

**Design and synthesis of plant oil-based UV-curable acrylates  
for sustainable coating applications**

by

Jonggeun Sung

B.S., Kansas State University, 2012

M.S., Kansas State University, 2014

AN ABSTRACT OF A DISSERTATION

submitted in partial fulfillment of the requirements for the degree

DOCTOR OF PHILOSOPHY

Department of Grain Science and Industry  
College of Agriculture

KANSAS STATE UNIVERSITY  
Manhattan, Kansas

2018

## Abstract

A demand in sustainable polymers has been increased because of the environment concerns and saving finite petroleum resources. Plant oils are promising renewable resources to produce environmentally friendly polymer applications. Soybean oil-based resins such as epoxidized soybean oil (ESO) and acrylated epoxidized soybean oil (AESO) have been well-known functionalized plant oils, but relatively low performances of their polymers and a competition with food production have been disadvantages. Thus, in this study, we designed new plant oil-based acrylates using non-food resources and achieved excellent properties of the acrylates for coatings and thermoset applications.

Firstly, we developed coating materials with high mechanical, thermal and coating performances using acrylated epoxidized camelina oil (AECO) as a main acrylate monomer with various meth(acrylates) as reactive diluents

Next, acrylated epoxidized cardanol modified fatty acids from camelina oil (AECFA) was successfully synthesized, and a phenolic structure with long aliphatic side chains with acrylic groups was obtained. The novel structure of AECFA provided rigidity into its polymer maintained with flexibility, and AECFA coating material showed better performances in terms of all properties such as mechanical, thermal, viscoelastic, and coating performances, as compared to commercial AESO resin.

Finally, acrylated epoxidized allyl 10-undecenoate (AEAU) was developed from 10-undecenoic acid, castor oil derivative. The single fatty ester structure with di-functional acrylates of AEAU had very lower viscosity and showed better thermoset performances than those of triglyceride-based acrylates such as AESO and AECO. Thus, AEAU had a potential to an alternative to AESO for thermoset applications.

**Design and synthesis of plant oil-based UV-curable acrylates  
for sustainable coating applications**

by

Jonggeun Sung

B.S., Kansas State University, 2012

M.S., Kansas State University, 2014

A DISSERTATION

submitted in partial fulfillment of the requirements for the degree

DOCTOR OF PHILOSOPHY

Department of Grain Science and Industry  
College of Agriculture

KANSAS STATE UNIVERSITY  
Manhattan, Kansas

2018

Approved by:

Major Professor  
Xiuzhi Susan Sun

# **Copyright**

Jonggeun Sung

2018

## Abstract

A demand in sustainable polymers has been increased because of the environment concerns and saving finite petroleum resources. Plant oils are promising renewable resources to produce environmentally friendly polymer applications. Soybean oil-based resins such as epoxidized soybean oil (ESO) and acrylated epoxidized soybean oil (AESO) have been well-known functionalized plant oils, but relatively low performances of their polymers and a competition with food production have been disadvantages. Thus, in this study, we designed new plant oil-based acrylates using non-food resources and achieved excellent properties of the acrylates for coatings and thermoset applications.

Firstly, we developed coating materials with high mechanical, thermal and coating performances using acrylated epoxidized camelina oil (AECO) as a main acrylate monomer with various meth(acrylates) as reactive diluents

Next, acrylated epoxidized cardanol modified fatty acids from camelina oil (AECFA) was successfully synthesized, and a phenolic structure with long aliphatic side chains with acrylic groups was obtained. The novel structure of AECFA provided rigidity into its polymer maintained with flexibility, and AECFA coating material showed better performances in terms of all properties such as mechanical, thermal, viscoelastic, and coating performances, as compared to commercial AESO resin.

Finally, acrylated epoxidized allyl 10-undecenoate (AEAU) was developed from 10-undecenoic acid, castor oil derivative. The single fatty ester structure with di-functional acrylates of AEAU had very lower viscosity and showed better thermoset performances than those of triglyceride-based acrylates such as AESO and AECO. Thus, AEAU had a potential to an alternative to AESO for thermoset applications.

# Table of Contents

Table of Contents .....	vi
List of Figures .....	x
List of Tables .....	xiv
List of Schemes .....	xv
Acknowledgements .....	xvi
Chapter 1 - Introduction .....	1
1.1. Overview .....	1
1.2. Objectives .....	2
1.3. References .....	4
Chapter 2 - Literature review .....	6
2.1. Plant oils .....	6
2.1.1. Fatty acids .....	6
2.1.2. Soybean oil .....	8
2.1.3. Camelina oil .....	8
2.1.4. Cardanol .....	9
2.1.5. References .....	11
2.2. Coating systems .....	15
2.2.1. Solvent-borne system .....	15
2.2.2. Water-borne system .....	16
2.2.3. UV-curable coating systems .....	17
2.2.4. Wood coating applications .....	18
2.2.5. References .....	21
2.3. Acrylate resins .....	24
2.3.1. Free-radical polymerization .....	24
2.3.2. Acrylates with aromatic structures .....	27
2.3.3. Polyurethane acrylates .....	29
2.3.4. Plant oil-based acrylates .....	30
2.3.5. References .....	34
2.4. Bio-inspired super-hydrophobic coating surfaces .....	39

2.4.1. Introduction.....	39
2.4.2. Special wettability surfaces in nature.....	41
2.4.3. Fabrication of super-hydrophobic surfaces.....	43
2.4.4. Conclusion .....	51
2.4.5. References.....	52
2.5. Fundamentals of biodegradable polymers .....	56
2.5.1. Introduction.....	56
2.5.2. Degradation mechanisms .....	58
2.5.3. Biodegradable polymers .....	66
2.5.4. Conclusion .....	73
2.5.5. References.....	75
Chapter 3 - Camelina oil-based acrylate with reactive diluents for bio-based wood coating applications .....	80
3.1. Abstract.....	80
3.2. Introduction.....	81
3.3. Materials and Methods.....	85
3.3.1. Materials .....	85
3.3.2. Synthesis of epoxidized camelina oil (ECO).....	86
3.3.3. Synthesis of acrylated epoxidized camelina oil (AECO).....	86
3.3.4. Preparation of UV-curable acrylates and coating materials.....	87
3.3.5. Measurements .....	88
3.4. Results and Discussion .....	90
3.4.1. FTIR analysis of CO and its derivatives .....	90
3.4.2. NMR analysis of CO and its derivatives.....	91
3.4.3. Viscosity of AECO resins with the RDs.....	94
3.4.4. Dynamic mechanical analysis of AECO:RDs polymers.....	95
3.4.5. Tensile properties of AECO:RDs polymers.....	100
3.4.6. Thermal degradation properties of AECO:RDs polymers .....	102
3.4.7. Coating performance of AECO:RDs polymers .....	105
3.5. Conclusion .....	107
3.6. References.....	108

Chapter 4 - Cardanol modified fatty acids from camelina oils for flexible bio-based acrylates coatings .....	113
4.1. Abstract.....	113
4.2. Introduction.....	114
4.3. Materials and Methods.....	121
4.3.1. Materials .....	121
4.3.2. Epoxidation and acrylation of camelina oil (ECO and AECO).....	121
4.3.3. Epoxidation and acrylation of cardanol glycidyl ether (ECGE and AECGE)..	122
4.3.4. Synthesis of free fatty acids from camelina oil (FACO) .....	123
4.3.5. Synthesis of cardanol modified fatty acids (CFA).....	124
4.3.6. Synthesis of epoxidized cardanol modified fatty acids (ECFA).....	124
4.3.7. Synthesis of acrylated epoxidized cardanol modified fatty acids (AECFA) ....	125
4.3.8. Preparation of UV-cured free-standing coating materials and coatings on wood .....	125
4.3.9. Measurements .....	126
4.4. Results and Discussion .....	128
4.4.1. Material synthesis and structure characterization using FTIR spectra .....	128
4.4.2. NMR spectra analysis and acrylate functionalities of the bio-based acrylates .	134
4.4.3. Bio-based content of the coating materials .....	138
4.4.4. Dynamic mechanical properties.....	139
4.4.5. Thermal degradation properties .....	141
4.4.6. Mechanical properties .....	144
4.4.7. Coating performance properties.....	146
4.5. Conclusion .....	148
4.6. References.....	149
Chapter 5 - Synthesis and characterization of di-functional acrylate from 10-undecenoic acid: A promising plant oil derivative for low viscous acrylate applications .....	155
5.1. Abstract.....	155
5.2. Introduction.....	156
5.3. Materials and Methods.....	160
5.3.1. Materials .....	160



5.3.2. Synthesis of allyl 10-undecenoate (AU) .....	161
5.3.3. Synthesis of epoxidized allyl 10-undecenoate (EAU) .....	161
5.3.4. Synthesis of acrylated epoxidized 10-undecenoate (AEAU).....	162
5.3.5. Preparation of UV-cured acrylates.....	163
5.3.6. Measurements .....	163
5.4. Results and Discussion .....	165
5.4.1. Structure characterization of AEAU and its intermediates .....	165
5.4.2. Rheological property of UA derivatives and the bio-based acrylates.....	171
5.4.3. Viscoelastic properties of the UV-cured acrylates.....	173
5.4.4. Tensile properties of the UV-cured acrylates .....	176
5.5.5. Thermal stability factors of the UV-cured acrylates .....	177
5.5.6. Possibility of AEAU as a reactive diluent for AESO resin.....	179
5.5. Conclusion .....	184
5.6. References.....	186
Chapter 6 - Conclusions and future works.....	190
6.1. Overall conclusions.....	190
6.2. Future works .....	191

## List of Figures

Figure 2.1: Compositions of CNSL: anacardic acid (a), cardanol (b), cardol (c), and 2-methyl cardol (d). .....	10
Figure 2.2: a) acrylic and b) methacrylic groups. ....	26
Figure 2.3: Initiation and propagation steps of free-radical polymerization (Noble and Coote, 2013). .....	27
Figure 2.4: Type I and Type II free-radical photoinitiators (Andrzejewska, 2001). ....	27
Figure 2.5: Typical bisphenol-A-based acrylate synthesis from epoxides of DGEBA (Mohtadizadeh et al., 2015). ....	29
Figure 2.6: Chemical structure of TMPTA. ....	29
Figure 2.7: Chemical structure of cardanol. ....	33
Figure 2.8: Plastic degradation process in the environment. ....	66
Figure 2.9: Poly(lactic acid) (a), and poly(lactide) (b). ....	72
Figure 2.10: Examples of PHAs from specific monomers (Shrivastav et al., 2013). ....	72
Figure 2.11: Chemical structure of PCL. ....	73
Figure 2.12: Chemical structure of PBS. ....	73
Figure 2.13: Example of AAC: poly(butylene adipate terephthalate) (PBAT). ....	73
Figure 3.1: Chemical structures of reactive diluents (HEA, HDED, EGDMA, MMA, LMA, and BDDMA) and free-radical photo-initiator (Darocur 1173). ....	85
Figure 3.2: FTIR spectra of camelina oil derivatives and cured AECO. ....	91
Figure 3.3: NMR spectra of ECO. ....	93
Figure 3.4: NMR spectra of AECO. ....	93

Figure 3.5: Viscosities of the AECO:RDs containing 3 wt% of Darocur 1173 at constant shear rate 1 s <sup>-1</sup> .....	95
Figure 3.6: Storage modulus (a) and tan δ (b) of the cured AECO containing petrochemical RDs. .....	98
Figure 3.7: Storage modulus (a) and tan δ (b) of the cured AECO containing bio-based RDs....	99
Figure 3.8: Tensile strengths of AECO:RDs polymers .....	101
Figure 3.9: Elongations at break of AECO:RDs polymers.....	102
Figure 3.10: Weight residues of AECO polymers containing petrochemical RDs as a function of temperature. ....	104
Figure 3.11: Weight residues of AECO polymers containing bio-based RDs as a function of temperature. ....	104
Figure 4.1: FTIR spectra of AECO, ECO, and camelina oil. ....	131
Figure 4.2: FTIR spectra of AECGE, ECGE, and CGE. ....	131
Figure 4.3: FTIR spectra of AECFA, ECFA, CFA, and FACO. ....	132
Figure 4.4: FTIR spectra of AESO and cured-AESO.....	132
Figure 4.5: FTIR spectra of AECO and cured-AECO.....	133
Figure 4.6: FTIR spectra of AECGE and cured-AECGE.....	133
Figure 4.7: FTIR spectra of AECFA and cured-AECFA. ....	134
Figure 4.8: NMR spectra of AECO. ....	136
Figure 4.9: NMR spectra of AECGE.....	136
Figure 4.10: NMR spectra of FACO.....	137
Figure 4.11: NMR spectra of CFA. ....	137
Figure 4.12: NMR spectra of ECFA. ....	137

Figure 4.13: NMR spectra of AECFA. ....	138
Figure 4.14: Storage modulus of AESO, AECO, AECGE, and AECFA as a function of temperature. .....	140
Figure 4.15: $\tan \delta$ of AESO, AECO, AECGE, and AECFA as a function of temperature. ....	140
Figure 4.16: Weight percentages of AESO, AECO, AECGE, and AECFA as a function of temperature. ....	143
Figure 4.17: Derivative weight loss of AESO, AECO, AECGE, and AECFA as a function of temperature. ....	143
Figure 4.18: Tensile strengths of the cured acrylates. ....	145
Figure 4.19: Elongations at break of the cured acrylates.....	145
Figure 5.1: Triglyceride-based acrylates from soybean oil (AESO) and camelina oil (AECO). 160	
Figure 5.2: Petrochemical reactive diluent, triethylene glycol dimethacrylate (TEGDMA).....	160
Figure 5.3: FTIR spectra of UA, AU, EAU, AEAU, and UV-cured AEAU.....	169
Figure 5.4: NMR spectra of UA. ....	169
Figure 5.5: NMR spectra of AU. ....	170
Figure 5.6: NMR spectra of EAU.....	170
Figure 5.7: NMR spectra of AEAU.....	171
Figure 5.8: Viscosities of UA and its derivatives, AESO, and AECO as a function of shear rate. .....	173
Figure 5.9: Storage modulus of the UV-cured acrylates as a function of temperature.....	175
Figure 5.10: $\tan \delta$ of the UV-cured acrylates as a function of temperature.....	175
Figure 5.11: Tensile stress of the UV-cured acrylates as a function of strain. ....	177
Figure 5.12: Residual weight of the UV-cured acrylates as a function of temperature.....	178

Figure 5.13: Derivative weight loss of the UV-cured acrylates as a function of temperature....	179
Figure 5.14: Viscosities of the neat AESO and the AESO resins containing AEAU and/or TEGDMA as reactive diluents.....	182
Figure 5.15: Tensile strengths of the AESO thermosets containing AEAU and/or TEGDMA as reactive diluents. ....	182
Figure 5.16: Elongations at break of the AESO thermosets containing AEAU and/or TEGDMA as reactive diluents. ....	183
Figure 5.17: Storage modulus of the AESO thermosets containing AEAU and/or TEGDMA as reactive diluents. ....	183
Figure 5.18: $\tan \delta$ of the AESO thermosets containing AEAU and/or TEGDMA as reactive diluents. ....	184

## List of Tables

Table 2.1: Common fatty acids in plant oils (Belgacem and Gandini, 2008; Pfister et al., 2011). C:DB is a ratio of the number of carbons in the fatty acid to the number of double bonds. ..	7
Table 2.2: Numbers of the double bonds and major fatty acid compositions of plant oils (Islam et al., 2014; Karak, 2012; Z. Petrovic, 2008).....	8
Table 3.1: Dynamic mechanical and tensile properties of the AECO:RDs polymers. ....	100
Table 3.2: Thermal stability factors of AECO:RDs polymers.....	103
Table 3.3: Coating performance properties of AECO-based coatings. Hardness* and adhesion* were measured at 3 days after the MEK rub tests were performed on the coatings. ....	106
Table 4.1: Thermal and mechanical properties of the AESO, AECO, AECGE, and AECFA polymers. $\sigma$ is tensile strength, and $\epsilon$ is elongation at break.....	141
Table 4.2: Coating performance properties of the cure acrylates. ....	147
Table 5.1: Properties of the UV-cured acrylates; $\sigma$ is tensile strength, and $\epsilon$ is elongation at break. ....	175
Table 5.2: Bio-content and viscosity of the AESO resins formulated with AEAU and/or TEGDMA including 3 wt% of photo-initiator. Viscoelastic and tensile properties of the UV-cured resins; $\eta$ is viscosity at shear rate of $1 \text{ s}^{-1}$ , $\sigma$ is tensile strength, and $\epsilon$ is elongation at break. ....	184

## List of Schemes

Scheme 3.1: Chemical pathway of synthesis of AECO from camelina oil. ....	84
Scheme 4.1: Synthesis route of AECO from camelina oil.....	118
Scheme 4.2: Synthesis route of AECGE from CGE.....	119
Scheme 4.3: Synthesis route of AECFA from camelina oil and CGE.....	120
Scheme 5.1: Synthesis route of AEAU from UA. ....	159

## **Acknowledgements**

This study was financially supported by U.S. Department of Agriculture National Institute of Food and Agriculture Biomass Research and Development Initiative program.

First, I would like to truly thank my advisor Dr. Xiuzhi Susan Sun. She has always supported and encouraged me to succeed in finishing my graduate study. I learned how to think as a doctor, how to behave professionally, and how to be a scientist from her. I will model myself on Dr. Sun as an excellent scientist, professor, mentor, and leader. I would also like to express appreciation to my committee, including Dr. Donghai Wang, Dr. Stefan H. Bossmann, and Dr. Yongcheng Shi, for their helpful comments and guidance, and I would like to thank my outside chair, Dr. Jennifer L. Anthony, for her service.

I would like to appreciate to Dr. Yonghui Li for supporting lab works, and thanks to all lab members of Bio-materials and Technology Lab and staffs of Department of Grain Science and Industry. Special thanks to my parents and parents in law, for their endless supports and encouragements.

Finally, but most importantly, special thanks to my wife Jiye Yoon for her love and great devotion to me and my daughter Lucia Y. Sung. I could never win through in the end without her.



# Chapter 1 - Introduction

## 1.1. Overview

UV-curing coating system has been focused as more environment-friendly technique in comparison with traditional solvent-borne coating system, because UV-curable resins need less volatile organic compounds, lower energy in the curing process, and shorter curing time (Bongiovanni et al., 2002; Landry et al., 2008; Schwalm, 2006). Therefore, in addition to coatings, photo-polymerization has been widely used for polymer applications including paints, printing inks, adhesives, composites, and dental resin (Andrzejewska, 2001). Acrylic resins including acrylate monomers have been well-known thermoset resins for UV-curing coatings, and petrochemicals such as diglycidyl ether bisphenol-A (Kardar et al., 2009; Mohtadizadeh et al., 2015) and epoxy novolac (Chattopadhyay et al., 2005) have been mainly used to produce commercial acrylic resins due to their excellent performances with competitive prices (Schwalm, 2006). Indeed, however, the petrochemicals are not renewable, and the price of the feedstocks can be fluctuated by various economic conditions and political issues (C. Zhang et al., 2017). Therefore, a demand for sustainable alternatives to the petrochemical resins have been extensively increased to reduce chemical pollutants and save petroleum resources (Crivello and Narayan, 1992; Meier et al., 2007).

Plant oils are promising sustainable resources in polymers and coating industries due to its renewability, abundancy, and flexibility of chemical modifications (Sharmin et al., 2015; Wool and Sun, 2005). Moreover, plant oils are intrinsically biodegradable and low toxic (Xia and Larock, 2010), and thus they have been already used for manufacturing surfactants, cosmetics, paints, coatings, lubricants, etc (Maisonneuve et al., 2013). Soybean is one of the major crops in the United States with 108 million metric tons of production in 2014 (US Department of Agriculture,

2015). Therefore, soybean oil has been one of the important renewable resources in chemical industry (Z. Petrovic, 2008; Williams and Hillmyer, 2008). Acrylated epoxidized soybean oil (AESO) is a well-known commercially available bio-based acrylate, and it can be formed as a transparent thermoset through free-radical polymerization under UV-radiation. However, relatively weak mechanical strength and low thermal properties of the AESO thermoset are disadvantages to producing high performance coating materials. In addition, using food resources in polymer applications can cause a dispute over a competition with food production, as soybean oil usages in industrial applications captured 15 % of global production of soybean oil (Belgacem and Gandini, 2008). Thus, this study is interested in designing sustainable resins for coating applications through using non-food resources such as camelina oil and cardanol.

## 1.2. Objectives

The overall purpose of this study was to investigate UV-curable coating materials and thermosets from non-food resources with improved performance properties through finding novel plant oils and developing chemical pathways.

The specific research objectives of this study are below:

1. **To design acrylated epoxidized camelina oil (AECO) resins formulated with various reactive diluents;** although UV-cured AECO compared to AESO showed excellent mechanical strength and coating ability, very high viscosity of AECO caused a difficulty in efficient coating process. Therefore, this research focused on finding appropriate reactive diluents and formulations to reduce the viscosity of AECO resins maintained with the properties (described in Chapter 3).
2. **To develop a sustainable alternative to AESO for producing high performance coating materials;** we were interested in the remarkable mechanical

strength and thermally stable structure of aromatic compounds, so cardanol was selected as a natural phenolic lipids to provide rigidity into triglyceride-based acrylate polymers. Therefore, a new acrylate was designed from a combined structure of cardanol and camelina oil (described in Chapter 4).

3. **To investigate very low viscous plant oil-based acrylate;** triglyceride-based acrylates are generally too viscous, so reactive diluents are additionally required to reduce the viscosity of the acrylates. However, typical reactive diluents such as styrene are volatile materials, which cause environmental hazardous and safety concerns in polymers manufacturing. Therefore, we focused on developing very low viscous bio-based acrylates that needs less or non-reactive diluents, and then a novel acrylate based on single fatty acid structure was synthesized from a castor oil derivative (described in Chapter 5).

### 1.3. References

- Andrzejewska, E. (2001). Photopolymerization kinetics of multifunctional monomers. *Progress in Polymer Science*, 26: 605-665.
- Belgacem, M. N., and Gandini, A. (2008). *Materials from vegetable oils: Major sources, properties and applications. Monomers, polymers and composites from renewable resources* (pp. 39-66) Elsevier.
- Bongiovanni, R., Montefusco, F., Priola, A., Macchioni, N., Lazzeri, S., Sozzi, L., and Ameduri, B. (2002). High performance UV-cured coatings for wood protection. *Progress in Organic Coatings*, 45: 359-363.
- Chattopadhyay, D., Panda, S. S., and Raju, K. (2005). Thermal and mechanical properties of epoxy acrylate/methacrylates UV cured coatings. *Progress in Organic Coatings*, 54: 10-19.
- Crivello, J. V., and Narayan, R. (1992). Epoxidized triglycerides as renewable monomers in photoinitiated cationic polymerization. *Chemistry of Materials*, 4: 692-699.  
doi:10.1021/cm00021a036
- Kardar, P., Ebrahimi, M., Bastani, S., and Jalili, M. (2009). Using mixture experimental design to study the effect of multifunctional acrylate monomers on UV cured epoxy acrylate resins. *Progress in Organic Coatings*, 64: 74-80.
- Landry, V., Riedl, B., and Blanchet, P. (2008). Nanoclay dispersion effects on UV coatings curing. *Progress in Organic Coatings*, 62: 400-408.
- Maisonneuve, L., Lebarbé, T., Grau, E., and Cramail, H. (2013). Structure–properties relationship of fatty acid-based thermoplastics as synthetic polymer mimics. *Polymer Chemistry*, 4: 5472-5517.
- Meier, M. A. R., Metzger, J. O., and Schubert, U. S. (2007). Plant oil renewable resources as green alternatives in polymer science. *Chemical Society Reviews*, 36: 1788-1802.  
doi:10.1039/b703294c
- Mohtadizadeh, F., Zohuriaan-Mehr, M., Hadavand, B. S., and Dehghan, A. (2015). Tetra-functional epoxy-acrylate as crosslinker for UV curable resins: Synthesis, spectral, and thermo-mechanical studies. *Progress in Organic Coatings*, 89: 231-239.
- Petrovic, Z. (2008). Polyurethanes from vegetable oils. *Polymer Reviews*, 48: 109-155.  
doi:10.1080/15583720701834224
- Schwalm, R. (2006). *UV coatings: Basics, recent developments and new applications* Elsevier.
- Sharmin, E., Zafar, F., Akram, D., Alam, M., and Ahmad, S. (2015). Recent advances in vegetable oils based environment friendly coatings: A review. *Industrial Crops and Products*, 76: 215-229.
- US Department of Agriculture. (2015). *Crop production 2014 summary*. (pp. 41-44). Washington, DC: US Department of Agriculture.
- Williams, C. K., and Hillmyer, M. A. (2008). Polymers from renewable resources: A perspective for a special issue of polymer reviews. *Polymer Reviews*, 48: 1-10.  
doi:10.1080/15583720701834133

- Wool, R. P., and Sun, X. S. (2005). *Bio-based polymers and composites*. Burlington: Academic Press.
- Xia, Y., and Larock, R. C. (2010). Vegetable oil-based polymeric materials: Synthesis, properties, and applications. *Green Chemistry*, 12: 1893-1909. doi:10.1039/c0gc00264j
- Zhang, C., Garrison, T. F., Madbouly, S. A., and Kessler, M. R. (2017). Recent advances in vegetable oil-based polymers and their composites. *Progress in Polymer Science*, 71: 91-143.

## Chapter 2 - Literature review

### 2.1. Plant oils

#### 2.1.1. Fatty acids


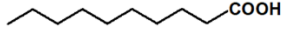
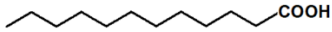
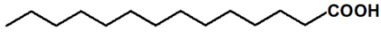

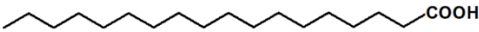
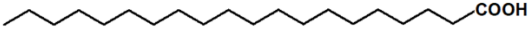
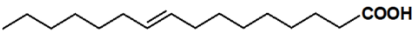
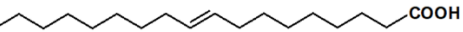
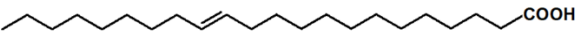
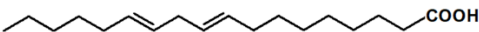
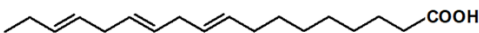
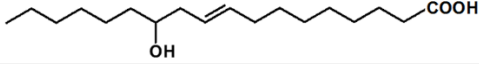
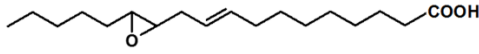
Most of plants contain oils at a range from very small amounts up to 80 wt% (C. Zhang et al., 2017), and the maximum oil content is typically obtained in plant seeds (Bockisch, 1998). Plant oils are mainly comprised of triglycerides, which are three fatty acids linked with a glycerin via ester bonds (J. J. La Scala et al., 2004). Fatty acids have important roles as fuels in metabolism through energy storage and transport (Rustan and Drevon, 2005). Triglycerides are the storage lipids in organic cells, which are surrounded by phospholipids and functional hydrophobic proteins (Christie, 2011). In addition, fatty acids are essential components of cell membranes as phospholipids, and they are also as thermal, electrical, and mechanical insulators (Rustan and Drevon, 2005).

Variety of fatty acids are found in terms of the different chain length, the number of carbons, degree of unsaturation sites, position of the unsaturated carbons, and presence of functional groups (e.g., hydroxyl and epoxy), depending on the species and growing conditions (Belgacem and Gandini, 2008; Islam et al., 2014; Pfister et al., 2011). The common fatty acids and their compositions in plant oils are listed in Table 2.1 and 2.2. Generally, five fatty acids such as palmitic, stearic, oleic, linoleic, and linolenic are key compositions of plant oils (Williams and Hillmyer, 2008). Most of the unsaturated carbons of plant oils are placed between 9th and 16th carbons of the fatty acids, and they are typically not conjugated whereas few oils such as tung oil contain conjugated C=C double bonds in their fatty acid chains (C. Zhang et al., 2017). In addition, some oils have functional groups in the fatty acids such as hydroxyl and oxirane; castor oil is mainly

composed of 87.5% ricinoleic acid, which contains one hydroxyl group at 12th carbon of the fatty acid (Salimon et al., 2010), and vernonia oil contains 72-80% vernolic acid, which has one oxirane ring between 12th and 13th carbons of the fatty acid (Baye and Becker, 2004).

The C=C double bonds of the fatty acids except the fatty acids containing conjugated C=C double bonds are not really reactive (C. Zhang et al., 2017), and thus other reactive groups such as epoxide and hydroxyl are functionalized on the fatty acids to be reactive intermediates or monomers for polymer applications (Del Rio et al., 2010). The unsaturation sites and ester groups of natural triglycerides can be chemically modified to obtain the reactive functional groups such as epoxides, acrylates, and hydroxyl groups on the fatty acids through using typical synthetic pathways in current polymer industries (Wool and Sun, 2005).

**Table 2.1: Common fatty acids in plant oils (Belgacem and Gandini, 2008; Pfister et al., 2011). C:DB is a ratio of the number of carbons in the fatty acid to the number of double bonds.**

Fatty acids	C:DB	Formula	Structure
Caprylic	8:0	C <sub>8</sub> H <sub>16</sub> O <sub>2</sub>	
Capric	10:0	C <sub>10</sub> H <sub>20</sub> O <sub>2</sub>	
Lauric	12:0	C <sub>12</sub> H <sub>24</sub> O <sub>2</sub>	
Myristic	14:0	C <sub>14</sub> H <sub>28</sub> O <sub>2</sub>	
Palmitic	16:0	C <sub>16</sub> H <sub>32</sub> O <sub>2</sub>	
Stearic	18:0	C <sub>18</sub> H <sub>36</sub> O <sub>2</sub>	
Arachidic	20:0	C <sub>20</sub> H <sub>40</sub> O <sub>2</sub>	
Palmitoleic	16:1	C <sub>16</sub> H <sub>30</sub> O <sub>2</sub>	
Oleic	18:1	C <sub>18</sub> H <sub>34</sub> O <sub>2</sub>	
Erucic	22:1	C <sub>22</sub> H <sub>42</sub> O <sub>2</sub>	
Linoleic	18:2	C <sub>18</sub> H <sub>32</sub> O <sub>2</sub>	
Linolenic	18:3	C <sub>18</sub> H <sub>30</sub> O <sub>2</sub>	
Ricinoleic	18:1:1OH	C <sub>18</sub> H <sub>34</sub> O <sub>3</sub>	
Vernolic	18:1:1 $\text{\textcircled{O}}$	C <sub>18</sub> H <sub>32</sub> O <sub>3</sub>	

**Table 2.2: Numbers of the double bonds and major fatty acid compositions of plant oils (Islam et al., 2014; Karak, 2012; Z. Petrovic, 2008).**

Name	C=C per triglyceride	Fatty acid composition (%)									
		Lauric	Myristic	Palmitic	Stearic	Palmitoleic	Oleic	Linoleic	Linolenic	Ricinoleic	Erucic
Soybean	4.6		0.1	10.6	0.1	4.0	23.3	53.7	7.6		
Palm	1.7	0.1	1	44.4	0.2	4.1	39.3	10	0.4		
Rapeseed	3.8		0.1	3.8	1.2	0.3	18.5	14.5	11.0		41.1
Linseed	6.6			6.0		4.0	22.0	16.0	52.0		
Corn	4.5		0.1	10.9	0.2	2.0	25.4	59.6	1.2		
Canola	3.9		1	4.0	0.3	1.8	60.9	21.0	8.8		0.7
Sunflower	4.7		0.1	7.0	4.5	0.1	18.7	67.5	0.8		6.6
Olive	2.8			9	0.6	2.7	80.3	6.3	0.7		
Castor	3.0			1.5	0.5		5	4	0.5	87.5	
Camelina	5.8			6.9	3.5	0.2	14.8	18.6	37.4		

### 2.1.2. Soybean oil

Soybean oil is one of the global plant oils with the largest volume, mainly produced in the United States, Brazil, and Argentina (C. Zhang et al., 2017), and approximately 15% of soybean oil was spent for industrial applications in the world (Belgacem and Gandini, 2008). In addition, 80-85% of unsaturated fatty acid composition of soybean oil with inexpensive price is suitable for a renewable raw material in polymer industries (Mihail and Petrovic, 2011; Z. Petrovic, 2008). Therefore, large series of researches have reported soybean oil-based polymers for various applications such as coatings (Dai et al., 2016; Habib and Bajpai, 2011; S. Ma et al., 2014a; Sung et al., 2015), pressure sensitive adhesives (Ahn et al., 2011; Ahn et al., 2013; Y. Li and Sun, 2014; Y. Li and Sun, 2015b), composites (Z. S. Liu et al., 2005; J. Lu et al., 2004; Uyama et al., 2003; Zhan and Wool, 2010), polyurethanes (Miao et al., 2013; Z. S. Petrovic et al., 2000; C. Zhang et al., 2013), and plasticizers (J. S. Choi and Park, 2004; Sung et al., 2015; D. Yang et al., 2014), etc.

### 2.1.3. Camelina oil

Camelina is an ancient oil seed crop that has originated in southeastern Europe and southwestern Asia, and it was importantly cultivated in Europe for centuries and replaced by

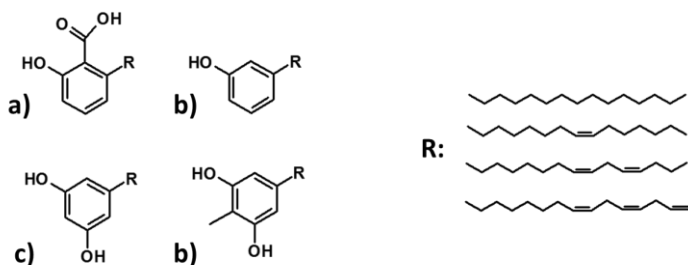


higher-yielding crops such as canola and wheat at the Middle ages (Kagale et al., 2014; N. Kim et al., 2015; Y. Li and Sun, 2015a). Camelina oil has been focused as a renewable raw material for polymer applications due to its highly unsaturated fatty acids (about 90% of fatty acids, 5.8 double bonds per triglyceride) in the oil (36-47% oil content in the seeds), which are advantages for producing strengthened polymers (N. Kim et al., 2015; Y. Li and Sun, 2015a). Camelina oil fatty acids are mainly composed of unsaturated fatty acids such as linolenic acid (C18:3, 37.4%), linoleic acid (C18:2, 18.6%), and oleic acid (C18:1, 14.8%) (N. Kim et al., 2015). The fatty acid compositions of camelina oil have been attractive for jet fuel, biodiesel, and lubricants productions (Kagale et al., 2014). Thus, camelina has been increasingly cultivated in the United States due to its beneficial applications in multiple industries (Iskandarov et al., 2014; Keske et al., 2013). In consideration of agricultural point of view, cultivation of camelina has several advantages such as using less water and fertilizer, needs for less herbicides and pesticides, and adaptability to severe weather and grow in marginal lands, as compared to common oil seed crops such as soybean, canola, etc. (Francis and Warwick, 2009; Iskandarov et al., 2014; Razeq et al., 2014). Furthermore, using camelina oil for polymer productions may not compete with food production because camelina oil is not a food resource. Currently, camelina meal and oil have been used to prepare polymers (Kasetaitė et al., 2014; N. Kim et al., 2015; Y. Li and Sun, 2015a; N. Reddy et al., 2012) and composites (Balanuca et al., 2014; J. T. Kim and Netravali, 2012).

#### **2.1.4. Cardanol**

Cashew nut shell liquid (CNSL) has been an attractive by-product of cashew nut production, as 450,000 metric ton of annual production was planned (Balachandran et al., 2013; Velmurugan and Loganathan, 2011), and 7-8% of growth per year was estimated (Lochab et al., 2014). Pristine CNSL is mainly composed of phenolic compounds with unsaturated alkyl side chains such as

anacardic acid (71.7%), cardanol (4.7%), cardol (18.7), 2-methyl cardol (2.7), and traces of polymeric materials (Figure 2.1) (Calò et al., 2007). CNSL is extracted from cashew nut shell through using solvent extraction, pyrolysis, and heat and supercritical carbon dioxide extraction (Lochab et al., 2014), and final compositions of CNSL is depending on the extracting processes (Balachandran et al., 2013). In order to obtain technical grade of CNSL, hot processing is used to extract cardanol from the nut shell as a major component; anacardic acid is converted to cardanol through decarboxylation, and cardol is removed by additional distillation process (Lochab et al., 2014; Mele and Vasapollo, 2008). Due to the abundancy of the raw materials with the simple extraction processes, CNSL is one of the natural phenolic chemicals for industrial uses with economic price (Sultania et al., 2011). The functional sites of cardanol such as the phenolic hydroxyl group and the C=C double bonds of the alkyl side chains are suitable for preparing a wide range of polymer applications such as coatings (Y. Choi et al., 2014; Darroman et al., 2015; Darroman et al., 2016; R. Liu et al., 2015), plasticizers (J. Chen et al., 2015; Greco et al., 2010; Hassouma et al., 2016), reactive diluents (J. Chen, Nie et al., 2015; Mi et al., 2012), synthetic resins (Hannoda et al., 2015; Jaillet, Darroman et al., 2014; Jaillet, Nouailhas et al., 2014), composites (Q. Chen et al., 2010; Maffezzoli et al., 2004; B. Rao and Palanisamy, 2011), surfactant (Dantas et al., 2009; Fontana et al., 2015; Tyman and Bruce, 2003), polyurethane (Suresh and Kishanprasad, 2005; Suresh, 2012), and nanocarrier (Bloise et al., 2014), etc.



**Figure 2.1: Compositions of CNSL: anacardic acid (a), cardanol (b), cardol (c), and 2-methyl cardol (d).**

## 2.1.5. References

- Ahn, B. K., Kraft, S., Wang, D., and Sun, X. S. (2011). Thermally stable, transparent, pressure-sensitive adhesives from epoxidized and dihydroxyl soybean oil. *Biomacromolecules*, 12: 1839-1843. doi:10.1021/bm200188u
- Ahn, B. K., Sung, J., Kim, N., Kraft, S., and Sun, X. S. (2013). UV-curable pressure-sensitive adhesives derived from functionalized soybean oils and rosin ester. *Polymer International*, 62: 1293-1301. doi:10.1002/pi.4420
- Balachandran, V. S., Jadhav, S. R., Vemula, P. K., and John, G. (2013). Recent advances in cardanol chemistry in a nutshell: From a nut to nanomaterials. *Chemical Society Reviews*, 42: 427-438.
- Balanuca, B., Lungu, A., Hanganu, A., Stan, L. R., Vasile, E., and Iovu, H. (2014). Hybrid nanocomposites based on POSS and networks of methacrylated camelina oil and various PEG derivatives. *European Journal of Lipid Science and Technology*, 116: 458-469.
- Baye, T., and Becker, H. C. (2004). Analyzing seed weight, fatty acid composition, oil, and protein contents in *vernonia galamensis* germplasm by near-infrared reflectance spectroscopy. *Journal of the American Oil Chemists' Society*, 81: 641-645.
- Belgacem, M. N., and Gandini, A. (2008). *Materials from vegetable oils: Major sources, properties and applications. Monomers, polymers and composites from renewable resources* (pp. 39-66) Elsevier.
- Bloise, E., Becerra-Herrera, M., Mele, G., Sayago, A., Carbone, L., D'Accolti, L., Mazzetto, S. E., and Vasapollo, G. (2014). Sustainable preparation of cardanol-based nanocarriers with embedded natural phenolic compounds. *ACS Sustainable Chemistry & Engineering*, 2: 1299-1304.
- Bockisch, M. (1998). *Fats and oils handbook*. (pp. 345). Champaign, IL: AOCS Press.
- Calò, E., Maffezzoli, A., Mele, G., Martina, F., Mazzetto, S. E., Tarzia, A., and Stifani, C. (2007). Synthesis of a novel cardanol-based benzoxazine monomer and environmentally sustainable production of polymers and bio-composites. *Green Chemistry*, 9: 754-759.
- Chen, J., Liu, Z., Li, K., Huang, J., Nie, X., and Zhou, Y. (2015). Synthesis and application of a natural plasticizer based on cardanol for poly (vinyl chloride). *Journal of Applied Polymer Science*, 132
- Chen, J., Nie, X., Liu, Z., Mi, Z., and Zhou, Y. (2015). Synthesis and application of polyepoxide cardanol glycidyl ether as biobased polyepoxide reactive diluent for epoxy resin. *ACS Sustainable Chemistry & Engineering*, 3: 1164-1171.
- Chen, Q., Xue, H., and Lin, J. (2010). Preparation of polypropylene-graft-cardanol by reactive extrusion and its composite material with bamboo powder. *Journal of Applied Polymer Science*, 115: 1160-1167.
- Choi, Y., Kim, K., Kim, D., Kim, H. J., Cha, S., and Lee, J. (2014). Synthesis and characterization of self-cross-linkable and bactericidal methacrylate polymers having renewable cardanol moieties for surface coating applications. *RSC Advances*, 4: 41195-41203.

- Choi, J. S., and Park, W. H. (2004). Effect of biodegradable plasticizers on thermal and mechanical properties of poly (3-hydroxybutyrate). *Polymer Testing*, 23: 455-460. doi:10.1016/j.polymertesting.2003.09.005
- Dai, J., Liu, X., Ma, S., Wang, J., Shen, X., You, S., and Zhu, J. (2016). Soybean oil-based UV-curable coatings strengthened by crosslink agent derived from itaconic acid together with 2-hydroxyethyl methacrylate phosphate. *Progress in Organic Coatings*, 97: 210-215.
- Dantas, T. C., Vale, T., Neto, A. D., Scatena Jr, H., and Moura, M. (2009). Micellization study and adsorption properties of an ionic surfactant synthesized from hydrogenated cardanol in air–water and in air–brine interfaces. *Colloid and Polymer Science*, 287: 81-87.
- Darroman, E., Durand, N., Boutevin, B., and Caillol, S. (2015). New cardanol/sucrose epoxy blends for biobased coatings. *Progress in Organic Coatings*, 83: 47-54.
- Darroman, E., Durand, N., Boutevin, B., and Caillol, S. (2016). Improved cardanol derived epoxy coatings. *Progress in Organic Coatings*, 91: 9-16.
- Del Rio, E., Galia, M., Cadiz, V., Lligadas, G., and Ronda, J. C. (2010). Polymerization of epoxidized vegetable oil derivatives: Ionic-coordinative polymerization of methylepoxyoleate. *Journal of Polymer Science Part A-Polymer Chemistry*, 48: 4995-5008. doi:10.1002/pola.24297
- Fontana, A., Guernelli, S., Zaccheroni, N., Zappacosta, R., Genovese, D., De Crescentini, L., and Riela, S. (2015). Micellization properties of cardanol as a renewable co-surfactant. *Organic & Biomolecular Chemistry*, 13: 9214-9222.
- Francis, A., and Warwick, S. (2009). The biology of canadian weeds. 142. *camelina alyssum* (mill.) thell.; *C. microcarpa* andrz. ex DC.; *C. sativa* (L.) crantz. *Canadian Journal of Plant Science*, 89: 791-810.
- Greco, A., Brunetti, D., Renna, G., Mele, G., and Maffezzoli, A. (2010). Plasticizer for poly (vinyl chloride) from cardanol as a renewable resource material. *Polymer Degradation and Stability*, 95: 2169-2174.
- Habib, F., and Bajpai, M. (2011). Synthesis and characterization of acrylated epoxidized soybean oil for UV cured coatings.
- Hannoda, Y., Akasaka, Y., and Shibata, M. (2015). Bio-based thermosetting bismaleimide resins using cardanyl linolenate and allyl cardanyl ether. *Reactive and Functional Polymers*, 97: 96-104.
- Hassouma, F., Mihai, I., Fetzer, L., Fouquet, T., Raquez, J., Laachachi, A., Ibn Al Ahrach, H., and Dubois, P. (2016). Design of new cardanol derivative: Synthesis and application as potential biobased plasticizer for poly (lactide). *Macromolecular Materials and Engineering*, 301: 1267-1278.
- Iskandarov, U., Kim, H. J., and Cahoon, E. B. (2014). *Camelina: An emerging oilseed platform for advanced biofuels and bio-based materials*. *Plants and BioEnergy* (pp. 131-140) Springer.
- Islam, M. R., Beg, M. D. H., and Jamari, S. S. (2014). Development of vegetable-oil-based polymers. *Journal of Applied Polymer Science*, 131

- Jaillet, F., Darroman, E., Ratsimihety, A., Auvergne, R., Boutevin, B., and Caillol, S. (2014). New biobased epoxy materials from cardanol. *European Journal of Lipid Science and Technology*, 116: 63-73.
- Jaillet, F., Nouailhas, H., Auvergne, R., Ratsimihety, A., Boutevin, B., and Caillol, S. (2014). Synthesis and characterization of novel vinyl ester prepolymers from cardanol. *European Journal of Lipid Science and Technology*, 116: 928-939.
- Kagale, S., Koh, C., Nixon, J., Bollina, V., Clarke, W. E., Tuteja, R., Spillane, C., Robinson, S. J., Links, M. G., . . . Parkin, I. A. (2014). The emerging biofuel crop camelina sativa retains a highly undifferentiated hexaploid genome structure. *Nature Communications*, 5: 3706. doi:10.1038/ncomms4706 [doi]
- Karak, N. (2012). Vegetable oil-based polymers: Properties, processing and applications. (pp. 322) Elsevier.
- Kasetaite, S., Ostrauskaite, J., Grazuleviciene, V., Svediene, J., and Bridziuviene, D. (2014). Camelina oil-and linseed oil-based polymers with bisphosphonate crosslinks. *Journal of Applied Polymer Science*, 131
- Keske, C. M., Hoag, D. L., Brandess, A., and Johnson, J. J. (2013). Is it economically feasible for farmers to grow their own fuel? A study of camelina sativa produced in the western united states as an on-farm biofuel. *Biomass and Bioenergy*, 54: 89-99.
- Kim, J. T., and Netravali, A. N. (2012). Non-food application of camelina meal: Development of sustainable and green biodegradable paper-camelina composite sheets and fibers. *Polymer Composites*, 33: 1969-1976.
- Kim, N., Li, Y., and Sun, X. S. (2015). Epoxidation of camelina sativa oil and peel adhesion properties. *Industrial Crops and Products*, 64: 1-8.
- La Scala, J. J., Sands, J. M., Orlicki, J. A., Robinette, E. J., and Palmese, G. R. (2004). Fatty acid-based monomers as styrene replacements for liquid molding resins. *Polymer*, 45: 7729-7737.
- Li, Y., and Sun, X. S. (2014). Di-hydroxylated soybean oil polyols with varied hydroxyl values and their influence on UV-curable pressure-sensitive adhesives. *Journal of the American Oil Chemists' Society*, 91: 1425-1432.
- Li, Y., and Sun, X. S. (2015a). Camelina oil derivatives and adhesion properties. *Industrial Crops and Products*, 73: 73-80.
- Li, Y., and Sun, X. S. (2015b). Synthesis and characterization of acrylic polyols and polymers from soybean oils for pressure-sensitive adhesives. *RSC Advances*, 5: 44009-44017.
- Liu, R., Zhang, X., Zhu, J., Liu, X., Wang, Z., and Yan, J. (2015). UV-curable coatings from multiarmed cardanol-based acrylate oligomers. *ACS Sustainable Chemistry & Engineering*, 3: 1313-1320.
- Liu, Z. S., Erhan, S. Z., and Xu, J. Y. (2005). Preparation, characterization and mechanical properties of epoxidized soybean oil/clay nanocomposites. *Polymer*, 46: 10119-10127. doi:10.1016/j.polymer.2005.08.065

- Lochab, B., Shukla, S., and Varma, I. K. (2014). Naturally occurring phenolic sources: Monomers and polymers. *RSC Advances*, 4: 21712-21752.
- Lu, J., Hong, C. K., and Wool, R. P. (2004). Bio-based nanocomposites from functionalized plant oils and layered silicate. *Journal of Polymer Science Part B-Polymer Physics*, 42: 1441-1450. doi:10.1002/polb.20027
- Ma, S., Jiang, Y., Liu, X., Fan, L., and Zhu, J. (2014). Bio-based tetrafunctional crosslink agent from gallic acid and its enhanced soybean oil-based UV-cured coatings with high performance. *RSC Advances*, 4: 23036-23042.
- Maffezzoli, A., Calo, E., Zurlo, S., Mele, G., Tarzia, A., and Stifani, C. (2004). Cardanol based matrix biocomposites reinforced with natural fibres. *Composites Science and Technology*, 64: 839-845.
- Mele, G., and Vasapollo, G. (2008). Fine chemicals and new hybrid materials from cardanol. *Mini-Reviews in Organic Chemistry*, 5: 243-253.
- Mi, Z., Nie, X., Liu, Z., and Wang, Y. (2012). Synthesis and effect of cardanol glycidyl ether as reactive diluent of epoxy resin system. *Journal of Bioprocess Engineering and Biorefinery*, 1: 202-206.
- Miao, S., Zhang, S., Su, Z., and Wang, P. (2013). Synthesis of bio-based polyurethanes from epoxidized soybean oil and isopropanolamine. *Journal of Applied Polymer Science*, 127: 1929-1936. doi:10.1002/app.37564
- Mihail, I., and Petrovic, Z. S. (2011). Polymerization of soybean oil with superacids. *Soybean: Applications and Technology*, : 365. doi:10.5772/10547
- Petrovic, Z. S., Guo, A., and Zhang, W. (2000). Structure and properties of polyurethanes based on halogenated and nonhalogenated soy-polyols. *Journal of Polymer Science Part A-Polymer Chemistry*, 38: 4062-4069. doi:10.1002/1099-0518(20001115)38:22<4062::AID-POLA60>3.0.CO;2-L
- Petrovic, Z. (2008). Polyurethanes from vegetable oils. *Polymer Reviews*, 48: 109-155. doi:10.1080/15583720701834224
- Pfister, D. P., Xia, Y., and Larock, R. C. (2011). Recent advances in vegetable oil-based polyurethanes. *ChemSusChem*, 4: 703-717.
- Rao, B., and Palanisamy, A. (2011). Monofunctional benzoxazine from cardanol for bio-composite applications. *Reactive and Functional Polymers*, 71: 148-154.
- Razeq, F. M., Kosma, D. K., Rowland, O., and Molina, I. (2014). Extracellular lipids of camelina sativa: Characterization of chloroform-extractable waxes from aerial and subterranean surfaces. *Phytochemistry*, 106: 188-196.
- Reddy, N., Jin, E., Chen, L., Jiang, X., and Yang, Y. (2012). Extraction, characterization of components, and potential thermoplastic applications of camelina meal grafted with vinyl monomers. *Journal of Agricultural and Food Chemistry*, 60: 4872-4879.

## 2.2. Coating systems

### 2.2.1. Solvent-borne system

Solvents have widely used as a major ingredient of organic coating formulation to dissolve or disperse the other ingredients such as viscous polymeric binders and additives (Sørensen et al., 2009). Dissolving coating resins in solvents lessens the viscosity of the coating formulation to enhance the processibility for conventional coating methods such as spraying or dipping (Sørensen et al., 2009). The evaporation rate of solvent and the viscous polymer dissolution are balanced by using blended solvents (Lambourne and Strivens, 1999). Furthermore, a good combination of the blended solvents is important because the solvents must dissolve all components in one system (Sørensen et al., 2009). Various solvents such as aliphatic and aromatic hydrocarbons (e.g. xylene and toluene), glycol esters and glycol ether, and alcohols have been used for the solvent-borne coating system (Kopeliovich, 2012; Sharmin et al., 2015; Sørensen et al., 2009). Including paints application, a solvent is contained up to 80 % of solid components (Kopeliovich, 2014). However, most of the solvents cause the environment concerns and health risks because of the volatile property at normal ambient conditions (Chang and Lu, 2013; Cheng et al., 2013b). The central nervous system of human body can be influenced by the exposure to solvent vapors, and risks of fire and explosion hazardous are increased in manufacturing process and storing chemicals (Sørensen et al., 2009). Therefore, a demand of more environment-friendly coating manufacturing has been increased to substitute for solvent-borne coatings (Weiss, 1997). In Europe, many solvent-borne coatings at market place have been banned by Europe legislations, which allow 300g/L of maximum solvent contents in coatings or paints. Consequently, other coatings such as water-borne, high solids coatings, and radiation curable coatings have been focused due to the less or non-solvent contents in the systems (Sharmin et al., 2015).

Nevertheless, the less or non-solvent based coating methods are less efficient for large-scale industry in comparison with conventional solvent-borne coatings (Johansson and Johansson, 2007). Therefore, several efforts for innovations of solvent-borne coatings have been studied to reduce the solvent contents using reactive diluents or low viscous polymer binders (Cheng et al., 2013b; Cheng et al., 2014; Johansson and Johansson, 2007; Ohlsson et al., 2012). In order to reduce the solvent contents in solvent-borne coatings maintained with other coating properties, compact hyper-branched polymers have been researched as a low viscous polymer binders or additives for alkyd resins due to the large number of functional sites with low viscosity (Cheng et al., 2013a; Cheng et al., 2013b; Cheng et al., 2014). Katarina and her co-workers have researched on fatty acid methyl esters from rapeseed oil as reactive diluents for solvent-borne coatings on metal coils (Johansson and Johansson, 2007; Johansson and Johansson, 2008; Ohlsson et al., 2012). The advantage of the fatty acid-based reactive diluents was high curing rate at high temperature due to the non-volatile characteristic of fatty acid-derivatives. However, those researches still used solvents and/or heats during the curing process.

### **2.2.2. Water-borne system**

Water-borne coating system is defined when water is used as primary solvent (80-100 % of total solvent), and they are specifically distinguished by polymer's solubility in water: water solution, water dispersion (colloidal) and emulsion (latex) (Sharmin et al., 2015). Generally, coating materials such as epoxy, acryl, urethanes, and alkyd resins are not easy to be soluble in water (Sørensen et al., 2009). Therefore, the water dispersion type has been mostly used for water-borne coatings (Sørensen et al., 2009). To produce water dispersion coating materials, hydrophilic groups are modified in the monomers, or dispersion agents are added into the coating ingredients (Sharmin et al., 2015). Compared to solvent-borne coating, the water-borne coatings clearly



exhibit environmental benefits of reduced volatile organic compounds emission and air pollutants (Chang and Lu, 2012). However, high performance engineering coatings were still based on the solvent-borne method while water-borne coatings were extensively used for building and home applications (Kiil, 2006). In addition, hydrophobic monomers such as triglycerides are hard to be used to water-borne coating due to the low water solubility (Sharmin et al., 2015). Biocides also must be needed in the water-borne coating formulations to impede the growths of bacterial and fungi (Sørensen et al., 2009).

Despite the water-borne coatings still need the technical challenges, this method has been strongly supported by economic pressure not only environmental regulation due to the higher costs of solvents in comparison with “cheap” water (Athawale and Nimbalkar, 2011). Water-borne coatings have been seriously considered as alternatives even though they have clear drawbacks (Broek, 1993). Therefore, efforts to improve the performance of water-borne coatings are also needed to achieve the similar properties of solvent-borne coatings for engineering applications such as automotive and aerospace products (Piçarra et al., 2014). In order to improve the performances of the water-borne coating, additions of inorganic nanoparticles and reactive agents have been widely studied (Dhoke et al., 2009; Keddie, 1997; A. Zhu et al., 2008).

### **2.2.3. UV-curable coating systems**

UV-curing is a widely used coating technique in industries for many materials including woods due to the low energy consumption, quick polymerization rate, selective curing area, less or non-VOC emission (Bongiovanni et al., 2002). In addition, UV-cured polymers generally show high chemical resistance because of the high cross-link density (Landry et al., 2008). Thermally sensitive materials can be also coated by UV-curing method because the radiation process is performed at normal temperature (Sharmin et al., 2015). From the advantages of photo-cured

polymers, the technique has been also extensively used for paints, printing inks, adhesives, composites, and dental resins (Andrzejewska, 2001). Since the UV-curing coating technology was firstly used in wood flooring industries in 1980s, 84 % of wood flooring market was conducted by the radiation curing method in 2005 due to the excellent processing benefits (Landry et al., 2010). The photo-polymerization is achieved at photosensitive functional groups such as vinyl or epoxides by free radical or cationic initiation under UV or visible light. Therefore, photo-curable coating materials are monomers or oligomers before they are cured as coatings on the target surface. Generally, three major components are formulated in the UV-curable coating resins: oligomers/monomers (e.g. acrylates, epoxies, and unsaturated polyesters), reactive diluents, and photo initiator (Sharmin et al., 2015). The oligomers have photosensitive reactive groups that can be polymerized under UV with initiators. The reactive diluents reduce the viscosity of the resins and take part into the polymer via co-polymerization with the oligomers (X. Wang and Soucek, 2013). In order to achieve the synergetic advantages, water-borne and UV-curing technologies have been combined to produce water-borne UV-curable polyurethane acrylates coatings (C. Y. Bai et al., 2006; C. Bai et al., 2007; Y. Zhang et al., 2011). Compared to traditional UV-curable coating, the waterborne UV-curable coating shows several advantages such as availability of using high molecular weight polymers, less viscosity, less odor, and an ease of the cleaning process after curing (Chang and Lu, 2013). However, drawbacks are limited to small size and simple shapes (Chang and Lu, 2013).

#### **2.2.4. Wood coating applications**

Since human started using tools, wood has been used as an important raw material for many different applications and reasons. Wood is abundant, economical, varied species, and attractive appearances (Nikolic et al., 2015). The natural material has been still focused as a green and

sustainable material in comparison with concrete, gypsum board, and fossil fuels-based synthetic materials for building, house, and furniture applications because of concerns of the environment and health risks (Lozhechnikova et al., 2017). Besides the issue of renewable material, wood is one of the important materials in construction because of high mechanical strength with relatively low weight, thermal insulation, humidity buffering properties, and some durability (Lozhechnikova et al., 2017; Nikolic et al., 2015). However, wood is easily harmed by high humidity, heat, chemical activity, and biological attacks (Graziola et al., 2012). Hydrophilic nature of wood can lead several practical problems, which influence the self-life of the materials (Lozhechnikova et al., 2017). Water into wood generates mechanical stress from the swelling-shrinkage cycle of the biomaterial matrix that causes changes in shapes such as twisting (Lozhechnikova et al., 2017) and mechanical deformation such as cracks and dinge (Xie et al., 2006). The damaged wood surfaces are also easily exposed to biological attacks such as insects and fungi (Eaton and Hale, 1993). Furthermore, the humid condition in the wood can accelerate the biological activity of microorganisms such as bacteria and fungi (Bussjaeger et al., 1999). The chemical components of wood such as lignin and aromatic polymer matrix are very susceptible to photo-degradation (Kalnins, 1966). Therefore, UV light directly degrades the wood surface, and the degradation causes the surface erosion (Xie et al., 2006). The weathering factors also cause roughness on surfaces, reduction of gloss, and discoloration (Xie et al., 2005). In order to protect the wood surface, the wood can be chemically modified to reduce the water absorption and swelling-shrinkage, and to prevent photo-degradation and biological attack (P. Evans et al., 2002; Navi and Girardet, 2000). The direct chemical modification on wood surface includes copper-chromium-arsenic preservatives (Xie et al., 2006), acid chlorides and anhydrides (Hill, 2007), and benzoyl chloride (P. Evans et al., 2002), etc. However, the chemical modification on the surface

is not an appropriate method to provide mechanical and optical performance characteristics such as hardness, scratch and impact resistance, and gloss.

Coating is covering a target surface with other polymeric materials, and it is the one of the powerful and popular techniques to enhance the surface properties of wood materials (Chang and Lu, 2012; Xie et al., 2006). Lifetime of wood products can be improved by guarding the wood substrates from light, moisture, mechanical damage, chemicals, and biological activities (Nikolic et al., 2015). Coating materials also enhance beauty of the wood surface via enhancing color and gloss (Wiemann, 2010). In addition, special functionalities such as UV-protect and fire retardant can be applied to coating for value added wood products (Chang and Lu, 2012; P. D. Evans et al., 2015).

## 2.2.5. References

- Andrzejewska, E. (2001). Photopolymerization kinetics of multifunctional monomers. *Progress in Polymer Science*, 26: 605-665.
- Athawale, V. D., and Nimbalkar, R. V. (2011). Waterborne coatings based on renewable oil resources: An overview. *Journal of the American Oil Chemists' Society*, 88: 159-185.
- Bai, C. Y., Zhang, X. Y., Dai, J. B., and Li, W. H. (2006). A new UV curable waterborne polyurethane: Effect of C C content on the film properties. *Progress in Organic Coatings*, 55: 291-295.
- Bai, C., Zhang, X., and Dai, J. (2007). Synthesis and characterization of PDMS modified UV-curable waterborne polyurethane dispersions for soft tact layers. *Progress in Organic Coatings*, 60: 63-68.
- Bongiovanni, R., Montefusco, F., Priola, A., Macchioni, N., Lazzeri, S., Sozzi, L., and Ameduri, B. (2002). High performance UV-cured coatings for wood protection. *Progress in Organic Coatings*, 45: 359-363.
- Broek, A. D. (1993). Environment-friendly paints: Their technical (im) possibilities. *Progress in Organic Coatings*, 22: 55-68.
- Bussjaeger, S., Daisey, G., Simmons, R., Spindel, S., and Williams, S. (1999). Mildew and mildew control for wood surfaces. *Journal of Coatings Technology*, 71: 67-69.
- Chang, C., and Lu, K. (2012). Natural castor oil based 2-package waterborne polyurethane wood coatings. *Progress in Organic Coatings*, 75: 435-443.
- Chang, C., and Lu, K. (2013). Linseed-oil-based waterborne UV/air dual-cured wood coatings. *Progress in Organic Coatings*, 76: 1024-1031.
- Cheng, G., Greenland, B. W., Lampard, C., Williams, N., Bahra, M. S., and Hayes, W. (2013a). Lightly branched comb polyesters: Application in fast drying solvent-borne coating formulations. *Reactive and Functional Polymers*, 73: 619-623.
- Cheng, G., Greenland, B. W., Lampard, C., Williams, N., Bahra, M. S., and Hayes, W. (2013b). Synthesis of novel hyperbranched polymers featuring oxazoline linear units and their application in fast-drying solvent-borne coating formulations. *Journal of Polymer Science Part A: Polymer Chemistry*, 51: 3964-3974.
- Cheng, G., Greenland, B. W., Lampard, C., Williams, N., Bahra, M. S., and Hayes, W. (2014). Hyperbranched polymers containing oxazoline monomers and succinic anhydride: Applications in fast drying, low solvent coating formulations. *Progress in Organic Coatings*, 77: 1516-1522.
- Dhoke, S. K., Khanna, A., and Sinha, T. J. M. (2009). Effect of nano-ZnO particles on the corrosion behavior of alkyd-based waterborne coatings. *Progress in Organic Coatings*, 64: 371-382.
- Eaton, R. A., and Hale, M. D. (1993). *Wood: Decay, pests and protection*. Chapman and Hall Ltd.

- Evans, P., Owen, N., Schmid, S., and Webster, R. (2002). Weathering and photostability of benzoylated wood. *Polymer Degradation and Stability*, 76: 291-303.
- Evans, P. D., Haase, J. G., Seman, A. S., and Kiguchi, M. (2015). The search for durable exterior clear coatings for wood. *Coatings*, 5: 830-864.
- Graziola, F., Girardi, F., Di Maggio, R., Callone, E., Miorin, E., Negri, M., Müller, K., and Gross, S. (2012). Three-components organic–inorganic hybrid materials as protective coatings for wood: Optimisation, synthesis, and characterisation. *Progress in Organic Coatings*, 74: 479-490.
- Hill, C. A. (2007). *Wood modification: Chemical, thermal and other processes* John Wiley & Sons.
- Johansson, K., and Johansson, M. (2007). The effect of fatty acid methyl esters on the curing performance and final properties of thermally cured solvent-borne coil coatings. *Progress in Organic Coatings*, 59: 146-151.
- Johansson, K., and Johansson, M. (2008). Fatty acid methyl ester as reactive diluent in thermally cured solvent-borne coil-coatings—The effect of fatty acid pattern on the curing performance and final properties. *Progress in Organic Coatings*, 63: 155-159.
- Kalnins, M. (1966). Surface characteristics of wood as they affect durability of finishes. part II. photochemical degradation of wood. *US Forest Service Research Paper FPL*, 57: 23-61.
- Keddie, J. L. (1997). Film formation of latex. *Materials Science and Engineering: R: Reports*, 21: 101-170.
- Kiil, S. (2006). Drying of latex films and coatings: Reconsidering the fundamental mechanisms. *Progress in Organic Coatings*, 57: 236-250.
- Kopeliovich, D. (2012). Hydrocarbon solvents. Retrieved from [http://www.substech.com/dokuwiki/doku.php?id=hydrocarbon\\_solvents](http://www.substech.com/dokuwiki/doku.php?id=hydrocarbon_solvents)
- Kopeliovich, D. (2014). Solvent-borne paints. Retrieved from [http://www.substech.com/dokuwiki/doku.php?id=solvent-borne\\_paints](http://www.substech.com/dokuwiki/doku.php?id=solvent-borne_paints)
- Lambourne, R., and Strivens, T. (1999). *Paint and surface coatings: Theory and practice* Elsevier.
- Landry, V., Blanchet, P., and Riedl, B. (2010). Mechanical and optical properties of clay-based nanocomposites coatings for wood flooring. *Progress in Organic Coatings*, 67: 381-388.
- Landry, V., Riedl, B., and Blanchet, P. (2008). Nanoclay dispersion effects on UV coatings curing. *Progress in Organic Coatings*, 62: 400-408.
- Lozhechnikova, A., Bellanger, H., Michen, B., Burgert, I., and Österberg, M. (2017). Surfactant-free carnauba wax dispersion and its use for layer-by-layer assembled protective surface coatings on wood. *Applied Surface Science*, 396: 1273-1281.
- Navi, P., and Girardet, F. (2000). Effects of thermo-hydro-mechanical treatment on the structure and properties of wood. *Holzforschung*, 54: 287-293.
- Nikolic, M., Lawther, J. M., and Sanadi, A. R. (2015). Use of nanofillers in wood coatings: A scientific review. *Journal of Coatings Technology and Research*, 12: 445-461.

- Ohlsson, K., Bergman, T., Sundell, P., Deltin, T., Tran, I., Svensson, M., and Johansson, M. (2012). Novel coil coating systems using fatty acid based reactive diluents. *Progress in Organic Coatings*, 73: 291-293.
- Piçarra, S., Fidalgo, A., Fedorov, A., Martinho, J. M., and Farinha, J. P. S. (2014). Smart polymer nanoparticles for high-performance water-borne coatings. *Langmuir*, 30: 12345-12353.
- Sharmin, E., Zafar, F., Akram, D., Alam, M., and Ahmad, S. (2015). Recent advances in vegetable oils based environment friendly coatings: A review. *Industrial Crops and Products*, 76: 215-229.
- Sørensen, P. A., Kiil, S., Dam-Johansen, K., and Weinell, C. (2009). Anticorrosive coatings: A review. *Journal of Coatings Technology and Research*, 6: 135-176.
- Wang, X., and Soucek, M. D. (2013). Investigation of non-isocyanate urethane dimethacrylate reactive diluents for UV-curable polyurethane coatings. *Progress in Organic Coatings*, 76: 1057-1067.
- Weiss, K. D. (1997). Paint and coatings: A mature industry in transition. *Progress in Polymer Science*, 22: 203-245.
- Wiemann, M. C. (2010). Characteristics and availability of commercially important woods. *Wood Handbook. Gen Tech Rep FPL-GTR-190. US Dep. Agric. for. Serv., for. Prod. Lab, Madison, WI*, : 44.
- Xie, Y., Krause, A., Mai, C., Miltz, H., Richter, K., Urban, K., and Evans, P. (2005). Weathering of wood modified with the N-methylol compound 1, 3-dimethylol-4, 5-dihydroxyethyleneurea. *Polymer Degradation and Stability*, 89: 189-199.
- Xie, Y., Krause, A., Miltz, H., and Mai, C. (2006). Coating performance of finishes on wood modified with an N-methylol compound. *Progress in Organic Coatings*, 57: 291-300.
- Zhang, Y., Asif, A., and Shi, W. (2011). Highly branched polyurethane acrylates and their waterborne UV curing coating. *Progress in Organic Coatings*, 71: 295-301.
- Zhu, A., Cai, A., Yu, Z., and Zhou, W. (2008). Film characterization of poly (styrene-butylacrylate-acrylic acid)-silica nanocomposite. *Journal of Colloid and Interface Science*, 322: 51-58.

## **2.3. Acrylate resins**

Acrylates such as epoxy acrylate, polyester acrylate, and urethane acrylates are typically used as major oligomers for free-radical UV curing resins due to their relative high reactivity and low volatility (B. Lee and Kim, 2006; Sharmin et al., 2015). UV-polymerization is strongly influenced by various conditions such as the number of acrylic functional groups, monomer structures, temperature, irradiation intensity and rate, and photoinitiator type (Andrzejewska, 2001). Photoinitiator were previously mentioned as the major component of UV-curable acrylates resins. To obtain high crosslinked polymer matrix, suitable photoinitiator should be selected (Andrzejewska, 2001). Therefore, this chapter introduces the basic free-radical polymerization principle and general type of acrylates.

### **2.3.1. Free-radical polymerization**

Free-radical polymerization has been one of the most important polymerization method in synthetic polymer industries since 1980s: over 40 % of global synthetic plastics and rubbers were manufactured by the free-radical polymerization process (Braun, 2010; Matyjaszewski and Davis, 2003). Acrylic compounds (contain acrylic or methacrylic groups) (Figure 2.2) are the extremely used photo-curable materials using free-radical polymerization due to the high reactivity of the acrylic functional groups (Andrzejewska, 2001). The acrylic materials become polymers through the three steps of the radical polymerization including initiation, propagation, and termination or/and chain-transfer. Free-radical intermediates are generated from photoinitiator under irradiation with appropriate wavelengths at the initiation step, and the radical from the initiator reacts with the vinyl group end of the acrylic monomer to form the initiated radical monomer (Figure 2.3) (Andrzejewska, 2001; Fairbanks et al., 2009). Then, the initiated monomer attacks the



other monomer, called propagation step. The chain length of polymer is increased by propagating of radical monomers.

The propagation of the polymerization is terminated when un-polymerized monomers or radical monomers are trapped in the polymerized matrix (Harikrishna et al., 2014). In addition, oxygen in atmosphere can react with the radicals, which is called oxygen inhibition (Andrzejewska, 2001; Braun, 2010). The oxygen inhibition significantly impedes the polymerization, and it can influence the conversion rate of the polymerization that is related to properties of the polymer (Andrzejewska, 2001; C. Y. Bai et al., 2006). The oxygen inhibition of acrylic group is more susceptible than that of methacrylate (Kloosterboer et al., 1989). The difference oxygen susceptibilities between acrylate and methacrylate may be caused by the stability of the radicals: the radical on secondary carbon of the acrylic group is less stable and higher reactive than the radical on tertiary carbon of the methacrylic group.

Generally, two types of photoinitiators (type I and II) for the radical polymerization are used, and they are described below (Figure 2.4) (Andrzejewska, 2001). Type I (e.g. Darocur 1173 and Irgacure 184) exhibits fast curing speed and high conversion rate under UV because the cleavage process at the initiation step is highly efficient (Andrzejewska, 2001; Mahendran et al., 2012). After the generation of the radicals from type I initiator, the benzoyl radical is the main initiating radicals to react with acrylates monomers (Andrzejewska, 2001). Otherwise, type II (e.g. benzophenone) needs hydrogen donors such as amines, ethers, and alcohols (RH in Figure 2.4) to form the ketyl radical and produce the active radical from the hydrogen donor. The ketyl radical is inactive, but the hydrogen donor radical ( $R^*$  in Figure 2.4) reacts with acrylate monomers for polymerization (Andrzejewska, 2001). Therefore, curing speed and double bond conversion rate of polymerization with type II initiator are slower than those of type I initiator due to its more steps

in the radical generation mechanism (Mahendran et al., 2012). In addition, the degree of polymerization or the crosslink density of the polymerization will be lower than those of the polymerization using type I initiator due to the higher oxygen susceptibility of the type II initiators (Oytun et al., 2013). Oxygen can react with radicals to produce peroxy radicals, which can reduce the speed of initiation and propagation steps or lead the early termination step due to the low reactivity of peroxy radicals, and type II initiator is more rapidly reacted with oxygen than type I initiator (Feng and Suh, 2009; Young and Lovell, 2011). In addition, the peroxy radicals can lead low shelf-life of the polymer product due to the easy bond scission of O-O- during using if they are included in the polymer matrix (Young and Lovell, 2011). Therefore, the oxygen inhibition phenomena is the most challenging problem of free radical polymerization technique, and several efforts to reduce the oxygen inhibition have been studied using additions of oxygen scavengers, additional active radicals, or reactive photoinitiators, and processing under inert atmosphere (Balta et al., 2007; Belon et al., 2010; Lalevée et al., 2012; Studer et al., 2003). Even though the major drawbacks of free-radical polymerization have been addressed, free-radical polymerization is one of the widely used techniques in polymer industry. Moreover, a high viscosity multifunctional acrylate typically shows lower double bond conversion than a low viscosity less functional acrylate shows because the high initial viscosity of the acrylate impedes the reaction diffusion (Anseth et al., 1994).

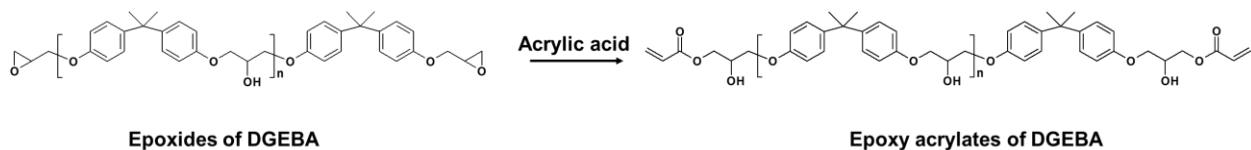


**Figure 2.2: a) acrylic and b) methacrylic groups.**

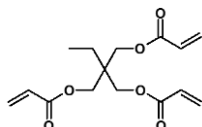


the chemical structure of polymers, crosslink density, and addition of crosslinkers (Chattopadhyay et al., 2005; Mohtadizadeh et al., 2015; Schwalm et al., 1997). From the results of Mohtadizadeh's works, the tetra-functional epoxy acrylate showed twice higher viscosity than that of the bi-functional epoxy acrylate. However, tensile strength, thermal decomposition temperature, glass transition temperature, and crosslink density were enhanced as the number of functional groups increased.

Trimethylolpropane triacrylate (TMPTA) (Figure 2.6) was used as a crosslinker to improve thermal and mechanical properties of epoxy novolac-based, and DGEBA-based acrylates and methacrylates by enhancements of crosslink densities (Chattopadhyay et al., 2005). The epoxy novolac-based acrylate showed seven times higher crosslink density with the 10 % TMPTA addition than that of the resin with 5 % of TMPTA addition, and the crosslink densities of DGEBA-based acrylate and methacrylate were improved more than twice while the TMPTA addition were increased from 5 % to 10 % of the total resins. Consequently, all acrylates and methacrylates of the research showed increases in mechanical strengths and glass transition temperatures. Similarly, A DGEBA-based acrylate was blended with combinations of multi-functional acrylates as crosslinker such as TMPTA, tripropylene glycol diacrylate (TPGDA), and 1,6-hexanedioldiacrylate (HDDA) (Kardar et al., 2009). In the results, higher TMPTA contents led the higher hardness, scratch strength, and glass transition temperatures. Fluorine modified DGEBA-based acrylates also showed excellent chemical resistances against hydrogen chloride and chloroform, but the high cost of fluorine materials was a problem, which should be solved for large-scale wood coating production (Bongiovanni et al., 2002).



**Figure 2.5: Typical bisphenol-A-based acrylate synthesis from epoxides of DGEBA (Mohtadizadeh et al., 2015).**



**Figure 2.6: Chemical structure of TMPTA.**

### 2.3.3. Polyurethane acrylates

Versatile properties of polyurethane can be achieved from the various hard and soft segments combinations; thus, polyurethanes have been widely used in many manufacturing industry (S. Lee et al., 2001). Polyurethane has been extensively used for many applications such as foams, cushion, rubber goods, synthetic leather, adhesives, paints, and fibers due to the ease of controlling the flexibility and the rigidity of the plastics (Guelcher, 2008; Tokiwa et al., 2009). In order to improve the performance of polyurethanes, acrylated polyurethanes were synthesized to add the benefits of polyacrylate such as good weather and water proofs into polyurethanes (Çanak and Serhatlı, 2013). Particularly, polyurethane acrylates have been widely used as oligomers/monomers for coating materials to provide toughness, abrasion resistance, and flexibility (Nabeth et al., 1996). Therefore, a lot of researches in UV-curable polyurethane acrylates have been performed to study various fields such as nanoparticles, water-borne application, UV-curing behavior, functional structure development, using reactive diluents, optimize formulation, etc. (Bao and Shi, 2010; Çanak and Serhatlı, 2013; Harikrishna et al., 2014; Nabeth et al., 1996; Patil et al., 2017; Pichavant and

Coqueret, 2008; Tathe and Jagtap, 2015; Tey et al., 2006; Um et al., 2016; F. Wang et al., 2008; Ye et al., 2016; Q. Zhang et al., 2016; Y. Zhang et al., 2011). Polyurethane acrylate resins are generally synthesized by the reaction of cyanate end groups (OCN-) of polyurethanes with hydroxyl acrylates such as 2-hydroxyethyl acrylate or 2-hydroxyethyl methacrylate (F. Wang et al., 2008).

Hyper-branched polyurethane acrylates were prepared for water-borne UV-curable coating, and improve hardness and solvent resistance were successfully enhanced by increases in acryl functionality in the polymer (Y. Zhang et al., 2011). From Bao and Shi, hyper-branched polyurethane acrylates were also prepared as an additive for commercial epoxy acrylate to merge the benefits of polyurethane acrylates and epoxy acrylates (Bao and Shi, 2010). The increases in the hyper-branched polyurethane acrylate additions definitely increased the acryl functionalities in the polymer blends, but the double bond conversions in cured polymers and tensile strengths were increased then further decreased as the hyper-branched polyurethane acrylate contents increased from 5 % to 30 % of the polymers. However, impact strengths and elongations were improved as the hyper-branched polyurethane acrylate contents increased.

#### **2.3.4. Plant oil-based acrylates**

The major groups of acrylates such as bisphenol-A-based and polyurethane-based are mostly derived from fossil fuels. Therefore, academia and industry have been seeking sustainable alternatives to the petroleum-based materials (Crivello and Narayan, 1992). Vegetable oils are significant resources as bio-based raw materials in coating industry due to the abundancy and the various chemical transformation ability (Sharmin et al., 2015). Soybean oil is one of the most applicable plant oils for bio-polymer applications because of the large composition of unsaturated fatty acids with inexpensive and easily available crops (Z. Petrovic, 2008; Williams and Hillmyer,

2008). Acrylated epoxidized soybean oil (AESO) is a typical type of soybean oil-based epoxy acrylates, and AESO is generally prepared by the ring-opening reaction of epoxides of epoxidized soybean oil (ESO) with acrylic acids (Campanella et al., 2011; Habib and Bajpai, 2011; J. La Scala and Wool, 2013). The most of commercial AESO products have been produced by the chemical pathway and formed acrylic esters on fatty chains, but the acrylic esters can lead high viscosity due to the intermolecular force among the esters of acrylic groups and triglycerides (Rengasamy and Mannari, 2013). Therefore, Regasamy and Mannari developed a new acrylate synthesis using 2-hydroxyethyl acrylate (HEA): the epoxides of ESO were reacted with the hydroxyl groups of HEA, and produced acryl ethers showed lower viscosity than commercial AESO (Rengasamy and Mannari, 2013). Zhang and co-workers directly prepared acrylate soybean oil (ASO) using a one-step reaction by the addition reaction of double bonds of soybean oil directly with acrylic acids (P. Zhang et al., 2013). However, the ASO did not contain hydroxyl groups because the acrylate directly modified on the double bond. The hydroxyl groups of epoxy acrylates provide polarity to the resins, which can enhance the wettability and the adhesiveness (Oprea et al., 2000). Therefore, the ASO may not be a good backbone material for coating polymers.

In comparison with soybean oil, linseed oil or camelina oil have a structural benefit from the higher degree of unsaturation on the fatty chains. Soybean oil fatty acids contains mostly oleic and linoleic acids (~80 % of total fatty acids), but camelina oil and linseed oil fatty acids are composed of 37 % and 51-55 % of linolenic acids, respectively (N. Kim et al., 2015; Vereshchagin and Novitskaya, 1965). Therefore, several researchers studied acrylates applications derived from camelina and linseed oils (Y. Li and Sun, 2015a; Mahendran et al., 2012). In addition, jatropha and palm oil has been researched as raw materials for epoxy and acrylate resin, polyurethane, and adhesives because the crops were produced for biodiesel in inexpensive prices (Aung et al., 2015).

Triglyceride-based polymer shows differences of properties in depending on the varied fatty acids, but they similarly show relatively low mechanical and thermal properties due to the long aliphatic chains, as compared to typical petrochemical-based polymers.

A bio-based acrylate monomer derived from itaconic acid was synthesized as a crosslink agent into AESO to enhance the coating performance and mechanical strength (Dai et al., 2016). Itaconic acid is a biochemical product of *Aspergillus terreus* from carbohydrate sources such as sugar, and it was ranked at top 12 of valuable bio-based chemicals from U.S department of Energy at 2004 (Pfeifer et al., 1952; Werpy et al., 2004). The itaconic acid-based crosslink agent (IG) was prepared by the ring-opening reaction of glycidyl methacrylate with itaconic acid, and AESO/IG copolymer showed higher tensile strength, lower elongation, and better coating performances such solvent resistance, pencil hardness, and adhesion strength, as compared to neat AESO polymer. In addition, little amounts of hydroxyethyl methacrylatephosphate (HMP) (2-4 % of total materials) was successfully added into AESO/IG copolymer as a co-crosslink agent to obtain the highest mechanical strength and coating performances. Itaconic acid was also used to synthesize bio-based UV-curable polyurethane acrylates for coating applications (Patil et al., 2017).

Even though soybean oil based resins are considered as a promising sustainable material, the low mechanical strength and glass transition temperatures of the resins are not sufficient for structural applications (Zhan and Wool, 2010). Thus, other plant oils such as cardanol or aromatic molecules such as vanillin acids have been extensively studied (C. Zhang et al., 2015; C. Zhang, Yan et al., 2015). Cardanol is a major component of cashew nutshell liquid, and it has been attractive bio-materials for a wide range of applications due to the unique chemical properties (Quirino et al., 2014). Cardanol is one of the unique aromatic structured lipids in nature (Lochab et al., 2014). The reactive hydroxyl groups of the phenol and the unsaturated aliphatic chains, as



shown in Figure 2.7, allow excellent functional flexibility (Balachandran et al., 2013). Therefore, many researchers have extensively studied cardanol as a raw material for epoxy and acrylate resins, polyurethane, flame retardants, antioxidants, and plasticizer, etc. Choi and co-workers developed antibacterial acrylate coatings using the co-polymerization of cardanylpropyl methacrylate (methacrylate modified on the phenol of cardanol) with methyl methacrylates (MMA) (Y. Choi et al., 2014). Liu's group prepared multi-armed acrylate oligomers from cardanol derivatives (R. Liu et al., 2015). Various bio-based polyols such as glycerol, xylitol, triglycerol, and sucrose were used as bodies, which were connected with the phenol group of cardanol. Then, the unsaturated aliphatic chains of the cardanol were modified as epoxy acrylates. All of the multi-armed acrylates coatings exhibited enhanced tensile strengths and elongations, adhesion, and hardness in comparison with AESO (R. Liu et al., 2015). However, the multi-armed acrylates showed over twenty times larger viscosities than that of AESO. Also, Liu and coworkers designed a high acrylate contents oligomer for a UV-curable application using cardanol derivatives and shell-type polyols, which contains sixteen hydroxyl groups on a molecule (R. Liu, Zhu et al., 2015). The cardanol derivatives were modified to the polyols, and the structure of the acrylate oligomer shaped a big shell containing branched long acrylic alkyl chains. The bio-based acrylate was compared to a commercial hyper-branched acrylate from petrochemicals, and it showed better surface mechanical properties such as indentation hardness and surface storage modulus (R. Liu et al., 2015).



**Figure 2.7: Chemical structure of cardanol.**

### 2.3.5. References

- Andrzejewska, E. (2001). Photopolymerization kinetics of multifunctional monomers. *Progress in Polymer Science*, 26: 605-665.
- Anseth, K. S., Wang, C. M., and Bowman, C. N. (1994). Reaction behaviour and kinetic constants for photopolymerizations of multi (meth) acrylate monomers. *Polymer*, 35: 3243-3250.
- Aung, M. M., Yaakob, Z., Abdullah, L. C., Rayung, M., and Li, W. J. (2015). A comparative study of acrylate oligomer on jatropha and palm oil-based UV-curable surface coating. *Industrial Crops and Products*, 77: 1047-1052.
- Bai, C. Y., Zhang, X. Y., Dai, J. B., and Li, W. H. (2006). A new UV curable waterborne polyurethane: Effect of C C content on the film properties. *Progress in Organic Coatings*, 55: 291-295.
- Balachandran, V. S., Jadhav, S. R., Vemula, P. K., and John, G. (2013). Recent advances in cardanol chemistry in a nutshell: From a nut to nanomaterials. *Chemical Society Reviews*, 42: 427-438.
- Balta, D. K., Arsu, N., Yagci, Y., Jockusch, S., and Turro, N. J. (2007). Thioxanthone-anthracene: A new photoinitiator for free radical polymerization in the presence of oxygen. *Macromolecules*, 40: 4138-4141.
- Bao, F., and Shi, W. (2010). Synthesis and properties of hyperbranched polyurethane acrylate used for UV curing coatings. *Progress in Organic Coatings*, 68: 334-339.
- Belon, C., Allonas, X., Croutxé-barghorn, C., and Lalevée, J. (2010). Overcoming the oxygen inhibition in the photopolymerization of acrylates: A study of the beneficial effect of triphenylphosphine. *Journal of Polymer Science Part A: Polymer Chemistry*, 48: 2462-2469.
- Bongiovanni, R., Montefusco, F., Priola, A., Macchioni, N., Lazzeri, S., Sozzi, L., and Ameduri, B. (2002). High performance UV-cured coatings for wood protection. *Progress in Organic Coatings*, 45: 359-363.
- Braun, D. (2010). Origins and development of initiation of free radical polymerization processes. *International Journal of Polymer Science*, 2009
- Campanella, A., Scala, J. J. L., and Wool, R. (2011). Fatty acid-based comonomers as styrene replacements in soybean and castor oil-based thermosetting polymers. *Journal of Applied Polymer Science*, 119: 1000-1010.
- Çanak, T. Ç, and Serhatlı, İ E. (2013). Synthesis of fluorinated urethane acrylate based UV-curable coatings. *Progress in Organic Coatings*, 76: 388-399.
- Chattopadhyay, D., Panda, S. S., and Raju, K. (2005). Thermal and mechanical properties of epoxy acrylate/methacrylates UV cured coatings. *Progress in Organic Coatings*, 54: 10-19.
- Choi, Y., Kim, K., Kim, D., Kim, H. J., Cha, S., and Lee, J. (2014). Synthesis and characterization of self-cross-linkable and bactericidal methacrylate polymers having renewable cardanol moieties for surface coating applications. *RSC Advances*, 4: 41195-41203.

- Crivello, J. V., and Narayan, R. (1992). Epoxidized triglycerides as renewable monomers in photoinitiated cationic polymerization. *Chemistry of Materials*, 4: 692-699.  
doi:10.1021/cm00021a036
- Dai, J., Liu, X., Ma, S., Wang, J., Shen, X., You, S., and Zhu, J. (2016). Soybean oil-based UV-curable coatings strengthened by crosslink agent derived from itaconic acid together with 2-hydroxyethyl methacrylate phosphate. *Progress in Organic Coatings*, 97: 210-215.
- Fairbanks, B. D., Schwartz, M. P., Bowman, C. N., and Anseth, K. S. (2009). Photoinitiated polymerization of PEG-diacrylate with lithium phenyl-2, 4, 6-trimethylbenzoylphosphinate: Polymerization rate and cytocompatibility. *Biomaterials*, 30: 6702-6707.
- Feng, L., and Suh, B. I. (2009). Acrylic resins resisting oxygen inhibition during free-radical photocuring. I. formulation attributes. *Journal of Applied Polymer Science*, 112: 1565-1571.
- Guelcher, S. A. (2008). Biodegradable polyurethanes: Synthesis and applications in regenerative medicine. *Tissue Engineering Part B: Reviews*, 14: 3-17.
- Habib, F., and Bajpai, M. (2011). Synthesis and characterization of acrylated epoxidized soybean oil for UV cured coatings.
- Harikrishna, R., Ponrathnam, S., and Rajan, C. (2014). Photopolymerization kinetics of bis-aromatic based urethane acrylate macromonomers in the presence of reactive diluent. *Progress in Organic Coatings*, 77: 225-231.
- Kardar, P., Ebrahimi, M., Bastani, S., and Jalili, M. (2009). Using mixture experimental design to study the effect of multifunctional acrylate monomers on UV cured epoxy acrylate resins. *Progress in Organic Coatings*, 64: 74-80.
- Kim, N., Li, Y., and Sun, X. S. (2015). Epoxidation of camelina sativa oil and peel adhesion properties. *Industrial Crops and Products*, 64: 1-8.
- Kloosterboer, J., Lijten, G., & Zegers, C. (1989). Formation of densely crosslinked polymer glasses by photopolymerization. Paper presented at the Abstracts of Papers of the American Chemical Society, , 197 28-PMSE.
- La Scala, J., and Wool, R. P. (2013). Fundamental thermo-mechanical property modeling of triglyceride-based thermosetting resins. *Journal of Applied Polymer Science*, 127: 1812-1826.
- Lalavée, J., Telitel, S., Tehfe, M. A., Fouassier, J. P., Curran, D. P., and Lacôte, E. (2012). N-Heterocyclic carbene boranes accelerate type I radical photopolymerizations and overcome oxygen inhibition. *Angewandte Chemie International Edition*, 51: 5958-5961.
- Lee, B., and Kim, H. (2006). Influence of isocyanate type of acrylated urethane oligomer and of additives on weathering of UV-cured films. *Polymer Degradation and Stability*, 91: 1025-1035.
- Lee, S., Yu, S., and Lee, Y. (2001). Degradable polyurethanes containing poly (butylene succinate) and poly (ethylene glycol). *Polymer Degradation and Stability*, 72: 81-87.
- Li, Y., and Sun, X. S. (2015). Camelina oil derivatives and adhesion properties. *Industrial Crops and Products*, 73: 73-80.

- Liu, R., Zhang, X., Zhu, J., Liu, X., Wang, Z., and Yan, J. (2015). UV-curable coatings from multiarmed cardanol-based acrylate oligomers. *ACS Sustainable Chemistry & Engineering*, 3: 1313-1320.
- Liu, R., Zhu, G., Li, Z., Liu, X., Chen, Z., and Ariyasivam, S. (2015). Cardanol-based oligomers with “hard core, flexible shell” structures: From synthesis to UV curing applications. *Green Chemistry*, 17: 3319-3325.
- Lochab, B., Shukla, S., and Varma, I. K. (2014). Naturally occurring phenolic sources: Monomers and polymers. *RSC Advances*, 4: 21712-21752.
- Mahendran, A. R., Wuzella, G., Aust, N., Kandelbauer, A., and Müller, U. (2012). Photocrosslinkable modified vegetable oil based resin for wood surface coating application. *Progress in Organic Coatings*, 74: 697-704.
- Matyjaszewski, K., and Davis, T. P. (2003). *Handbook of radical polymerization* John Wiley & Sons.
- Mohtadizadeh, F., Zohuriaan-Mehr, M., Hadavand, B. S., and Dehghan, A. (2015). Tetra-functional epoxy-acrylate as crosslinker for UV curable resins: Synthesis, spectral, and thermo-mechanical studies. *Progress in Organic Coatings*, 89: 231-239.
- Nabeth, B., Gerard, J., and Pascault, J. (1996). Dynamic mechanical properties of UV-curable polyurethane acrylate with various reactive diluents. *Journal of Applied Polymer Science*, 60: 2113-2123.
- Noble, B. B., and Coote, M. L. (2013). First principles modelling of free-radical polymerisation kinetics. *International Reviews in Physical Chemistry*, 32: 467-513.
- Oprea, S., Vlad, S., Stanciu, A., and Macoveanu, M. (2000). Epoxy urethane acrylate. *European Polymer Journal*, 36: 373-378.
- Oytun, F., Kahveci, M. U., and Yagci, Y. (2013). Sugar overcomes oxygen inhibition in photoinitiated free radical polymerization. *Journal of Polymer Science Part A: Polymer Chemistry*, 51: 1685-1689.
- Park, Y., Lim, D., Kim, H., Park, D., and Sung, I. (2009). UV-and thermal-curing behaviors of dual-curable adhesives based on epoxy acrylate oligomers. *International Journal of Adhesion and Adhesives*, 29: 710-717.
- Patil, D. M., Phalak, G. A., and Mhaske, S. (2017). Design and synthesis of bio-based UV curable PU acrylate resin from itaconic acid for coating applications. *Designed Monomers and Polymers*, 20: 269-282.
- Petrovic, Z. (2008). Polyurethanes from vegetable oils. *Polymer Reviews*, 48: 109-155. doi:10.1080/15583720701834224
- Pfeifer, V., Vojnovich, C., and Heger, E. (1952). Itaconic acid by fermentation with *aspergillus terreus*. *Industrial & Engineering Chemistry*, 44: 2975-2980.
- Pichavant, L., and Coqueret, X. (2008). Optimization of a UV-curable acrylate-based protective coating by experimental design. *Progress in Organic Coatings*, 63: 55-62.

- Quirino, R. L., Garrison, T. F., and Kessler, M. R. (2014). Matrices from vegetable oils, cashew nut shell liquid, and other relevant systems for biocomposite applications. *Green Chemistry*, 16: 1700-1715.
- Rengasamy, S., and Mannari, V. (2013). Development of soy-based UV-curable acrylate oligomers and study of their film properties. *Progress in Organic Coatings*, 76: 78-85. doi:10.1016/j.porgcoat.2012.08.012
- Schwalm, R., Häußling, L., Reich, W., Beck, E., Enenkel, P., and Menzel, K. (1997). Tuning the mechanical properties of UV coatings towards hard and flexible systems. *Progress in Organic Coatings*, 32: 191-196.
- Sharmin, E., Zafar, F., Akram, D., Alam, M., and Ahmad, S. (2015). Recent advances in vegetable oils based environment friendly coatings: A review. *Industrial Crops and Products*, 76: 215-229.
- Shen, L., Li, Y., Zheng, J., Lu, M., and Wu, K. (2015). Modified epoxy acrylate resin for photocurable temporary protective coatings. *Progress in Organic Coatings*, 89: 17-25.
- Studer, K., Decker, C., Beck, E., and Schwalm, R. (2003). Overcoming oxygen inhibition in UV-curing of acrylate coatings by carbon dioxide inerting, part I. *Progress in Organic Coatings*, 48: 92-100.
- Tathe, D. S., and Jagtap, R. (2015). Biobased reactive diluent for UV-curable urethane acrylate oligomers for wood coating. *Journal of Coatings Technology and Research*, 12: 187-196.
- Tey, J., Soutar, A., Mhaisalkar, S., Yu, H., and Hew, K. (2006). Mechanical properties of UV-curable polyurethane acrylate used in packaging of MEMS devices. *Thin Solid Films*, 504: 384-390.
- Tokiwa, Y., Calabia, B., Ugwu, C., and Aiba, S. (2009). Biodegradability of plastics. *International Journal of Molecular Sciences*, 10: 3722-3742. doi:10.3390/ijms10093722
- Um, M. S., Ham, D. S., Cho, S. K., Lee, S., Kim, K. J., Lee, J. H., Choa, S., Jung, H. W., and Choi, W. J. (2016). Surface mechanical properties of poly (urethane acrylate)/silica hybrid interpenetrating polymer network (IPN) coatings. *Progress in Organic Coatings*, 97: 166-174.
- Vereshchagin, A., and Novitskaya, G. V. (1965). The triglyceride composition of linseed oil. *Journal of the American Oil Chemists Society*, 42: 970-974.
- Wang, F., Hu, J., and Tu, W. (2008). Study on microstructure of UV-curable polyurethane acrylate films. *Progress in Organic Coatings*, 62: 245-250.
- Werpy, T., Petersen, G., Aden, A., Bozell, J., Holladay, J., White, J., Manheim, A., Eliot, D., Lasure, L., and Jones, S. (2004). *Top Value Added Chemicals from Biomass. Volume 1- Results of Screening for Potential Candidates from Sugars and Synthesis Gas*,
- Williams, C. K., and Hillmyer, M. A. (2008). Polymers from renewable resources: A perspective for a special issue of polymer reviews. *Polymer Reviews*, 48: 1-10. doi:10.1080/15583720701834133

- Ye, C., Lu, L., Pei, X., Hu, Y., Chen, J., and Wang, Y. (2016). Development and characterization of transparent waterborne polyurethane acrylate/fullerenols thin-film nanocomposite as thermal-insulating coating. *Polymer Science Series B*, 58: 601-609.
- Young, R. J., and Lovell, P. A. (2011). *Introduction to polymers* CRC press.
- Zhan, M., and Wool, R. P. (2010). Biobased composite resins design for electronic materials. *Journal of Applied Polymer Science*, 118: 3274-3283.
- Zhang, C., Madbouly, S. A., and Kessler, M. R. (2015). Renewable polymers prepared from vanillin and its derivatives. *Macromolecular Chemistry and Physics*, 216: 1816-1822.
- Zhang, C., Yan, M., Cochran, E. W., and Kessler, M. R. (2015). Biorenewable polymers based on acrylated epoxidized soybean oil and methacrylated vanillin. *Materials Today Communications*, 5: 18-22.
- Zhang, P., Xin, J., and Zhang, J. (2013). Effects of catalyst type and reaction parameters on one-step acrylation of soybean oil. *ACS Sustainable Chemistry & Engineering*, 2: 181-187.
- Zhang, Q., Huang, C., Wang, H., Hu, M., Li, H., and Liu, X. (2016). UV-curable coating crosslinked by a novel hyperbranched polyurethane acrylate with excellent mechanical properties and hardness. *RSC Advances*, 6: 107942-107950.
- Zhang, Y., Asif, A., and Shi, W. (2011). Highly branched polyurethane acrylates and their waterborne UV curing coating. *Progress in Organic Coatings*, 71: 295-301.

## 2.4. Bio-inspired super-hydrophobic coating surfaces

### 2.4.1. Introduction

The wettability is defined as a behavior of liquid on a surface, and it is one of the important key properties of the solid surfaces that has to be understanding to manipulate technical applications (Dorrer and Ruehe, 2009). Wettability of the solid surfaces is influence by both surface roughness and the surface energy of the materials (Nakajima et al., 1999). Surface wettability is generally classified by the water contact angle of the surface. Hydrophilic surface is defined as the water contact angle in the range of  $0^\circ \leq \theta < 90^\circ$ , and hydrophobic surface has the water contact angle in the range of  $90^\circ < \theta \leq 180^\circ$  (X. Zhang et al., 2008). Furthermore, a surface having the water contact angle between  $0^\circ$  to  $10^\circ$  is defined as a super-hydrophobic surface, and a surface wetting in the water contact angle range of  $150^\circ < \theta \leq 180^\circ$  is called as a super-hydrophobic surface and non-wetting property (Marmur, 2012; Nakajima et al., 1999). The super-hydrophobicity generally leads small sliding or tilting angle (lower than  $10^\circ$ ) because the droplets on the super-hydrophobic surface can easily move by the small gravitational force applied when the surface was tilted (X. Zhang et al., 2008).

The super-hydrophobicity of the rough lotus leaves in nature is a well-known example of self-cleaning properties, also it called as “lotus effect” (X. Zhang et al., 2008). When the surfaces are exposed by dusts or contaminants, the super-hydrophobic roughness can lead self-cleaning of the surface because adhered particles are easily removed by the rolling off droplets. Due to the super-hydrophobicity of the rough surface, self-cleaning effect has been great interested in the surfaced modified applications such as satellite dishes, solar energy panels, photovoltaics, exterior windows, heat exchanger surfaces of air conditioning systems, wall paints, medical tools, and non-soiling

clothes (Dorrer and Ruehe, 2009; M. Ma and Hill, 2006). The non-wetting surface prevents forming contaminants, ice, and fog on the surface of the above equipment (M. Ma and Hill, 2006).

The research on special wetting surfaces such as super-hydrophobic surfaces has been started when Ollivier found the water contact angle of closed  $180^\circ$  of a surface coated with soot, arsenic trioxide, and lycopodium powder in 1907 (Jiang et al., 2015). Then, stearic acid deposited galena rough surface achieved the water contact angle of  $160^\circ$  in 1923 (X. Zhang et al., 2008). Wenzel firstly described the theoretical model to understand the relationship between surface roughness and wettability of solid-liquid interface in 1936 (Wenzel, 1936), called Wenzel model. Afterward, Cassie and Baxter proposed the new model that considered for the surface wetting properties of liquid-air interfaces not only solid-liquid interfaces when air is trapped between liquid and rough solid surface in 1944 (Cassie and Baxter, 1944). These two models have been a key role to understand the surface wettability even though they have limitations to clarify the real conditions (Si and Guo, 2015). In addition, the two models clearly showed that super-hydrophobicity needs the low surface energy of materials and the high surface roughness (X. Zhang et al., 2008). Since “lotus effect” and its self-cleaning properties was studied in 1997, super-hydrophobic surfaces in nature have been actively researched by the impression from plants and animals (X. Zhang et al., 2008). Accordingly, many researchers have been effort to artificially fabricate the super-hydrophobic surfaces roughness and modify the surface materials, and potential applications have been researched by the bio-inspired super-hydrophobic surfaces. From Essential Science Indicators Database, super-hydrophobic surfaces were top 7th research in materials science and technology area from 2006 to 2010 (Si and Guo, 2015).

In this chapter, special wettable surfaces in natures and current researches on fabrication of super-hydrophobic surfaces are described.



## **2.4.2. Special wettability surfaces in nature**

### **2.4.2.1. Hierarchical surfaces**

The best example of super-hydrophobic surface is lotus leaves (M. Ma and Hill, 2006). Barthlott and Neinhuis firstly characterize the surface characteristics and self-cleaning property of lotus leaf and other plants (Barthlott and Neinhuis, 1997). They found the impressive self-cleaning ability of the lotus leaf due to the surface roughness, reduced particle adhesion, and water repellency of the unique surface, and it has been called “Lotus effect” (Barthlott and Neinhuis, 1997). The epicuticular wax is crystal structure, and they are spread on the microscale papillae of the leaves. The natural hierarchical surface, which is composed of papillae covered with epicuticular wax is likely to enhance super-hydrophobicity and self-cleaning effect (Barthlott and Neinhuis, 1997; Sun et al., 2005). Many super-hydrophobic surfaces in nature including plants, insects, and animals have hierarchical surfaces that enhance hydrophobicity (H. Guo et al., 2015). Air trapping at the second or higher level of roughness prevents water penetrating to the surface (M. Ma et al., 2008).

Water strider is a good example of hierarchical super-hydrophobic surface for standing on the water surface (Gao and Jiang, 2004). In order to obtain extreme hydrophobicity, the legs of water strider are composed of spindle-shape microscale setae and nanoscale grooved structures on the setae (Gao and Jiang, 2004). Several researches to fabricate artificial super-hydrophobic surface have been designed hierarchical surfaces (Bhushan et al., 2009; H. Guo et al., 2015; Sahoo and Kandasubramanian, 2014). Ice adhesion or freezing outdoor surfaces can be reduced or delayed using water repellency and self-cleaning of super-hydrophobic surface coatings (Yao et al., 2011).

#### ***2.4.2.2. Anisotropic surface structures***

Current technology reduces the friction of water on boats and swimsuits using bio-inspired surface structures such as shark skin, as it is called low drag property (Bixler and Bhushan, 2012; Bixler and Bhushan, 2013). The fish is clean when they are exposed to the oil-polluted water because the surface of fish scale is super-oleophobic in water while the fish scale is super-hydrophilic (M. Liu et al., 2009), and it is also self-cleaning property in the marine environment. Butterfly wing and rice leaf shows more efficient self-cleaning than other plants leave such as lotus leaf because they have also low drag property on the surface not only lotus effect property (Bixler and Bhushan, 2013). In addition, a low drag surface often leads antifouling properties: biofouling is undesirable micro- or macro-organism accumulation on surfaces (Bixler and Bhushan, 2012).

Rice leaf, butterfly wing, fish scales, and shark skin have anisotropic arranged surfaces roughness (Bhushan, 2009; Zheng et al., 2007). Rice leaf and butterfly wing surfaces have longitudinal channels (the arrow direction in the figure) that lead drag reduction. The hierarchical papillae and epicuticular waxy surface structure of rice leaf provides super-hydrophobicity and lotus effect (Bixler and Bhushan, 2013). Butter fly wings also contain longitudinal channels in the scale-like structures that leads surface roughness to drag reduction and self-cleaning properties (Bixler and Bhushan, 2013). Shark skin and fish scales lead high flow rates towards the longitudinal direction (the arrow directions) due to the anisotropic riblets on the surfaces, and the low drag properties and the surface roughness leads antifouling and self-cleaning properties in the marine environment (Bixler and Bhushan, 2013). From Bixler and Bhushan, drag reduction, self-cleaning, and antifouling surfaces are attractive for many engineering applications such as airplanes, wind turbines, ship hulls, medical devices, and pipelines.

#### ***2.4.2.3. Aligned nano-pillars and nano-pots shape surfaces***

Eyes of mosquito, and wings of dragonfly and cicada need to be dry and clean (Sun et al., 2005; Yu et al., 2015). Nanostructures of the surfaces of the wings contain aligned pillar/pots that provide super-hydrophobicity and low adhesion properties, and Cicada and dragonfly wings efficiently reduce the dust adhesion on the wing (W. Lee et al., 2004). The eyes of mosquito are composed of arranged microscale hemisphere sensory units covered with nanoscale pots (Yu et al., 2015). The aligned rough surface of the mosquito's eye provides super-hydrophobicity and anti-fogging properties (Yu et al., 2015).

#### ***2.4.2.4. Rough fibrous surfaces***

Some plants' leaves contain fibrous surfaces that enhance hydrophobicity for water repellency and self-cleaning (Miyachi et al., 2006). Silver ragwort shows the water contact angle around  $150^\circ$  due to the densely covered fibers (diameters about 6  $\mu\text{m}$ ) (Miyachi et al., 2006). The fibers of silver ragwort have also hierarchical surface on the fibers that influence the extreme hydrophobicity. The underside of Ramee leaf shows super-hydrophobicity that water contact angle is around  $164^\circ$  (Z. Guo et al., 2011). Fibers with diameter around 2  $\mu\text{m}$  leads the super-hydrophobic roughness. In addition, the fibers also have second-level hierarchical grooves that extremely increase the hydrophobicity (Z. Guo and Liu, 2007). Similarly, Chinese watermelon skin exhibit  $159^\circ$  (H. Guo et al., 2015).

### **2.4.3. Fabrication of super-hydrophobic surfaces**

Previously mentioned, super-hydrophobicity is determined with two keys parameters that are low surface energy materials and rough surface morphology. Methods for producing super-hydrophobic surfaces are generally categorized by two criteria due to steps of the fabrication: the first method is making rough surface from a low surface energy materials (one-step), and the other

method is making a rough surface, then modifying the surface with low surface energy materials (two-step) (M. Ma and Hill, 2006; X. Zhang et al., 2008). The one-step process beneficially has a simplicity, but it is often limited to small-scale products. In contrast, the two-step process is easily used to make bulk productions (M. Ma and Hill, 2006). Otherwise, the producing methods for super-hydrophobic surface are also classified as top-down or bottom-up methods due to the start point of fabrications. top-down methods produce highly controlled morphology of the surfaces (ex. etching and lithography) and bottom-up methods produce random topography on the surface (ex. chemical vapor deposition, electrospinning, dip-coating, and self-assembly) (Jiang et al., 2015). In this chapter, raw materials with fabrication strategies for super-hydrophobic surfaces are introduced.

#### ***2.4.3.1. Silica-based materials***

Silica nanoparticles are the most widely used materials in super-hydrophobic surfaces researches (Yu et al., 2015). Silica-base materials are intrinsically hydrophilic, but they can be super-hydrophobic when they are modified with low surface materials or to form appropriate roughness. In addition, the excellent optical transparency is another advantage for producing surface roughness without losing optical properties (Si and Guo, 2015; Yu et al., 2015). Hydrophobic coating for anti-reflection and water-repellency properties on glass substrates for self-cleaning solar cell applications was derived from poly-diallyldimethyl ammonium chloride (PDDA) with SiO<sub>2</sub> nanoparticles multilayer coated with perfluorooctyltriethoxysilane (POTS) as a low surface energy fluoroalkyl material (X. Li et al., 2013). The maximum optical transmittance of the coated glass was 99% when the non-coated glass substrate showed 91.3% transmittance, and highest water contact angle was 135 ° with a low reflection around 0.3 % (X. Li et al., 2013). The research successfully produced excellent optical properties in compared with commercial

solar cell cover glass (92-93% transmittance). However, the water contact angle of the coating was not into the super-hydrophobic surface because it was much lower than  $150^\circ$ . The hydrophobicity of the coating surface was caused by the porous roughness of the PDDA with  $\text{SiO}_2$  nanoparticles multilayer surface and the fluorinated coating. This research is one of good example to show that high transparency is difficultly maintained with high roughness of the surface.

The competitiveness between transparency and super-hydrophobicity are generally happened because an increase of roughness for super-hydrophobicity leads an increase of light scattering that reduce the transparency (Yao et al., 2011; Yu et al., 2015). Nanoscale roughness should be lower than the visible light wave length (380-760 nm) for transparent surfaces, and anti-reflective super-hydrophobic coatings enhance the performance of optical and electric devices such as solar cells and lens (Yao et al., 2011). Therefore, super-hydrophobicity with excellent transparency properties on same surface has been great interests on antireflective coating applications (Yao et al., 2011). Shang et al. made vinyl functionalized  $\text{SiO}_2$  nano-sphere (average diameter of 500 nm) coating for glass substrate using two different methods such as dip coating and spraying methods to obtain super-hydrophobic surface (Shang et al., 2013). The super-hydrophobic  $\text{SiO}_2$  coating showed water contact angles of  $158^\circ$  and  $145.7^\circ$  using dip coating and spraying methods, respectively when multi-layers of coatings were applied on glass surfaces. However, the vinyl functionalized  $\text{SiO}_2$  nano-sphere were oxidized and degraded above  $200^\circ\text{C}$ , and the  $\text{SiO}_2$  was deprived of its super-hydrophobicity.

Another well-known silica-based material is polydimethylsiloxane (PDMS) that has low surface energy (M. Ma and Hill, 2006). Khorasni et al. obtained porous PDMS surface without using chemical modification (Khorasani et al., 2005).  $\text{CO}_2$ -pulsed laser made porosities on the PDMS surface, and the water contact angle reached around  $175^\circ$  while non-laser treated PDMS

surface exhibited the water contact angle of 105 °. Similarly, rough surface PDMS composites was obtained by laser etching, and the water contact angle and sliding angle were 160 ° and lower than 5 ° (Jin et al., 2005). PDMS was also used as a hydrophobic polymer matrix for containing SiO<sub>2</sub> nanoparticles to prepare super-hydrophobic nano-coating (K. Li et al., 2014). The water contact angle of the PDMS/ SiO<sub>2</sub> coating was 153 ° due to the hierarchical roughness after heat curing at 100-200 °C, and interestingly, the heat treatment above 400 °C of the coating produce the new SiO<sub>2</sub> nanoparticles from PDMS fragments. Thus, the optical transparency increased from 40 % to 80 % after the heat curing temperature increased from 200 °C to 400 °C without losing the super-hydrophobicity. Afterwards, the super-hydrophobic surface was changed to be super-hydrophilic with the water contact angle was around 0 ° when the heat treatment temperature was over 500 °C. The hydroxyl groups modified hierarchical surface leaded the extremely super-hydrophilic property.

#### ***2.4.3.2. Fluorocarbon-based materials***

Fluorinated materials are extremely low surface energy materials because -CF<sub>3</sub> terminated surface without roughness showed the water contact angle of 120 ° (Decker and Garoff, 1997). Therefore, making roughness on the fluorinated materials directly leads super hydrophobic properties (M. Ma and Hill, 2006). Poly(tetrafluoroethalene) (PTFE, and also called Teflon) is well known long chain fluorocarbon polymer (chemical structure is [CF<sub>2</sub>-CF<sub>2</sub>]<sub>n</sub>) with providing extremely low surface energy due to the low polarized C-F bonds (Crick and Parkin, 2010). Several methods have been researched to provide roughness on PTFE polymer surface using mechanical extension (J. L. Zhang et al., 2004), plasma etching (Milella et al., 2009), and silica microsphere addition on the surface (J. Li et al., 2006). Otherwise, fluorocarbon polymers were used with other roughness agents such as nanoparticles. Hsieh et al. invented fluoro-containing silica nanoparticles

using a mixture of commercial silica particles (diameter of 20 nm) with perfluoroalkyl methacrylic copolymer (product of DuPont Co) for wood coating (Hsieh et al., 2011). The fluoro-containing silica nanoparticles exhibited excellent surface roughness and low surface energy of the coating materials. Therefore, the coating obtained maximal water contact angle of  $168.3^\circ$  (super-hydrophobicity) and the contact angle of  $153.6^\circ$  for sunflower oil drop (superoleophobicity).

Fluoroalkyl silane (FAS) has been widely used to modify rough surfaces (hydrophobic but not super-hydrophobic) with low surface energy materials for super-hydrophobic properties (Yu et al., 2015). The  $\text{CF}_3$  terminated fluoroalkyl chain is very hydrophobic, but the silicon-end group is hydrophilic that become reactive (hydroxyl ending group) during hydration, and the reactive silicon-end group is then reacted with the hydroxyl group of the surface using dehydration reaction process (Crick and Parkin, 2010). FAS also directly used to modify the surface of the nanoparticles for super-hydrophobic particles themselves. Sheen et al. modified  $\text{SiO}_2$  with a fluorinated material to obtain low surface energy nanoparticles for super-amphiphobic (hydrophobic and oleophobic) surfaces (Sheen et al., 2008). The coating surface exhibited various liquid repellency against water, diiodomethane, soybean oil, and diesel fuel etc. which are the contact angles of  $167.5^\circ$ ,  $158.6^\circ$ ,  $146.6^\circ$ , and  $140.4^\circ$ . Similarly, Zhou et al, obtained excellent durable super-hydrophobic coating (the water contact angle of  $171^\circ$ ) on fabric substrates using the fluorinated silica nanoparticles with PDMS as a silica polymer and additional fluoroalkyl silane treatment (Zhou et al., 2012). They observed that the super-hydrophobicity was led by mainly the roughness of the nanoparticles rather than the PDMS or the additional fluorinated treatment. PDMS polymer matrix was durable enough. In addition, the PDMS surface still exhibited the surface roughness after the nanoparticles was removed by abrasion or washing tests because the remaining hole made the surface very rough like a porous surface.

#### ***2.4.3.3. Carbon-based nanomaterials***

High electrical and thermal conductive carbon materials such as carbon nanotube (CNT), carbon nanofiber(CNF), and graphene have been interested in super-hydrophobic coatings due to their excellent properties for various applications (Si and Guo, 2015; Yu et al., 2015). Meng and Park prepared super-hydrophobic and transparent multi-walled CNT films modified with fluoropolymer (FP), which was composed of acrylic silane and commercial acrylic fluorocarbon, on glass substrates using dip-coating process (Meng and Park, 2010). The coating surface exhibited the water contact angle of 160.2 ° and the optical transparency of 83.5% via seven times of dip-coating process. Similarly, Men et al. produced fluoroalkyl silane modified multi walled CNT coating using a spray gun, and the water contact angles of 163 ° and the sliding angles lower than 5 ° were maintained from 25 °C to 400 °C condition (X. Zhu et al., 2014).

Graphene has been interested in materials field due to the excellent properties from the unique two-dimensional carbon backbone. However, the two-dimensional structures lead challenges to make surface roughness for super-hydrophobicity (Si and Guo, 2015). Choi and Park modified graphene oxide sheets with commercial FP (called “Nafion”) using reduction of the hydroxyl groups of the graphene oxide sheets (B. G. Choi and Park, 2012). From controlling the FP concentration in the reduction of the graphene oxide sheet, roughness of the petal-like structures on the surface were controlled. The Nafion/graphene hybrid film showed the super-hydrophobicity (water contact angle of 160 °) and 80 % optical transmittance. Otherwise, Jang et al. simply used SiO<sub>2</sub> nanoparticles to make dinge-like surface structures after removing the SiO<sub>2</sub> nanoparticles from the graphene oxide sheet (J. Lee et al., 2013). Super-hydrophobic transparent graphene sheet with the water contact angle larger than 150 ° and 72.7% transparency was obtained.



#### **2.4.3.4. Polymers**

Polymers are one of the most attractive materials to fabricate super-hydrophobic surfaces due to their processibility, cost effectiveness, flexibility, and molecular diversity (Si and Guo, 2015). Hong et al. obtained super-hydrophobic polystyrene (PS) surface using anodic aluminum oxide (AAO) nanoporous template (Hong et al., 2013). In the study, four types of AAO templates with short and long, and simple and stepped shapes nanopores produced different length and shape of nanopillars on PS surfaces. The simple-short, simple-long, stepped-short, and stepped-long nanopillars surfaces showed the water contact angles of 103.9 °, 109.3 °, 111.9 °, and 150.6 °, respectively. The authors observed that the Cassie-Baxter state contact angles were much higher on stepped nanopillars rather than simple shaped nanopillars, and the length of nanopillars did not influence to the Cassie-Baxter state contact angles. However, the Wenzel state contact angles were influenced by the length of the nanopillars: the long nanopillars exhibited higher the Wenzel state contact angles rather than the short nanopillars on both simple and stepped structures. Therefore, stepped-long nanopillars surface showed the super-hydrophobicity due to the high degree of hierarchical and roughness (Hong et al., 2013). Similarly using the template nanoimprinting method, vertically aligned polyacrylonitrile (PAN) fibers showed contact angle larger than 170 ° using AAO template: smooth PAN surface showed the water contact angle of 100 ° (Feng et al., 2002). Polyvinyl alcohol (PVA) fibers also vertically aligned when they were formed in AAO template, and it showed super-hydrophobic property even though PVA is intrinsically hydrophilic (Feng et al., 2003).

Electrospinning has been widely used to produce polymeric fibers with diameters of micro and nano-size, and the electrospun fibers mats will be super-hydrophobic when the roughness of the surfaces is high enough (M. Ma et al., 2008). The hydrophobicity of the electrospun fiber mats

were increased by simple super-hydrophobic coating. Pefluoroalkyl ethyl methacrylate (PPFEMA) were coating on the polycaprolactone (PCL) electrospun fibers (average fibers diameter of 100 nm and beads diameter of 2  $\mu\text{m}$ ) using chemical vapor deposition (M. L. Ma et al., 2005). The PPFEMA exhibited excellent super-hydrophobicity (the water contact angle of 175  $^\circ$ ) due to the surface roughness of the PCL mats and extremely low surface energy of PPFEMA beads.

Several researchers prepared super-hydrophobic surfaces using bio-based polymers such as polylactic acid (PLA), castor oil-based polymer, and fatty acids. Giuntoli et al. prepared fluorofunctionalized PLA polymers for water repellent coating of stone (Giuntoli et al., 2012). Fluorinated PLA was obtained by the ring-opening reaction of lactide with fluorinated alcohols at 130  $^\circ\text{C}$ . Giuntoli et al. observed water repellency via weight loss experiments in controlled humid conditions. Mulazim et al. prepared castor oil-based UV-curable highly hydrophobic coating (Mulazim et al., 2013). Castor oil was modified with isocyanatopropyltriethoxysilane as an alkoxy silane, and the silane modified castor oil was hydrolyzed as a single silane modified fatty acid. The hydrolyzed silane modified castor oil were added to norbonyl acrylate as a main acrylate monomer with silica nanoparticles, and hydrophobilization agents such as fluorinate silane and alkyl silane. The hybrid coating showed the highest hydrophobicity (water contact angle of 143  $^\circ$ ) when all the hydrophobilization agents and silica nanoparticles were applied together into the polymer coating (Mulazim et al., 2013). The silane modified castor oil was a key role to binding the hydrophobilization agents, and the surface roughness was leaded by the silica nanoparticles. Wang et al. produced super-hydrophobic coating on a copper surface using fatty acid (myristic acid:  $\text{CH}_3(\text{CH}_2)_{12}\text{COOH}$ ) (S. T. Wang et al., 2006). The copper plate was oxidized by the fatty acid in ethanol to form the copper carboxylate ( $\text{Cu}(\text{CH}_3(\text{CH}_2)_{12}\text{COOH})_2$ ), and the copper

carboxylate was assembled itself to grow flower-like cluster coating on the copper surface. The water contact angle of the fatty acid cluster coating was 162 °.

#### **2.4.4. Conclusion**

Many scientists have been developed super-hydrophobic surfaces from various interests such as fundamental adhesion theory, thermodynamic behaviors on the surfaces, investigations of natural special wetting behaviors, and bio-inspired special wettability surface for various applications. Despite researcher's effort, several challenging is still remained. Firstly, most of the researches for practical applications are still limited to lab scale productions (X. Zhang et al., 2008). The super-hydrophobic coating should be fabricated by using inexpensive materials, low energy consumption, and simple fabrication methods for industrial large productions. However, many researches reached the superhydrophobicity using the additional hydrophobization agents such as fluoroalkyl silane or fluorocarbon materials which are commercially expensive. Secondly, mechanical stability of the fabricated surface is concerned because micro- or nano-structures would be easily destroyed and losing the roughness (Y. Zhang et al., 2012). Finally, only few researches prepared the super-hydrophobic surfaces using bio-based materials, and many bio-based super-hydrophobic surfaces were fabricated with other main ingredients which are not bio-based. The problems will be solved from scientists' devotion, and the special wettability surface applications will make our life be better.

## 2.4.5. References

- Barthlott, W., and Neinhuis, C. (1997). Purity of the sacred lotus, or escape from contamination in biological surfaces. *Planta*, 202: 1-8. doi:10.1007/s004250050096
- Bhushan, B. (2009). Biomimetics: Lessons from nature - an overview. *Philosophical Transactions of the Royal Society A-Mathematical Physical and Engineering Sciences*, 367: 1445-1486. doi:10.1098/rsta.2009.0011
- Bhushan, B., Jung, Y. C., and Koch, K. (2009). Micro-, nano- and hierarchical structures for superhydrophobicity, self-cleaning and low adhesion. *Philosophical Transactions of the Royal Society A-Mathematical Physical and Engineering Sciences*, 367: 1631-1672. doi:10.1098/rsta.2009.0014
- Bixler, G. D., and Bhushan, B. (2012). Bioinspired rice leaf and butterfly wing surface structures combining shark skin and lotus effects. *Soft Matter*, 8: 11271-11284. doi:10.1039/c2sm26655e
- Bixler, G. D., and Bhushan, B. (2013). Fluid drag reduction and efficient self-cleaning with rice leaf and butterfly wing bioinspired surfaces. *Nanoscale*, 5: 7685-7710. doi:10.1039/c3nr01710a
- Cassie, A. B. D., and Baxter, S. (1944). Wettability of porous surfaces. *Transactions of the Faraday Society*, 40: 546-551. doi:10.1039/TF9444000546
- Choi, B. G., and Park, H. S. (2012). Superhydrophobic graphene/nafion nanohybrid films with hierarchical roughness. *Journal of Physical Chemistry C*, 116: 3207-3211. doi:10.1021/jp207818b
- Crick, C. R., and Parkin, I. P. (2010). Preparation and characterisation of super-hydrophobic surfaces. *Chemistry-a European Journal*, 16: 3568-3588. doi:10.1002/chem.200903335
- Decker, E. L., and Garoff, S. (1997). Contact line structure and dynamics on surfaces with contact angle hysteresis. *Langmuir*, 13: 6321-6332. doi:10.1021/la970528q
- Dorrer, C., and Ruehe, J. (2009). Some thoughts on superhydrophobic wetting. *Soft Matter*, 5: 51-61. doi:10.1039/b811945g
- Feng, L., Li, S. H., Li, H. J., Zhai, J., Song, Y. L., Jiang, L., and Zhu, D. B. (2002). Superhydrophobic surface of aligned polyacrylonitrile nanofibers. *Angewandte Chemie-International Edition*, 41: 1221-+. doi:10.1002/1521-3773(20020402)41:73.0.CO;2-G
- Feng, L., Song, Y. L., Zhai, J., Liu, B. Q., Xu, J., Jiang, L., and Zhu, D. B. (2003). Creation of a superhydrophobic surface from an amphiphilic polymer. *Angewandte Chemie-International Edition*, 42: 800-802. doi:10.1002/anie.200390212
- Gao, X. F., and Jiang, L. (2004). Water-repellent legs of water striders. *Nature*, 432: 36-36. doi:10.1038/432036a
- Giuntoli, G., Rosi, L., Frediani, M., Sacchi, B., and Frediani, P. (2012). Fluoro-functionalized PLA polymers as potential water-repellent coating materials for protection of stone. *Journal of Applied Polymer Science*, 125: 3125-3133. doi:10.1002/app.36469

- Guo, H., Li, Q., Zhao, H., Zhou, K., and Feng, X. (2015). Functional map of biological and biomimetic materials with hierarchical surface structures. *Rsc Advances*, 5: 66901-66926. doi:10.1039/c5ra09490a
- Guo, Z., and Liu, W. (2007). Biomimic from the superhydrophobic plant leaves in nature: Binary structure and unitary structure. *Plant Science*, 172: 1103-1112. doi:10.1016/j.plantsci.2007.03.005
- Guo, Z., Liu, W., and Su, B. (2011). Superhydrophobic surfaces: From natural to biomimetic to functional. *Journal of Colloid and Interface Science*, 353: 335-355. doi:10.1016/j.jcis.2010.08.047
- Hong, D., Ryu, I., Kwon, H., Lee, J., and Yim, S. (2013). Preparation of superhydrophobic, long-neck vase-like polymer surfaces. *Physical Chemistry Chemical Physics*, 15: 11862-11867. doi:10.1039/c3cp51833g
- Hsieh, C., Chang, B., and Lin, J. (2011). Improvement of water and oil repellency on wood substrates by using fluorinated silica nanocoating. *Applied Surface Science*, 257: 7997-8002. doi:10.1016/j.apsusc.2011.04.071
- Jiang, T., Guo, Z., and Liu, W. (2015). Biomimetic superoleophobic surfaces: Focusing on their fabrication and applications. *Journal of Materials Chemistry A*, 3: 1811-1827. doi:10.1039/c4ta05582a
- Jin, M. H., Feng, X. J., Xi, J. M., Zhai, J., Cho, K. W., Feng, L., and Jiang, L. (2005). Superhydrophobic PDMS surface with ultra-low adhesive force. *Macromolecular Rapid Communications*, 26: 1805-1809. doi:10.1002/marc.200500458
- Khorasani, M. T., Mirzadeh, H., and Kermani, Z. (2005). Wettability of porous polydimethylsiloxane surface: Morphology study. *Applied Surface Science*, 242: 339-345. doi:10.1016/j.apsusc.2004.08.035
- Lee, J., Yoon, J., and Jang, J. (2013). A route towards superhydrophobic graphene surfaces: Surface-treated reduced graphene oxide spheres. *Journal of Materials Chemistry A*, 1: 7312-7315. doi:10.1039/c3ta11434a
- Lee, W., Jin, M. K., Yoo, W. C., and Lee, J. K. (2004). Nanostructuring of a polymeric substrate with well-defined nanometer-scale topography and tailored surface wettability. *Langmuir*, 20: 7665-7669. doi:10.1021/la049411+
- Li, J., Fu, J., Cong, Y., Wu, Y., Xue, L. J., and Han, Y. C. (2006). Macroporous fluoropolymeric films templated by silica colloidal assembly: A possible route to super-hydrophobic surfaces. *Applied Surface Science*, 252: 2229-2234. doi:10.1016/j.apsusc.2005.03.224
- Li, K., Zeng, X., Li, H., Lai, X., and Xie, H. (2014). Effects of calcination temperature on the microstructure and wetting behavior of superhydrophobic polydimethylsiloxane/silica coating. *Colloids and Surfaces A-Physicochemical and Engineering Aspects*, 445: 111-118. doi:10.1016/j.colsurfa.2014.01.024
- Li, X., He, J., and Liu, W. (2013). Broadband anti-reflective and water-repellent coatings on glass substrates for self-cleaning photovoltaic cells. *Materials Research Bulletin*, 48: 2522-2528. doi:10.1016/j.materresbull.2013.03.017

- Liu, M., Wang, S., Wei, Z., Song, Y., and Jiang, L. (2009). Bioinspired design of a superoleophobic and low adhesive water/solid interface. *Advanced Materials*, 21: 665-+. doi:10.1002/adma.200801782
- Ma, M. L., Mao, Y., Gupta, M., Gleason, K. K., and Rutledge, G. C. (2005). Superhydrophobic fabrics produced by electrospinning and chemical vapor deposition. *Macromolecules*, 38: 9742-9748. doi:10.1021/ma0511189
- Ma, M., and Hill, R. M. (2006). Superhydrophobic surfaces. *Current Opinion in Colloid & Interface Science*, 11: 193-202. doi:10.1016/j.cocis.2006.06.002
- Ma, M., Hill, R. M., and Rutledge, G. C. (2008). A review of recent results on superhydrophobic materials based on micro- and nanofibers. *Journal of Adhesion Science and Technology*, 22: 1799-1817. doi:10.1163/156856108X319980
- Marmur, A. (2012). Hydro- hygro- oleo- omni-phobic? terminology of wettability classification (vol 8, pg 6867, 2012). *Soft Matter*, 8: 12134-12134. doi:10.1039/C2SM25443C
- Meng, L., and Park, S. (2010). Effect of fluorination of carbon nanotubes on superhydrophobic properties of fluoro-based films. *Journal of Colloid and Interface Science*, 342: 559-563. doi:10.1016/j.jcis.2009.10.022
- Milella, A., Di Mundo, R., Palumbo, F., Favia, P., Fracassi, F., and d'Agostino, R. (2009). Plasma nanostructuring of polymers: Different routes to superhydrophobicity. *Plasma Processes and Polymers*, 6: 460-466. doi:10.1002/ppap.200930011
- Miyauchi, Y., Ding, B., and Shiratori, S. (2006). Fabrication of a silver-ragwort-leaf-like superhydrophobic micro/nanoporous fibrous mat surface by electrospinning. *Nanotechnology*, 17: 5151-5156. doi:10.1088/0957-4484/17/20/019
- Mulazim, Y., Cakmakci, E., and Kahraman, M. V. (2013). Photo-curable highly water-repellent nanocomposite coatings. *Journal of Vinyl & Additive Technology*, 19: 31-38. doi:10.1002/vnl.20309
- Nakajima, A., Fujishima, A., Hashimoto, K., and Watanabe, T. (1999). Preparation of transparent superhydrophobic boehmite and silica films by sublimation of aluminum acetylacetonate. *Advanced Materials*, 11: 1365-1368. doi:10.1002/(SICI)1521-4095(199911)11:163.0.CO;2-F
- Sahoo, B. N., and Kandasubramanian, B. (2014). Recent progress in fabrication and characterisation of hierarchical biomimetic superhydrophobic structures. *Rsc Advances*, 4: 22053-22093. doi:10.1039/c4ra00506f
- Shang, Q., Wang, M., Liu, H., Gao, L., and Xiao, G. (2013). Facile fabrication of water repellent coatings from vinyl functionalized SiO<sub>2</sub> spheres. *Journal of Coatings Technology and Research*, 10: 465-473. doi:10.1007/s11998-012-9465-z
- Sheen, Y., Huang, Y., Liao, C., Chou, H., and Chang, F. (2008). New approach to fabricate an extremely super-amphiphobic surface based on fluorinated silica nanoparticles. *Journal of Polymer Science Part B-Polymer Physics*, 46: 1984-1990. doi:10.1002/polb.21535
- Si, Y., and Guo, Z. (2015). Superhydrophobic nanocoatings: From materials to fabrications and to applications. *Nanoscale*, 7: 5922-5946. doi:10.1039/c4nr07554d

- Sun, T. L., Feng, L., Gao, X. F., and Jiang, L. (2005). Bioinspired surfaces with special wettability. *Accounts of Chemical Research*, 38: 644-652. doi:10.1021/ar040224c
- Wang, S. T., Feng, L., and Jiang, L. (2006). One-step solution-immersion process for the fabrication of stable bionic superhydrophobic surfaces. *Advanced Materials*, 18: 767-+. doi:10.1002/adma.200501794
- Wenzel, R. N. (1936). Resistance of solid surfaces to wetting by water. *Industrial & Engineering Chemistry*, 28: 988-994. doi:10.1021/ie50320a024
- Yao, X., Song, Y., and Jiang, L. (2011). Applications of bio-inspired special wettable surfaces. *Advanced Materials*, 23: 719-734. doi:10.1002/adma.201002689
- Yu, S., Guo, Z., and Liu, W. (2015). Biomimetic transparent and superhydrophobic coatings: From nature and beyond nature. *Chemical Communications*, 51: 1775-1794. doi:10.1039/c4cc06868h
- Zhang, J. L., Li, J. A., and Han, Y. C. (2004). Superhydrophobic PTFE surfaces by extension. *Macromolecular Rapid Communications*, 25: 1105-1108. doi:10.1002/marc.200400065
- Zhang, X., Shi, F., Niu, J., Jiang, Y., and Wang, Z. (2008). Superhydrophobic surfaces: From structural control to functional application. *Journal of Materials Chemistry*, 18: 621-633. doi:10.1039/b711226b
- Zhang, Y., Xia, H., Kim, E., and Sun, H. (2012). Recent developments in superhydrophobic surfaces with unique structural and functional properties. *Soft Matter*, 8: 11217-11231. doi:10.1039/c2sm26517f
- Zheng, Y., Gao, X., and Jiang, L. (2007). Directional adhesion of superhydrophobic butterfly wings. *Soft Matter*, 3: 178-182. doi:10.1039/b612667g
- Zhou, H., Wang, H., Niu, H., Gestos, A., Wang, X., and Lin, T. (2012). Fluoroalkyl silane modified silicone rubber/nanoparticle composite: A super durable, robust superhydrophobic fabric coating. *Advanced Materials*, 24: 2409-2412. doi:10.1002/adma.201200184
- Zhu, X., Zhang, Z., Ge, B., Men, X., and Zhou, X. (2014). Fabrication of a superhydrophobic carbon nanotube coating with good reusability and easy repairability. *Colloids and Surfaces A-Physicochemical and Engineering Aspects*, 444: 252-256. doi:10.1016/j.colsurfa.2013.12.066

## **2.5. Fundamentals of biodegradable polymers**

### **2.5.1. Introduction**

Plastic is a well-known name to various materials of industrial products in our modern life. Chemically, the term of plastic is defined as a long chain polymer that has a high molecular weight of a hydrocarbon molecule (Ghosh et al., 2013; Scott, 1999). Plastics have been annually produced over 300 million tons by 2015 (Halden, 2010), and the widespread usage of plastics for versatile applications is caused by the excellent performance properties such as mechanical strength, flexibility, barrier properties, durability, and easy fabrication processes (Singh and Sharma, 2008). In addition, the stability and the durability of plastics with low manufacturing costs have led to the dramatically increased demand of plastics products (Ghosh et al., 2013). The obvious truth is that plastics lead the fast growth of manufacturing technology, which strongly encourages many innovations in our modern lives. However, drawbacks of usages of plastics have been clearly identified from an environmental point of view. Most of current plastics are stable and durable in the natural environment even though the durability is not required for all applications; the durability is not desirable for many disposable applications such as packaging and containers; approximately 30% of the global plastic was consumed to produce packaging applications (Shah et al., 2008). Therefore, the low rate of plastic degradation has become a great concern in the environment. Plastics are generally composed of long chain hydrocarbons, which show great resistances against microbial attacks due to the very balanced charges on the backbones of the polymers (Ghosh et al., 2013). Therefore, the accumulation of plastic wastes in the environment has been a problem leading to global environmental pollution and chemical waste management (Singh and Sharma, 2008). One of the most widely used synthetic polymers is polyethylene (PE) with 140 million tons of global production annually, and synthetic polymers like PE can be oxidized when they are



exposed to ultra violet irradiation from sun light, called photo-oxidation (Sivan, 2011). Then, the oxidized plastics are fragmented and degraded to small particles and micro-plastics that have been accumulated to the environment for few decades (Sivan, 2011). Consequently, the micro-plastic can be into our food chain through ingestion by wild and marine animals (Teuten et al., 2009).

In the US, produced plastic waste in 2010 was 31 million tons, and only 8% of the waste was recycled (Ghosh et al., 2013). Packaging materials are good example of leading huge environmental accumulation of plastic waste because 41% of worldwide plastics consumption is used in packaging product such as polyethylene (PE), polypropylene (PP), polystyrene (PS), and polyethylene terephthalate (PET) (Bastarrachea et al., 2010; Shah et al., 2008). Conventional methods of waste managements are landfills and burning the wastes. However, both methods cause serious environmental problems such as unfertile lands due to the pH change of the soil and hazardous greenhouse gases containing furans and dioxins that cause dangerous problem in human hormone (Ghosh et al., 2013). In addition, the most extensively used raw materials for the polymer productions are derived from fossil fuels such as oil and coal (M. M. Reddy et al., 2013). Moreover, the usages of the natural resources should be reduced to follow current global efforts such as reductions of carbon emission. Due to the concern of plastic wastes and resources, bio-based and biodegradable polymers can be most appropriate alternatives (Sudesh and Iwata, 2008). Biodegradable plastics encourage several benefits to the environment such as increases of soil fertility, reducing accumulation of plastic materials, and saving the waste management cost (Tokiwa et al., 2009). From the efforts for reducing packaging plastic wastes, over 50% of biodegradable plastic is consumed for packaging applications in 2015 with estimated annual growth rate of 33% until 2023 (Scarfato et al., 2015).

My graduate researches have focused on synthesis of cross-linked plant oil-based polymers, which are not intrinsically biodegradable. Therefore, there was a lack of knowledges of biodegradable materials and also general degradation mechanisms of plastics. This review helped to improve understanding of fundamentals of biodegradable polymers. This chapter covered general degradation mechanisms of plastics including biodegradation, and most popular biodegradable polymers in markets were introduced.

### **2.5.2. Degradation mechanisms**

Polymer properties are affected by chemical, physical, and/or biological influences as results of environmental factors such as light, heat, moisture, chemicals, and biological activity (Shah et al., 2008). A polymer matrix begins macromolecular fragmentation to smaller molecules or monomers when the polymer is exposed to the environment conditions, and this is called polymer degradation (Krzan et al., 2006). The polymer degradations result cracking, erosion, bond scission, discoloration, and phase separation, which directly change mechanical, thermal, optical, and electrical properties of polymers (Shah et al., 2008). The plastic degradation has two steps process (Figure 2.8) (Krzan et al., 2006). The first step is disintegration of polymer molecules, called depolymerization or deterioration, which long polymer chains are broken to small oligomers, monomers, or fragments by abiotic and biotic factors. The second step is called as mineralization that convert the small molecules and fragments into digestion products such as CO<sub>2</sub>, water, and cell biomass (aerobic digestion) and CO<sub>2</sub>, CH<sub>4</sub>, and cell biomass (anaerobic digestion) by microorganisms. The degradations are classified by various factors such as photo (light), hydrolytic (moisture), thermal (heat), oxidative (oxygen), mechanical (stress), and bio (microorganism) degradations (Krzan et al., 2006). In nature, combinations of those factors accelerate degradations of polymers (Lucas et al., 2008). The degradations are strongly influenced

by chemical structures, molecular weight, morphology of the polymers, and environmental conditions such as temperature and pH (Marin et al., 2013).

Biodegradation is defined as the degradation process (initiated or propagated) by microorganism (Ammala et al., 2011; Gu et al., 2000). Most of polymers are too large to be directly mineralized by microorganisms because only small oligomers or monomers can pass into the microbial cells (Shah et al., 2008). Therefore, depolymerization or deterioration of polymer is a required first step for completed biodegradation, and the abiotic degradation (photo, thermal, hydrolytic, and mechanical) have important roles to lead or accelerated biodegradation (Lucas et al., 2008; Palmisano and Pettigrew, 1992). In this section, abiotic and biotic degradation mechanisms and factors are discussed.

#### *2.5.2.1. Abiotic mechanisms*

**Photo-degradation.** Photo degradation naturally refers to most polymers in mild environmental condition by the reaction with oxygen under light (Ammala et al., 2011). Free radicals are released from the polymer frameworks when polymers are exposed to light (normally UV and visible light), and oxidizing susceptible polymer bonds are broken by the attack of the free radicals (Krzan et al., 2006; Singh and Sharma, 2008). Finally, the broken part of the polymer backbone contains various oxidative functional groups such as carboxylic acids, hydro-carboxylic acids, esters, aldehydes and alcohols (Ammala et al., 2011). Therefore, photo degradation is also called photo-oxidative degradation. The UV radiation directly leads photo degradation, and visible light enhances thermal degradation (Shah et al., 2008).

C-C and C-H bonds can be directly dissociated by UV radiation and formed to free radicals (Plotnikov, 1988). Metallic catalysts residues in commercial polymers acts like photosensitive impurities, which can be a source of free radical generation for photo degradation (Singh and

Sharma, 2008). From the strategy, photosensitive additives such as prooxidant agents were intentionally added to the plastic bags, packaging, and agricultural films for increases in degradability (Shyichuk et al., 2001; Weiland et al., 1995). C=C sites also generate high reactive free radicals such as hydroxyl and macroalkoxyl radicals in the polymer structures through the oxidation of the double bond (Carlsson and Wiles, 1976). UV-radiation near 290 to 400 nm wavelengths in the sun light affects the shelf lives of polymers for outdoor applications (Rånby, 1989). Polyethylene, polyether, and polyurethanes are susceptible to oxidative degradation because free radicals are easily formed from the polymer structures (Marin et al., 2013). The main photo degradation occurrence is the ether part of the polyether, and the oxidation of the ether forms ester or aldehyde end group (Nagai et al., 2005). In contrast, polyesters and silicon contain polymers are less susceptible against to the oxidation (Lyu and Untereker, 2009). Photo degradation leads changes in physical and optical properties such as reduction of molecular weight, mechanical strength, and flexibility, and yellowing issue of the polymers (Singh and Sharma, 2008). The photo degradation is one of important factors in abiotic degradation because most of plastics predispose to absorb the energy of UV leading oxidation and cleavage (Lucas et al., 2008; Shah et al., 2008).

**Thermal degradation.** Oxidation of the carbons in polymers is generated by supplying required heat energy, so thermal degradation is also categorized in oxidative degradation as similar as photo degradation (Krzan et al., 2006; Singh and Sharma, 2008). A difference between photo and thermal degradations is that photo degradation is generated on the surface of the polymer, but thermal degradation randomly occurs all over the polymer (Tayler, 2004). The depolymerization reaction of thermal degradation tends to start at imperfect or weak polymer chain such initiator residues, peroxide, or ether (Singh and Sharma, 2008). Thermal degradation entails a result of

molecular weight reduction via bond scissions of the polymer structure, and typical property changes are observed such as cracking, flexibility reduction, and color change (Shah et al., 2008). Both oxidative degradations of thermal and photo tend to increase the degradability with reduction of the density of polymers (Ammala et al., 2011). In addition, branched structures exhibit higher rate of oxidative degradation in comparison to linear structures: isotactic polypropylene > low-density polyethylene > linear low-density polyethylene > high-density polyethylene (Chiellini et al., 2006).

**Hydrolytic degradation.** Hydrolysis is one of the common chemical degradations in environment (He et al., 2004). Hydrolytic degradation is caused by the reaction of polymers with water, and the polymer backbone is reduced on main or side chains (Marin et al., 2013). For the reaction with water, polymers must involve hydrolyzable groups such as esters, ethers, anhydrides, amides, or ester amides (urethane) (Lucas et al., 2008). Those groups are well-known functional groups in several synthetic and natural biodegradable polymers such as poly(lactic acid) (PLA), poly( $\epsilon$ -caprolactone) (PCL), poly(ethylene terephthalate) (PET), poly(3-hydroxybutyrate) (PHB), poly(butylene succinate) (PBS), poly(butylene adipate) (PBA), and starch, etc. In addition, the first stage of the degradation is commonly performed by non-enzymatic (abiotic) hydrolysis in the case of various polyesters (Pitt et al., 1981). Abiotic hydrolysis is one of the significant reactions for starting the degradation of high molecular weight biodegradable polymers such as PLA, PLA derivatives, and PBS (Nakayama et al., 1996).

Hydrolytic degradation on ester groups of biodegradable polymers such as PLA and PCL exhibit higher degradability in basic condition than the degradability in acidic condition (Jung et al., 2006). The rate of the hydrolytic degradation is more influenced by the water accessibility into the aliphatic polyester chain than the intrinsic rate of the bond scission on ester groups (Marin et

al., 2013). Therefore, amorphous regions of polymers are more preferred for easy of hydrolytic degradation in comparison with crystalline region because water molecules can easily penetrate into the loosely organized amorphous matrix (Lucas et al., 2008).

**Mechanical degradation.** Mechanical degradation has not extensively studied in polymer degradation fields, compared to photo and hydrolytic degradations (Ammala et al., 2011). It might be caused by lots of different road conditions such as material installation, ageing, pressure during usages, environmental stress, etc (Lucas et al., 2008). Mechanical damages influence the acceleration of other degradations; Busfield and Taba reported that shear forces on the polymer surface increased the rate of photo degradation because of the change of the morphology from the stress (Busfield and Taba, 1996). In addition, mechanical damage can initiate or accelerate biodegradation even though mechanical degradation factors are not majority during biodegradation process (Briassoulis, 2005).

#### ***2.5.2.2. Biotic degradation mechanism (biodegradation)***

Biodegradation is performed by microorganisms such as fungi and bacteria, and this involves completed degradations of polymer products by biological activity (Marin et al., 2013). Therefore, depolymerization or deterioration, and mineralization by microorganisms are included for the term of biodegradation (Figure 2.8) (Shah et al., 2008). Previously mentioned, most of polymers cannot be directly digested (mineralized) by the organisms because the size of polymers is generally larger than the cell membranes (Shah et al., 2008). Thus, biodeterioration and biodepolymerization (also called as biofragmentation) are required for the first step of biodegradation, results in tiny fragments and monomers (Lucas et al., 2008). The abiotic deterioration and abiotic depolymerization are not clearly distinguished in chronological order because they may occur at same time or synergistically happen during the degradation. However, biotic deterioration

(biodeterioration) firstly starts to break down the polymer to tiny particles, and then biotic depolymerization (biodepolymerization) generates oligomers and monomers from the particles for the next step (mineralization) (Kumar Sen and Raut, 2015; Lucas et al., 2008). The metabolite products from the mineralization process should be non-toxic to the environment and joined the carbon cycle (Singh and Sharma, 2008). Biodegradation process is strongly affected by microorganism's activities, so the degradability is susceptible to environmental parameters such as temperature, water, pH, and oxygen (Krzan et al., 2006). In this chapter, deterioration, depolymerization, and mineralization by microorganisms are explained, respectively.

**Biodeterioration.** Biodeterioration is commonly combined with abiotic degradation factors through physical and chemical actions (Lucas et al., 2008). Biodeterioration is generated by living organisms such as bacteria, algae, protozoa, and fungi, which can grow on the surface and/or inside of the polymers (Hueck, 2001; Wallström et al., 2005). The living organisms form biofilms (colonization) on the surface of polymers, resulting in serious damages to the plastic products (Gu, 2003). The adhered microbial species on the polymer surface physically destroy the polymer matrix, resulting in cracks, because the adhesives of living organisms can penetrate into the pores of the polymer surface and increase the size of the pores (Cappitelli et al., 2006). In addition, filamentous microbial species make widespread colony like mycelium in polymers, and then, the penetrating frame of the microorganism accelerates cracks and alterations of the pore size (Bonhomme et al., 2003).

The biofilms and mycelium also contribute biodeterioration via chemical activity such as acidic erosion and oxidation. Chemolithotrophic microbes consume inorganic materials such as ammonia, nitrites, and hydrogen sulfide as energy and electron sources (Lucas et al., 2008). Then, products of Chemolithotrophic metabolism are strong acids such as nitric acid or sulfuric acid.

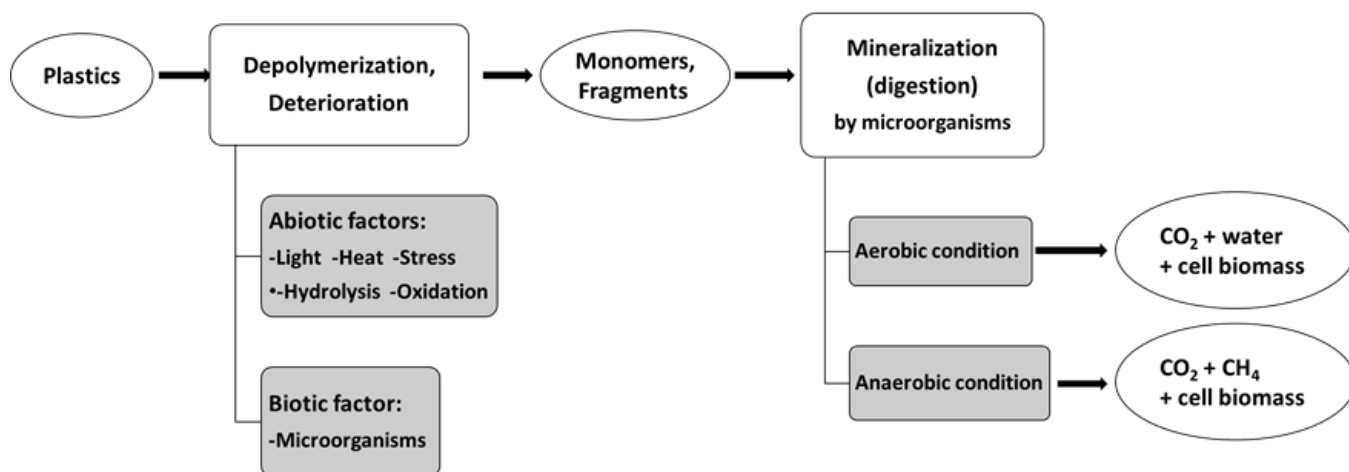
Otherwise, chemoorganotrophic microbes use organic compounds as carbon and energy sources, and they produce organic acids such as oxalic, citric, gluconic, and fumaric acids (Alcamo, 1998; Jennings and Lysek, 1996). In addition, succinic, adipic, lactic acid, and butane diols are generated by abiotic and biotic hydrolysis of biodegradable polymer such as PBS, PBA, and PLA. (Göpferich, 1996; Lindström et al., 2004; Tan et al., 2008). The active acids and diols of microbes' metabolites and hydrolysis products are possible to react with the polymer material, resulting in acceleration of surface erosions (Lugauskas et al., 2003). Furthermore, some filamentous bacteria and fungi can consume the organic acids from the hydrolysis as carbon sources to assembly mycelium (synergistically affect physical biodeterioration) (Hakkarainen et al., 2000). This chemical activity of surface erosion is expected as a major cause of biodeterioration (Warscheid and Braams, 2000).

**Biofragmentation.** Biofragmentation is a depolymerization process by enzymes of microorganisms for breaking down the polymer to small molecules such as oligomers and monomers. Enzymes are as biological catalysts that reduce the activation energy of chemical degradation reactions such as hydrolysis and oxidation (Chandra and Rustgi, 1998; Lucas et al., 2008). Many biodegradable polymers involve enzymatic hydrolysis of esters, amides, or urethane bonds (Eubeler et al., 2009). The enzyme, which causes hydrolysis reaction, is called hydrolase. Ester group is a susceptible group for the hydrolysis under natural conditions (abiotic factors) (Eubeler et al., 2009), and enzymatic hydrolysis for the ester cleavages has also similar mechanism that involves water attacking to ester bonds. Various biodegradable polyesters such as PHB, poly(ethylene adipate) PEA, PCL are depolymerized by enzymatic hydrolysis using hydrolases, which are named “depolymerase” coming after the name of the polymer (e.g. PCL depolymerase and PEA depolymerase) (Lucas et al., 2008). If the polymer includes crystalline region, hydrophobic area, and steric hinder structure (e.g. poly(vinyl alcohol) (PVC) and lignin), it is hard



to be degraded by bond scission reaction such as hydrolysis (Lucas et al., 2008). In this case, some biologically venerable groups such as alcohols and peroxides are modified in polymer matrix by oxidative enzymes such as oxidase and peroxidase (Lucas et al., 2008).

**Mineralization.** Mineralization in degradation of plastic is that microorganisms digest the fragmented polymers aerobically or anaerobically and produce metabolites such as carbon dioxide and biomass (Krzan et al., 2006). Aerobic biodegradation is performed in wild nature, and anaerobic biodegradation occurs in dregs and landfills (Shah et al., 2008). In addition, composts and soil allow partial aerobic and anaerobic biodegradations (Shah et al., 2008). Aerobic mineralization produces CO<sub>2</sub>, water, and cell biomass, otherwise CO<sub>2</sub>, CH<sub>4</sub>, and cell biomass are released by anaerobic mineralization (Krzan et al., 2006). 100 % mineralization means that all polymer materials are consumed, and it relates to that all carbons of the materials are converted to CO<sub>2</sub> (aerobically) or CO<sub>2</sub> and CH<sub>4</sub> (anaerobically) (Kyrikou and Briassoulis, 2007). Fully biodegradable materials have to be decomposed to the metabolites in the common disposed environments within one year (Leja and Lewandowicz, 2010). Monitoring of CO<sub>2</sub> or CH<sub>4</sub> are requisitely used to prove mineralization process for determine biodegradability (discussed in the next chapter).



## **Figure 2.8: Plastic degradation process in the environment.**

### **2.5.3. Biodegradable polymers**

Many kinds of biodegradable polymers have been studied, and they are classified by the origin of the polymer as synthetic or natural polymers. The natural polymers have two categories such as polysaccharide and protein groups. The synthetic polymer groups are categorized by the chemical structures and repeat units of polymers. Mostly researched and commercialized synthetic biodegradable polymers are aliphatic polyesters because of the high biodegradability by esters repeat groups and synthetic diversity (Tokiwa et al., 2009; Vroman and Tighzert, 2009). Therefore, this chapter mainly introduced synthetic biodegradable polyesters and polyurethanes.

#### ***2.5.3.1. Poly(lactic acid/lactide) [PLA]***

Poly(lactic acid) or poly(lactide) (PLA), shown in Figure 2.9, is a biodegradable aliphatic polyester based on renewable resources, which are obtained from microbial fermentation of plants resources such as corn starch and sugar cane. PLA is synthesized using condensation of lactic acid or ring-opening polymerization of lactide (Niaounakis, 2014). PLA is classified in three isomers such as poly(L-lactide), poly(D-lactide), and poly(DL-lactide) (Tokiwa et al., 2009). PLA is the most applicable biobased and biodegradable thermoplastic, and it is the firstly commercialized renewable polymers at a large-scale production (Rudnik and Briassoulis, 2011). The high melting temperature of PLA (typically 150 °C) is suitable for various processing methods such as injection molding, formation of film, spinning, blow-molding, expansion molding, and extrusion (Sudesh and Iwata, 2008). In addition, PLA has been used and studied to apply for packaging, clothing, and biomedical applications due to the excellent properties such as high mechanical strength, good barrier properties, biocompatibility, and biodegradability (Chuensangjun et al., 2012). The rate of

biodegradability of PLA is depending on the molecular weight and chemical composition, so PLA can be used for both biodegradable goods and durable products due to appropriate synthetic formulations and conditions (Chuensangjun et al., 2013; Yuryev et al., 2016). PLA is typically degraded by firstly hydrolysis at high temperature (60 °C) and then enzymatic degradation (called hydro-biodegradable) (Rudnik and Briassoulis, 2011; Sudesh and Iwata, 2008). The depolymerization process of PLA is not strongly affected by microorganisms because the PLA polymer matrix is less vulnerable to microbes in comparison with other biodegradable aliphatic polyesters such as poly(glycolic acid) (PGA) (more hydrophilic structure) (Tansengco and Tokiwa, 1997). Therefore, lactide and glycolide co-polymer (PLGA) (copolymer of PLA and PGA) has been used for biodegradable sutures and have potentials for other medical applications such as drug delivery, and implantable screws and pins due to the toughness of PLA, the high biodegradability of PGA, and the biocompatibility of the degraded products (Niaounakis, 2014). From another approach, starch is added to PLA for an improvement of biodegradability and reduction of the manufacturing cost (Shah et al., 2008). However, plasticizers such as glycerol are requisitely added to the PLA/starch blends because of the high brittleness of the blend polymer (Shah et al., 2008). Several scientists have focused on the good mechanical properties and the high melting temperature of PLA. Therefore, blends of PLA with various engineering plastics such as polycarbonate (PC) and poly(trimethylene terephthalate) (PTT) were researched for durable applications (Yuryev et al., 2016; H. Zou et al., 2010).

#### ***2.5.3.2. Poly(hydroxyalkanoates) [PHAs]***

PHA is biologically synthesized by bacteria from various substrates such as glucose and fatty acids, and a wide variety of PHA copolymers are built by the specific functional groups on the various PHA monomers (Figure 2.10) (Shrivastav et al., 2013). PLA is normally cheaper and more

available in biopolymer market in compared with PHA, and applications of PLA have outpaced PHA's applications (G. Chen, 2009). PLA can be hydrolyzed, but it is not typically deteriorated or depolymerized from pristine plastic level using only microorganisms (Gomez et al., 2012). In contrast, PHA can be depolymerized by bacteria and fungi under both aerobic and anaerobic conditions (Gomez et al., 2012). Therefore, PHA is more easily biodegradable under various conditions in compared with PLA (Sudesh and Iwata, 2008). PHB, a well-known type of PHA, showed 90 % of degradation in 5 days at 50 °C using a thermotolerant *Aspergillus* sp strain (Sanchez et al., 2000). In addition, a PHB film was completely degraded on the surface of the soil in tropical conditions within 50 days (Sudesh and Iwata, 2008). Furthermore, PHAs have at least 150 structural different monomers due to the various available bacteria and substrates for the biosynthesis of PHA while PLA has only two different monomers such as D- and L-lactic acids. Consequently, PHA can have a wide range of applications due to its diverse material properties from the various monomers (Rehm, 2010). Therefore, PHA has been researched for various applications including packaging plastics, medical usages, drug delivery, fibers, and biofuels (G. Chen, 2009). However, the high cost of producing PHA and falling oil prices after 2008 made polymer industries lose interests in PHA researches (G. Chen, 2009; Verlinden et al., 2007). To overcome the economical hindrance, many researchers have been developed to reach high substrate conversion rate, more efficient fermentation process, high purity of the products, and economic substrates usages (Verlinden et al., 2007).

### ***2.5.3.3. Poly( $\epsilon$ -caprolactone) [PCL]***

PCL, shown in Figure 2.11, is a petrochemical-based aliphatic polyester, produced by ring-opening polymerization of  $\epsilon$ -caprolactone using organic metal complex catalyst such as zing alkoxide and aluminum triflate (Niaounakis, 2014). PCL has semi-crystalline structures (50 % of

degree of crystallinity) with low melting and glass transition temperatures (60 °C and - 60°C) (Niaounakis, 2014; Tokiwa et al., 2009). In compared with other aliphatic biodegradable polyesters such as PLA and PGA, PCL has lower melting temperature; it leads rheological and viscoelastic benefits for a wide range of fabrication techniques such as electro spinning, gravity spinning, and micro-particles formation (Cipitria et al., 2011). *Penisillium* sp. strain 26-1 completely degraded PCL in isolated soil in 12 days (Tokiwa et al., 2009). In addition, PCL was fully degraded by *Aspergillus* sp. strain ST-01 in isolated soil at 50 °C during 6 days incubation. (Sanchez et al., 2000). The biodegradability of PCL was increased by blending with other biodegradable aliphatic polymers such as poly(ethylene succinate) (PES) and PHB (Niaounakis, 2014; Seretoudi et al., 2002). The blending between aliphatic polymers generally reduces the crystallinity and melting temperature as behaviors of general copolymers, which increase the susceptibility of degradation (Tokiwa et al., 2009). In other reason, starch blended PCL was investigated in order to reduce the total cost of the product because starch is one of the cheap natural polymers (Ratto et al., 1999). PCL is a biocompatible due to the non-toxic materials (Tsujiimoto et al., 2015). Even though general biocompatible and biodegradable polymers have a potential for biomedical applications, PCL has disadvantages of poor wettability, low cell attachment, and uncontrolled biological action with the polymer due to the intrinsic hydrophobic structure of PCL (Place et al., 2009). Therefore, coating, plasma treatment, and chemical treatment have been researched to obtain the moderate hydrophilicity of PCL surface for tissue engineering applications (Cipitria et al., 2011).

#### **2.5.3.4. Poly(butylene succinate) [PBS]**

PBS, shown in Figure 2.12, is a petrochemical biobased aliphatic polyesters, resulting in similar properties of PET, PE, PP (Niaounakis, 2014; Shah et al., 2008). The melting temperature

of PBS is around 113 °C, and PBS is synthesized by the condensation reaction between adipic acid and 1,4-butanediol (Takiyama and Fujimaki, 1994; Tokiwa et al., 2009). PBS shows lower biodegradation rate than that of PCL due to the high crystalline structure (Niaounakis, 2014). In addition, microorganisms for degrading PBS has lower ratio of them to the total microorganisms in the environment, as compared with PCL degrading microorganisms (Tokiwa et al., 2009). Therefore, PBS is generally mixed with starch to increase the rate of degradability and also reduce the cost of the products (Shah et al., 2008). The biodegradation of PBS needs hydrolysis process as a first step, so PBS is hydro-biodegradable (similar with PLA degradation process) (Shah et al., 2008). Major application of PBS is agricultural mulch film, and packaging films and bags. From the data of SK Chemical in Korea, a leading producer of PBS, their PBS products *showed* 50 % degradation of the film (40 um thickness) after 1 month in garden soil (Shah et al., 2008).

#### ***2.5.3.5. Aliphatic-aromatic co-polyesters [AAC]***

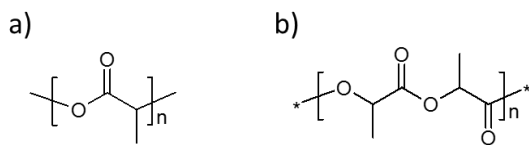
In order to increase performance properties such as strengths, aliphatic polyesters are modified with aromatic polyesters such as terephthalate. Characteristics of AACs are combined of biodegradability of aliphatic polyesters with excellent mechanical strength of aromatic polyesters (Shah et al., 2008; Tokiwa et al., 2009). It was firstly invented by PCL with aromatic polyesters such as PET, poly(butylene terephthalate) (PBT), poly(ethylene isophthalate) (PEIP), which were degraded by hydrolysis of *R. delamar* lipase (Tokiwa and Suzuki, 1981). The biodegradability of the lipase for the AACs was drastically decrease by increases in contents of aromatic polyesters (Tokiwa et al., 2009). Currently, poly(butylene adipate terephthalate) (PBAT), shown in Figure 2.13, is mainly produced to replace low-density PE with similar performance properties for food wraps and plastic bags (Shah et al., 2008). PBAT has excellent properties such as high elongation at break (700 %), fracture resistance, and water and oil repellent properties with full

biodegradability (Niaounakis, 2014). However, relatively high costs of the polymer impede a wide range of applications (Niaounakis, 2014).

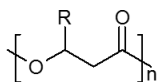
#### ***2.5.3.6. Polyurethanes***

Polyurethane has been extensively used for many applications such as foams, cushion, rubber goods, synthetic leather, adhesives, paints, and fibers due to the ease of controlling the flexibility and the rigidity of the plastics (Guelcher, 2008; Tokiwa et al., 2009). Polyurethanes are generally synthesized by two monomers, which are isocyanates for hard segments and polyols for soft segments with additions of chain extenders such as carbon chains containing amine end groups (Guelcher, 2008). Versatile properties of polyurethane can be achieved from the various hard and soft segments combinations; thus polyurethanes have been widely used in many manufacturing industry (S. Lee et al., 2001). The reaction of  $\text{N}=\text{C}=\text{O}$  bonds of isocyanates with hydroxyl groups of polyols generates urethane linkages and form a prepolymer of isocyanates and polyols, and then the reaction of  $\text{N}=\text{C}=\text{O}$  end groups of the prepolymer with amines of chain extenders generates urea bonds and form a polyurethane (Guelcher, 2008). The urethane bonds of polyurethanes are vulnerable to microbial attacks (Shah et al., 2008), and the biodegradability of polyurethanes is strongly influenced by the chemical compositions of the monomers (Ratner et al., 2004). Polyesters-based polyols such as PCL and poly(D, L-lactide) are most preferred monomers for biodegradable polyurethanes since the ester groups are easily depolymerized by hydrolysis from chemical and enzymatic activities (Doppalapudi et al., 2014). The biodegradability of polyurethanes is increase by increases in containing aliphatic structures of both isocyanates and polyols instead of containing aromatic structures, and toxicity of the degradation products is increased by the higher aromatic structure contents (Doppalapudi et al., 2014; S. Lee et al., 2001). The degradation process of the general polyester-based polyurethane was described (Guelcher,

2008); firstly, urethane and urea fragments, and alpha hydroxyl acid (from soft segments) are produced by the hydrolysis of the ester linkages of the soft segment in polyurethane, and alpha hydroxyl acids (from soft segments), and the urethane and urea linkages are then partially hydrolyzed by enzymatic activities. The final products of the degradation are varied by the composition of the polyurethanes (Guelcher, 2008). The degradation rate can be manipulated by the degree of the ester bonds in the soft segments, whereas the hard segments including urethane bonds are not easily hydrolyzed (Vroman and Tighzert, 2009). Therefore, aliphatic isocyanates such as 1,4-diisocyanatobutan are preferred for biodegradable polyurethanes, as compared to aromatic isocyanates (Doppalapudi et al., 2014).

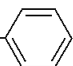


**Figure 2.9: Poly(lactic acid) (a), and poly(lactide) (b).**



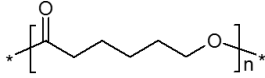
R:  $\text{CH}_3$  Poly(3-hydroxyalkanoates) [PHB]

$\text{CH}_2\text{-CH}_3$  Poly(3-hydroxyvalerate) [PHV]

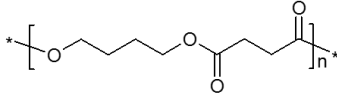
$\text{CH}_2\text{-}$   Poly(3-hydroxy-5-phenylvalerate) [PHPV]

**Figure 2.10: Examples of PHAs from specific monomers (Shrivastav et al., 2013).**

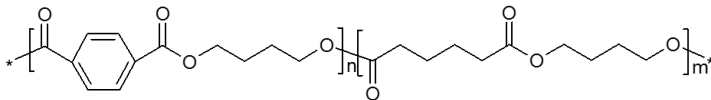




**Figure 2.11: Chemical structure of PCL.**



**Figure 2.12: Chemical structure of PBS.**



**Figure 2.13: Example of AAC: poly(butylene adipate terephthalate) (PBAT).**

#### 2.5.4. Conclusion

This chapter covered the biodegradation mechanisms of polymers, which involve also abiotic degradations, and popular synthetic biodegradable polymers were described. Currently, many scientists have studied biodegradable polymers, and several biodegradable plastics have been commercially available in markets. However, several problems impede widespread of biodegradable usages. The biodegradable polyesters and starch/polyesters blends are still expensive compared to conventional synthetic plastics (Singh and Sharma, 2008). In addition, the facilities for sorting, recycling, and composting of biodegradable plastics are insufficient (Singh and Sharma, 2008). Furthermore, there are also controversial questions that the manufacturing of biodegradable polymers is not always sustainable (Gerngross and Slater, 2000). PLA and PHA are good examples of the concern about the sustainability even though they are biobased materials. The raw material of PLA is lactic acid, which is obtained from fermentation of starch and sugars,

and the sources of the starch and sugars are corn, sugarcane, sugar beet, potato, cassava, rice, wheat, and sweet potato (Sudesh and Iwata, 2008). Therefore, PLA production spends foods for human, and the raw material supplies for PLA will be limited because of the inadequate feedstocks for growing human population in the future (Sudesh and Iwata, 2008). PHA has also similar concerns with that of PLA. The major raw materials for large-scale PHA production are vegetable oils such as palm and soybean oils. Even though vegetable oils are not major foods for human, they are important raw materials for bio-diesel, which has been increasingly demanded in fuel industries (Sudesh and Iwata, 2008). These issues can cause an increase in the cost of the raw materials, and the price competitiveness of the biobased materials against petrochemical materials would be worse. Therefore, economic manufacturing costs for the biodegradable plastics, new non-food resources, and improvements of infrastructures for biodegradable plastics wastes have to be considered and studied in future.

## 2.5.5. References

- Alcamo, I. E. (1998). *Schaum's outline of theory and problems of microbiology* McGraw Hill Professional.
- Ammala, A., Bateman, S., Dean, K., Petinakis, E., Sangwan, P., Wong, S., Yuan, Q., Yu, L., Patrick, C., and Leong, K. (2011). An overview of degradable and biodegradable polyolefins. *Progress in Polymer Science*, 36: 1015-1049.
- Bastarrachea, L., Dhawan, S., Sablani, S. S., Mah, J., Kang, D., Zhang, J., and Tang, J. (2010). Biodegradable poly (butylene adipate-co-terephthalate) films incorporated with nisin: Characterization and effectiveness against *listeria innocua*. *Journal of Food Science*, 75: E215-E224.
- Bonhomme, S., Cuer, A., Delort, A., Lemaire, J., Sancelme, M., and Scott, G. (2003). Environmental biodegradation of polyethylene. *Polymer Degradation and Stability*, 81: 441-452.
- Briassoulis, D. (2005). The effects of tensile stress and the agrochemical vapam on the ageing of low density polyethylene (LDPE) agricultural films. part I. mechanical behaviour. *Polymer Degradation and Stability*, 88: 489-503.
- Busfield, W. K., and Taba, P. (1996). Photo-oxidative degradation of mechanically stressed polyolefins. *Polymer Degradation and Stability*, 51: 185-196.
- Cappitelli, F., Principi, P., and Sorlini, C. (2006). Biodeterioration of modern materials in contemporary collections: Can biotechnology help? *Trends in Biotechnology*, 24: 350-354.
- Carlsson, D., and Wiles, D. (1976). The photooxidative degradation of polypropylene. part I. photooxidation and photoinitiation processes. *Journal of Macromolecular Science—Reviews in Macromolecular Chemistry*, 14: 65-106.
- Chandra, R., and Rustgi, R. (1998). Biodegradable polymers. *Progress in Polymer Science*, 23: 1273-1335.
- Chen, G. (2009). A microbial polyhydroxyalkanoates (PHA) based bio- and materials industry. *Chemical Society Reviews*, 38: 2434-2446. doi:10.1039/b812677c
- Chiellini, E., Corti, A., D'antone, S., and Baciù, R. (2006). Oxo-biodegradable carbon backbone polymers—oxidative degradation of polyethylene under accelerated test conditions. *Polymer Degradation and Stability*, 91: 2739-2747.
- Chuensangjun, C., Pechyen, C., Chisti, Y., & Sirisansaneeyakul, S. (2012). Lipase-catalysed polymerization of lactic acid and the properties of the polymer. Paper presented at the *Advanced Materials Research*, , 506 154-157.
- Chuensangjun, C., Pechyen, C., and Sirisansaneeyakul, S. (2013). Degradation behaviors of different blends of polylactic acid buried in soil. *Energy Procedia*, 34: 73-82.
- Cipitria, A., Skelton, A., Dargaville, T., Dalton, P., and Hutmacher, D. (2011). Design, fabrication and characterization of PCL electrospun scaffolds—a review. *Journal of Materials Chemistry*, 21: 9419-9453.

- Doppalapudi, S., Jain, A., Khan, W., and Domb, A. J. (2014). Biodegradable polymers—an overview. *Polymers for Advanced Technologies*, 25: 427-435.
- Eubeler, J. P., Zok, S., Bernhard, M., and Knepper, T. P. (2009). Environmental biodegradation of synthetic polymers I. test methodologies and procedures. *TrAC Trends in Analytical Chemistry*, 28: 1057-1072.
- Gerngross, T. U., and Slater, S. C. (2000). How green are green plastics? *Scientific American*, 283: 36-41.
- Ghosh, S. K., Pal, S., and Ray, S. (2013). Study of microbes having potentiality for biodegradation of plastics. *Environmental Science and Pollution Research*, 20: 4339-4355.
- Gomez, J., Méndez, B., Nickel, P., Pettinari, M., Prieto, M., and Silva, L. (2012). Making green polymers even greener: Towards sustainable production of polyhydroxyalkanoates from agroindustrial by-products. () InTech.
- Göpferich, A. (1996). Mechanisms of polymer degradation and erosion. *Biomaterials*, 17: 103-114.
- Gu, J., Ford, T., Mitton, D., and Mitchell, R. (2000). *Microbial corrosion of metals. the uhlig corrosion handbook*.
- Gu, J. (2003). Microbiological deterioration and degradation of synthetic polymeric materials: Recent research advances. *International Biodeterioration & Biodegradation*, 52: 69-91. doi:[http://dx.doi.org/10.1016/S0964-8305\(02\)00177-4](http://dx.doi.org/10.1016/S0964-8305(02)00177-4)
- Guelcher, S. A. (2008). Biodegradable polyurethanes: Synthesis and applications in regenerative medicine. *Tissue Engineering Part B: Reviews*, 14: 3-17.
- Hakkarainen, M., Karlsson, S., and Albertsson, A. (2000). Rapid (bio) degradation of polylactide by mixed culture of compost microorganisms—low molecular weight products and matrix changes. *Polymer*, 41: 2331-2338.
- Halden, R. U. (2010). Plastics and health risks. *Annual Review of Public Health*, Vol 31, 31: 179-194. doi:[10.1146/annurev.publhealth.012809.103714](https://doi.org/10.1146/annurev.publhealth.012809.103714)
- He, Y., Qian, Z., Zhang, H., and Liu, X. (2004). Alkaline degradation behavior of polyesteramide fibers: Surface erosion. *Colloid and Polymer Science*, 282: 972-978.
- Hueck, H. (2001). The biodeterioration of materials—an appraisal. *International Biodeterioration & Biodegradation*, 48: 5-11.
- Jennings, D. H., and Lysek, G. (1996). *Fungal biology: Understanding the fungal lifestyle*. Bios Scientific Publishers Ltd.
- Jung, J. H., Ree, M., and Kim, H. (2006). Acid-and base-catalyzed hydrolyses of aliphatic polycarbonates and polyesters. *Catalysis Today*, 115: 283-287.
- Krzan, A., Hemjinda, S., Miertus, S., Corti, A., and Chiellini, E. (2006). Standardization and certification in the area of environmentally degradable plastics. *Polymer Degradation and Stability*, 91: 2819-2833.
- Kumar Sen, S., and Raut, S. (2015). Microbial degradation of low density polyethylene (LDPE): A review. *Journal of Environmental Chemical Engineering*, 3: 462-473. doi:<http://dx.doi.org/10.1016/j.jece.2015.01.003>

- Kyrikou, I., and Briassoulis, D. (2007). Biodegradation of agricultural plastic films: A critical review. *Journal of Polymers and the Environment*, 15: 125-150.
- Lee, S., Yu, S., and Lee, Y. (2001). Degradable polyurethanes containing poly (butylene succinate) and poly (ethylene glycol). *Polymer Degradation and Stability*, 72: 81-87.
- Leja, K., and Lewandowicz, G. (2010). Polymer biodegradation and biodegradable polymers—a review. *Polish Journal of Environmental Studies*, 19: 255-266.
- Lindström, A., Albertsson, A., and Hakkarainen, M. (2004). Development of a solid-phase extraction method for simultaneous extraction of adipic acid, succinic acid and 1, 4-butanediol formed during hydrolysis of poly (butylene adipate) and poly (butylene succinate). *Journal of Chromatography A*, 1022: 171-177.
- Lucas, N., Bienaime, C., Belloy, C., Queneudec, M., Silvestre, F., and Nava-Saucedo, J. (2008). Polymer biodegradation: Mechanisms and estimation techniques—A review. *Chemosphere*, 73: 429-442.
- Lugauskas, A., Levinskait, L., and Pečiulyt, D. (2003). Micromycetes as deterioration agents of polymeric materials. *International Biodeterioration & Biodegradation*, 52: 233-242.
- Lyu, S., and Untereker, D. (2009). Degradability of polymers for implantable biomedical devices. *International Journal of Molecular Sciences*, 10: 4033-4065.
- Marin, E., Briceno, M. I., and Caballero-George, C. (2013). Critical evaluation of biodegradable polymers used in nanodrugs. *International Journal of Nanomedicine*, 8: 3071-3090. doi:10.2147/IJN.S47186 [doi]
- Nagai, Y., Nakamura, D., Miyake, T., Ueno, H., Matsumoto, N., Kaji, A., and Ohishi, F. (2005). Photodegradation mechanisms in poly (2, 6-butylenenaphthalate-co-tetramethyleneglycol)(PBN–PTMG). I: Influence of the PTMG content. *Polymer Degradation and Stability*, 88: 251-255.
- Nakayama, A., Kawasaki, N., Arvanitoyannis, I., Aiba, S., and Yamamoto, N. (1996). Synthesis and biodegradation of poly ( $\gamma$ -butyrolactone-co-L-lactide). *Journal of Environmental Polymer Degradation*, 4: 205-211.
- Niaounakis, M. (2014). *Biopolymers: Processing and products* William Andrew.
- Palmisano, A. C., and Pettigrew, C. A. (1992). Biodegradability of plastics. *Bioscience*, 42: 680-685.
- Pitt, G., Gratzl, M., Kimmel, G., Surles, J., and Sohindler, A. (1981). Aliphatic polyesters II. the degradation of poly (DL-lactide), poly ( $\epsilon$ -caprolactone), and their copolymers in vivo. *Biomaterials*, 2: 215-220.
- Place, E. S., George, J. H., Williams, C. K., and Stevens, M. M. (2009). Synthetic polymer scaffolds for tissue engineering. *Chemical Society Reviews*, 38: 1139-1151.
- Plotnikov, V. (1988). Effect of mechanical stresses on photochemical degradation of polymeric molecules. Paper presented at the Dokl Akad Nauk SSSR, , 301 376-379.
- Rånby, B. (1989). Photodegradation and photo-oxidation of synthetic polymers. *Journal of Analytical and Applied Pyrolysis*, 15: 237-247.

- Ratner, B. D., Hoffman, A. S., Schoen, F. J., and Lemons, J. E. (2004). *Biomaterials science: An introduction to materials in medicine* Academic press.
- Ratto, J. A., Stenhouse, P. J., Auerbach, M., Mitchell, J., and Farrell, R. (1999). Processing, performance and biodegradability of a thermoplastic aliphatic polyester/starch system. *Polymer*, 40: 6777-6788.
- Reddy, M. M., Vivekanandhan, S., Misra, M., Bhatia, S. K., and Mohanty, A. K. (2013). Biobased plastics and bionanocomposites: Current status and future opportunities. *Progress in Polymer Science*, 38: 1653-1689. doi:10.1016/j.progpolymsci.2013.05.006
- Rehm, B. H. A. (2010). Bacterial polymers: Biosynthesis, modifications and applications. *Nature Reviews Microbiology*, 8: 578-592. doi:10.1038/nrmicro2354
- Rudnik, E., and Briassoulis, D. (2011). Degradation behaviour of poly (lactic acid) films and fibres in soil under mediterranean field conditions and laboratory simulations testing. *Industrial Crops and Products*, 33: 648-658.
- Sanchez, J. G., Tsuchii, A., and Tokiwa, Y. (2000). Degradation of polycaprolactone at 50° C by a thermotolerant aspergillus sp. *Biotechnology Letters*, 22: 849-853.
- Scarfato, P., Di Maio, L., and Incarnato, L. (2015). Recent advances and migration issues in biodegradable polymers from renewable sources for food packaging. *Journal of Applied Polymer Science*, 132
- Scott, G. (1999). Polymers in modern life. In G. Scott (Ed.), (pp. 1-18) *The Royal Society of Chemistry*. doi:10.1039/9781847551726-00001
- Seretoudi, G., Bikiaris, D., and Panayiotou, C. (2002). Synthesis, characterization and biodegradability of poly (ethylene succinate)/poly ( $\epsilon$ -caprolactone) block copolymers. *Polymer*, 43: 5405-5415.
- Shah, A. A., Hasan, F., Hameed, A., and Ahmed, S. (2008). Biological degradation of plastics: A comprehensive review. *Biotechnology Advances*, 26: 246-265.
- Shrivastav, A., Kim, H., and Kim, Y. (2013). Advances in the applications of polyhydroxyalkanoate nanoparticles for novel drug delivery system. *Biomed Research International*, : 581684. doi:10.1155/2013/581684
- Shyichuk, A., Stavychna, D., and White, J. (2001). Effect of tensile stress on chain scission and crosslinking during photo-oxidation of polypropylene. *Polymer Degradation and Stability*, 72: 279-285.
- Singh, B., and Sharma, N. (2008). Mechanistic implications of plastic degradation. *Polymer Degradation and Stability*, 93: 561-584.
- Sivan, A. (2011). New perspectives in plastic biodegradation. *Current Opinion in Biotechnology*, 22: 422-426.
- Sudesh, K., and Iwata, T. (2008). Sustainability of biobased and biodegradable plastics. *CLEAN–Soil, Air, Water*, 36: 433-442.
- Takiyama, E., and Fujimaki, T. (1994). " BIONOLLE", biodegradable plastic through chemical synthesis. *Studies in Polymer Science*, 12: 150-150.

- Tan, F. T., Cooper, D. G., Marić, M., and Nicell, J. A. (2008). Biodegradation of a synthetic copolyester by aerobic mesophilic microorganisms. *Polymer Degradation and Stability*, 93: 1479-1485.
- Tansengco, M., and Tokiwa, Y. (1997). Thermophilic microbial degradation of polyethylene succinate. *World Journal of Microbiology and Biotechnology*, 14: 133-138.
- Taylor, D. R. (2004). Mechanistic aspects of the effects of stress on the rates of photochemical degradation reactions in polymers. *Journal of Macromolecular Science, Part C*, 44: 351-388. doi:10.1081/MC-200033682
- Teuten, E. L., Saquing, J. M., Knappe, D. R., Barlaz, M. A., Jonsson, S., Bjorn, A., Rowland, S. J., Thompson, R. C., Galloway, T. S., . . . Takada, H. (2009). Transport and release of chemicals from plastics to the environment and to wildlife. *Philosophical Transactions of the Royal Society of London. Series B, Biological Sciences*, 364: 2027-2045. doi:10.1098/rstb.2008.0284 [doi]
- Tokiwa, Y., Calabria, B., Ugwu, C., and Aiba, S. (2009). Biodegradability of plastics. *International Journal of Molecular Sciences*, 10: 3722-3742. doi:10.3390/ijms10093722
- Tokiwa, Y., and Suzuki, T. (1981). Hydrolysis of copolyesters containing aromatic and aliphatic ester blocks by lipase. *Journal of Applied Polymer Science*, 26: 441-448.
- Tsujimoto, T., Takayama, T., and Uyama, H. (2015). Biodegradable shape memory polymeric material from epoxidized soybean oil and polycaprolactone. *Polymers*, 7: 2165-2174.
- Verlinden, R. A. J., Hill, D. J., Kenward, M. A., Williams, C. D., and Radecka, I. (2007). Bacterial synthesis of biodegradable polyhydroxyalkanoates. *Journal of Applied Microbiology*, 102: 1437-1449. doi:10.1111/j.1365-2672.2007.03335.x
- Vroman, I., and Tighzert, L. (2009). Biodegradable polymers. *Materials*, 2: 307-344.
- Wallström, S., Strömberg, E., and Karlsson, S. (2005). Microbiological growth testing of polymeric materials: An evaluation of new methods. *Polymer Testing*, 24: 557-563.
- Warscheid, T., and Braams, J. (2000). Biodeterioration of stone: A review. *International Biodeterioration & Biodegradation*, 46: 343-368.
- Weiland, M., Daro, A., and David, C. (1995). Biodegradation of thermally oxidized polyethylene. *Polymer Degradation and Stability*, 48: 275-289.
- Yuryev, Y., Mohanty, A. K., and Misra, M. (2016). Hydrolytic stability of polycarbonate/poly (lactic acid) blends and its evaluation via poly (lactic) acid median melting point depression. *Polymer Degradation and Stability*, 134: 227-236.
- Zou, H., Yi, C., Wang, L., and Xu, W. (2010). Crystallization, hydrolytic degradation, and mechanical properties of poly (trimethylene terephthalate)/poly (lactic acid) blends. *Polymer Bulletin*, 64: 471-481.

## **Chapter 3 - Camelina oil-based acrylate with reactive diluents for bio-based wood coating applications**

### **3.1. Abstract**

Acrylated plant oils have been used as coating resins. The coating materials derived from the plant oils with low unsaturation fatty acids, such as soybean oil, usually have low film strength and better flexibility. While other plant oils with higher unsaturation fatty acids such as camelina oil or linseed oil, usually have high film strength and less flexibility. In addition, to brittleness, the acrylated resin from plant oils with a high degree of unsaturated fatty acids is found to be too viscous to use, which limits its applications, as coating resins. In this study, we identify and characterize reactive diluents for enhancements of processibility and performance properties of the acrylated resin. Camelina oil is used because camelina is revalued as a non-food oilseed crop in biofuel and biopolymer industries due to its high oil content (36-47% in seed) that is composed of 90% of unsaturated fatty acids. Acrylated epoxidized camelina oil (AECO) was synthesized through the epoxidation of camelina oil (CO), followed by the ring-opening reaction of epoxidized camelina oil (ECO) with acrylic acids. Synthesis of ECO and AECO were confirmed by Fourier transform infrared (FTIR) spectroscopy and  $^1\text{H}$  nuclear magnetic resonance (NMR). Several mono- and di-(meth)acrylates, namely, 2-hydroxyethyl acrylate (HEA), 1,6-hexanediol ethoxylate diacrylate (HDEDA), and ethylene glycol dimethacrylate (EGDMA), methyl methacrylate (MMA), lauryl methacrylate (LMA), and 1,4-butanediol dimethacrylate (BDDMA) were then respectively formulated with AECO at 10 wt% of AECO as reactive diluents. The lowest viscosity (4.2 Pa·s) was obtained for AECO:MMA resin. All the AECO formulations with an addition of a photoinitiator were cured under UV lighting to prepare AECO-based films and coatings on wood surface, which were characterized for the mechanical, dynamic mechanical, thermal, and coating



performance properties. The highest tensile strength (22.0 MPa) and pencil hardness (4H) were achieved for the cured AECO:EGDMA resin, and the AECO:HEA film and coating showed the excellent flexibility (8% of elongation at break) and adhesion (4B) with comparable tensile strength (21.2 MPa).

### **3.2. Introduction**

UV-curing coating system has been widely used in industries due to its low energy consumption and volatile organic compound emission, processing at normal temperature, quick polymerizations, and selective curing area (Bongiovanni et al., 2002; Schwalm, 2006; Sharmin et al., 2015). In addition, the radiation curing technique has been spotlighted as a more environment-friendly coating method because of the less or non-solvent contents in the formulation, as compared to traditional solvent-borne coating systems (Sharmin et al., 2015). Consequently, 84% of wood flooring market used the radiation curing method in 2005 due to its processing benefits (Landry et al., 2010). Acrylates such as epoxy acrylate and polyurethane acrylates are typical monomers/oligomers for UV-curable resins due to their high reactivity, excellent adhesion on target surface, hardness, and chemical resistance (B. Lee and Kim, 2006; Park et al., 2009; Shen et al., 2015), and petrochemicals have been widely used to produce the acrylates for UV-curing coating materials as well (Schwalm, 2006). To reduce carbon emission and save fossil fuels, “green” UV-curable materials are needed as alternatives to petroleum-based materials (Meier et al., 2007). Therefore, plant oils such as soybean and castor oil have been important renewable resources in polymer industry because they are abundant, naturally non-toxic, and capable of chemical functionalization (Mahendran et al., 2012; Wool and Sun, 2005). Various oil-based UV-curable coatings have been prepared from soybean oil (Habib and Bajpai, 2011; Rengasamy and Mannari, 2013; Sung et al., 2015), castor oil (Mishra et al., 2015; Q. Wang et al., 2016), linseed oil (Chang

and Lu, 2013; Mahendran et al., 2012; K. Zou and Soucek, 2004), jatropha oil (Aung et al., 2015), and palm oil (Rosli et al., 2003).

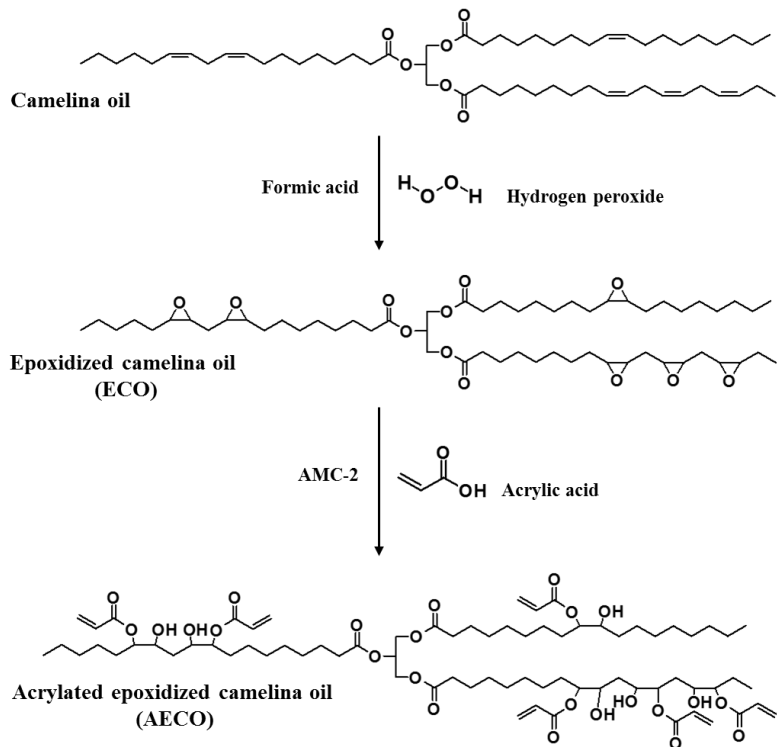
Camelina is an oil seed crop, and camelina oil (CO) has been attractive in biopolymer industry because of its high oil content in the seed (36-47%) containing high degree of unsaturated fatty acids (about 90% of fatty acids, 5.8 double bonds per triglyceride), which are suitable for making high-performance biopolymers; soybean oil contains 18-22% of oil content in the seed and 4.6 double bonds per mole of unsaturation (N. Kim et al., 2015; Y. Li and Sun, 2015a). The fatty acid composition of CO is also promising for producing jet fuel, biodiesel, and lubricants (Kagale et al., 2014). Moreover, CO is a non-food resource, so using the oil in polymer industries is free from the controversy that biopolymers derived edible oils lead a competition with food production. Thus, camelina has been increasingly cultivated in the United States due to its beneficial applications in multiple industries (Iskandarov et al., 2014; Keske et al., 2013). Although camelina is a strong candidate for the sustainable feedstock of biofuel and bioproducts, the relatively high cost of camelina processing is one of the challenges of using camelina in industries partly due to the lack of co-products from camelina (Y. Li and Sun, 2015a). Currently, only few applications such as polymers (Kasetaite et al., 2014; N. Kim et al., 2015; Y. Li and Sun, 2015a; N. Reddy et al., 2012) and composites (Balanuca et al., 2014; J. T. Kim and Netravali, 2012) have been investigated using camelina meal and oil. Therefore, developing high value co-products from camelina can improve the economics of camelina.

With this in mind, acrylated epoxidized camelina oil (AECO) was prepared according to the epoxy ring-opening of epoxidized camelina oil (ECO), which was synthesized from CO using hydrogen peroxide with formic acid, with acrylic acids (Scheme 3.1) (Y. Li and Sun, 2015a). High mechanical strength and thermal properties of AECO polymer were achieved, as compared to

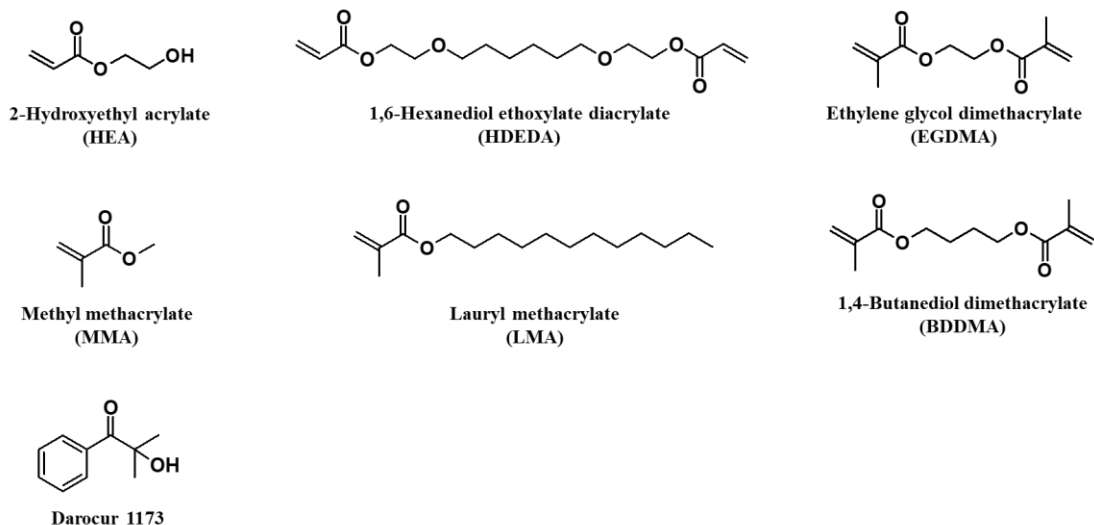
typical plant oil-based acrylates such as acrylated epoxidized soybean oil (AESO) due to the higher functionality of AECO. However, the acrylic esters and triglycerides of the plant oil-based acrylates can cause high viscosity of the resins due to the enhanced intermolecular forces among the esters of the acrylates and the triglyceride (Rengasamy and Mannari, 2013). Thus, in this study, a reactive diluent (RD) such as styrene is required to reduce the viscosity of plant oil-based acrylates qualified with performance properties of the products (J. La Scala and Wool, 2013). Styrene is one of the mostly used RDs for thermoset polymers, but the use of styrene raises concerns about environmental hazardous and health risks due to its high volatility and carcinogenicity (Cousinet et al., 2015). Hence, various low viscous mono- and multi-(meth)acrylates have been used or synthesized as RDs for many polymer applications such as plant oil-based thermosets (Campanella et al., 2009; Campanella et al., 2011), dental composites (Kilambi et al., 2009; H. Lu et al., 2005), polyester resins (Cousinet et al., 2015), liquid molding resins (Stanzione et al., 2012), and bone replacement materials (Schuster et al., 2007a; Schuster et al., 2007b). Therefore, the objective of this work is to find adequate (meth)acrylates as RDs to reduce the viscosity of AECO and improve performance properties of AECO polymer for UV-curable wood coating applications.

In this context, different candidates derived from petroleum and renewable resources were selected as RDs for this study (Figure 3.1): petrochemical (meth)acrylates such as 2-hydroxyethyl acrylate (HEA); 1,6-hexanediol ethoxylate diacrylate (HDEDA); and ethylene glycol dimethacrylate (EGDMA). Bio-based (meth)acrylates such as methyl methacrylate (MMA, regarded as a bio-based chemical because it can be synthesized from bio-methanol that is derived from glycerol as a renewable resource (van Bennekom et al., 2012); lauryl methacrylate (LMA, synthesized from lauryl alcohol that is prepared by hydrogenation of fatty acid (Kreutzer, 1984));

and 1,4-butanediol dimethacrylate (BDDMA, synthesized from butanediol that is derived from succinic acid (Bozell and Petersen, 2010)). These RDs were incorporated into the AECO at 10 wt% of AECO, and the resins were UV-cured in the presence of 3 wt% Darocur 1173 as a photoinitiator. Viscosities of the resins were estimated, and mechanical, dynamic mechanical, thermal properties, and gel content of the polymers were obtained using the cured acrylate films. Coating performance tests were conducted on the cured acrylate coatings on wood panels, and two commercial wood finishes for interior wood applications were also investigated by the coating performance tests as comparison targets. Structure characterization of CO and its derivatives were performed by Fourier transform infrared (FTIR) spectroscopy and  $^1\text{H}$  nuclear magnetic resonance (NMR).



**Scheme 3.1: Chemical pathway of synthesis of AECO from camelina oil.**



**Figure 3.1: Chemical structures of reactive diluents (HEA, HDEDA, EGDMA, MMA, LMA, and BDDMA) and free-radical photo-initiator (Darocur 1173).**

### 3.3. Materials and Methods

#### 3.3.1. Materials

Camelina oil (CO) was provided by Montana gluten Free Processors (Belgrade, MT). Darocur 1173 (2-hydroxyl-2-methyl-1-phenylpropan-1-one) was supplied by BASF (Florham Park, NJ). AMC-2 (a 40-60% solution of chromium(III) 2-ethylhexanoate in a mixture of di(heptyl, nonyl, undecyl) phthalates) was purchased from Ampac Fine Chemicals (Rancho Cordova, CA). 2-hydroxyethyl acrylate (HEA) (96 wt%), and 1,6-hexanediol ethoxylate diacrylate (HDEDA) (>90 wt%), ethylene glycol dimethacrylate (EGDMA) (98 wt%), methyl methacrylate (MMA) (99 wt%), lauryl methacrylate (LMA) (96 wt%), 1,4-butanediol dimethacrylate (BDDMA) (95 wt%) were obtained from Sigma-Aldrich (St. Louis, MO). 0.1 N hydrogen bromide in acetic acid, formic acid (88 wt%), hydrogen peroxide (30 wt%), Acrylic acid (>99 wt%), ethyl acetate, ethyl ether, toluene, methyl ethyl ketone, anhydrous magnesium sulfate, Celite 545, sodium bicarbonate, and hydroquinone were purchased from Sigma-Aldrich (St. Louis, MO) and Fisher Scientific

(Waltham, MA). Minwax Polycrylic Protective Finish (PC) and Minwax Fast-Drying Polyurethane (PU) were produced by Minwax Company (Upper Saddle River, NJ).

### **3.3.2. Synthesis of epoxidized camelina oil (ECO)**

ECO was produced from CO using formic acid and hydrogen peroxide (Scheme 3.1), and the epoxidation of CO has been modified according to our previous research (N. Kim et al., 2015; Y. Li and Sun, 2015a). 94.7 g of formic acid (88 wt%, 33.3 wt% of CO) was added to 250 g of CO (0.28 mol) in a 1000 mL of an Erlenmeyer flask with a magnetic stirrer. The flask was placed in an ice/water bath, and the mixture was vigorously stirred while 374.9 g of hydrogen peroxide (30 wt%, 3.3 mol) was gradually added to the mixture. The flask was covered, and the mixture was stirred for 16 hours. The flask was placed in the water bath during the reaction time to maintain the temperature of the reactants below 40 °C. At the end of the reaction, the product was extracted with ethyl acetate. The organic layer was then separated from the water layer using a separatory funnel, and the organic phase was washed with water and saturated sodium bicarbonate solution to remove the acid and hydrogen peroxide. The organic phase was dried over magnesium sulfate, followed by Celite filtration. The ethyl acetate was evaporated using a rotary evaporator under a tap vacuum at 45 °C, and extra drying of the product was performed under high-pressure vacuum at 85 °C. 245 g of ECO was obtained.

### **3.3.3. Synthesis of acrylated epoxidized camelina oil (AECO)**

The epoxide of ECO was reacted with acrylic acid in the present of AMC-2 as a catalyst to produce AECO (Scheme 3.1). 1.2 g of AMC-2 was added to 60 g of ECO (0.062 mol) in a 500 mL Erlenmeyer flask, and 0.198 g of hydroquinone (0.33 wt% of ECO) was added to the mixture as a free-radical polymerization inhibitor. The flask was equipped with a magnetic stirrer and a

stopper, and placed in an oil bath at 80 °C. After the mixture temperature reached at 80 °C, acrylic acid (23.62 g, 0.328 mol) was added by five stepwise additions of one fifth of the acrylic acid at 0, 2, 4, 6, and 8 hours from the beginning of the reaction. The reaction was maintained with another 4 hours after the last step of acrylic acid addition, and the temperature of the mixture were kept on 80 °C during the reaction. At the end of the reaction, the mixture was dissolved in ethyl ether after the flask was cooled to room temperature. The unreacted components were then removed by several extractions with water and saturated sodium bicarbonate solution using a separatory funnel. The organic phase was dried over magnesium sulfate and filtered by Celite. 60.5 g of product was collected after evaporating ethyl ether under vacuum at 50 °C.

#### **3.3.4. Preparation of UV-curable acrylates and coating materials**

AECO was mixed with RDs such as HEA, HDEDA, EGDMA, MMA, LMA, or BDDMA at a 10:1 weight ratio, and a total of 3 wt% Darocur 1173 was added to the resins as a free-radical polymerization initiator. The resin mixture was mixed by a vortex and a sonicator following careful heating the mixture via using a heat gun. The mixed resin was spread over a glass plate at 160 um thickness using a film casting knife (BYK-Gardener USA, Columbia, MD). Then, the glass plate with spread resin was carried twice under UV irradiation (1.8 kW, 6-in (300 W in<sup>-1</sup>) lamps) at conveyor rate of 10 ft min<sup>-1</sup> through using a F300 UV system equipped with a LC6B benchtop conveyor (Fusion UV system, Gaithersburg, MD). The UV-cured resin was carefully peeled from the glass plate as a free-standing film for characterization of the cured acrylates. For measurements of coating performances of the resins, coatings on wood panels were prepared. The wood panel was covered with the acrylic resin using a brush, and the resin was cured by the same UV system previously mentioned at approximately 50 um thickness. The commercial wood finish (PC and PU) was spread onto the wood panel using the brush, and it was completely dried at room

temperature for 24 hours. After the drying time, second and third coat were applied for PC and PU to obtain the thickness (~50  $\mu\text{m}$ ), respectively.

### 3.3.5. Measurements

FTIR spectra of the acrylates monomers and polymers were monitored at a range from 400  $\text{cm}^{-1}$  to 4000  $\text{cm}^{-1}$  with 4  $\text{cm}^{-1}$  of resolution using Perkin-Elmer Spectrum 400 FTIR spectroscopy (Waltham, MA). Varian 600 MHz spectrometer with deuterated chloroform as a solvent was employed at room temperature for  $^1\text{H}$  NMR spectra of CO and its derivatives. Determination of epoxy contents of ECO were compiled with the test method A of ASTM D 1652-97. Viscosities of the acrylate monomers were estimated using a Bohlin CVOR 150 rheometer (Marlvern Instruments, Southborough, MA) equipped with a PP 20 parallel plate on 500  $\mu\text{m}$  of gap size. The viscosities were isothermally measured at 25  $^\circ\text{C}$  with a constant shear rate of 1  $\text{s}^{-1}$ .

Tensile properties of the UV-cured acrylates were estimated according to ASTM D 882-12 using a tensile tester (TT-1100, ChemInstruments, Fairfield, OH). Strips (17.78 cm length, 1.27 cm width, and 0.13-0.15 mm thickness) of cured acrylates were prepared by cropping the free-standing films using a dual-blade shear cutter (JDC Precision Cutter 1000, Thwing-Albert Instrument Company, West Berlin, NJ) according to ASTM D 6287-09. Each end of the strip was respectively held on a fixed grip and a moving grip of the tensile tester with 12.7 cm of initial grip separation, and a test was performed at a constant rate of grip separation of 2.54  $\text{cm min}^{-1}$ . Tensile strength and elongation at break were determined as the average values of the three precision tests.

Measurements of viscoelastic properties of the polymers were conducted with dynamic mechanical analysis (DMA) using TA DMA Q800 (New Castle, DE). A strip (2 cm length, 1.27 cm width, and 0.13-0.15 thickness) was obtained from the free-standing cured films and then applied to tension/film clamp of the DMA. The specimen was heated from -50  $^\circ\text{C}$  to 200  $^\circ\text{C}$  at a



rate of 3 °C min<sup>-1</sup> with a tensile mode at 1 Hz of a frequency and 15 μm of amplitude. Storage modulus, loss modulus, and tan δ were obtained. Thermogravimetric analysis (TGA) was used to observe thermal decomposition behavior of the polymer using PerkinElmer Pyris 1 TGA (Norwalk, CT). The cured acrylates (9-10 mg) were tested in a heating range of 50 °C to 650 °C at a rate of 20 °C min<sup>-1</sup> under a nitrogen atmosphere.

The adhesion of the coatings to wood was measured using crosshatch cut test according to ASTM D 3359-02, and the pencil hardness of the coatings was determined according to ASTM D 3363-00. The solvent resistance of the coatings was evaluated by the test method A of ASTM D 5402-06 using methyl ethyl ketone (MEK) as a solvent. The surface of the coatings was rubbed with cotton gauze, which was soaked in MEK, and maximum numbers of double rubs (one forward and one backward motion) were reported until the coating started to peel off or be deformed. The specular gloss of the coatings was obtained using a glossmeter according to ASTM D 523-14.

The gel content of the cured acrylates was evaluated by immersion test in toluene (Y. Li and Sun, 2015b; Vendamme and Eevers, 2013). Approximately 0.12 g of the strips of the cured acrylate films were immersed in 20 mL toluene in a vial for 3 weeks at room temperature, and the specimens were then dried in an oven at 130 °C for 3 hours. The gel content was calculated using Eq. (1):

$$\text{Gel content} = \frac{w_f}{w_i} \times 100 \quad (1)$$

where  $w_i$  and  $w_f$  are the weights of the specimens before and after immersion in toluene.

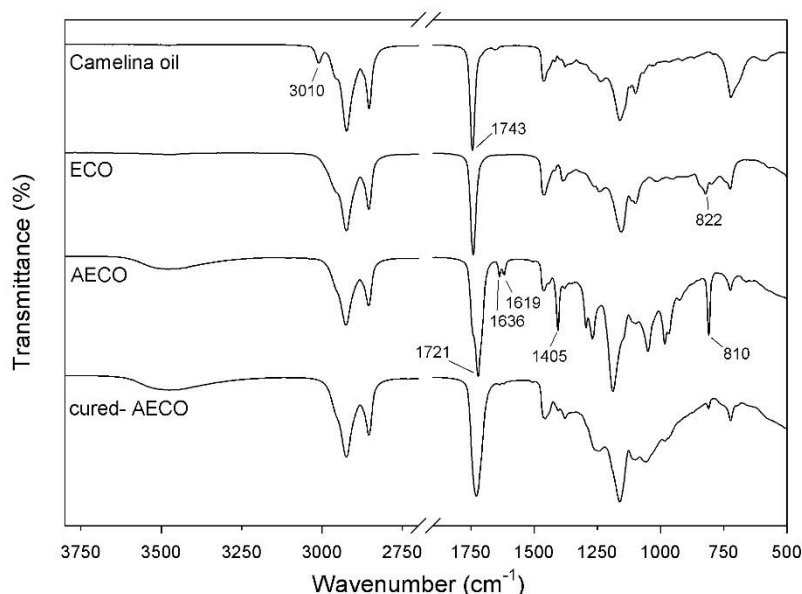
## 3.4. Results and Discussion

### 3.4.1. FTIR analysis of CO and its derivatives

Fatty acid compositions of CO are mainly linolenic acid (37.4%), linoleic acid (18.6%), oleic acid (14.8%), and gondoic acid (13.2%); the average number of C=C double bonds per mole of CO and molecular weight of CO were estimated to be 5.8 and 892 g/mol, respectively (N. Kim et al., 2015). To produce ECO, oxirane was modified on the unsaturated site of CO using hydrogen peroxide as an oxygen donor and formic acid as an oxygen carrier. The molar ratio of hydrogen peroxide to the C=C site was 1.1:1 for the epoxidation reaction. However, 4.78 epoxides per triglyceride, which corresponded to an average epoxy contents of 7.76% (following ASTM D1652) and an epoxy conversion rate of 82.4%, was obtained because of side reactions such as ring-opening with formic acid (N. Kim et al., 2015). The epoxidation of CO was monitored using FTIR spectra (Figure 3.2). The appearance of the peak at  $822\text{ cm}^{-1}$  in ECO spectra represented the C-O-C stretching of epoxide groups, and the C-H stretching peak of C=C double bonds at  $3010\text{ cm}^{-1}$  in CO spectra disappeared in the ECO spectra due to the consumption of C=C double bonds of CO during the epoxidation reaction.

Acrylic groups were grafted on the triglyceride of CO using the ring-opening reaction of the epoxides of ECO with acrylic acids. To produce maximally functionalized acrylates, one epoxide group was reacted with 1.1 moles of acrylic acids (J. La Scala and Wool, 2013). In the FTIR spectra of AECO (Figure 3.2), the modified acrylic groups were strongly evidenced by the appeared peaks of C=C double bonds of acrylate groups of AECO at 810, 1405, 1619, and  $1636\text{ cm}^{-1}$ . In addition, the broad peaks of hydroxyl groups were observed around  $3450\text{ cm}^{-1}$  since new hydroxyl groups were generated by the ring-opening of epoxides. The C=O stretching peak of carbonyl groups of acrylates at  $1721\text{ cm}^{-1}$  were appeared in the FTIR spectra of AECO. Therefore, the C=O stretching

peak of carbonyl groups of triglycerides at  $1743\text{ cm}^{-1}$  were overlapped with the peak of acrylates. The C=C double bonds peaks at 810, 1405, 1619, and  $1636\text{ cm}^{-1}$  in AECO spectra were mostly reduced at the spectra of cured-AECO since the reactive double bonds of the acrylate groups were successfully participated in the free-radical polymerization.



**Figure 3.2: FTIR spectra of camelina oil derivatives and cured AECO.**

### 3.4.2. NMR analysis of CO and its derivatives

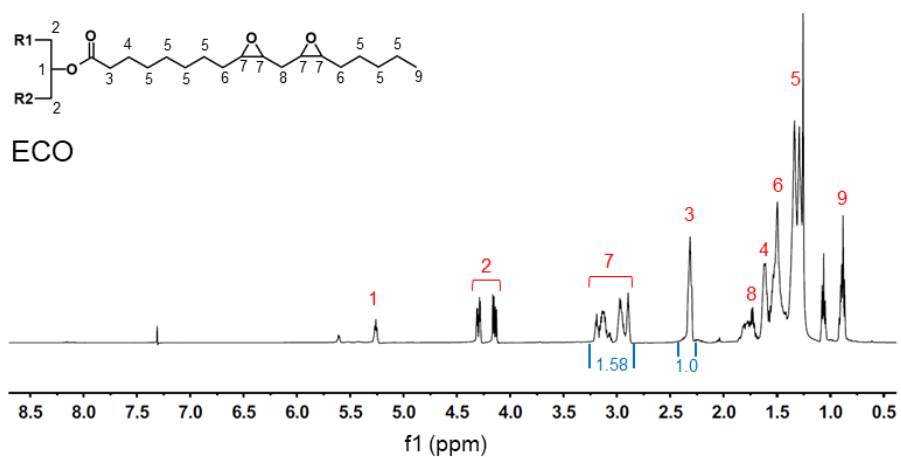
The synthesis of ECO and AECO was monitored by  $^1\text{H}$  NMR, and all peak assignments of protons were marked in Figure 3.3 and 3.4. Structural characterization of CO was previously confirmed by  $^1\text{H}$  NMR (Y. Li and Sun, 2015a), and estimation of functionality of ECO and AECO was based on the relative peaks of the NMR spectra, respectively. As shown in Figure 3.3, the peaks of the epoxide protons were observed at 2.9-3.2 ppm (peak 7) in the spectra of ECO after the epoxidation of CO, and typical triglyceride peaks at 5.26 ppm (peak 1, glycerol protons), 4.1-4.3 ppm (peak 2, glycerol protons), and 2.3 ppm (peak 3,  $\alpha$ -methylene proton) appeared in the

spectra of ECO (Habib and Bajpai, 2011; Y. Li and Sun, 2015a). The peak 7 in the spectra of ECO disappeared in the spectra of AECO (Figure 3.4) due to the acrylation reaction of ECO. The new peaks at 5.7-6.5 ppm (9 a-c in AECO spectra) represented the double bond of the acrylic groups of AECO. Following Eq. (2) and (3), the numbers of epoxy groups per molecule of ECO ( $N_e$ ) and acrylate groups per molecule of AECO ( $N_a$ ), respectively, were estimated using peak 3 as an internal standard (J. La Scala, 2002).

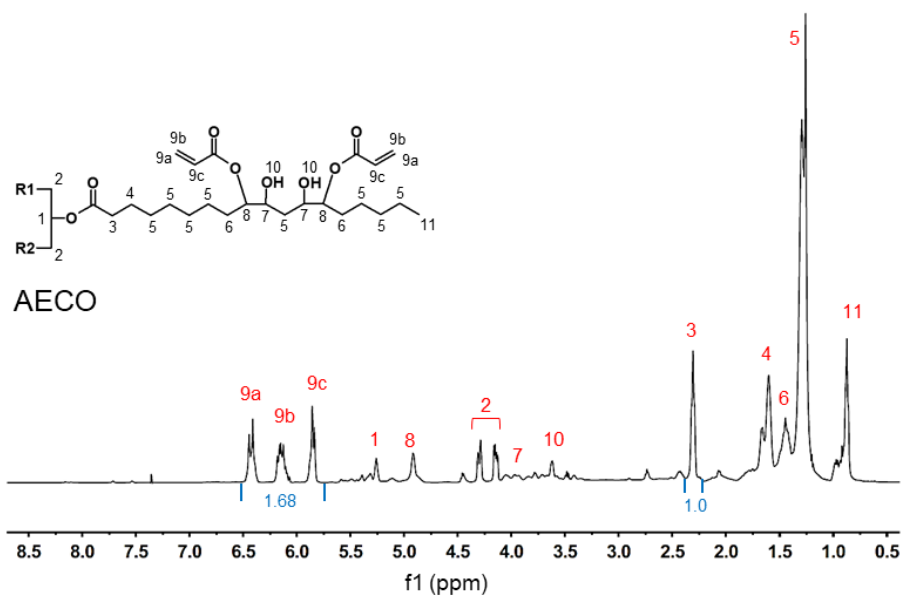
$$N_e = \frac{A_{2.9-3.2ppm}}{2A_{proton}} \quad (2)$$

$$N_a = \frac{A_{5.7-6.5ppm}}{3A_{proton}} \quad (3)$$

where  $A_{2.9-3.2ppm}$  and  $A_{5.7-6.5ppm}$  are the area of the corresponding peaks and noted in the spectra of ECO and AECO, respectively.  $A_{proton}$  is the area per  $\alpha$ -methylene proton per molecule, which was calculated by dividing the area of peak 3 by 6 (the number of protons per molecule for peak 3). From Eq. (2) and (3), the numbers of epoxy and acryl groups of ECO and AECO were calculated to be 4.74 and 3.36 per molecule, respectively. The epoxy content based on the NMR spectra was very similar to the measured epoxy content (4.78 per molecule) using the test method of ASTM D1652.



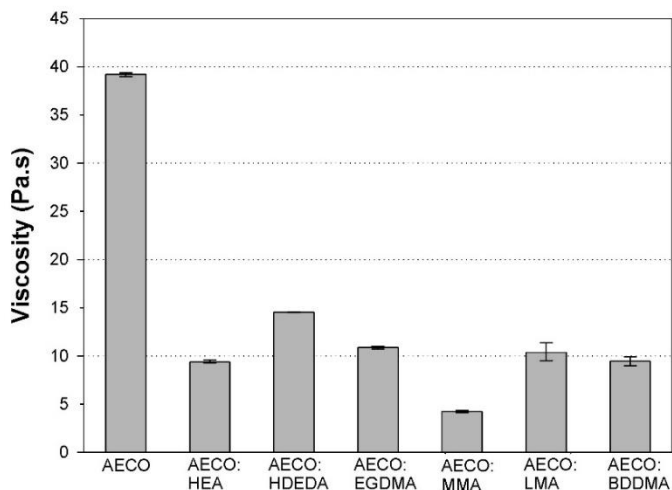
**Figure 3.3: NMR spectra of ECO.**



**Figure 3.4: NMR spectra of AECO.**

### 3.4.3. Viscosity of AECO resins with the RDs

AECO had an increased viscosity of 65.7 Pa·s at a shear rate of  $1 \text{ s}^{-1}$  while CO and ECO had a viscosity of 0.08 and 0.57 Pa·s at the same shear rate, respectively. The high viscosity of AECO was caused by an increased hydrogen bonding and dipole-dipole interaction due to the high polar hydroxyl and ester groups of the acrylic functionalized triglyceride (Y. Li and Sun, 2015a). The viscosity of neat AECO was decreased to 39.2 Pa·s with an addition of 3 wt% Darocur 1173 to the resin because the photoinitiator could act as a diluent due to its small molecular size. Viscosities of AECO resins containing various RDs (10 wt% of AECO) and the photoinitiator (3 wt% of total resin) are shown in Figure 3.5. The viscosities of the resins with the RDs were significantly reduced and varied by the molecular structures and the acryl functionalities of the RDs. The AECO:MMA resin has the lowest viscosity of 4.2 Pa·s because MMA structure was the smallest among the RDs contained with one methacrylate functional group. Similarly, HEA and LMA also had one acrylic functional group, however, the tail of hydroxyl group on HEA and the long aliphatic carbons of LMA could lead higher polarity of the resins and lower molecular mobility of the RDs into the resins. Therefore, AECO:HEA and AECO:LMA resins showed more than two times higher viscosity (9.4 Pa·s of AECO:HEA and 10.4 Pa·s of AECO:LMA) than that of AECO:MMA resin. The difunctional RDs such as HDEDA, LMA, and BDDMA led less reductions of the viscosity of AECO than that of MMA, and it is because the large number of acrylic functional groups of the RDs inhibited the mobility of the RDs into the AECO resins due to the increased intermolecular interaction between AECO and the RDs. In addition, HDEDA had the longest molecular chain and the highest molecular weight containing two acrylic functional groups. Therefore, AECO:HDEDA resin exhibited the highest viscosity (14.5 Pa·s) among all the AECO:RD resins.



**Figure 3.5: Viscosities of the AECO:RDs containing 3 wt% of Darocur 1173 at constant shear rate  $1 \text{ s}^{-1}$ .**

#### 3.4.4. Dynamic mechanical analysis of AECO:RDs polymers

Viscoelastic behaviors of AECO polymer and AECO:RDs copolymers were observed using DMA under oscillating force, and important properties of the analysis were summarized in Table 3.1. Tensile storage modulus ( $E'$ ) and  $\tan \delta$  of the polymers were plotted in Figure 3.6 and 3.7, and glass transition temperature ( $T_g$ ) of the polymers was determined as the temperature of the maximum height of  $\tan \delta$  plots. Crosslink density ( $\nu_e$ ) of the polymeric networks was estimated by using  $E'$  values in the rubbery region of the curves of  $E'$  (Figure 3.6.a and 3.7.a).  $E'$  at the temperature,  $T$  (100 °C greater than  $T_g$ ), was taken to calculate  $\nu_e$  following Eq. (4) (Asif et al., 2005; Sung et al., 2015).

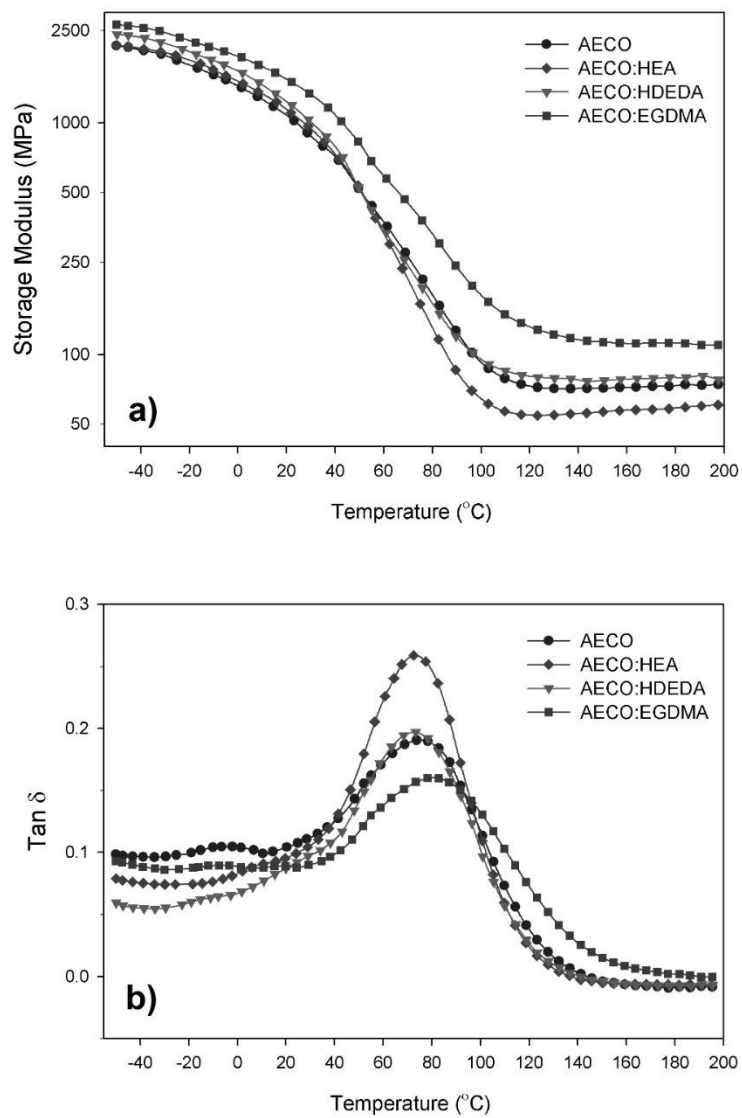
$$\nu_e = \frac{E'}{3RT} \quad (4)$$

where  $R$  is the gas constant, and  $T$  is the absolute temperature. The cured AECO including no RDs showed  $T_g$  of 75.1 °C and  $\nu_e$  of  $6.5 \text{ kmol m}^{-3}$ . Compared to the neat AECO polymer, AECO:HEA and AECO:MMA copolymers exhibited obviously low  $E'$  at the rubbery plateaus in

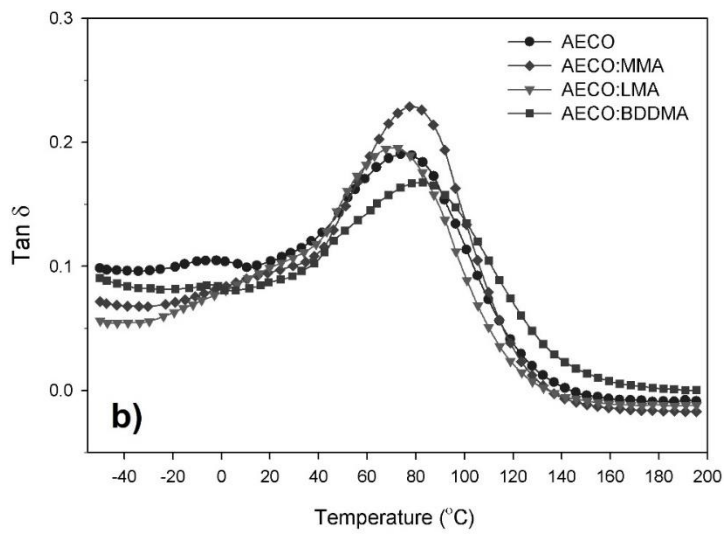
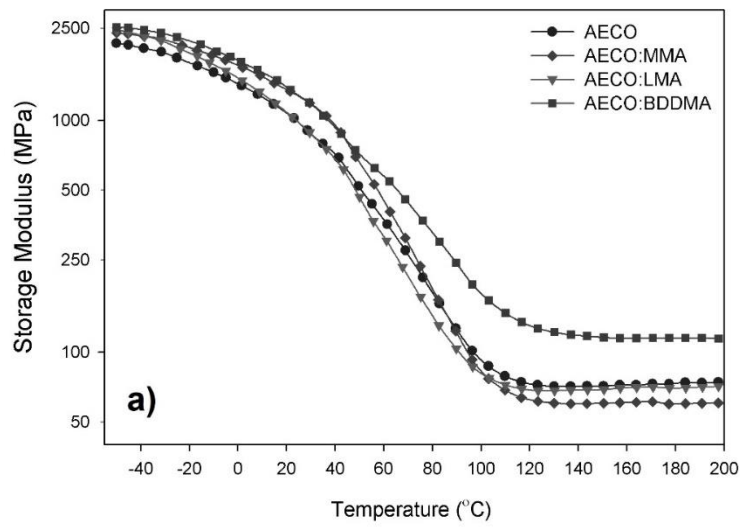
Figure 3.6.a and 3.7.a and large intensity of  $\tan \delta$  in Figure 3.6.b and 3.7.b. Otherwise, AECO formulated with EGDMA and BDDMA copolymers had very high  $E'$  at the rubbery region and low intensity of the damping factor. Therefore, AECO:HEA and AECO:MMA copolymers had loosely crosslinked networks, while the polymeric networks of AECO:EGDMA and AECO:BDDMA copolymers were compactly closed. For comparison with AECO:HEA copolymer ( $T_g$  of 72.9 °C),  $T_g$  of AECO:MMA copolymer was obviously greater (78.9 °C), while having a similarly loosely crosslinked system. This result indicates that MMA caused lower rotational mobility of the copolymer because the methyl group next to the vinyl group of the methacrylate could act as an anchor in the polymeric network under the oscillation forces during the DMA test. The three-dimensional effect of the methyl group on segment motion in crosslink networks was reported (Chattopadhyay et al., 2005). For the formulations of AECO with the monoacrylates RDs, the additions of HEA, MMA, and LMA onto AECO slightly reduced  $v_e$  of the AECO polymeric network to 5.2-6.4 kmol m<sup>-3</sup>. This result was expected because a copolymerization with monoacrylate can reduce  $v_e$  of acrylate polymers (Prandato et al., 2015). However,  $v_e$  of AECO and the difunctional RDs (HDEDA, EGDMA, and BDDMA) copolymers were improved in comparison with that of AECO polymer. Therefore, we know that the diacrylates RDs acted as a crosslink agent in addition to a diluent for the resin systems. In the case of the diacrylates,  $T_g$  and  $v_e$  of the cured AECO was significantly improved by incorporation of EGDMA (81.1 °C and 9.9 kmol m<sup>-3</sup>) and BDDMA (81.9 °C and 10.2 kmol m<sup>-3</sup>), respectively, but  $v_e$  of AECO:HDEDA copolymer (7.1 kmol m<sup>-3</sup>) was slightly higher than that of AECO polymer. This result suggests that the relatively short molecular chains of EGDMA and BDDMA compared to HDEDA caused more tightly crosslinked polymer networks.



It has been known that the narrower width of  $\tan \delta$  peak is associated with the increment in the homogeneity of polymer systems (H. Lu et al., 2001; B. S. Rao and Palanisamy, 2008), and diacrylates typically produce more heterogeneous polymeric networks than those of monoacrylates due to the different reactivity of the vinyl functional groups of the diacrylates (Anseth and Bowman, 1995; Dušek and Ilavský, 1975a; Dušek and Ilavský, 1975b). Here, the AECO might present a heterogeneous polymeric structure due its multi-functional groups. As compared to AECO polymer, significantly narrower glass transition regions were observed for the formulations of AECO with HEA, HDEDA, MMA, and LMA, respectively. (Figure 3.6.b and 3.7.b), as demonstrated with the half peak widths of  $\tan \delta$  peaks in Table 3.1. Interestingly, small monoacrylates such as HEA and MMA significantly improved homogeneity of the AECO-based polymers because AECO:HEA and AECO:MMA copolymers exhibited the much narrower half peak widths of  $\tan \delta$  peaks (56.5 and 61.6 °C, respectively) than that of AECO polymer (94.1 °C). This result indicates that the less functional groups on the more simple backbone structures of the RDs could increase the structural homogeneity of the polymers, as compared to AECO monomer. However, the half peak width of  $\tan \delta$  peak of AECO:EGDMA copolymer (89.6 °C) was not significantly smaller than that of AECO polymer (94.1 °C), and AECO:BDDMA copolymer showed the largest half peak widths of  $\tan \delta$  peaks (101.2 °C) among all the polymers. A heterogeneity of polymers can be caused by incompletely cured regions due to the trapped radicals, which are isolated in the highly crosslinked regions of polymer structures under curing (Kilambi et al., 2007; Wenand and McCormick, 2000). Therefore, the relatively heterogeneous networks of AECO:EGDMA and AECO:BDDMA copolymers compared to the other AECO:RDs copolymers could be due to their high values of  $v_e$ .



**Figure 3.6: Storage modulus (a) and tan  $\delta$  (b) of the cured AECO containing petrochemical RDs.**



**Figure 3.7: Storage modulus (a) and tan  $\delta$  (b) of the cured AECO containing bio-based RDs.**

**Table 3.1: Dynamic mechanical and tensile properties of the AECO:RDs polymers.**

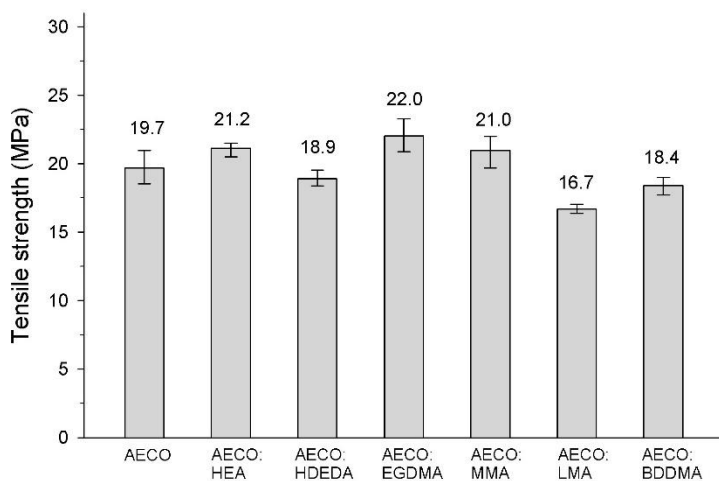
Samples	$T_g$ (°C)	Half peak width (°C)	Crosslink density (kmol m <sup>-3</sup> )	Tensile strength (MPa)	Elongation at break (%)
AECO	75.1	94.1	6.5	19.7±1.3	7.1±0.5
AECO:HEA	72.9	56.5	5.2	21.2±0.6	8.0±0.8
AECO:HDEDA	72.6	70.2	7.1	18.9±0.6	6.1±0.5
AECO:EGDMA	81.1	89.6	9.9	22.0±1.3	4.0±0.4
AECO:MMA	78.9	61.6	5.3	21.0±1.2	5.9±0.7
AECO:LMA	70.3	80.3	6.4	16.7±0.3	6.4±0.6
AECO:BDDMA	81.9	101.2	10.2	18.4±0.7	4.1±0.3

### 3.4.5. Tensile properties of AECO:RDs polymers

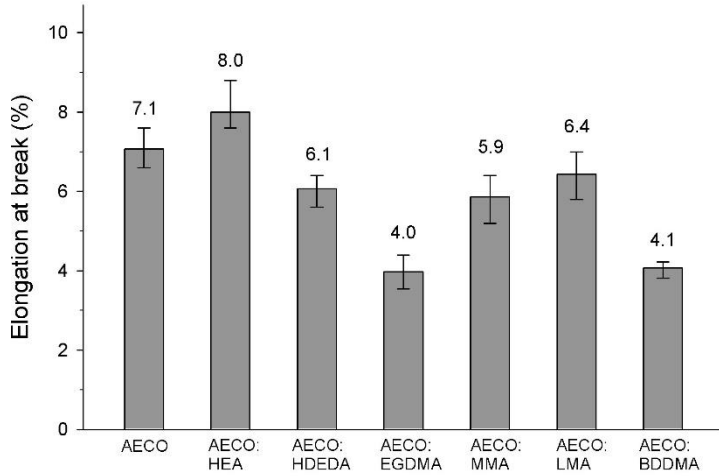
Tensile strength and elongation at break of UV-cured AECO and AECO:RD resins are shown in Figure 3.8 and 3.9, respectively, and summarized in Table 3.1. The elongation at break of all samples were at a range from 4 to 8%, thus the cured acrylates could be defined as rigid materials which generally shows elongation at break less than 7% (Dai et al., 2016). The AECO polymer had tensile strength of 19.7 MPa and elongation at break of 7.1%, and all the formulations with the RDs except HEA reduced the flexibility of the polymers. Compared to AECO, the AECO:RDs resins contained fewer numbers of the long and flexible aliphatic chains due to the lower compositions of triglycerides, and could result in the decreases of the flexibilities of the polymers. Therefore, the least reduction of the flexibility (0.7% below the elongation at break of AECO polymer) was obtained for AECO:LMA copolymer due to the long aliphatic side chain of LMA structure, and thereby the side chains could lead poor strength (tensile strength of 16.7 MPa) of the AECO:LMA copolymer among all the samples. Interestingly, only AECO:HEA copolymer had an improvement of elongation at break (8%) while the tensile strength (21.2 MPa) was slightly upgraded, as compared to AECO polymer. The additional hydroxyl group of HEA can increase the mechanical performance of the polymer due to the hydrogen bonds of the polymeric networks (Schuster et al., 2007a). However, the AECO:HEA copolymer rapidly lost the stiffness at the

elevated temperatures, as demonstrated with the slope of the glass transition region in Figure 3.6.a. The weak strength over mild temperatures can be due to the low bond energy of the hydrogen bonds in polymer networks (Schuster et al., 2007a).

Typically, highly crosslinked networks of polymers cause increases in brittleness and rigidity of the materials (Can et al., 2006). Thus, AECO:EGDMA and AECO:BDDMA copolymers showed the lowest elongations at break around 4%. However, AECO:EGDMA copolymer had significantly higher tensile strength (22 MPa) than that of AECO:BDDMA copolymers (18.4 MPa), while they exhibited very similar  $T_g$ ,  $v_e$ , and elongation at break. This result suggests that the less heterogeneous polymer structure of AECO:EGDMA resulted better toughness of the polymer, and it is in concurrence with that more homogeneous system is more rigid at the temperature below its  $T_g$  when they have similar  $T_g$  (Kilambi et al., 2009). Similarly, the upgraded tensile strength of AECO:MMA copolymer compared to that of AECO polymer also could be due to its higher homogeneity and  $T_g$  although AECO:MMA copolymer had lower  $v_e$ .



**Figure 3.8: Tensile strengths of AECO:RDs polymers**



**Figure 3.9: Elongations at break of AECO:RDs polymers**

### 3.4.6. Thermal degradation properties of AECO:RDs polymers

Thermal decomposition behaviors and stability factors of AECO polymer and AECO:RDs copolymers were obtained using TGA, and the TGA curves are shown in Figure 3.10 and 3.11. The values of  $T_{d,5\%}$  (the degradation temperature for 5% weight loss),  $T_{d,30\%}$  (the degradation temperature for 30% weight loss),  $T_{d,max}$  (the temperature of maximum degradation rate), and  $T_s$  (the statistic heat-resistant index) are tabulated in Table 3.2.  $T_s$  was calculated using Eq. (5) (Aouf et al., 2013; Lehrle and Williams, 1994).

$$T_s = 0.49[T_{d,5\%} + 0.6(T_{d,30\%} - T_{d,5\%})] \quad (5)$$

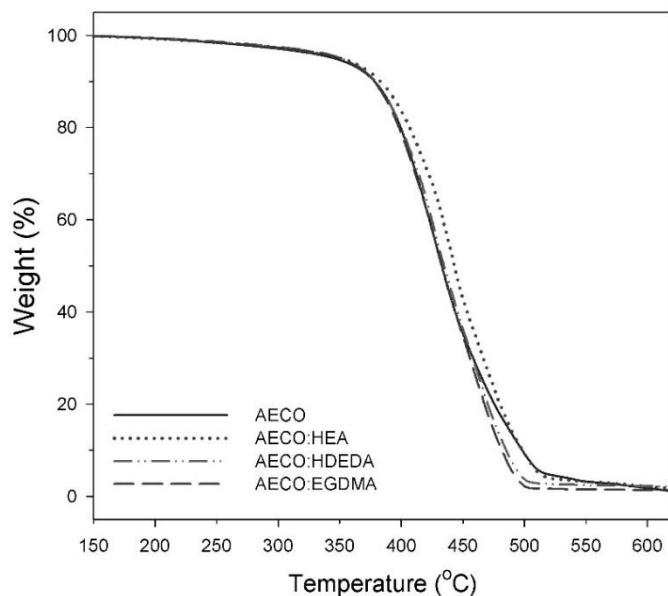
In Figure 3.10 and 3.11, all cured coating materials were stable under heating up to around 220 °C since most of weight (>99%) of the polymers remained. Then, unreacted monomers and oligomers in the crosslinked structures were firstly decomposed at a temperature range from 220 to 340 °C (C. Zhang et al., 2015), and major degradation stages, resulted from depolymerization of thermosets and char formation, were observed at a temperature range from 340 to 500 °C (K.

Liu et al., 2015). Overall,  $T_s$  of AECO polymer was slightly improved after being formulated with the RDs, and all the cured acrylates were thermally stable since  $T_s$  values of the cured acrylates were above 188, which was comparable to  $T_s$  values of thermally stable epoxy resin such as diglycidyl ether of bisphenol A (DGEBA) (S. Ma, Liu et al., 2014).

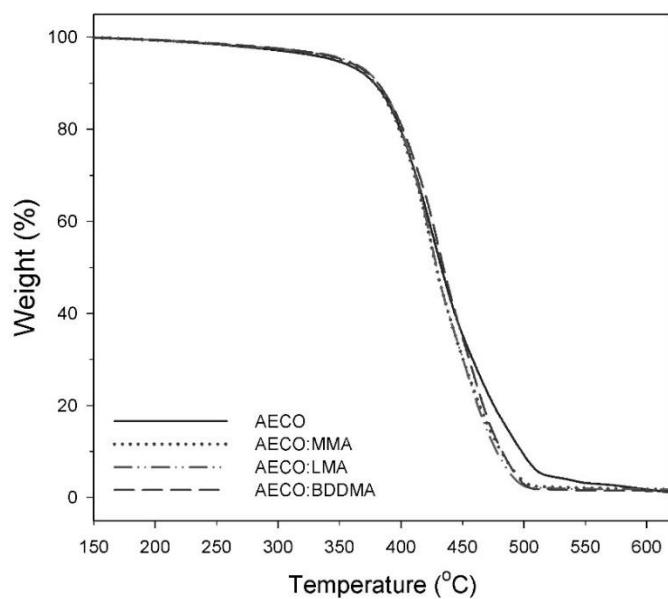
No significant differences among all the cured acrylates were observed at the first degradation stages, and all AECO:RDs copolymers showed higher  $T_{d,5\%}$  than that of AECO polymer (345.5 °C) at the initial of the major degradation stage. Although, however, AECO:HEA copolymer showed the least crosslinked networks, AECO:HEA copolymer had comparatively higher thermal stability at the temperature range of the rapid degradation, as demonstrated with the highest  $T_{d,30\%}$  (421.9 °C) and  $T_{d,max}$  (438.4 °C). In addition, the maximum  $T_s$  value (192.8) was also obtained for AECO:HEA copolymer. Herein, we know that other factors besides the crosslink density also influence the thermal stability of polymers; the thermal stability factors of crosslinked polymers are complicatedly affected by the polymeric network structure, crosslinking, chemical structure and composition, remaining polar groups, cohesive energy between molecular chains, and rigidity of molecular chains, etc. (Chattopadhyay et al., 2004; Kashiwagi et al., 1985).

**Table 3.2: Thermal stability factors of AECO:RDs polymers.**

Samples	$T_{d,5\%}$ (°C)	$T_{d,30\%}$ (°C)	$T_{d,max}$ (°C)	$T_s$
AECO	345.4	412.1	430.8	188.9
AECO:HEA	350.6	421.9	438.4	192.8
AECO:HDEDA	351.1	413.9	424.1	190.5
AECO:EGDMA	350.3	411.4	432.0	189.6
AECO:MMA	350.3	411.2	421.7	189.6
AECO:LMA	355.6	411.5	427.8	190.7
AECO:BDDMA	353.4	414.9	432.6	191.2



**Figure 3.10: Weight residues of AECO polymers containing petrochemical RDs as a function of temperature.**



**Figure 3.11: Weight residues of AECO polymers containing bio-based RDs as a function of temperature.**



### 3.4.7. Coating performance of AECO:RDs polymers

Coating performance of the cured AECO polymers on wood panels were measured in terms of MEK resistance, gloss, hardness, and adhesion (Table 3.3). Wood panels were also coated with two commercial wood finishes (PC and PU) as comparison targets, respectively. Gel contents of the AECO:RDs polymers were measured to estimate curing degree of the different polymers. The gloss of the coatings on wood panels was measured on 60 ° angle, and the gloss of AECO coating (88.9 °) were reduced by incorporations with the RDs. However, all the coatings showed high glossy coating surfaces without hazy regions. All the bio-based polymers showed excellent cured coating systems because the gel content of AECO and AECO;RDs polymers were maintained at a range of 96 to 97%. The RDs addition at 10 wt% to AECO did not significantly influence the gel content of AECO polymer. The gel content of PC and PU were not measured because free-standing films were not able to be made due to their strong adhesion on glass plates.

All the AECO-based coatings on wood panels showed excellent resistance to MEK rubs since all the coatings were not peeled from the panels or deformed after over 250 times of double rubs. However, both PC and PU coatings on wood panels were very weakened to MEK resistance (lower than 25 times of double rubs). After the MEK rub tests, the surfaces of the AECO-based coatings were slightly scratched, but were not visually deformed. The hardness and adhesion of the coatings after the MEK rub test remained the same. AECO:EGDMA coating showed the highest hardness of 4H, and other coatings containing the diacrylates RDs (HDEDA and BDDMA) had better hardness, as compared to AECO and AECO formulated with the monoacrylate RDs coatings. The result of the hardness is corresponding to the crosslink densities of the polymers; the polymers with higher crosslink density tend to show better hardness for coatings than that of the less crosslinked polymers. In contrast, AECO formulated with the diacrylates RDs coatings, which had

relatively higher crosslink densities and lower elongations at break than those of other coatings, showed the low adhesions on the wood surface because the cut areas of the brittle polymers were easy to be broken and removed from the substrate during cutting process in the adhesion test. Otherwise, the highest adhesions of the bio-based coatings were obtained for AECO:HEA and AECO:LMA copolymers, and it can be due to their relatively low crosslink density and  $T_g$ , which resulted less brittleness of polymer networks. In addition, the more polar groups such as hydroxyls in the AECO:HEA system can contribute to an increase in adhesion (Deka and Karak, 2009). After the MEK rub test, the adhesion strengths of AECO:EGDMA and AECO:BDDMA coatings were maintained at 2B, while other coatings had decreases in adhesion strengths. The result suggests that the high crosslink density and acryl functionality due to the addition of EGDMA and BDDMA into the AECO resins improved the solvent resistances of the coatings under the MEK rub test, and thereby the adhesion strengths of AECO:EGDMA and AECO:BDDMA coatings might not be significantly influenced by the solvent. Although PC and PU were damaged by the MEK rubbing, they exhibited better adhesion strengths on wood surface than that of the AECO-based coating materials.

**Table 3.3: Coating performance properties of AECO-based coatings. Hardness\* and adhesion\* were measured at 3 days after the MEK rub tests were performed on the coatings.**

Samples	Gloss (60°)	Gel contents (%)	MEK resistance	Hardness	Hardness*	Adhesion	Adhesion*
AECO	88.9	96.0	>250	2H	2H	3B	2B
AECO:HEA	82.9	96.0	>250	1H	1H	4B	3B
AECO:HDEDA	74.1	96.1	>250	3H	3H	2B	1B
AECO:EGDMA	87.0	96.6	>250	4H	4H	2B	2B
AECO:MMA	79.0	96.0	>250	2H	2H	3B	2B
AECO:LMA	78.6	96.8	>250	2H	2H	4B	3B
AECO:BDDMA	79.2	96.4	>250	3H	3H	2B	2B
PC	71.4		<25	2H		5B	
PU	93.1		<25	3H		4B	

### 3.5. Conclusion

Different mono- and di-functional (meth)acrylates derived from petroleum and bio-based resources were evaluated as reactive diluents to reduce the high viscosity of AECO and enhance the performance properties of AECO-based wood coating materials. The formulation of AECO with EGDMA successfully improved mechanical strengths (tensile strength and hardness) and thermal properties (crosslink density and  $T_g$ ) of AECO polymer, but the increase in brittleness of the copolymer resulted the reductions of the flexibility of the polymer and the adhesion strengths on wood surface. Contrariwise, AECO:HEA copolymer compared to AECO polymer showed the enhanced tensile strength and thermal stability although the flexibility was improved, and the highest adhesion of 4B was obtained for AECO:HEA copolymer among all the coating materials. The viscosity of AECO were mostly reduced by incorporation with MMA as a bio-based RD. In addition, the coating performance, mechanical properties, and thermal stability of AECO:MMA coating system were comparable to the neat AECO coating material. The results suggested that HEA and MMA are practical RDs to produce AECO-based resins for wood coating applications.

### 3.6. References

- Anseth, K. S., and Bowman, C. N. (1995). Kinetic gelation predictions of species aggregation in tetrafunctional monomer polymerizations. *Journal of Polymer Science Part B: Polymer Physics*, 33: 1769-1780.
- Aouf, C., Nouailhas, H., Fache, M., Caillol, S., Boutevin, B., and Fulcrand, H. (2013). Multi-functionalization of gallic acid. synthesis of a novel bio-based epoxy resin. *European Polymer Journal*, 49: 1185-1195.
- Asif, A., Shi, W. F., Shen, X. F., and Nie, K. M. (2005). Physical and thermal properties of UV curable waterborne polyurethane dispersions incorporating hyperbranched aliphatic polyester of varying generation number. *Polymer*, 46: 11066-11078.  
doi:10.1016/j.polymer.2005.09.046
- Aung, M. M., Yaakob, Z., Abdullah, L. C., Rayung, M., and Li, W. J. (2015). A comparative study of acrylate oligomer on jatropha and palm oil-based UV-curable surface coating. *Industrial Crops and Products*, 77: 1047-1052.
- Balanuca, B., Lungu, A., Hanganu, A., Stan, L. R., Vasile, E., and Iovu, H. (2014). Hybrid nanocomposites based on POSS and networks of methacrylated camelina oil and various PEG derivatives. *European Journal of Lipid Science and Technology*, 116: 458-469.
- Bongiovanni, R., Montefusco, F., Priola, A., Macchioni, N., Lazzeri, S., Sozzi, L., and Ameduri, B. (2002). High performance UV-cured coatings for wood protection. *Progress in Organic Coatings*, 45: 359-363.
- Bozell, J. J., and Petersen, G. R. (2010). Technology development for the production of biobased products from biorefinery carbohydrates—the US department of energy’s “Top 10” revisited. *Green Chemistry*, 12: 539-554.
- Campanella, A., La Scala, J. J., and Wool, R. P. (2009). The use of acrylated fatty acid methyl esters as styrene replacements in triglyceride-based thermosetting polymers. *Polymer Engineering & Science*, 49: 2384-2392.
- Campanella, A., Scala, J. J. L., and Wool, R. (2011). Fatty acid-based comonomers as styrene replacements in soybean and castor oil-based thermosetting polymers. *Journal of Applied Polymer Science*, 119: 1000-1010.
- Can, E., Wool, R., and Küsefoğlu, S. (2006). Soybean-and castor-oil-based thermosetting polymers: Mechanical properties. *Journal of Applied Polymer Science*, 102: 1497-1504.
- Chang, C., and Lu, K. (2013). Linseed-oil-based waterborne UV/air dual-cured wood coatings. *Progress in Organic Coatings*, 76: 1024-1031.
- Chattopadhyay, D., Panda, S. S., and Raju, K. (2005). Thermal and mechanical properties of epoxy acrylate/methacrylates UV cured coatings. *Progress in Organic Coatings*, 54: 10-19.
- Chattopadhyay, D., Rohini Kumar, D., Sreedhar, B., and Raju, K. (2004). Thermal stability and dynamic mechanical behavior of acrylic resin and acrylic melamine coatings. *Journal of Applied Polymer Science*, 91: 27-34.

- Cousinet, S., Ghadban, A., Fleury, E., Lortie, F., Pascault, J., and Portinha, D. (2015). Toward replacement of styrene by bio-based methacrylates in unsaturated polyester resins. *European Polymer Journal*, 67: 539-550.
- Dai, J., Liu, X., Ma, S., Wang, J., Shen, X., You, S., and Zhu, J. (2016). Soybean oil-based UV-curable coatings strengthened by crosslink agent derived from itaconic acid together with 2-hydroxyethyl methacrylate phosphate. *Progress in Organic Coatings*, 97: 210-215.
- Deka, H., and Karak, N. (2009). Bio-based hyperbranched polyurethanes for surface coating applications. *Progress in Organic Coatings*, 66: 192-198.
- Dušek, K., & Ilavský, M. (1975a). Cyclization in crosslinking polymerization. I. chain polymerization of a bis unsaturated monomer (monodisperse case). Paper presented at the *Journal of Polymer Science: Polymer Symposia*, , 53(1) 57-73.
- Dušek, K., & Ilavský, M. (1975b). Cyclization in crosslinking polymerization. II. chain polymerization of a bis unsaturated monomer (polydisperse case). Paper presented at the *Journal of Polymer Science: Polymer Symposia*, , 53(1) 75-88.
- Habib, F., and Bajpai, M. (2011). Synthesis and characterization of acrylated epoxidized soybean oil for UV cured coatings.
- Iskandarov, U., Kim, H. J., and Cahoon, E. B. (2014). *Camelina: An emerging oilseed platform for advanced biofuels and bio-based materials*. *Plants and BioEnergy* (pp. 131-140) Springer.
- Kagale, S., Koh, C., Nixon, J., Bollina, V., Clarke, W. E., Tuteja, R., Spillane, C., Robinson, S. J., Links, M. G., . . . Parkin, I. A. (2014). The emerging biofuel crop camelina sativa retains a highly undifferentiated hexaploid genome structure. *Nature Communications*, 5: 3706. doi:10.1038/ncomms4706 [doi]
- Kasetaite, S., Ostrauskaite, J., Grazuleviciene, V., Svediene, J., and Bridziuviene, D. (2014). Camelina oil-and linseed oil-based polymers with bisphosphonate crosslinks. *Journal of Applied Polymer Science*, 131
- Kashiwagi, T., Hirata, T., and Brown, J. E. (1985). Thermal and oxidative degradation of poly (methyl methacrylate) molecular weight. *Macromolecules*, 18: 131-138.
- Keske, C. M., Hoag, D. L., Brandess, A., and Johnson, J. J. (2013). Is it economically feasible for farmers to grow their own fuel? A study of camelina sativa produced in the western united states as an on-farm biofuel. *Biomass and Bioenergy*, 54: 89-99.
- Kilambi, H., Cramer, N. B., Schneidewind, L. H., Shah, P., Stansbury, J. W., and Bowman, C. N. (2009). Evaluation of highly reactive mono-methacrylates as reactive diluents for BisGMA-based dental composites. *Dental Materials*, 25: 33-38.
- Kilambi, H., Reddy, S. K., Schneidewind, L., Lee, T. Y., Stansbury, J. W., and Bowman, C. N. (2007). Design, development, and evaluation of monovinyl acrylates characterized by secondary functionalities as reactive diluents to diacrylates. *Macromolecules*, 40: 6112-6118.
- Kim, J. T., and Netravali, A. N. (2012). Non-food application of camelina meal: Development of sustainable and green biodegradable paper-camelina composite sheets and fibers. *Polymer Composites*, 33: 1969-1976.

- Kim, N., Li, Y., and Sun, X. S. (2015). Epoxidation of camelina sativa oil and peel adhesion properties. *Industrial Crops and Products*, 64: 1-8.
- Kreutzer, U. R. (1984). Manufacture of fatty alcohols based on natural fats and oils. *Journal of the American Oil Chemists' Society*, 61: 343-348.
- La Scala, J. (2002). The effects of triglyceride structure on the properties of plant oil-based polymers, PhD dissertation. University of Delaware,
- La Scala, J., and Wool, R. P. (2013). Fundamental thermo-mechanical property modeling of triglyceride-based thermosetting resins. *Journal of Applied Polymer Science*, 127: 1812-1826.
- Landry, V., Blanchet, P., and Riedl, B. (2010). Mechanical and optical properties of clay-based nanocomposites coatings for wood flooring. *Progress in Organic Coatings*, 67: 381-388.
- Lee, B., and Kim, H. (2006). Influence of isocyanate type of acrylated urethane oligomer and of additives on weathering of UV-cured films. *Polymer Degradation and Stability*, 91: 1025-1035.
- Lehrle, R. S., and Williams, R. J. (1994). Thermal degradation of bacterial poly (hydroxybutyric acid): Mechanisms from the dependence of pyrolysis yields on sample thickness. *Macromolecules*, 27: 3782-3789.
- Li, Y., and Sun, X. S. (2015a). Camelina oil derivatives and adhesion properties. *Industrial Crops and Products*, 73: 73-80.
- Li, Y., and Sun, X. S. (2015b). Synthesis and characterization of acrylic polyols and polymers from soybean oils for pressure-sensitive adhesives. *RSC Advances*, 5: 44009-44017.
- Liu, K., Madbouly, S. A., and Kessler, M. R. (2015). Biorenewable thermosetting copolymer based on soybean oil and eugenol. *European Polymer Journal*, 69: 16-28.
- Lu, H., Lovell, L. G., and Bowman, C. N. (2001). Exploiting the heterogeneity of cross-linked photopolymers to create high-T<sub>g</sub> polymers from polymerizations performed at ambient conditions. *Macromolecules*, 34: 8021-8025.
- Lu, H., Stansbury, J. W., Nie, J., Berchtold, K. A., and Bowman, C. N. (2005). Development of highly reactive mono-(meth) acrylates as reactive diluents for dimethacrylate-based dental resin systems. *Biomaterials*, 26: 1329-1336.
- Ma, S., Liu, X., Fan, L., Jiang, Y., Cao, L., Tang, Z., and Zhu, J. (2014). Synthesis and properties of a Bio-Based epoxy resin with high epoxy value and low viscosity. *ChemSusChem*, 7: 555-562.
- Mahendran, A. R., Wuzella, G., Aust, N., Kandelbauer, A., and Müller, U. (2012). Photocrosslinkable modified vegetable oil based resin for wood surface coating application. *Progress in Organic Coatings*, 74: 697-704.
- Meier, M. A. R., Metzger, J. O., and Schubert, U. S. (2007). Plant oil renewable resources as green alternatives in polymer science. *Chemical Society Reviews*, 36: 1788-1802.  
doi:10.1039/b703294c

- Mishra, V., Mohanty, I., Patel, M. R., and Patel, K. I. (2015). Development of green waterborne UV-curable castor oil-based urethane acrylate coatings: Preparation and property analysis. *International Journal of Polymer Analysis and Characterization*, 20: 504-513.
- Park, Y., Lim, D., Kim, H., Park, D., and Sung, I. (2009). UV-and thermal-curing behaviors of dual-curable adhesives based on epoxy acrylate oligomers. *International Journal of Adhesion and Adhesives*, 29: 710-717.
- Prandato, E., Livi, S., Melas, M., Auclair, J., Verney, V., Fleury, E., and Méchin, F. (2015). Effect of bio-based monomers on the scratch resistance of acrylate photopolymerizable coatings. *Journal of Polymer Science Part B: Polymer Physics*, 53: 379-388.
- Rao, B. S., and Palanisamy, A. (2008). Synthesis, photo curing and viscoelastic properties of triacrylate compositions based on ricinoleic acid amide derived from castor oil. *Progress in Organic Coatings*, 63: 416-423. doi:10.1016/j.porgcoat.2008.07.001
- Reddy, N., Jin, E., Chen, L., Jiang, X., and Yang, Y. (2012). Extraction, characterization of components, and potential thermoplastic applications of camelina meal grafted with vinyl monomers. *Journal of Agricultural and Food Chemistry*, 60: 4872-4879.
- Rengasamy, S., and Mannari, V. (2013). Development of soy-based UV-curable acrylate oligomers and study of their film properties. *Progress in Organic Coatings*, 76: 78-85. doi:10.1016/j.porgcoat.2012.08.012
- Rosli, W. W., Kumar, R., Zah, S. M., and Hilmi, M. M. (2003). UV radiation curing of epoxidized palm oil–cycloaliphatic diepoxide system induced by cationic photoinitiators for surface coatings. *European Polymer Journal*, 39: 593-600.
- Schuster, M., Turecek, C., Kaiser, B., Stampfl, J., Liska, R., and Varga, F. (2007a). Evaluation of biocompatible photopolymers I: Photoreactivity and mechanical properties of reactive diluents. *Journal of Macromolecular Science, Part A*, 44: 547-557.
- Schuster, M., Turecek, C., Mateos, A., Stampfl, J., Liska, R., and Varga, F. (2007b). Evaluation of biocompatible photopolymers II: Further reactive diluents. *Monatshefte Für Chemie-Chemical Monthly*, 138: 261-268.
- Schwalm, R. (2006). *UV coatings: Basics, recent developments and new applications* Elsevier.
- Sharmin, E., Zafar, F., Akram, D., Alam, M., and Ahmad, S. (2015). Recent advances in vegetable oils based environment friendly coatings: A review. *Industrial Crops and Products*, 76: 215-229.
- Shen, L., Li, Y., Zheng, J., Lu, M., and Wu, K. (2015). Modified epoxy acrylate resin for photocurable temporary protective coatings. *Progress in Organic Coatings*, 89: 17-25.
- Stanzione, J. F., Sadler, J. M., La Scala, J. J., and Wool, R. P. (2012). Lignin model compounds as Bio-Based reactive diluents for liquid molding resins. *ChemSusChem*, 5: 1291-1297.
- Sung, J., Li, Y., and Sun, X. S. (2015). Plasticization effects of dihydroxyl soybean oil improve flexibilities of epoxy-based films for coating applications. *Journal of Applied Polymer Science*, 132: 41773. doi:10.1002/app.41773
- van Bennekom, J. G., Venderbosch, R. H., and Heeres, H. J. (2012). Biomethanol from glycerol. Biodiesel-feedstocks, production and applications () InTech.

- Vendamme, R., and Eevers, W. (2013). Sweet solution for sticky problems: Chemoreological design of self-adhesive gel materials derived from lipid biofeedstocks and adhesion tailoring via incorporation of isosorbide. *Macromolecules*, 46: 3395-3405.
- Wang, Q., Chen, G., Cui, Y., Tian, J., He, M., and Yang, J. (2016). Castor oil based biethiol as a highly stable and self-initiated oligomer for photoinitiator-free UV coatings. *ACS Sustainable Chemistry & Engineering*, 5: 376-381.
- Wenand, M., and McCormick, A. V. (2000). A kinetic model for radical trapping in photopolymerization of multifunctional monomers. *Macromolecules*, 33: 9247-9254.
- Wool, R. P., and Sun, X. S. (2005). *Bio-based polymers and composites*. Burlington: Academic Press.
- Zhang, C., Yan, M., Cochran, E. W., and Kessler, M. R. (2015). Biorenewable polymers based on acrylated epoxidized soybean oil and methacrylated vanillin. *Materials Today Communications*, 5: 18-22.
- Zou, K., and Soucek, M. D. (2004). UV-Curable Organic-Inorganic hybrid film coatings based on epoxidized cyclohexene derivatized linseed oil. *Macromolecular Chemistry and Physics*, 205: 2032-2039.



## **Chapter 4 - Cardanol modified fatty acids from camelina oils for flexible bio-based acrylates coatings**

### **4.1. Abstract**

Novel bio-based acrylate was designed through the epoxy ring-opening reaction of cardanol glycidyl ether (CGE) with fatty acids from camelina oil (FACO), followed by epoxidation of unsaturated chains and then acrylation of the epoxides. Cardanol- and camelina oil-based acrylates were also respectively synthesized for comparison purposes. The bio-based acrylate coatings were then produced under UV-radiation from the acrylates monomers with an addition of a photo-initiator. Polymerization of the acrylates and synthesis of the monomers were observed using Fourier transform infrared (FTIR) spectroscopy, and the chemical structures and acryl contents of the acrylates were confirmed by proton nuclear magnetic resonance ( $^1\text{H}$  NMR). The mechanical and thermal properties of the cured acrylates were evaluated using tensile test, dynamic mechanical analysis (DMA), and thermogravimetric analysis (TGA). Observation of resistances to water, solvent, and hydrolytic degradation were conducted to water and toluene uptake test, methyl ethyl ketone (MEK) rub test, and a degradation test under sodium hydroxide solution. Gel content was measured to evaluate performance of the coatings, and other coating performances including gloss, adhesion, and pencil hardness were determined using the wood panel coated with the cured acrylates. Compared to acrylated epoxidized soybean oil (AESO) coating, the acrylate derived from the cardanol modified fatty acids showed higher tensile strength, hardness, glass transition temperature, thermal decomposition temperature at maximum degradation rate, and resistances to solvent and hydrolytic condition of the cured coating. Therefore, the newly designed acrylate is a great alternative to AESO

## 4.2. Introduction

Petroleum-based acrylic resins have mainly been used for UV-curing coatings (Schwalm, 2006). For example, epoxy acrylates, which are commonly based on diglycidyl ether bisphenol-A (DGEBA) (Kardar et al., 2009; Mohtadizadeh et al., 2015) and epoxy novolac (Chattopadhyay et al., 2005), are produced by epoxy ring-opening with acrylic acids. They are widely used for acrylic oligomers/monomers in UV-curable resins due to their good adhesion, hardness, and chemical resistance (Park et al., 2009; Shen et al., 2015). The process of UV-curing is still one of the important coating techniques in industries due to its low energy consumption, quick polymerization rate, selective curing area, and less volatile organic compound emission (Bongiovanni et al., 2002; Landry et al., 2008; Schwalm, 2006). In addition, thermally sensitive materials can be coated by the UV-curing system due to the radiation process at normal temperature (Sharmin et al., 2015). The photo-polymerization method has also been extensively used for paints, printing inks, adhesives, composites, and dental resins (Andrzejewska, 2001). Therefore, UV-curable sustainable alternatives to the petrochemicals are needed to reduce carbon emission and conserve natural resources (Meier et al., 2007). Due to the abundance of crops, and containing chemically active sites such as double bond and esters, vegetable oils are significant sustainable resources in polymers and coating industries (Sharmin et al., 2015; Wool and Sun, 2005). Soybean oil is one of the promising plant oils for bio-polymer applications in North America because of the large composition of unsaturated fatty acids with inexpensive and abundant crops (Z. Petrovic, 2008; Williams and Hillmyer, 2008). Acrylated epoxidized soybean oil (AESO) is commercially available and generally prepared by the ring-opening reaction of epoxidized soybean oil (ESO) with acrylic acids (J. La Scala and Wool, 2013; K. Liu et al., 2015; J. Lu et al., 2005), and it can be polymerized under UV-radiation using free-radical photoinitiators.

However, AESO is limited by its relatively low mechanical strength and glass transition temperature due to the flexible aliphatic chains of fatty acids (Dai et al., 2016; Zhan and Wool, 2010). Thus, AESO has been copolymerized with rigid petrochemical monomers such as styrene (Can et al., 2006; Fu et al., 2010), divinylbenzene (F. Li et al., 2001), and bisphenol-A (Can et al., 2002) to improve the mechanical and thermal properties. Recently, bio-based crosslink agents derived from itaconic acid (Dai et al., 2015; Dai et al., 2016), vanillin (C. Zhang et al., 2015), gallic acid (S. Ma et al., 2014a), and eugenol (K. Liu et al., 2015) were reacted with AESO to increase bio-contents and strength of the polymer. Mechanical strength and glass transition temperature of AESO polymer were successfully improved with increments of the bio-based additives; however, brittleness of the polymers was undesirably increased. In addition, using edible plant oils for producing polymers can cause a competition with food production. Therefore, developing UV-curable coating material derived from non-food resources is an interest of this research, and the new coating should exhibit better performances than AESO polymer does.

Cardanol, a major distillate from cashew nutshell liquid (CNSL), is an abundant and inexpensive agricultural byproduct from cashew nut production. Cardanol is a phenolic structure containing C<sub>15</sub> unsaturated aliphatic chain at *meta* position of the phenol (Balachandran et al., 2013; R. Liu et al., 2015). The aromatic structure with functional flexibility due to the reactive hydroxyl groups and unsaturated aliphatic carbons have been attractive for a wide range of applications such as coatings (Y. Choi et al., 2014; Darroman et al., 2015; Darroman et al., 2016; R. Liu et al., 2015), plasticizers (J. Chen et al., 2015; Greco et al., 2010; Hassouma et al., 2016), reactive diluents (J. Chen et al., 2015; Mi et al., 2012), synthetic resins (Hannoda et al., 2015; Jaillet et al., 2014; Jaillet et al., 2014), composites (Q. Chen et al., 2010; Maffezzoli et al., 2004; B. Rao and Palanisamy, 2011), surfactant (Dantas et al., 2009; Fontana et al., 2015; Tyman and Bruce, 2003), polyurethane

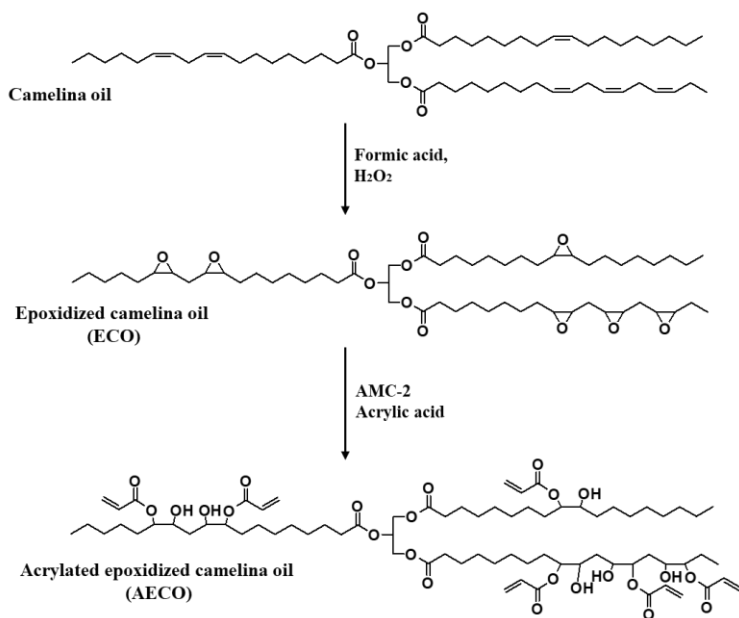
(Suresh and Kishanprasad, 2005; Suresh, 2012), nanocarrier (Bloise et al., 2014) and so on (Balachandran et al., 2013; Quirino et al., 2014). Cardanol glycidyl ether (CGE) can be produced by the reaction of cardanol with epichlorohydrin (J. Chen et al., 2015; Suresh and Kishanprasad, 2005), and it has been commercialized as a reactive diluent for coating resins by Cardolite Corporation (Newark, NJ) (R. Liu et al., 2015). The structure of CGE is shown in Scheme 1b. The CGE was directly used as a plasticizer for poly(vinyl chloride) (PVC), and it showed a potential to an alternative of petrochemical plasticizers in PVC applications due to its good mechanical and thermal properties with processibility (J. Chen et al., 2015). Cardanol-based diol has been synthesized by the ring-opening reaction of CGE with water, and a polyurethane was produced using the diol and diphenyl methane diisocyanate (Suresh and Kishanprasad, 2005). Chen et al. has reported CGE-based reactive diluent through epoxidation of the unsaturated chain of CGE for petroleum-based epoxy resins (J. Chen et al., 2015). The reactive diluent led improvements of mechanical and thermal performances of DGEBA polymer while the viscosity of the resin was significantly reduced. Additionally, CGE has been used to investigate branched and hyper-branched acrylates for UV-curing applications through modifications of CGE on bio-based and petroleum-based polyols, respectively (R. Liu et al., 2015; R. Liu et al., 2015). The cured hyper-branched acrylates showed better surface mechanical properties such as indentation hardness and surface storage modulus compared to petrochemical hyper-branched acrylate. The branched acrylates coatings also exhibited enhanced mechanical and coating functionalities compared to AESO coating, whereas viscosities of the cardanol-based acrylates were over fifteen times more than that of AESO.

Camelina (*Camelina sativa*) is a non-food oilseed crop, and cultivation of camelina has increased in the United States due to its application for biofuel (Iskandarov et al., 2014; Keske et

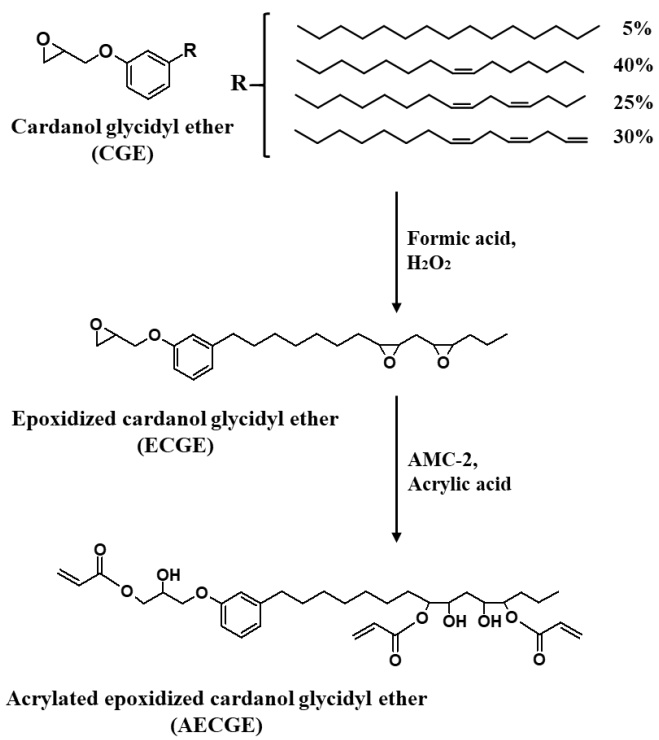
al., 2013). In comparison with common oilseed crops (e.g., soybean, canola, sunflower, and rapeseed), camelina is beneficial to agronomic conditions which are low water and fertilizer uses, adaptability to severe climates (e.g., cold and semiarid), ability to grow in marginal lands, and low requirements of herbicides and pesticides (Francis and Warwick, 2009; Iskandarov et al., 2014; Razeq et al., 2014). Camelina seed contains 36-47% oil, which is higher than 18-22% of oil in soybean (Moser, 2012). 90% of camelina oil (CO) is unsaturated fatty acids (5.8 double bonds per triglyceride), whereas soybean oil contains 84% unsaturated fatty acids (4.6 double bonds per triglyceride) (N. Kim et al., 2015; Y. Li and Sun, 2015a). Therefore, CO derivatives are expected to obtain higher functionality than that of soybean oil derivatives due to its higher degree of unsaturation (Y. Li and Sun, 2015a), and the structural benefits of CO are more suitable to strengthen the biopolymer. Even though camelina has a great potential as a natural resource of fuel and polymer, the camelina market is challenging, partly because of lack of high value co-products production (Y. Li and Sun, 2015a). A few applications such as composites (Balanuca et al., 2014) and polymers (Kasetaitė et al., 2014; N. Kim et al., 2015; Y. Li and Sun, 2015a) derived from CO have been reported.

As previously mentioned, developing high performance acrylate coatings derived from non-food resources was the objective of this study. Thus, acrylated epoxidized camelina oil (AECO) and acrylated epoxidized cardanol glycidyl ether (AECGE) were preliminarily synthesized through the synthesis routes shown in Scheme 4.1 and 4.2. First, epoxidized camelina oil (ECO) and epoxidized cardanol glycidyl ether (ECGE) were derived from CO and CGE, respectively, using hydrogen peroxide with formic acid. Then, AECO and AECGE were obtained by the ring-opening reaction of the epoxides with acrylic acid. The AECO and AECGE polymers showed better mechanical strength than that of AESO polymer, but the rigid polymers exhibited poor flexibilities.

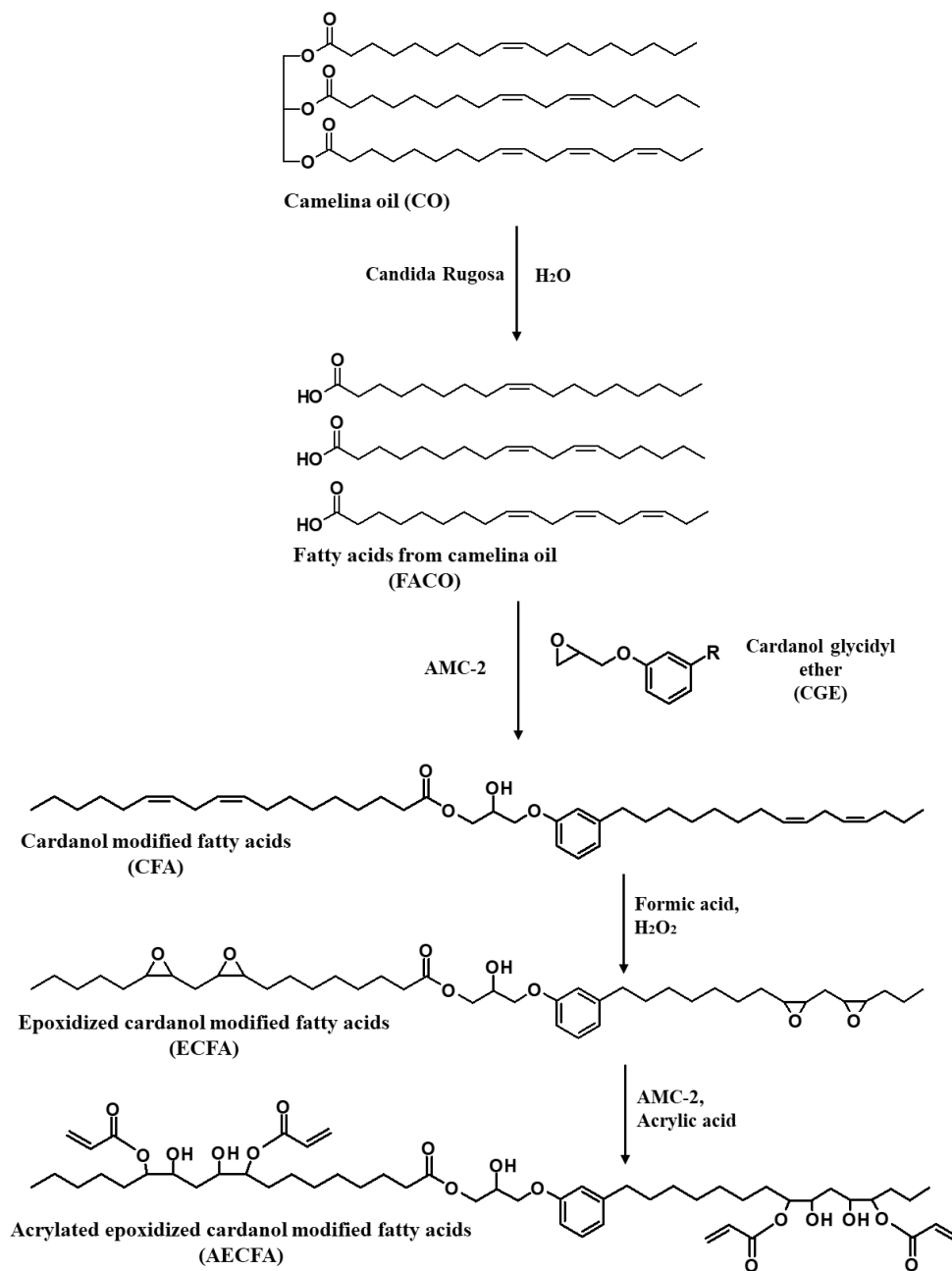
Therefore, cardanol modified fatty acids (CFA, Scheme 4.3) were designed to provide flexibility onto the phenolic structure through an addition of a flexible fatty acid chain. Acrylated epoxidized cardanol modified fatty acids (AECFA) was synthesized, followed by epoxidation of CFA and then acrylation of the epoxides. In this study, commercial AESO was used as a bench mark comparison target, and all acrylates were cured under UV-radiation. Mechanical properties of the cured acrylates were conducted by tensile test, and the coating performance in terms of water and solvent absorption, solvent resistance, gel content, hydrolytic degradation, gloss, adhesion on wood, and pencil hardness of the polymers were evaluated. Characterization methods including Fourier transform infrared (FTIR) spectroscopy, nuclear magnetic resonance ( $^1\text{H}$  NMR), thermogravimetric analysis (TGA), and dynamic mechanical analysis (DMA) were employed.



**Scheme 4.1: Synthesis route of AECO from camelina oil.**



**Scheme 4.2: Synthesis route of AECGE from CGE.**



**Scheme 4.3: Synthesis route of AECFA from camelina oil and CGE.**



## 4.3. Materials and Methods

### 4.3.1. Materials

Cardanol glycidyl ether (CGE) was donated by Cardolite Corporation (Newark, NJ). Camelina oil (CO) was supplied by Montana Gluten Free Processors (Belgrade, MT). Acrylated epoxidized soybean oil (AESO) was purchased from Sigma-Aldrich (St. Louis, MO). Darocur 1173 (2-hydroxyl-2-methyl-1-phenylpropan-1-one) was provided by BASF (Florham Park, NJ). AMC-2 (a 40-60% solution of chromium(III) 2-ethylhexanoate in a mixture of di(heptyl, nonyl, undecyl) phthalates) was supplied by Ampac Fine Chemicals (Rancho Cordova, CA). 0.1 N hydrogen bromide in acetic acid, formic acid (88 wt%), immobilized *Candida Rugosa* (>100 U/g), hydrogen peroxide (30 wt%), acrylic acid (>99 wt%), ethyl acetate, methyl ethyl ketone (MEK), toluene, ethyl ether, anhydrous magnesium sulfate, sodium bicarbonate, and hydroquinone were purchased from Sigma-Aldrich (St. Louis, MO) and Fisher Scientific (Waltham, MA).

### 4.3.2. Epoxidation and acrylation of camelina oil (ECO and AECO)

Epoxidation of CO was carried out according to our previous research with some modifications (N. Kim et al., 2015; Y. Li and Sun, 2015a). One hundred g of CO (0.112 mol) and 37.1 g of formic acid (88 wt%, 33.3 wt% of CO) was added to a 1000 mL of an Erlenmeyer flask placed in an ice/water bath with a magnetic stirrer. Then, 149.9 g of hydrogen peroxide (30 wt%, 1.323 mol) was gradually added to the flask, and the mixture was covered and stirred for 16 hours in the water bath without ice refills. To separate the organic layer from the water layer, 200 mL of ethyl acetate was added to the mixture using a separatory funnel at the end of the reaction. The product in the organic layer was washed by water and saturated sodium bicarbonate solution to remove the acid and hydrogen peroxide. The organic layer was dried over magnesium sulfate and

then filtrated by Celite. The ethyl acetate was evaporated using the rotary evaporator under vacuum at 45 °C, and 98.5 g of ECO was collected.

Acrylation of ECO was performed with a reaction of the epoxide with acrylic acid in the present of AMC-2 and hydroquinone as a catalyst and a free-radical polymerization inhibitor. 60 g of ECO (0.062 mol), 0.198 g of hydroquinone (0.33 wt% of ECO), and 1.2 g of AMC-2 were mixed in a 500 mL Erlenmeyer flask equipped with a magnetic stirrer. The ECO contained 4.8 epoxides per molecule, and 1.1 moles of acrylic acids per epoxide group was added to obtain a maximally acrylated monomer (J. La Scala and Wool, 2013). After the mixture temperature was maintained at 80 °C with an oil bath, 23.62 g of acrylic acid (0.328 mol) was separately added by a five-step addition at 0, 2, 4, 6, and 8 hours from the initial addition to prevent free radical polymerizations of acrylic acids. The reaction was continued for another 4 hours after the last addition of acrylic acid. The product was dissolved in ethyl ether at a separatory funnel, and the unreacted components such as excess of acids, catalyst, and inhibitor were then extracted by water and saturated sodium bicarbonate solution. Drying the organic phase was conducted by magnesium sulfate for water absorbing and Celite filtration for removing magnesium sulfate. After evaporating the solvent under vacuum at 50 °C, 60.5 g of product was obtained.

#### **4.3.3. Epoxidation and acrylation of cardanol glycidyl ether (ECGE and AECGE)**

Epoxidation of CGE was similarly performed as the synthesis of ECO. The process began with 150 g of CGE (0.42 mol) mixed with 56.82 g of formic acid (88 wt%, 33.3 wt% of CGE) in a 1000 mL Erlenmeyer flask placed in an ice/water bath. The mixture was stirred by a magnetic stirrer, and 171.6 g of hydrogen peroxide (30 wt%, 1.541 mol) was gradually added to the flask. The flask was capped and stirred for 16 hours in the water bath without ice refills. At the end of the reaction, 300 mL of ethyl acetate was added to the mixture in a separatory funnel to remove

the water layer of the mixture. The product was purified and concentrated by the same purification and drying procedure as the described above for ECO synthesis, and 157.2 g of ECGE was collected.

Using the stoichiometric reaction with acrylic acid (1.1 mol of acrylic acid per epoxide group), AECGE was prepared from ECGE. Then, 20 g of ECGE (0.0526 mmol, 2.39 epoxide groups per molecule) were added to a 125 mL Erlenmeyer flask equipped with a magnetic stirrer, and 0.066 g of hydroquinone (0.33 wt% of ECGE), and 0.4 g of AMC-2 were added to the flask. The mixture temperature was maintained at 80 °C with an oil bath, and 9.965 g of acrylic acid (0.138 mol) was separately added by three-step additions at 0, 2, and 4 hours from the initial addition. The mixture was additionally stirred for another 6 hours after the last addition of acrylic acid. At the end of the reaction, the product was purified with the ether extraction using water and saturated sodium bicarbonate solution, dried over magnesium sulfate, then filtered by Celite. After evaporating the solvent under vacuum at 50 °C, 20.1 g of AECGE was obtained.

#### **4.3.4. Synthesis of free fatty acids from camelina oil (FACO)**

Free fatty acids were prepared via a lipase-catalyzed hydrolysis of camelina oil using immobilized *Candida Rugosa*, the reaction temperature and the oil/water phase ratio was motivated by Chen's research (W. Chen et al., 2014). The hydrolysis of camelina oil was performed at a 250 mL in an Erlenmeyer flask. Phase ratio of the reaction mixture was 0.9 v/v (35 mL of CO and 38.9 mL of water), then the enzyme (3.59 g, 5 wt% of the oil/water mixture) was added. The reactor was capped and placed in an oil bath at 33 °C with magnetic stirring. The reaction time was 36 hours, and 150 mL of ethyl alcohol was then added to the mixture to dissolve the mixture. The enzyme was separated from the mixture using Celite filtration. Alcohol and water were removed by a rotary evaporator under vacuum at 80 °C. Two layers were observed, and 29 g

of the upper layer was collected as the product. This reaction and further synthetic routes of cardanol modified fatty acids epoxide and acrylate were described in Scheme 4.3.

#### **4.3.5. Synthesis of cardanol modified fatty acids (CFA)**

The epoxy ring of CGE was opened with FACO using AMC-2 as a catalyst, and a stoichiometric ratio of an epoxide group and a fatty acid was 1:1.1 (Scheme 4.3). Next, CGE (20 g, 56 mmol) and FACO (17.55g, approximately 61.6 mmol) were mixed with AMC-2 (0.2 g, 1 wt% of CGE) in a 125 mL of an Erlenmeyer flask equipped with a magnetic stirrer. The flask was capped and stirred in an oil bath at 100 °C for 24 hours. The product was dissolved in ethyl ether and then the unreacted FACO and the catalyst were washed using water and saturated sodium bicarbonate solution. The organic layer was dried over magnesium sulfate, filtered by Celite, and evaporated under vacuum at 50 °C. Then, 33.6 g of CFA was obtained.

#### **4.3.6. Synthesis of epoxidized cardanol modified fatty acids (ECFA)**

Using a 125 mL Erlenmeyer flask, 15 g of CFA (approximately 23 mmol) and 5.68 g of formic acid (88 wt%, 33.3 wt% of CF) were placed in an ice/water bath. Next, 19.98 g of hydrogen peroxide (30 wt%, 176 mmol) was gradually added to the flask, and the mixture was capped and stirred for 16 hours in the water bath without ice refills. At the end of the reaction, the water layer of the mixture was removed from the organic layer through adding 80 mL of ethyl acetate in a separatory funnel. The product in the organic layer was washed by water and saturated sodium bicarbonate to remove the acid and hydrogen peroxide. The solvent was dried over magnesium sulfate and then filtrated by Celite. The ethyl acetate was evaporated using the rotary evaporator under vacuum at 45 °C, and 13.8 g of ECFA was collected.

#### **4.3.7. Synthesis of acrylated epoxidized cardanol modified fatty acids (AECFA)**

To prepare AECFA, ECFA was reacted with acrylic acid in the presence of AMC-2 and hydroquinone as a catalyst and a free-radical inhibitor (Scheme 4.3). Next, 11.6 g of ECFA (approximately 17 mmol), 0.038 g of hydroquinone (0.33 wt% of ECFA), and 0.23 g of AMC-2 were mixed in a 125 mL Erlenmeyer flask equipped with a magnetic stirrer. The ECFA contained epoxy content of 7.4% by weight, and the mole ratio of oxirane to acrylic acid of 1:1.1 was used for the acrylation of ECFA. After the mixture temperature was maintained at 80 °C with an oil bath, 4.33 g of acrylic acid (60 mmol) was added by a four-step addition at 0, 2, 4, and 6 hours from the initial addition, respectively, and the reaction was continued for another 4 hours after the last addition of acrylic acid. Finally, the product was purified with the ether extraction using water and saturated sodium bicarbonate solution, dried over magnesium sulfate, then filtered by Celite. Twelve g of product was obtained after evaporating the solvent under vacuum at 50 °C.

#### **4.3.8. Preparation of UV-cured free-standing coating materials and coatings on wood**

The UV-curable acrylic resins were prepared by the addition of free-radical polymerization initiator Darocur 1173 (3 wt% of acrylate) to AESO, AECO, AECGE, and AECFA, respectively. The mixture was carefully heated using a heat gun, and it was mixed well with the aid of a vortex mixer and a sonicator. The mixture was spread over a glass panel using a film casting knife (BYK-Gardener USA, Columbia, MD) at 160  $\mu\text{m}$  wet thickness. The spread acrylic resin containing the photoinitiator was passed twice through a F300 UV system (1.8 kW, 6-in (300 W  $\text{in}^{-1}$ ) lamps) equipped with a LC6B benchtop conveyor (Fusion UV system, Gaithersburg, MD) at a conveyor rate of 10  $\text{ft min}^{-1}$ . The cured coating material was peeled from the glass and then stored for characterization of free-standing coating materials. The acrylic resin mixture was spread onto wood using a brush and then cured by the same UV system previously mentioned to obtain coatings

on wood (approximately 50  $\mu\text{m}$ ) for characterization of adhesion, pencil hardness, MEK resistance, and gloss.

#### 4.3.9. Measurements

Epoxy content was estimated according to the test method A of ASTM D 1652-97. The FTIR spectra were obtained by Perkin-Elmer Spectrum 400 FTIR spectroscopy (Waltham, MA). The spectra were monitored at a range from  $400\text{ cm}^{-1}$  to  $4000\text{ cm}^{-1}$  with  $4\text{ cm}^{-1}$  of resolution.  $^1\text{H}$  NMR was performed at room temperature using a Varian 600 MHz spectrometer with deuterated chloroform as a solvent.

TGA was performed with PerkinElmer Pyris 1 TGA (Norwalk, CT) to evaluate thermal stability of the cured coating materials. Under a nitrogen atmosphere, 9-10 mg of each sample was accurately weighed and heated from  $50\text{ }^\circ\text{C}$  to  $750\text{ }^\circ\text{C}$  at a rate of  $20\text{ }^\circ\text{C min}^{-1}$ . Next, DMA was acquired with TA DMA Q800 (New Castle, DE) equipped with a tension/film clamp to obtain viscoelastic properties of the cured coating materials. Specimens (2cm long, 1.27 cm wide, and 0.13-0.15 mm thick) were applied on the DMA, and the tests were conducted in 1 Hz of a frequency,  $15\text{ }\mu\text{m}$  of amplitude, and a heating range of  $-50\text{ }^\circ\text{C}$  to  $200\text{ }^\circ\text{C}$  at a rate of  $3\text{ }^\circ\text{C min}^{-1}$ . Glass transition temperature ( $T_g$ ) was obtained as a temperature of maximum  $\tan \delta$  peak, and calculation of crosslink density was based on elastic modulus on the rubbery region (Sung et al., 2015).

Mechanical properties of the coating materials were measured using a tensile tester (TT-1100, ChemInstruments, Fairfield, OH). Free-standing cured coating materials were cropped to 1.27 cm wide using a dual-blade shear cutter (JDC Precision Cutter 1000, Thwing-Albert Instrument Company, West Berlin, NJ) according to ASTM D 6287-09, and a strip of the sample was tested with 5.08 cm of initial grip separation and  $2.54\text{ cm min}^{-1}$  of a rate of grip separation. At least five

strips of each sample were conducted with the test, and tensile strength and elongation at break were obtained as the average of the three precision measurements.

The adhesion on wood was determined by a crosshatch cut test method according to ASTM D 3359-02, and the pencil hardness of the coatings (approximately 50  $\mu\text{m}$  thick) was obtained according to ASTM D 3363-00. The specular gloss of the coatings was measured using a glossmeter according to ASTM D523-14. The solvent resistance of the coatings on wood panels was measured according to the test method A of ASTM D5402-06 using MEK as a solvent. The coatings were rubbed with MEK-soaked cotton gauze, and the resistance was estimated as numbers of double rub (one forward and one backward motion). The solvent and water resistance of the cured acrylates were determined by uptake tests of the free-standing coating materials in film form according to 24 hours immersion in toluene and water, respectively. The cured coating film specimens (1.27 cm long and wide with 0.13-0.15 mm thickness) were weighed and then immersed in the liquids in vials, and the vials were covered and placed in the oven at 25 °C for 24 hours. At the end of the experiments, the solvent and water drops of the surfaces of the sample specimens were carefully removed by wiping using wipers without pressing the samples. Then, the samples were immediately weighed, and the difference between the weights of each sample before and after the immersions were obtained. Hydrolytic degradation test was similarly performed with 24 hours immersion in 1 M NaOH aqueous solution. The described specimens were weighed and soaked in the NaOH solution in vials, and the vials were covered and placed in the oven at 25 °C for 24 hours. The specimens were washed by distilled water after the certain period of time, and they were dried in the oven at 60 °C for 24 hours. The weight percent loss or gain of the hydrolytic degradation and water-solvent uptakes tests was determined by subtracting the weight of the tested sample from the initial weight and then multiplying 100. The gel content of the cured acrylates

film was measured by immersion test in toluene (Y. Li and Sun, 2015b; Vendamme and Eevers, 2013). The cured films (approximately 0.15 g) were immersed in 20mL of toluene for 10 days at room temperature. At the end of the tests, the samples were dried in an oven at 130 °C for 3 hours. The gel content was determined as the percentage values of the differences between the weights of the specimens before and after immersion in toluene, and averages of three precise measurements of each sample were obtained for accuracy.

## **4.4. Results and Discussion**

### **4.4.1. Material synthesis and structure characterization using FTIR spectra**

The C=C double bonds per one mole of camelina oil were estimated to be 5.8 (N. Kim et al., 2015), and 7.76 wt% of the average epoxy content (4.8 epoxides per mole) of ECO was measured after the epoxidation of camelina oil using formic acid and hydrogen peroxide. Then, acrylate functional groups were modified on camelina oil triglycerides through the ring-opening reaction of the epoxides of ECO with acrylic acids (Scheme 4.1), and the epoxy content of AECO was measured to be 0.3 wt%. The epoxidation and acrylation of camelina oil were monitored using FTIR spectra (Figure 4.1). The epoxidation of camelina oil was evidenced by the appeared peak of the C-O-C stretching of oxiranes at 822 cm<sup>-1</sup> and the disappeared peak of C-H stretching of C=C double bonds at 3010 cm<sup>-1</sup> in the FTIR spectra of camelina oil and ECO. The peak of C=O stretching of carbonyl groups of the triglyceride was remained at 1743 cm<sup>-1</sup> during the epoxidation of camelina oil. After the acrylation of ECO, the broad absorption band around 3450 cm<sup>-1</sup> indicated newly generated hydroxyl groups from the ring-opening of the epoxides, and the peak around 1721 cm<sup>-1</sup> represented C=O stretching of carbonyl groups of acrylates on AECO. In addition, the



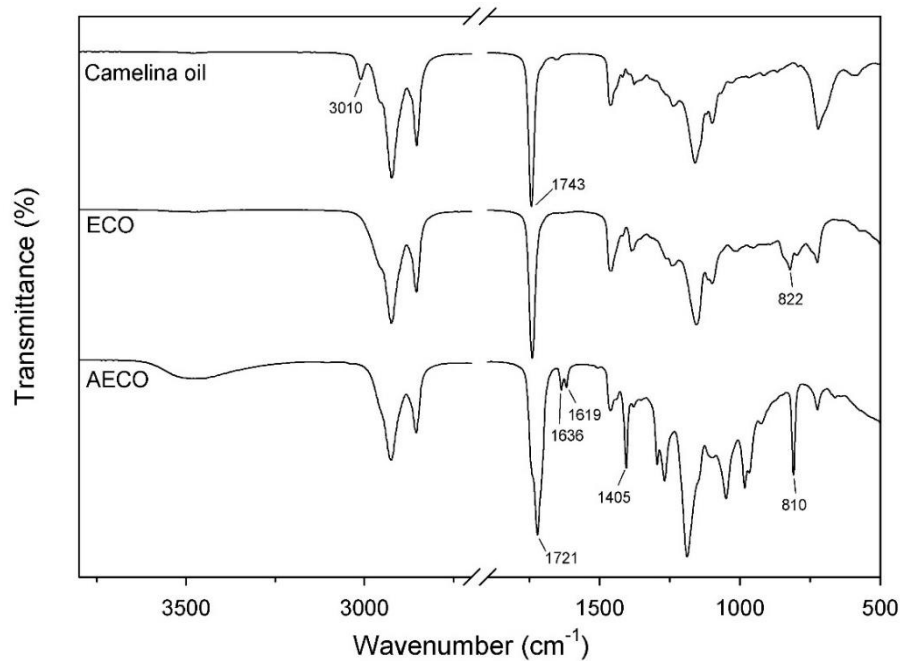
acrylation was strongly evidenced by the new peaks at 810, 1405, 1619, and 1636  $\text{cm}^{-1}$ , which represented C=C double bonds of acrylate groups of AECO.

The cardanol derivative, CGE, was modified to form ECGE and then AECGE through the same epoxidation and acrylation methods of ECO and AECO synthesis (Scheme 4.2). In the spectra of CGE (Figure 4.2), the peaks at 1450 and 1588  $\text{cm}^{-1}$  and the peaks at 1155 and 1260  $\text{cm}^{-1}$  were attributed to symmetric and asymmetric C=C stretching of benzene ring. The peaks at 776, 858, and 910  $\text{cm}^{-1}$  indicated the terminal epoxy group of CGE (J. Chen et al., 2015). The epoxy content of CGE was measured to be 4.24 wt% (approximately 0.95 epoxides per molecule), and C=C double bonds per one mole of CGE was estimated to be 1.8 from the provider. The peak of C-H stretching of C=C double bonds of the aliphatic chain at 3007  $\text{cm}^{-1}$  in the spectra of CGE were removed in the spectra of ECGE through the epoxidation of the side chain of CGE. Furthermore, the enlarged peaks of 844 and 776  $\text{cm}^{-1}$  of the spectra of ECGE were attributed to the vibration of oxirane groups on the aliphatic chain (J. Chen et al., 2015). The C=O stretching peak of acrylates at 1721  $\text{cm}^{-1}$  and the broad hydroxyl band around 3450  $\text{cm}^{-1}$  in AECGE spectra were generated by the acrylation of epoxides, and the peaks at 810, 1405, and 1636  $\text{cm}^{-1}$  also indicated C=C double bonds of acrylate groups of AECGE. The epoxy content of ECGE was measured to be 9.9 wt%, and it was reduced to 0.4 wt% in AECGE through the oxirane ring opening in the acrylation reaction.

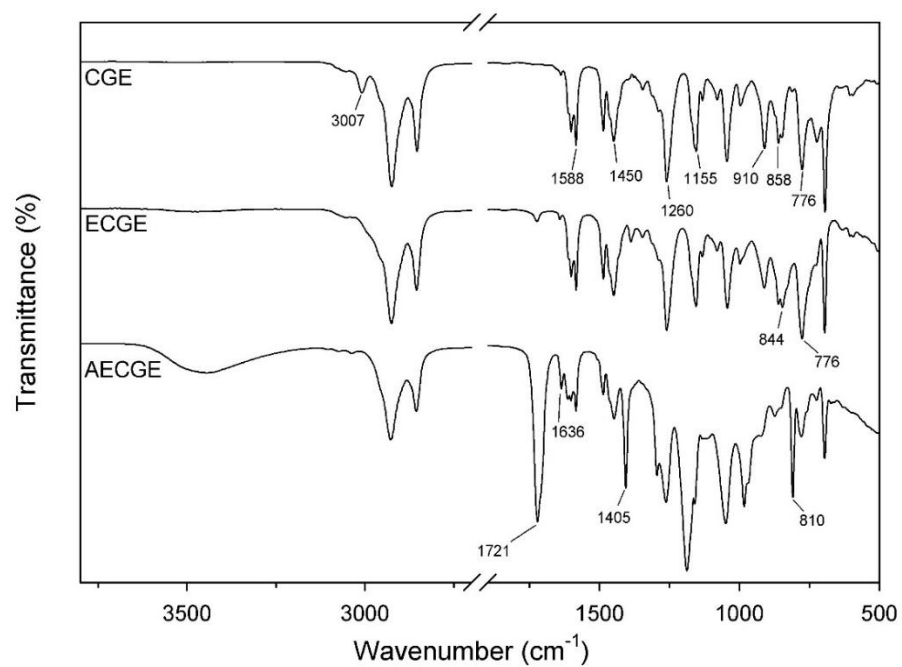
The FACO was derived from the lipase hydrolysis of camelina oil (Scheme 4.3), and the broad band from 2500 to 3500  $\text{cm}^{-1}$  of the spectra of FACO represented carboxylic acids of the free fatty acids (Figure 4.3). In addition, the C=O stretching peak shift from 1743 to 1708  $\text{cm}^{-1}$  in FACO spectra strongly indicated that most of triglycerides of camelina oil were formed to free fatty acids. The broad acid band and the C=O stretching peak of FACO at 1708  $\text{cm}^{-1}$  disappeared

in the spectra of CFA because the acid group of FACO was reacted with the terminal epoxide of CGE to form CFA through the epoxy ring-opening reaction in Scheme 4.3. The reaction of CGE and FACO was also strongly evidenced by the new C=O stretching peak of esters of CFA at 1740  $\text{cm}^{-1}$  and the O-H band around 3500  $\text{cm}^{-1}$  in CFA spectra. The terminal epoxy peak of CGE at 858  $\text{cm}^{-1}$  in CGE spectra (Figure 4.2) were obviously reduced by the reaction with FACO in CFA spectra (Figure 4.3), and 0.3 wt% of the epoxy content of CFA was measured. The peaks 1155, 1260, 1450, 1588, and 3010  $\text{cm}^{-1}$  of CFA indicated that the CFA structure included benzene rings and unsaturated aliphatic chains. After epoxidation of CFA, the peak of C=C double bonds of the aliphatic chain at 3010  $\text{cm}^{-1}$  in the spectra of CFA were removed in the spectra of ECFA. In addition, the peaks at 776, 822, and 844  $\text{cm}^{-1}$  in ECFA spectra were attributed to the oxirane groups on aliphatic chains, which were same as the peaks of ECO (822  $\text{cm}^{-1}$ ) and ECGE (776 and 844  $\text{cm}^{-1}$ ). In the spectra of AECFA, the new peaks of C=C double bonds of acrylates at 810, 1405, 1636  $\text{cm}^{-1}$  and the enlarged O-H band around 3500  $\text{cm}^{-1}$  were results from the acrylation reaction of epoxides. Finally, 7.44 wt% of epoxy content of ECFA were reduced to 0.3 wt% through the acrylation of ECFA.

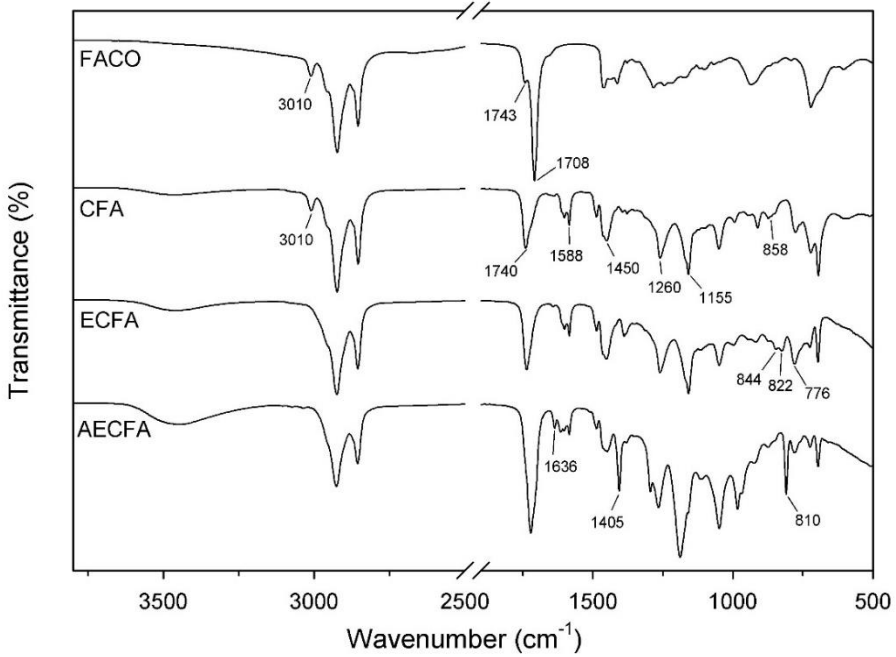
The AESO, AECO, AECGE, and AECFA resins were monitored by FTIR at before and after UV-curing (respectively, Figure 4.4, 4.5, 4.6, and 4.7). For example, the peaks of acrylic C=C double bounds shown at 810, 1405, and 1636  $\text{cm}^{-1}$  in AECFA spectra (Figure 4.7) and at 810, 1405, 1619, and 1636  $\text{cm}^{-1}$  in AESO spectra (Figure 4.4) were mostly disappeared after the resins were cured by the UV system.



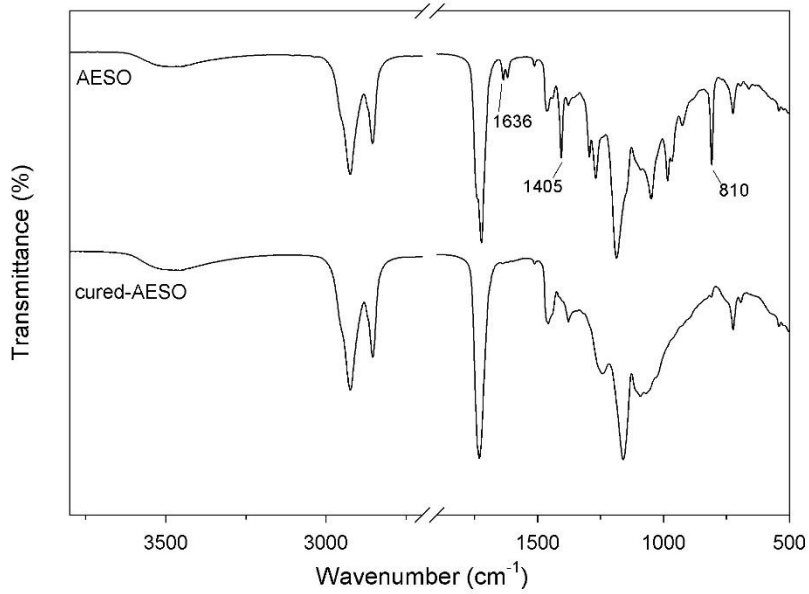
**Figure 4.1: FTIR spectra of AECO, ECO, and camelina oil.**



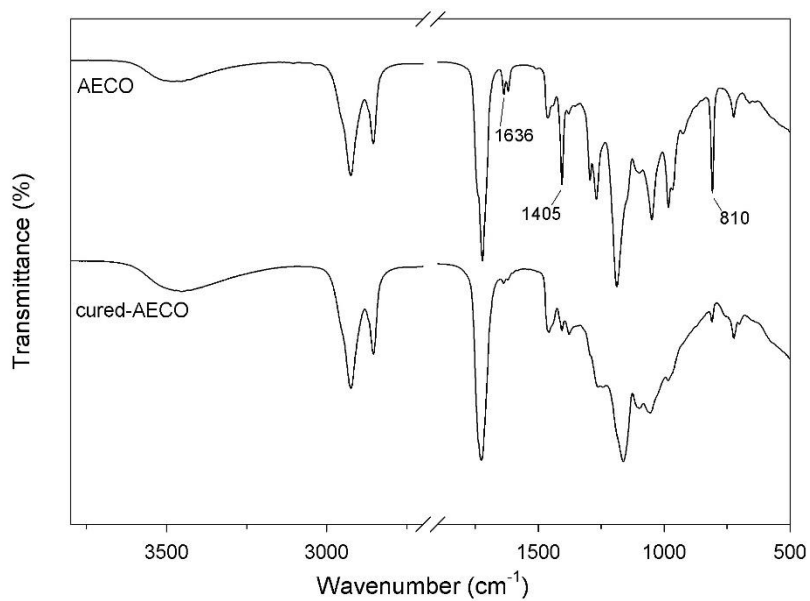
**Figure 4.2: FTIR spectra of AECGE, ECGE, and CGE.**



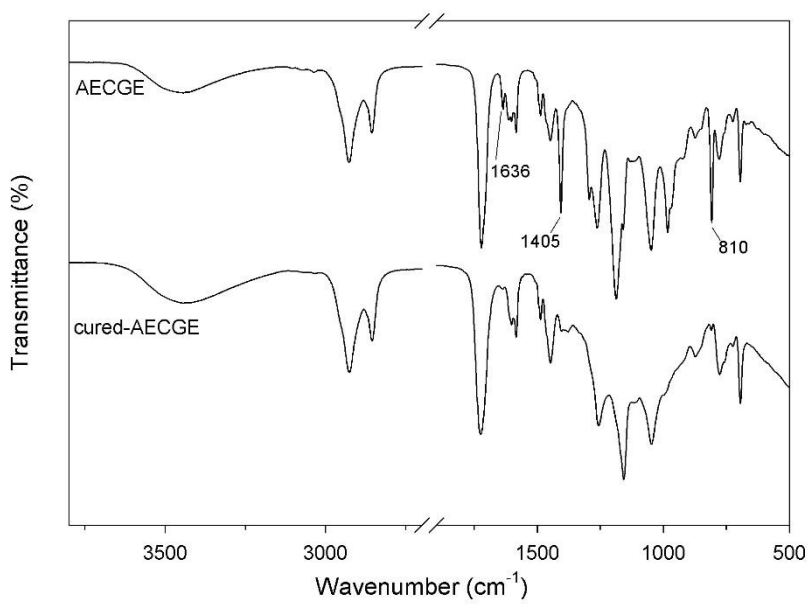
**Figure 4.3: FTIR spectra of AECFA, ECFA, CFA, and FACO.**



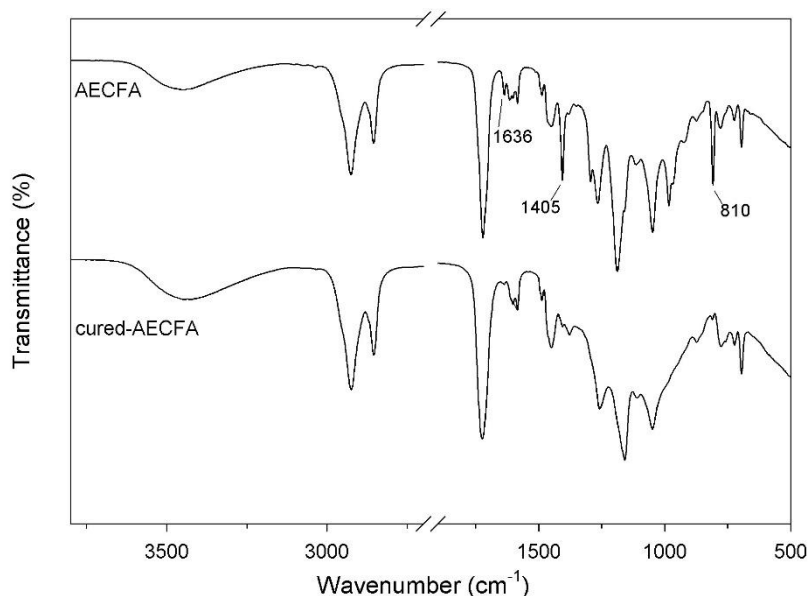
**Figure 4.4: FTIR spectra of AESO and cured-AESO.**



**Figure 4.5: FTIR spectra of AECO and cured-AECO.**



**Figure 4.6: FTIR spectra of AECGE and cured-AECGE.**



**Figure 4.7: FTIR spectra of AECFA and cured-AECFA.**

#### 4.4.2. NMR spectra analysis and acrylate functionalities of the bio-based acrylates

The structural characterization of AECO, AECGE, and AECFA (Figure 4.8, 4.9, and 4.13, respectively) and AECFA intermediates (Figure 4.10, 4.11, and 4.12, respectively) were confirmed by  $^1\text{H}$  NMR, and all peak assignments of protons were marked in the figures as well as used to estimate acrylate functionality of the resins. As shown in Figure 4.8, AECO had several typical peaks of triglyceride such as the peaks of glycerol protons at 5.25-5.4 ppm (peak 1) and at 4.1-4.35 ppm (peak 2), and the peak of the  $\alpha$ -methylene proton at 2.3 ppm (peak 3) (Habib and Bajpai, 2011; Y. Li and Sun, 2015a). In AECGE spectra (Figure 4.9), the peaks of the aromatic protons at 6.7-7.2 ppm (peak 1-3) and the peak of the methylene proton in  $-\text{CH}_2\text{-Ar}$  group at 2.55 ppm (peak 4) indicated the phenolic structure containing the aliphatic chain of AECGE (Suresh, 2012). Successful acrylation for AECO and AECGE synthesis was confirmed by the three peaks at 5.7-6.5 ppm, which represented the protons in the vinyl groups of the acrylates (peak 9 a-c of AECO

(Figure 4.8) and peak 15 a-c of AECGE (Figure 4.9), respectively (Y. Li and Sun, 2015a; R. Liu et al., 2015).

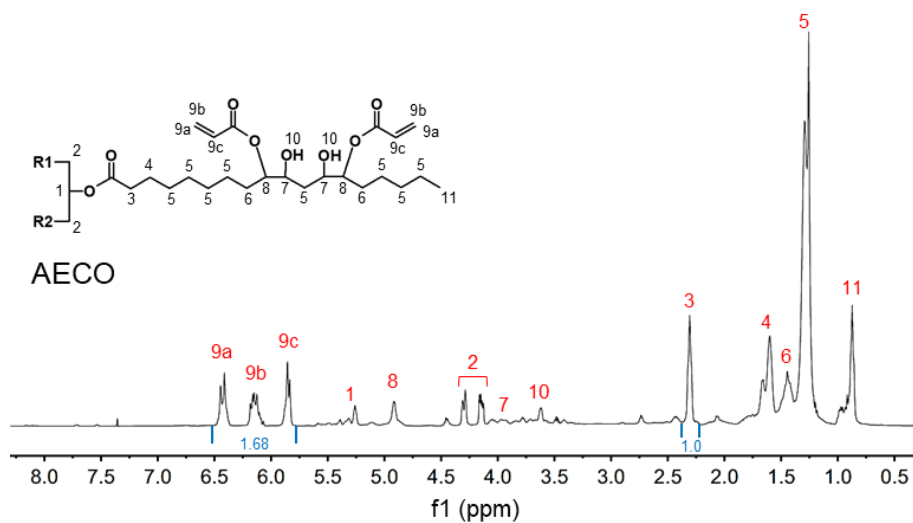
The unsaturated aliphatic chain of FACO was presented at peak 4 (at 2.06 ppm, allylic methylene protons), peak 5 (at 5.35 ppm, olefinic protons), and peak 6 (2.8 ppm, double allylic protons) in the spectra of FACO (Figure 4.10). After the reaction of FACO with CGE, the structure of CFA was strongly evidenced by the new peaks of at 3.9-4.3 ppm (peak 12-14) in Figure 4.11 that were attributed to protons of the glycerol as a result of epoxy ring-opening reaction with acid (Jaillet et al., 2014). After epoxidation of CFA, the peaks of the epoxide protons appeared at 2.8-3.2 ppm (peak 8) in the spectra of ECFA (Figure 4.12) and disappeared after acrylation. The new three peaks located at 5.7-6.5 ppm (peak 17 a-c) in the spectra of AECFA (Figure 4.13), indicating the double bond of the acrylate groups.

The number of acrylate groups ( $N_a$ ) in AECO, AECGE, and AECFA were estimated following Eq. (1) using methylene proton as internal standard (J. La Scala, 2002):

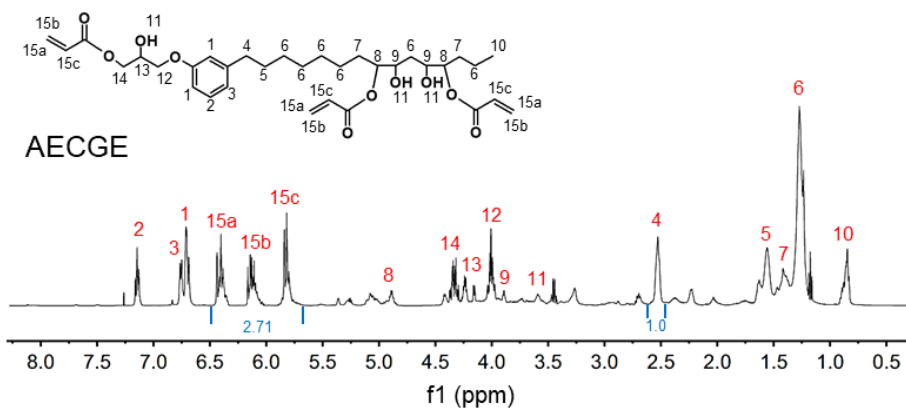
$$N_a = \frac{A_{5.7-6.5ppm}}{3A_{proton}} \quad (1)$$

Where  $A_{5.7-6.5ppm}$  is the area of the corresponding peak and noted in the spectra. In the case of AECO (Figure 4.8),  $A_{proton}$  is the area per peak 3 (internal standard) per molecule that was calculated by dividing the area of peak 3 by the number of the protons per molecule (i.e., 6 protons for peak 3). In Figure 4.9 and 4.13, the values of  $A_{proton}$  for AECGE and AECFA were respectively estimated by dividing the area of peak 4 as the internal standard by 2 (the number of the protons for peak 4) per molecule. From Eq. (1), the acrylate functionalities of AECO, AECGE, and AECFA were calculated to be 3.36, 1.81, and 2.25 per molecule, respectively. Then, acryl conversion rates were calculated from the acryl functionality based on the measured epoxy content;

the conversion rates of 70.3, 75.7, and 68.8 % were obtained for AECO, AECGE, and AECFA, respectively.



**Figure 4.8: NMR spectra of AECO.**



**Figure 4.9: NMR spectra of AECGE.**



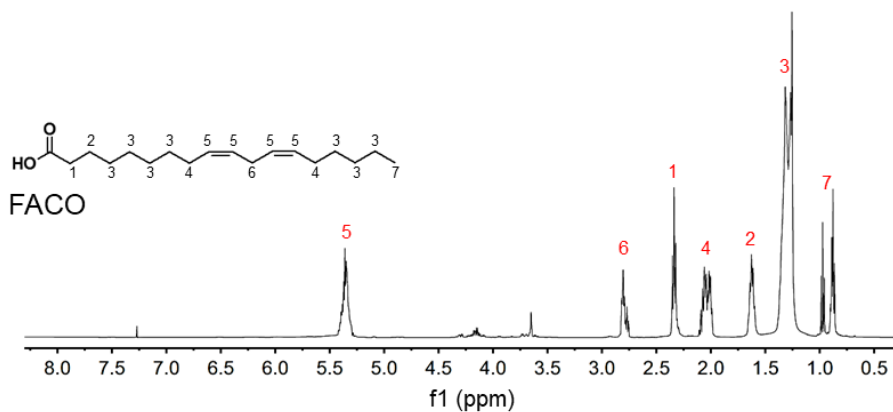


Figure 4.10: NMR spectra of FACO.

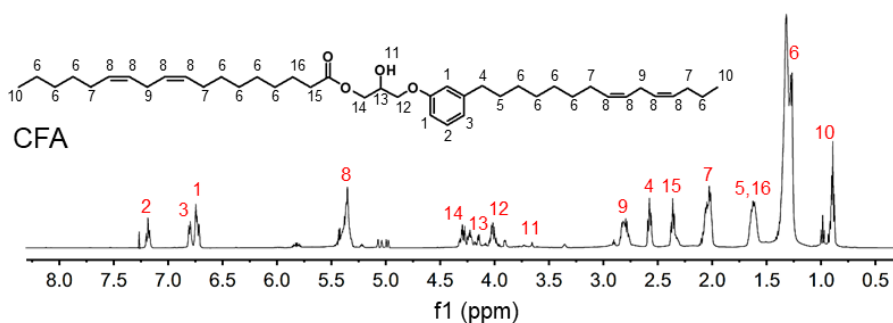


Figure 4.11: NMR spectra of CFA.

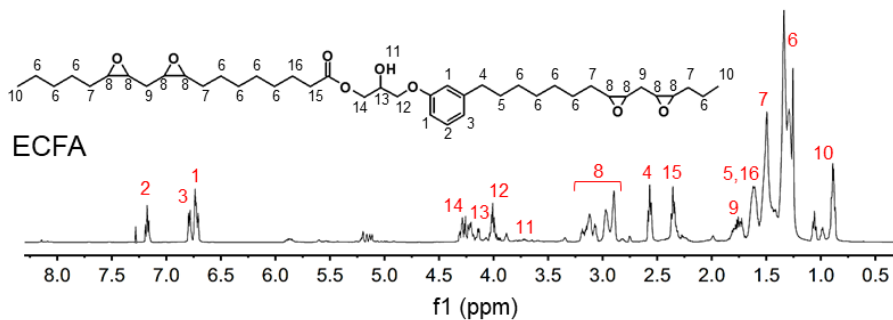
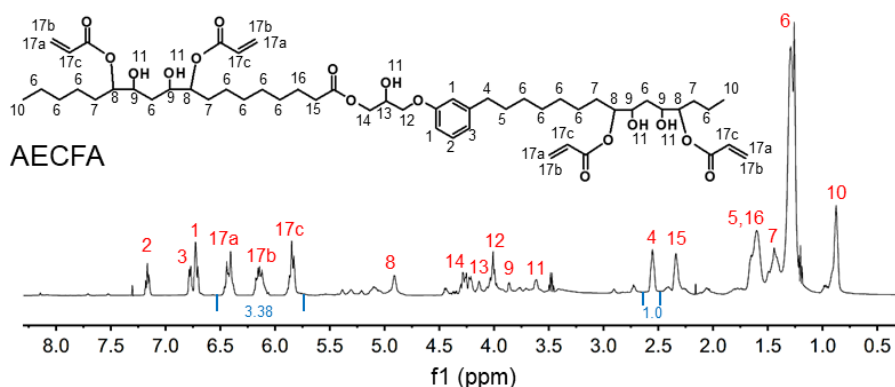


Figure 4.12: NMR spectra of ECFA.



**Figure 4.13: NMR spectra of AECFA.**

#### 4.4.3. Bio-based content of the coating materials

The United States Department of Agriculture (USDA) defines bio-based product as “a commercial product excluding food and fuel is derived from plants or other renewable feedstocks, and composed in whole or in significant part of biological products”. Therefore, a minimum bio-based content is required criteria to obtain USDA Certified Bio-based Product Label for the product. International standards such as ASTM D6866 and ISO 16620 have been established for the examination of the bio-based content. USDA specifies that product testing is conducted following ASTM D6866, which defines the bio-based content as “a percent of the mass of the bio-based carbon in the total organic carbon of the product” (Dai et al., 2015; Kunioka et al., 2014). Thus, 100% bio-based content was obtained for AESO and AECO, respectively, since acrylic acid can be produced from renewable resources such as 3-hydroxypropionic acid (Ondrey, 2014). The bio-based content of AECGE and AECFA were calculated to be 90.9 and 94.4%, respectively, because CGE was typically produced by epoxidation of cardanol with epichlorohydrin that was regarded as a petrochemical (J. Chen et al., 2015; Suresh and Kishanprasad, 2005).

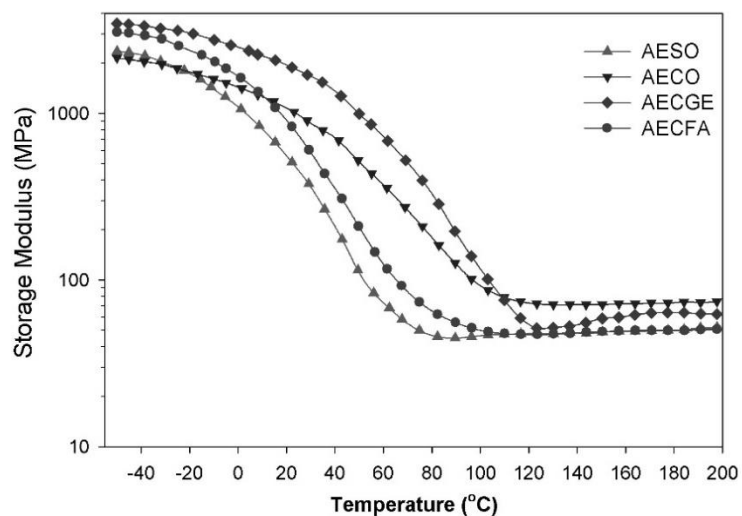
#### 4.4.4. Dynamic mechanical properties

Dynamic mechanical properties of UV-cured samples were measured using DMA, and storage modulus ( $E'$ ) and  $\tan \delta$  are plotted as a function of temperature in Figure 4.14 and 4.15, respectively.  $T_g$  of the cured polymers were determined as the temperature of the peaks of the  $\tan \delta$  curves in Figure 4.15. Since all plots of  $E'$  reached at rubbery states at high temperatures (above 150 °C) in Figure 4.14,  $E'$  at 100 °C greater than  $T_g$  in the rubbery plateau region were used to estimate the crosslink densities ( $\nu_e$ ) following Eq. (2) (Asif et al., 2005; Sung et al., 2015):

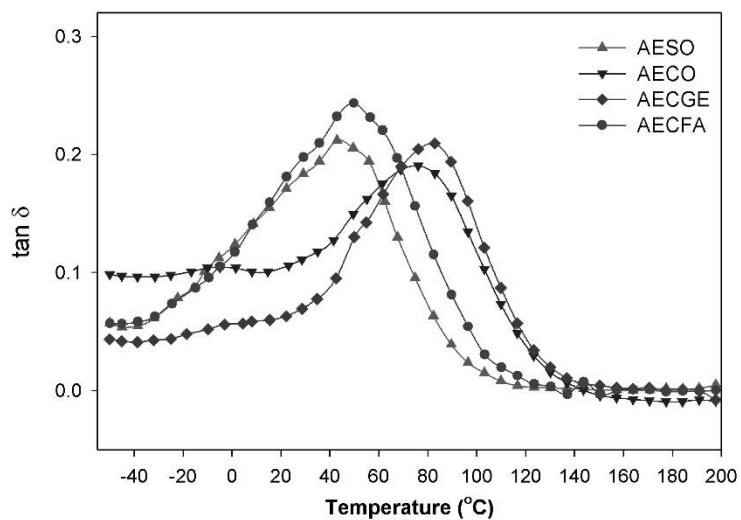
$$E' = 3\nu_e RT \quad (2)$$

where  $R$  is the gas constant and  $T$  is the absolute temperature.

Table 4.1 shows  $E'$  at 25 °C,  $T_g$ , and  $\nu_e$ . Obviously, the highest  $E'$  at 25 °C (1820 MPa) and  $T_g$  (81.9 °C) were obtained for AECGE polymer, and  $E'$  of AECGE polymer were higher than that of AESO, AECO, and AECFA polymers at both glass and glass transition regions in Figure 4.14. These results were expected because aromatic structures enhance rigidity of polymer networks as rotational mobility of the polymer decreases, which contribute to improvements of  $E'$ ,  $T_g$ , and strength of polymer (Stanzione III et al., 2012). The AECFA polymer also showed higher  $E'$  at 25 °C (737 MPa) and  $T_g$  (52.7 °C) than those of AESO polymer (457 MPa and 46.9 °C) even though AECFA and AESO polymers had same  $\nu_e$  of 4.6 kmol m<sup>-3</sup>. This result may be due to the rigid benzene rings of AECFA polymer. In comparison between the two triglyceride-based acrylates (AECO and AESO), AECO polymer exhibited obviously higher  $E'$  at all regions,  $\nu_e$ , and  $T_g$  relative to AESO polymer shown in Figure 4.14 and 4.15. This can be explained by that AECO may contain more functional groups than that of AESO due to the higher unsaturation of the triglyceride structure. The higher functionality of AECO, compared to AESO, could lead to a more tightly-crosslinked network.



**Figure 4.14: Storage modulus of AESO, AECO, AECGE, and AECFA as a function of temperature.**



**Figure 4.15:  $\tan \delta$  of AESO, AECO, AECGE, and AECFA as a function of temperature.**

**Table 4.1: Thermal and mechanical properties of the AESO, AECO, AECGE, and AECFA polymers.  $\sigma$  is tensile strength, and  $\epsilon$  is elongation at break.**

Samples	$E'$ at 25 °C (MPa)	$T_g$ (°C)	$v_e$ (kmol m <sup>-3</sup> )	$T_{d,5\%}$ (°C)	$T_{d,30\%}$ (°C)	$T_{d,max}$ (°C)	$T_s$	$R_{600}$ (%)	$\sigma$ (MPa)	$\epsilon$ (%)
AESO	457	46.9	4.6	313	413	428	183	1.3	9.5±0.5	11.5±1.5
AECO	970	75.1	6.5	345	412	431	189	1.7	19.5±0.6	7.7±0.8
AECGE	1820	81.9	5.6	313	427	473	187	4.6	28.6±1.1	4.8±0.3
AECFA	737	52.7	4.6	317	407	441	182	3.5	15.7±1.0	11.7±2.2

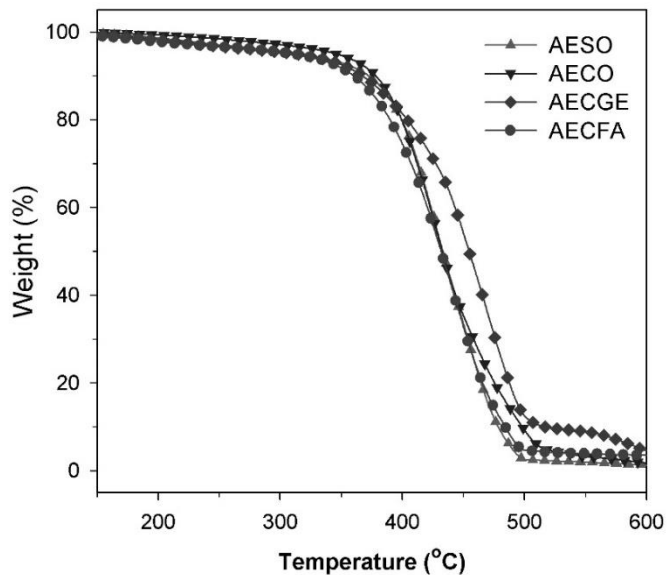
#### 4.4.5. Thermal degradation properties

Thermal degradation profiles and stability factors of the UV-cured polymers were observed by TGA, and the TGA thermograms are shown in Figure 4.16 and 4.17. Thermal stability factors including the degradation temperatures for 5% weight loss ( $T_{d,5\%}$ ) and 30% weight loss ( $T_{d,30\%}$ ), the temperature of maximum degradation rate ( $T_{d,max}$ ), the statistic heat-resistant index ( $T_s$ ), and the char residue at 600 °C ( $R_{600}$ ) are listed in Table 4.1.  $T_s$  was estimated from  $T_{d,5\%}$  and  $T_{d,30\%}$  using Eq. (3) (Aouf et al., 2013; Lehrle and Williams, 1994):

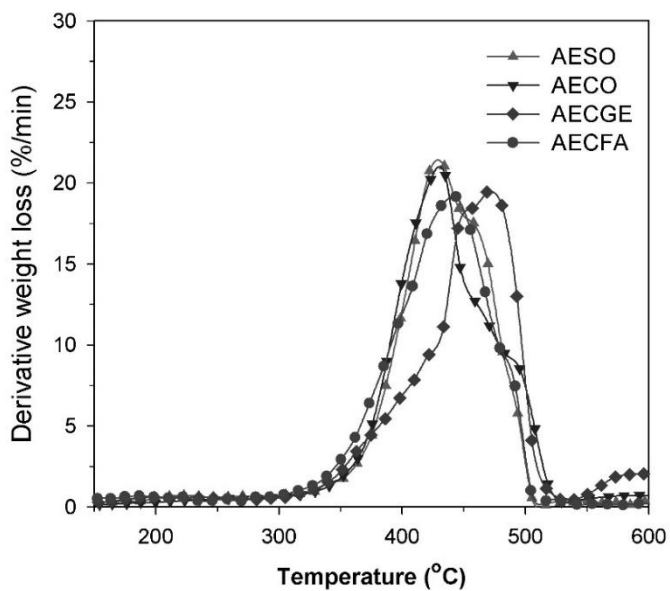
$$T_s = 0.49[T_{d,5\%} + 0.6(T_{d,30\%} - T_{d,5\%})] \quad (3)$$

The TGA curves mainly indicate three degradation stages. The first degradation (200-320 °C) was caused by unreacted acrylates and oligomers in the crosslinked matrix (C. Zhang et al., 2015). The second degradation (320-500 °C) was the fastest decomposition range, which was attributed to the depolymerization of the crosslinked structure and char formation, and the third degradation (above 500 °C) was believed to be the degradation of char residues (K. Liu et al., 2015). The  $T_{d,5\%}$  of AECO is the highest, and AECO was the most stable in the first degradation stages in Figure 4.16. It could be due to the highest crosslink density and storage modulus at the rubbery region of AECO polymer, which were confirmed by DMA test. All the samples were thermally stable because  $T_s$  values were at a range from 182 to 189;  $T_s$  of 185 was reported by cured diglycidyl ether of bisphenol-A (DGEBA), a well-known thermally stable epoxy resin, when using an amino-

based curing agent (S. Ma et al., 2014). The  $T_s$  of the cured acrylate was increased with the increased crosslink density of the polymer. Increased crosslink density of polymer generally leads an increment of thermal stability, but it is also strongly influenced by chemical structure of the polymer network (S. Ma et al., 2014b). At the second degradation stage, AESO and AECO polymers showed relatively faster initial degradation rates (slopes of beginning of the second degradation ranges in Figure 4.16) compared to AECGE and AECFA polymers, which contained the aromatic structures in the polymer networks. In addition, AECFA exhibited higher  $T_{d,max}$  (441 °C) than that of AESO and AECO (428 and 431 °C), while crosslink densities of AESO and AECO were obviously similar and higher than that of AECFA, respectively. These results are in concurrence with that phenolic structures are thermally stable (Jaillet et al., 2014). As ester linkage is easily cleaved during thermal degradation (Khosravi and Musa, 2011), The AECGE polymer exhibited dominantly high  $T_{d,max}$  and temperature range of the main decomposition step because AECGE contained less thermally cleavable ester groups than that of AESO, AECO, and AECFA, which were mainly composed of esters of fatty acids. At the third degradation step, AECGE and AECFA polymers showed bigger residues ( $R_{600}$ ) of 4.6 and 3.5% than 1.3 and 1.7% of AESO and AECO since aromatic structure has a tendency for high char formation under thermal degradation (Ellzey et al., 2006). Enhanced thermal stability and high char residue by aromatic contents in polymers have been reported by several researchers (K. Liu et al., 2015; R. Liu et al., 2015; S. Ma et al., 2014a).



**Figure 4.16: Weight percentages of AESO, AECO, AECGE, and AECFA as a function of temperature.**



**Figure 4.17: Derivative weight loss of AESO, AECO, AECGE, and AECFA as a function of temperature.**

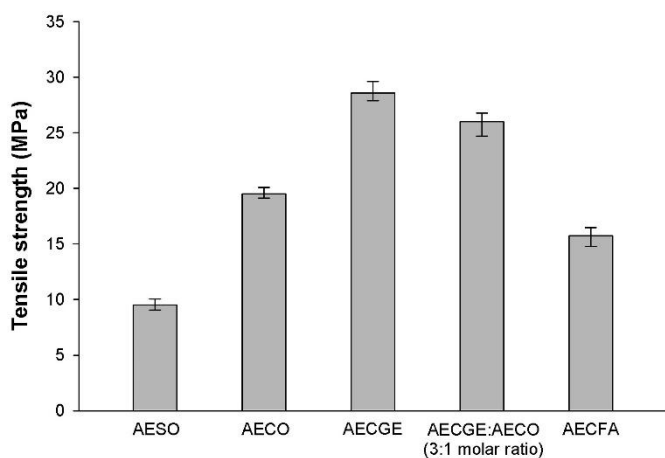
#### 4.4.6. Mechanical properties

The mechanical properties of the coating materials were estimated by tensile testing; tensile strength and elongation at break for the UV-cured acrylic polymer are shown in Figure 4.18 and 4.19, respectively, and summarized in Table 4.1. The order of tensile strength is corresponding to the order of  $E'$  at 25 °C of the DMA test. The AECO polymer showed the higher tensile strength and the lower elongation at break than those of AESO polymer; this result is consistent with another finding that the higher crosslink density leads to enhanced strength and brittleness (Can et al., 2006). While AESO and AECO polymers exhibited tensile strengths of 9.5 and 19.5 MPa, AECGE polymer showed the highest tensile strength of 28.6 MPa because the aromatic nature of cardanol can contribute to the strength of the polymer (R. Liu et al., 2015). However, as expected, AECGE polymer had the lowest elongation at break of 4.8% defined as a rigid material since the elongation was below 7% (Dai et al., 2016). Compared to AESO polymer, AECO and AECGE polymers are beneficial to mechanical strength. However, the brittleness is not desirable for flexible coating applications. Otherwise, high elongations at break of 11.5 and 11.7% of AESO and AECFA polymers were similarly obtained. Interestingly, AECFA polymer showed 1.65 times larger tensile strength (15.7 MPa) than that of the AESO polymer, while having the same crosslink densities. Compared to AESO polymer, the better strength of AECFA maintained with the flexibility was possibly due to the combination of the benzene ring with the aliphatic chains from both cardanol and fatty acid.

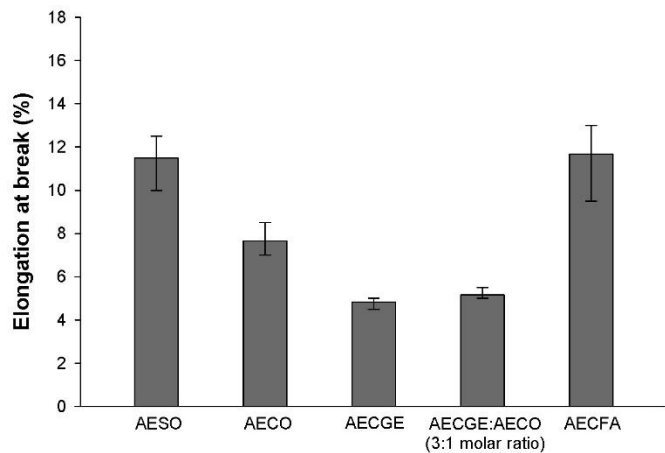
For comparison with AECFA polymer, which was equimolar chemical structure of cardanol and fatty acid, a copolymer of AECGE and AECO at 3 to 1 molar ratio was also tested to observe the effect of the benzene ring on mechanical properties when the phenolic structure was simply mixed with triglyceride in an acrylic resin. Then, 26 MPa and 5.2% of tensile strength and



elongation at break were obtained from AECGE:AECO (3:1 molar ratio) copolymer. It is easy to know that no synergetic improvements of strength or flexibility were observed in the copolymer system compared to neat AECO and AECGE polymers.



**Figure 4.18: Tensile strengths of the cured acrylates.**



**Figure 4.19: Elongations at break of the cured acrylates.**

#### 4.4.7. Coating performance properties

Coating performance of the cured acrylates were examined by investigations of water and solvent uptakes, gel content, and hydrolytic degradation using free-standing coating materials in film form. In addition, gloss, adhesion, pencil hardness, and MEK resistance of the coating materials on wood panels were measured. The results are summarized in Table 4.2. Water and solvent uptake tests were performed to examine penetrations of water and solvent into the coating materials. All cured acrylates showed good water resistances without significant differences on the uptakes. However, AESO polymer clearly exhibited the lowest solvent resistance compared to other polymers during toluene uptake test. It can be attributed in terms of the low crosslink density and the lack of the aromatic structure of AESO polymer. In addition, the solvent resistance of AECFA polymer was slightly better than that of AECO polymer even though AECFA polymer networks were more loosely crosslinked. Herein, we can know that the benzene segment in the acrylates systems is the most important key to prevent solvent migration on the polymers. The result of the gel content is corresponding to the result of the solvent uptake test although all the samples did not show remarkable differences on the gel content. As all the coating materials had the gel contents at a range of 96 to 97%, the coatings can be regarded as being highly cured. In addition, all the coatings on wood panels exhibited excellent resistances to MEK rubs because the surface of the coatings was not deformed after 250 times of double rubs.

Hydrolytic degradation is one of the common chemical degradation that occurs in the environment due to the reaction of polymers with water (He et al., 2004; Marin et al., 2013), and a degradation test in alkaline conditions has been used for bioplastics such as poly(lactic acid) and polyurethane (De Jong et al., 2001; S. Lee et al., 2001). The AECGE polymer showed the lowest weight loss of 1.21% in 1M NaOH solution during 24 hours, while other polymers exhibited

weight loss from 2.78 to 3.09%. Compared to the other polymers containing fatty acids, less hydrolyzable groups such as esters in AECGE polymer may lead the lower weight loss during the degradation.

The gloss of the cured coatings on 60 ° angle was measured, and the values of AESO and AECO polymers were relatively higher than those of AECGE and AECFA polymers. However, all cured samples had high glossiness on wood surface without haziness. A cross hatch cut test was performed to the cured acrylates on wood, the result is corresponding to the result of elongations at break in Table 4.2; flexible polymers (AESO and AECFA) had better adhesion strengths than that of the brittle polymers (AECO and AECGE). Fewer cross cut areas were maintained on the brittle polymers because the edges and the intersections of the cut areas of the brittle coating materials were more easily damaged during the cutting process. Otherwise, highest pencil hardness of 5H was obtained for AECGE polymer, and AECO and AECFA polymers showed 2H while AESO polymer had lowest value of HB. Therefore, we know that high  $T_g$  and the phenolic structure provided better hardness of the coating materials; Liu's research also reported similar results (R. Liu et al., 2015).

**Table 4.2: Coating performance properties of the cure acrylates.**

Samples	Water uptake (%)	Toluene uptake (%)	Gel content (%)	1M NaOH weight loss (%)	Gloss (60°)	Adhesion	Pencil hardness	MEK resistance
AESO	0.52 ± 0.5	15.0 ± 0.9	96.0 ± 0.3	3.09 ± 0.4	89.4	4B	HB	>250
AECO	0.45 ± 0.1	11.8 ± 1.0	96.4 ± 0.6	2.78 ± 0.7	88.9	3B	2H	>250
AECGE	1.22 ± 0.2	9.1 ± 0.7	97.1 ± 0.4	1.21 ± 0.1	79.9	3B	5H	>250
AECFA	0.52 ± 0.1	10.1 ± 0.1	96.8 ± 0.4	2.94 ± 0.8	72.2	4B	2H	>250

## 4.5. Conclusion

The bio-based acrylates, AECO, AECGE, and AECFA were successfully synthesized from cardanol and camelina oil. The AECGE polymer showed excellent tensile strength, hardness, thermal properties, and resistances to solvent and hydrolytic degradation due to its rigid benzene ring; however, its high brittleness is an obstacle for applying to flexible coating applications. The AECO polymer presents fairly lower flexibility and higher rigidity than AESO polymer due to its higher functionality. The rigidity of AECGE polymer was considerably upgraded by the introduction of the fatty acids on the structure as shown in the AECFA polymer. Although the strength of AECFA polymer is lower than AECGE polymer, it is much higher than AESO polymer. Since the unique chemical structure of AECFA, which is the combined feature of the flexible aliphatic chains of both fatty acids and cardanol and the rigid aromatic hydrocarbon; AECFA showed more toughened polymer network with better thermal stability and coating performances than those of AESO while the flexibility was maintained. These results indicated that AECFA derived from non-food crops has a great potential to a substitute for soybean oil-based acrylates such as AESO.

## 4.6. References

- Andrzejewska, E. (2001). Photopolymerization kinetics of multifunctional monomers. *Progress in Polymer Science*, 26: 605-665.
- Aouf, C., Nouailhas, H., Fache, M., Caillol, S., Boutevin, B., and Fulcrand, H. (2013). Multi-functionalization of gallic acid. synthesis of a novel bio-based epoxy resin. *European Polymer Journal*, 49: 1185-1195.
- Asif, A., Shi, W. F., Shen, X. F., and Nie, K. M. (2005). Physical and thermal properties of UV curable waterborne polyurethane dispersions incorporating hyperbranched aliphatic polyester of varying generation number. *Polymer*, 46: 11066-11078.  
doi:10.1016/j.polymer.2005.09.046
- Balachandran, V. S., Jadhav, S. R., Vemula, P. K., and John, G. (2013). Recent advances in cardanol chemistry in a nutshell: From a nut to nanomaterials. *Chemical Society Reviews*, 42: 427-438.
- Balanuca, B., Lungu, A., Hanganu, A., Stan, L. R., Vasile, E., and Iovu, H. (2014). Hybrid nanocomposites based on POSS and networks of methacrylated camelina oil and various PEG derivatives. *European Journal of Lipid Science and Technology*, 116: 458-469.
- Bloise, E., Becerra-Herrera, M., Mele, G., Sayago, A., Carbone, L., D'Accolti, L., Mazzetto, S. E., and Vasapollo, G. (2014). Sustainable preparation of cardanol-based nanocarriers with embedded natural phenolic compounds. *ACS Sustainable Chemistry & Engineering*, 2: 1299-1304.
- Bongiovanni, R., Montefusco, F., Priola, A., Macchioni, N., Lazzeri, S., Sozzi, L., and Ameduri, B. (2002). High performance UV-cured coatings for wood protection. *Progress in Organic Coatings*, 45: 359-363.
- Can, E., Küsefoğlu, S., and Wool, R. (2002). Rigid thermosetting liquid molding resins from renewable resources. II. copolymers of soybean oil monoglyceride maleates with neopentyl glycol and bisphenol A maleates. *Journal of Applied Polymer Science*, 83: 972-980.
- Can, E., Wool, R., and Küsefoğlu, S. (2006). Soybean-and castor-oil-based thermosetting polymers: Mechanical properties. *Journal of Applied Polymer Science*, 102: 1497-1504.
- Chattopadhyay, D., Panda, S. S., and Raju, K. (2005). Thermal and mechanical properties of epoxy acrylate/methacrylates UV cured coatings. *Progress in Organic Coatings*, 54: 10-19.
- Chen, J., Liu, Z., Li, K., Huang, J., Nie, X., and Zhou, Y. (2015). Synthesis and application of a natural plasticizer based on cardanol for poly (vinyl chloride). *Journal of Applied Polymer Science*, 132
- Chen, J., Nie, X., Liu, Z., Mi, Z., and Zhou, Y. (2015). Synthesis and application of polyepoxide cardanol glycidyl ether as biobased polyepoxide reactive diluent for epoxy resin. *ACS Sustainable Chemistry & Engineering*, 3: 1164-1171.
- Chen, Q., Xue, H., and Lin, J. (2010). Preparation of polypropylene-graft-cardanol by reactive extrusion and its composite material with bamboo powder. *Journal of Applied Polymer Science*, 115: 1160-1167.

- Chen, W., Sun, S., Liang, S., Peng, L., Wang, Y., and Shen, M. (2014). Lipase-catalyzed hydrolysis of linseed oil: Optimization using response surface methodology. *Journal of Oleo Science*, 63: 619-628.
- Choi, Y., Kim, K., Kim, D., Kim, H. J., Cha, S., and Lee, J. (2014). Synthesis and characterization of self-cross-linkable and bactericidal methacrylate polymers having renewable cardanol moieties for surface coating applications. *RSC Advances*, 4: 41195-41203.
- Dai, J., Liu, X., Ma, S., Wang, J., Shen, X., You, S., and Zhu, J. (2016). Soybean oil-based UV-curable coatings strengthened by crosslink agent derived from itaconic acid together with 2-hydroxyethyl methacrylate phosphate. *Progress in Organic Coatings*, 97: 210-215.
- Dai, J., Ma, S., Wu, Y., Han, L., Zhang, L., Zhu, J., and Liu, X. (2015). Polyesters derived from itaconic acid for the properties and bio-based content enhancement of soybean oil-based thermosets. *Green Chemistry*, 17: 2383-2392.
- Dantas, T. C., Vale, T., Neto, A. D., Scatena Jr, H., and Moura, M. (2009). Micellization study and adsorption properties of an ionic surfactant synthesized from hydrogenated cardanol in air–water and in air–brine interfaces. *Colloid and Polymer Science*, 287: 81-87.
- Darroman, E., Durand, N., Boutevin, B., and Caillol, S. (2015). New cardanol/sucrose epoxy blends for biobased coatings. *Progress in Organic Coatings*, 83: 47-54.
- Darroman, E., Durand, N., Boutevin, B., and Caillol, S. (2016). Improved cardanol derived epoxy coatings. *Progress in Organic Coatings*, 91: 9-16.
- De Jong, S., Arias, E. R., Rijkers, D., Van Nostrum, C., Kettenes-Van den Bosch, J., and Hennink, W. (2001). New insights into the hydrolytic degradation of poly (lactic acid): Participation of the alcohol terminus. *Polymer*, 42: 2795-2802.
- Ellzey, K. A., Ranganathan, T., Zilberman, J., Coughlin, E. B., Farris, R. J., and Emrick, T. (2006). Deoxybenzoin-based polyarylates as halogen-free fire-resistant polymers. *Macromolecules*, 39: 3553-3558.
- Fontana, A., Guernelli, S., Zaccheroni, N., Zappacosta, R., Genovese, D., De Crescentini, L., and Riela, S. (2015). Micellization properties of cardanol as a renewable co-surfactant. *Organic & Biomolecular Chemistry*, 13: 9214-9222.
- Francis, A., and Warwick, S. (2009). The biology of canadian weeds. 142. *Camelina alyssum* (mill.) thell.; *C. microcarpa* andrz. ex DC.; *C. sativa* (L.) crantz. *Canadian Journal of Plant Science*, 89: 791-810.
- Fu, L., Yang, L., Dai, C., Zhao, C., and Ma, L. (2010). Thermal and mechanical properties of acrylated epoxidized-soybean oil-based thermosets. *Journal of Applied Polymer Science*, 117: 2220-2225.
- Greco, A., Brunetti, D., Renna, G., Mele, G., and Maffezzoli, A. (2010). Plasticizer for poly (vinyl chloride) from cardanol as a renewable resource material. *Polymer Degradation and Stability*, 95: 2169-2174.
- Habib, F., and Bajpai, M. (2011). Synthesis and characterization of acrylated epoxidized soybean oil for UV cured coatings.

- Hannoda, Y., Akasaka, Y., and Shibata, M. (2015). Bio-based thermosetting bismaleimide resins using cardanyl linolenate and allyl cardanyl ether. *Reactive and Functional Polymers*, 97: 96-104.
- Hassouma, F., Mihai, I., Fetzer, L., Fouquet, T., Raquez, J., Laachachi, A., Ibn Al Ahrach, H., and Dubois, P. (2016). Design of new cardanol derivative: Synthesis and application as potential biobased plasticizer for poly (lactide). *Macromolecular Materials and Engineering*, 301: 1267-1278.
- He, Y., Qian, Z., Zhang, H., and Liu, X. (2004). Alkaline degradation behavior of polyesteramide fibers: Surface erosion. *Colloid and Polymer Science*, 282: 972-978.
- Iskandarov, U., Kim, H. J., and Cahoon, E. B. (2014). *Camelina: An emerging oilseed platform for advanced biofuels and bio-based materials*. *Plants and BioEnergy* (pp. 131-140) Springer.
- Jaillet, F., Darroman, E., Ratsimihety, A., Auvergne, R., Boutevin, B., and Caillol, S. (2014). New biobased epoxy materials from cardanol. *European Journal of Lipid Science and Technology*, 116: 63-73.
- Jaillet, F., Nouailhas, H., Auvergne, R., Ratsimihety, A., Boutevin, B., and Caillol, S. (2014). Synthesis and characterization of novel vinylester prepolymers from cardanol. *European Journal of Lipid Science and Technology*, 116: 928-939.
- Kardar, P., Ebrahimi, M., Bastani, S., and Jalili, M. (2009). Using mixture experimental design to study the effect of multifunctional acrylate monomers on UV cured epoxy acrylate resins. *Progress in Organic Coatings*, 64: 74-80.
- Kasetaite, S., Ostrauskaite, J., Grazuleviciene, V., Svediene, J., and Bridziuviene, D. (2014). Camelina oil-and linseed oil-based polymers with bisphosphonate crosslinks. *Journal of Applied Polymer Science*, 131
- Keske, C. M., Hoag, D. L., Brandess, A., and Johnson, J. J. (2013). Is it economically feasible for farmers to grow their own fuel? A study of camelina sativa produced in the western united states as an on-farm biofuel. *Biomass and Bioenergy*, 54: 89-99.
- Khosravi, E., and Musa, O. M. (2011). Thermally degradable thermosetting materials. *European Polymer Journal*, 47: 465-473.
- Kim, N., Li, Y., and Sun, X. S. (2015). Epoxidation of camelina sativa oil and peel adhesion properties. *Industrial Crops and Products*, 64: 1-8.
- Kunioka, M., Taguchi, K., Ninomiya, F., Nakajima, M., Saito, A., and Araki, S. (2014). Biobased contents of natural rubber model compound and its separated constituents. *Polymers*, 6: 423-442.
- La Scala, J. (2002). The effects of triglyceride structure on the properties of plant oil-based polymers, PhD dissertation. University of Delaware,
- La Scala, J., and Wool, R. P. (2013). Fundamental thermo-mechanical property modeling of triglyceride-based thermosetting resins. *Journal of Applied Polymer Science*, 127: 1812-1826.

- Landry, V., Riedl, B., and Blanchet, P. (2008). Nanoclay dispersion effects on UV coatings curing. *Progress in Organic Coatings*, 62: 400-408.
- Lee, S., Yu, S., and Lee, Y. (2001). Degradable polyurethanes containing poly (butylene succinate) and poly (ethylene glycol). *Polymer Degradation and Stability*, 72: 81-87.
- Lehrle, R. S., and Williams, R. J. (1994). Thermal degradation of bacterial poly (hydroxybutyric acid): Mechanisms from the dependence of pyrolysis yields on sample thickness. *Macromolecules*, 27: 3782-3789.
- Li, F., Hanson, M., and Larock, R. (2001). Soybean oil–divinylbenzene thermosetting polymers: Synthesis, structure, properties and their relationships. *Polymer*, 42: 1567-1579.
- Li, Y., and Sun, X. S. (2015a). Camelina oil derivatives and adhesion properties. *Industrial Crops and Products*, 73: 73-80.
- Li, Y., and Sun, X. S. (2015b). Synthesis and characterization of acrylic polyols and polymers from soybean oils for pressure-sensitive adhesives. *RSC Advances*, 5: 44009-44017.
- Liu, K., Madbouly, S. A., and Kessler, M. R. (2015). Biorenewable thermosetting copolymer based on soybean oil and eugenol. *European Polymer Journal*, 69: 16-28.
- Liu, R., Zhang, X., Zhu, J., Liu, X., Wang, Z., and Yan, J. (2015). UV-curable coatings from multiarmed cardanol-based acrylate oligomers. *ACS Sustainable Chemistry & Engineering*, 3: 1313-1320.
- Liu, R., Zhu, G., Li, Z., Liu, X., Chen, Z., and Ariyasivam, S. (2015). Cardanol-based oligomers with “hard core, flexible shell” structures: From synthesis to UV curing applications. *Green Chemistry*, 17: 3319-3325.
- Lu, J., Khot, S., and Wool, R. P. (2005). New sheet molding compound resins from soybean oil. I. synthesis and characterization. *Polymer*, 46: 71-80.
- Ma, S., Jiang, Y., Liu, X., Fan, L., and Zhu, J. (2014). Bio-based tetrafunctional crosslink agent from gallic acid and its enhanced soybean oil-based UV-cured coatings with high performance. *RSC Advances*, 4: 23036-23042.
- Ma, S., Liu, X., Fan, L., Jiang, Y., Cao, L., Tang, Z., and Zhu, J. (2014). Synthesis and properties of a Bio-Based epoxy resin with high epoxy value and low viscosity. *ChemSusChem*, 7: 555-562.
- Ma, S., Liu, X., Jiang, Y., Fan, L., Feng, J., and Zhu, J. (2014). Synthesis and properties of phosphorus-containing bio-based epoxy resin from itaconic acid. *Science China Chemistry*, 57: 379-388.
- Maffezzoli, A., Calo, E., Zurlo, S., Mele, G., Tarzia, A., and Stifani, C. (2004). Cardanol based matrix biocomposites reinforced with natural fibres. *Composites Science and Technology*, 64: 839-845.
- Marin, E., Briceno, M. I., and Caballero-George, C. (2013). Critical evaluation of biodegradable polymers used in nanodrugs. *International Journal of Nanomedicine*, 8: 3071-3090. doi:10.2147/IJN.S47186 [doi]



- Meier, M. A. R., Metzger, J. O., and Schubert, U. S. (2007). Plant oil renewable resources as green alternatives in polymer science. *Chemical Society Reviews*, 36: 1788-1802. doi:10.1039/b703294c
- Mi, Z., Nie, X., Liu, Z., and Wang, Y. (2012). Synthesis and effect of cardanol glycidyl ether as reactive diluent of epoxy resin system. *Journal of Bioprocess Engineering and Biorefinery*, 1: 202-206.
- Mohtadizadeh, F., Zohuriaan-Mehr, M., Hadavand, B. S., and Dehghan, A. (2015). Tetra-functional epoxy-acrylate as crosslinker for UV curable resins: Synthesis, spectral, and thermo-mechanical studies. *Progress in Organic Coatings*, 89: 231-239.
- Moser, B. R. (2012). Biodiesel from alternative oilseed feedstocks: Camelina and field pennycress. *Biofuels*, 3: 193-209.
- Ondrey, G. (2014). A step closer to bio-based acrylic acid. *Chemical Engineering*, 121: 18-18.
- Park, Y., Lim, D., Kim, H., Park, D., and Sung, I. (2009). UV-and thermal-curing behaviors of dual-curable adhesives based on epoxy acrylate oligomers. *International Journal of Adhesion and Adhesives*, 29: 710-717.
- Petrovic, Z. (2008). Polyurethanes from vegetable oils. *Polymer Reviews*, 48: 109-155. doi:10.1080/15583720701834224
- Quirino, R. L., Garrison, T. F., and Kessler, M. R. (2014). Matrices from vegetable oils, cashew nut shell liquid, and other relevant systems for biocomposite applications. *Green Chemistry*, 16: 1700-1715.
- Rao, B., and Palanisamy, A. (2011). Monofunctional benzoxazine from cardanol for biocomposite applications. *Reactive and Functional Polymers*, 71: 148-154.
- Razeq, F. M., Kosma, D. K., Rowland, O., and Molina, I. (2014). Extracellular lipids of camelina sativa: Characterization of chloroform-extractable waxes from aerial and subterranean surfaces. *Phytochemistry*, 106: 188-196.
- Schwalm, R. (2006). *UV coatings: Basics, recent developments and new applications* Elsevier.
- Sharmin, E., Zafar, F., Akram, D., Alam, M., and Ahmad, S. (2015). Recent advances in vegetable oils based environment friendly coatings: A review. *Industrial Crops and Products*, 76: 215-229.
- Shen, L., Li, Y., Zheng, J., Lu, M., and Wu, K. (2015). Modified epoxy acrylate resin for photocurable temporary protective coatings. *Progress in Organic Coatings*, 89: 17-25.
- Stanzione III, J. F., Sadler, J. M., La Scala, J. J., Reno, K. H., and Wool, R. P. (2012). Vanillin-based resin for use in composite applications. *Green Chemistry*, 14: 2346-2352.
- Sung, J., Li, Y., and Sun, X. S. (2015). Plasticization effects of dihydroxyl soybean oil improve flexibilities of epoxy-based films for coating applications. *Journal of Applied Polymer Science*, 132: 41773. doi:10.1002/app.41773
- Suresh, K. I. (2012). Rigid polyurethane foams from cardanol: Synthesis, structural characterization, and evaluation of polyol and foam properties. *ACS Sustainable Chemistry & Engineering*, 1: 232-242.

- Suresh, K. I., and Kishanprasad, V. S. (2005). Synthesis, structure, and properties of novel polyols from cardanol and developed polyurethanes. *Industrial & Engineering Chemistry Research*, 44: 4504-4512.
- Tyman, J. H., and Bruce, I. E. (2003). Synthesis and characterization of polyethoxylate surfactants derived from phenolic lipids. *Journal of Surfactants and Detergents*, 6: 291-297.
- Vendamme, R., and Eevers, W. (2013). Sweet solution for sticky problems: Chemoreological design of self-adhesive gel materials derived from lipid biofeedstocks and adhesion tailoring via incorporation of isosorbide. *Macromolecules*, 46: 3395-3405.
- Williams, C. K., and Hillmyer, M. A. (2008). Polymers from renewable resources: A perspective for a special issue of polymer reviews. *Polymer Reviews*, 48: 1-10.  
doi:10.1080/15583720701834133
- Wool, R. P., and Sun, X. S. (2005). *Bio-based polymers and composites*. Burlington: Academic Press.
- Zhan, M., and Wool, R. P. (2010). Biobased composite resins design for electronic materials. *Journal of Applied Polymer Science*, 118: 3274-3283.
- Zhang, C., Yan, M., Cochran, E. W., and Kessler, M. R. (2015). Biorenewable polymers based on acrylated epoxidized soybean oil and methacrylated vanillin. *Materials Today Communications*, 5: 18-22.

## **Chapter 5 - Synthesis and characterization of di-functional acrylate from 10-undecenoic acid: A promising plant oil derivative for low viscous acrylate applications**

### **5.1. Abstract**

Low viscous fatty ester-based acrylate, acrylated epoxidized allyl 10-undecenoate (AEAU), was prepared through lipase-catalyzed esterification of 10-undecenoic acid with allyl alcohol using Novozyme 435, followed by epoxidation of the unsaturated fatty ester and then acrylation of the epoxides. Compared to triglyceride-based acrylates such as acrylated epoxidized soybean oil (AESO) and acrylated epoxidized camelina oil (AECO), the viscosity of AEAU achieved was much lower (1.264 Pa·s at 1 s<sup>-1</sup>), whereas AESO and AECO were highly viscous (28.5 Pa·s and 70.8 Pa·s, respectively, at 1 s<sup>-1</sup>). The AEAU thermoset has a mechanical strength of 25 MPa, while AESO or AECO has about 9.5 MPa and 19.5 MPa, respectively. AEAU also has good balance of flexibility and thermal stability. Additionally, AEAU as an additive into AESO improved mechanical and thermal properties of the AESO thermoset with reduced viscosity of the AESO resin, and significantly enhanced the performance properties of the AESO polymer maintained with high bio-content was found using a combined bio- and petroleum-based reactive diluent of AEAU and triethylene glycol dimethacrylate (TEGDMA). Thus, AEAU has great potential to a bio-based acrylate itself or an additive for various thermoset applications due to its low viscosity monomer with excellent polymer properties.

## 5.2. Introduction

Vinyl ester resin, mainly composed of monomers with acrylic or methacrylic groups, is one of the well-known thermoset resins for various applications in manufacturing industries such as transportation, construction, automotive, marine, and composites due to its excellent thermal and mechanical properties, resistances to corrosion and degradation with inexpensive price (J. J. La Scala et al., 2005; Rosu et al., 2009; X. Yang et al., 2015; C. Zhang et al., 2015). The acrylate monomers are crosslinked by free-radical polymerization of the vinyl groups of the acrylates. Reactive diluents such as styrene are also added to the vinyl ester resin for a reduction of the resin viscosity and an enhancement of the polymer performance (J. J. La Scala et al., 2005; C. Zhang et al., 2015). The acrylate monomers are typically derived from bisphenol-A (X. Yang et al., 2015), which is a petrochemical and regarded as a toxic chemical to living organisms (Chrysanthos et al., 2011; S. Ma et al., 2014). In addition, styrene is highly volatile and a carcinogenic material derived from fossil resources (Cousinet et al., 2015). Therefore, renewable building blocks such as triglyceride (J. La Scala and Wool, 2005; J. La Scala and Wool, 2013; X. Yang et al., 2015), fatty acid (J. J. La Scala et al., 2004), and vanillin (C. Zhang et al., 2015; C. Zhang et al., 2015), etc., has been studied as the component of the resin to increase sustainability and reduce the hazardous risks.

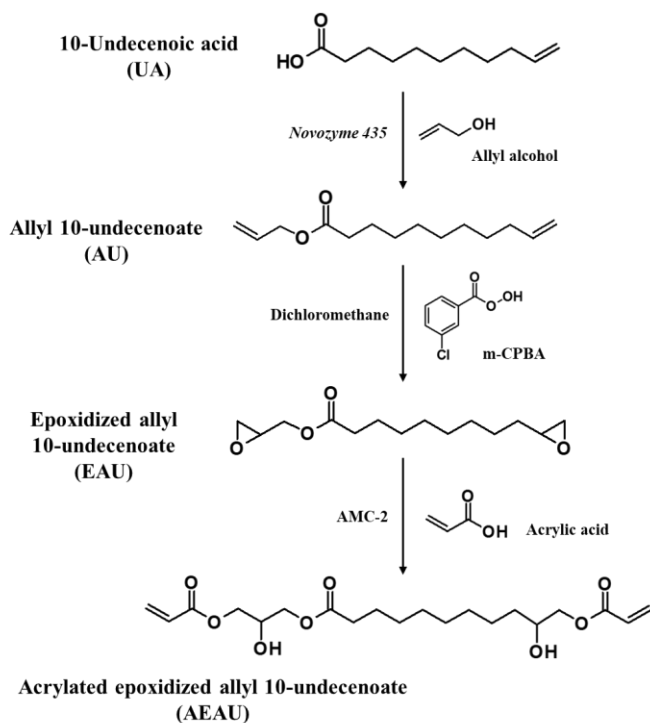
Plant oils are important resources in polymer industries due to the abundancy of crops, its intrinsic non-toxicity, they also contain unsaturation parts and ester groups that allow further chemical modifications (Sharmin et al., 2015; Wool and Sun, 2005). Acrylated epoxidized soybean oil (AESO) is a commercially available bio-based acrylate and is free-radically polymerized under UV-radiation using photo-initiators. However, soybean is a food resource, and inherently flexible aliphatic chain of the triglyceride structure causes low mechanical strength and glass transition

temperature of the AESO thermoset (X. Yang et al., 2015; Zhan and Wool, 2010). Therefore, we prepared acrylated epoxidized camelina oil (AECO) to develop a high-performance plant oil-based acrylate for coating applications from non-food resources (Sung and Sun, Under Review); high functionality resin was obtained because camelina oil has more unsaturated sites on the triglyceride (5.8 double bond) than that of soybean oil (4.6 double bond) (N. Kim et al., 2015; Y. Li and Sun, 2015a). As we expected, the better mechanical strength and thermal properties were achieved for the AECO thermoset in comparison with the AESO thermoset. However, the poor flexibility was attributed to the rigidity of the AECO polymer, and moreover, the viscosity of AECO was larger than twice of that of AESO because it had more polar groups such as acrylic and hydroxyl groups. Therefore, the viscosity will limit its applications, and reactive diluents should be required to use AECO as a backbone matrix of thermosets. The high viscosity issue is typical for the acrylates derived from natural triglycerides due to the intermolecular forces from the hydroxyl and the ester groups of the large molecular weight monomers (Rengasamy and Mannari, 2013). Thus, reactive diluents such as styrene are needed for the plant oil-based resins including AESO (also for petroleum-based resins) to meet low viscosity requirements of practical applications such as liquid molding resins for composites (Campanella et al., 2009; Campanella et al., 2011). In order to replace styrene, various bio-based reactive diluents have been prepared for thermoset polymers (Campanella et al., 2009; Campanella et al., 2011; J. J. La Scala et al., 2004; Sadler et al., 2012; Stanzione et al., 2012; X. Yang et al., 2015). However, complete styrene replacements were difficult because the viscosity reduction performance of styrene was overwhelming due to the remarkably lower viscosity of styrene, as compared to the bio-based reactive diluents (Cousinet et al., 2015). Therefore, the aim of this study is developing a low viscous plant-oil based acrylate monomer, which may need less or no reactive diluents for thermoset applications.

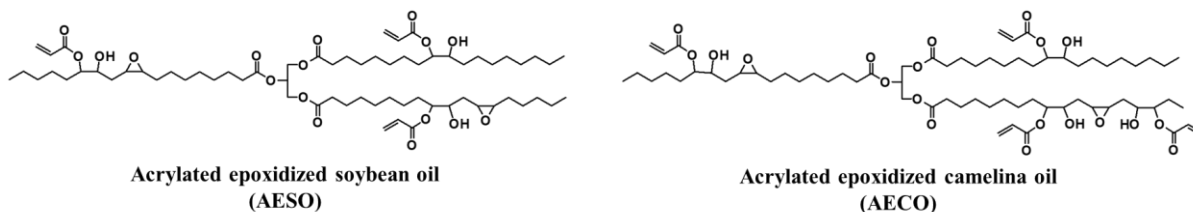
A triglyceride structure is comprised of three fatty acids, which are linked by a glycerol center through ester bonds (J. J. La Scala et al., 2004), and the branched and large molecular structure of the triglyceride is a disadvantage to building low viscous resins because the structural drawback and modified polar functional groups can synergistically cause high viscosity in the resins. Therefore, fatty ester-based monomers will be indubitably less viscous, as compared to triglyceride-based monomers if they have the same functional groups. This is in accordance with the study from Campanella et al., for developing styrene replacements using acrylated epoxidized fatty acid methyl ester from soybean oil, which had much lower viscosity than that of AESO (Campanella et al., 2009). However, fatty ester-based thermosets compared to triglyceride-based thermosets may have a difficulty in obtaining rigidity and high thermal stability due to its low molecular weight of the fatty ester-based monomers. Thus, to produce strengthened thermosets from fatty esters in this study, we hypothesized an additional unsaturated site on the ester side of a fatty acid would enhance the reactivity in addition to the unsaturated fatty acid chain, which would improve acryl functionality and mechanical strength of the polymer.

In this study, allyl 10-undecenoate (AU), which is a fatty ester containing two terminal unsaturated carbons, was designed from 10-undecenoic acid (or undecylenic acid) (UA) through enzymatic esterification of UA with allyl alcohol (Scheme 5.1). UA is a derivative from castor oil, which contains one terminal C=C double bond on the C11 fatty acid, and it has already been an ingredient for pharmaceutical and cosmetic products (Bigot et al., 2016). Currently, UA has been used as a precursor for polymer preparations such as polyamide 11 (Nylon 11, commercial name is Rilsan by Arkema) (Van der Steen and Stevens, 2009), polyurethane (Lligadas et al., 2010; Lluch et al., 2013), polyester (Pang et al., 2014), and epoxy resins (C. Li et al., 2016; C. Li et al., 2017). Acrylated epoxidized allyl 10-undecenoate (AEAU) was synthesized from UA, followed

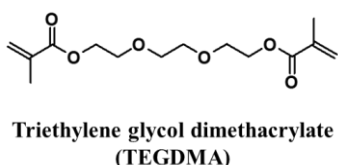
by epoxidation of AU and then acrylation of the epoxy intermediate (Scheme 5.1). The structures and the corresponding functionalities of AEAU and its intermediates were evaluated by analysis of  $^1\text{H}$  nuclear magnetic resonance (NMR) and Fourier transform infrared spectroscopy (FTIR), and rheological behaviors of all the derivatives were monitored at 25 °C. AEAU was cured under UV-radiation after an addition of Darocur 1173 as a free-radical polymerization initiator, and then, performance of the thermoset was estimated in terms of mechanical, viscoelastic, and thermal degradation properties. Triglyceride-based acrylates such as commercial AESO and synthesized AECO (Figure 5.1), were used as comparison targets. Moreover, a special experiment was performed to evaluate the possibility of AEAU as a bio-based reactive diluent for AESO resin, and triethylene glycol dimethacrylate (TEGDMA) (Figure 5.2) was also used for AESO resin as a petrochemical reactive diluent.



**Scheme 5.1: Synthesis route of AEAU from UA.**



**Figure 5.1: Triglyceride-based acrylates from soybean oil (AESO) and camellina oil (AECO).**



**Figure 5.2: Petrochemical reactive diluent, triethylene glycol dimethacrylate (TEGDMA).**

## 5.3. Materials and Methods

### 5.3.1. Materials

10-undecenoic acid (UA, 98%), acrylated epoxidized soybean oil (AESO), allyl alcohol ( $\geq 99\%$ ), lipase acrylic resin from *Candida antarctica* (Novozyme 435,  $\geq 5,000$  U/g), acrylic acid ( $>99\%$ ), hydroquinone, sodium sulfite, and anhydrous magnesium sulfate were purchased from Sigma-Aldrich (St. Louis, MO). m-Chloroperoxybenzoic acid (m-CPBA, 70–75%), 0.1 N hydrogen bromide in acetic acid, dichloromethane, toluene, ethyl ether, Celite 545, and sodium bicarbonate were purchased from Fisher Scientific (Waltham, MA). Darocur 1173 (2-hydroxyl-2-methyl-1-phenylpropan-1-one) was supplied by BASF (Florham Park, NJ). AMC-2 (a 40-60% solution of chromium(III) 2-ethylhexanoate in a mixture of di(heptyl, nonyl, undecyl) phthalates)



was provided by Ampac Fine Chemicals (Rancho Cordova, CA). Acrylated epoxidized camelina oil (AECO) were prepared as described in our previous work.(Sung and Sun, Under Review)

### **5.3.2. Synthesis of allyl 10-undecenoate (AU)**

AU was prepared via enzymatic esterification of UA with excess of allyl alcohol in the molar ratio of 1 to 5 using immobilized *Candida antarctica*, Novozyme 435. The reaction began with 50 g of UA (0.27 mol) mixed with 74.7 g of allyl alcohol (1.36 mol) and 2.5 g of Novozyme 435 (5 wt% of UA) in a 500-mL Erlenmeyer flask equipped with a magnetic stirrer. The temperature was maintained at 50 °C with an oil bath, and the mixture was covered and stirred for 24 hours at 50 °C. At the end of the reaction, the enzyme was removed from the mixture using Celite filtration. The excess of allyl alcohol and water were separated from the product using a rotary evaporator under vacuum at 80 °C. The enzyme residues were additionally removed by a centrifugation at 10,000 rpm for 15 min, and 57.2 g of the supernatant was collected as the final product. This reaction and further preparations of the epoxy and the acrylate from AU were described in Scheme 5.1.

### **5.3.3. Synthesis of epoxidized allyl 10-undecenoate (EAU)**

EAU was synthesized from AU according to our previous research with some modifications.(C. Li et al., 2016) 63.7 g of m-CPBA (0.267 mol) was dissolved in 200 mL of dichloromethane at a 500-mL Erlenmeyer flask placed in an ice/water bath. The mixture was vigorously agitated by a magnetic stirrer, and 20 g of AU (approximately 0.089 mol) was gradually added by drop-additions using a 50-mL separatory funnel for 30 min. After the addition of AU, the mixture was covered and stirred for 24 hours in the water bath without ice refills. At the end of the reaction, the dichloromethane in the mixture was evaporated under vacuum at room temperature, and 250 mL of ethyl ether was then added into the mixture. After the mixture was

completely dissolved in the ethyl ether at a 1000-mL separatory funnel, the product was purified by several extractions following the order of 150 mL of 10 wt% sodium sulfite solution (three times repetition), 150 mL of saturated sodium bicarbonate solution (five times repetition), and 50 mL of water. The organic phase was dried over magnesium sulfate, and the magnesium sulfate was then removed by Celite filtration. 18.7 g of EAU was obtained after evaporating the ethyl ether under vacuum at 60 °C. The epoxy content of EAU was measured to be 1.75 per molecule.

#### **5.3.4. Synthesis of acrylated epoxidized 10-undecenoate (AEAU)**

The ring-opening reaction of EAU with acrylic acids was performed to prepare AEAU. For obtaining maximum acryl functionality, one epoxide group was reacted with 1.1 moles of acrylic acids (J. La Scala and Wool, 2013). 17.84 g of EAU (approximately 0.071 mol) was charged into a 250-mL round-bottomed flask equipped with a magnetic stirrer and a stopper, and 0.0892 g of hydroquinone (0.5 wt% of EAU) and 0.357 g of AMC-2 (2 wt% of EAU) were added to the flask as a free-radical inhibitor and a catalyst. The mixture was stirred and maintained at 80 °C, and then 9.83 g of acrylic acid (0.136 mol) was separately added by a three-step addition: one third of the total acrylic acid at initial addition, and the addition of second third and the final at 2 and 4 hours from the beginning of the reaction, respectively. After the final addition of acrylic acid, the reaction was continued for additional 6 hours. 200 mL of ethyl ether was added to the mixture at the end of the reaction for ether extraction. Using a 500-mL separatory funnel, purifications of the product were performed with the ether extraction through water washing (100 mL, five times repeat) and using saturated sodium bicarbonate solution (30 mL). Magnesium sulfate was used to absorb water residues in the organic phase and then removed by Celite filtration. Finally, the solvent was evaporated under vacuum at 45 °C, and 23.2 g of AEAU was collected.

### 5.3.5. Preparation of UV-cured acrylates

AEAU, AESO, or AECO were used as acrylic monomer/oligomers to prepare bio-based acrylates. Darocur 1173 (3 wt% of total resin) was added to the resins, and they were mixed well through using a vortex mixer and a sonicator following warming the mixture using a heat gun. Using a film casting knife (BYK-Gardener USA, Columbia, MD), the resin mixture was spread over a glass panel at 4-in width and 160  $\mu\text{m}$  thickness. Then the resin over the glass panel was immediately cured twice using a F300 UV system ((1.8 kW, 6-in (300 W  $\text{in}^{-1}$ ) lamps) equipped with a LC6B benchtop conveyor (Fusion UV system, Gaithersburg, MD) at a conveyor rate of 10  $\text{ft min}^{-1}$ . The cured resin was peeled from the glass panel at one day after UV-curing and stored as an acrylate film (0.13-0.14 mm thickness) for investigation of thermoset properties. For testing AEAU as a reactive diluent, AESO, AEAU, and TEGDMA were mixed at weight ratios of 8:2:0, 8:1:1, and 8:0:2, respectively. The mixed acrylates were UV-cured after additions of 3 wt% of Darocur 1173 and then stored as films according to the same method as mentioned.

### 5.3.6. Measurements

$^1\text{H}$  nuclear magnetic resonance (NMR) spectra were provided by a Varian 600 MHz spectrometer at room temperature with deuterated chloroform as a solvent, and Fourier transform infrared spectroscopy (FTIR) analysis was performed on Perkin-Elmer Spectrum 400 FTIR spectroscopy (Waltham, MA) at spectra range from 400  $\text{cm}^{-1}$  to 4000  $\text{cm}^{-1}$  with 4  $\text{cm}^{-1}$  of resolution. Epoxy content of the epoxide was measured according to the test method A of ASTM D 1652-97 using 0.1 N hydrogen bromide in acetic acid as a titrant. Viscosities of UA and its derivatives were measured using a Bohlin CVOR 150 rheometer (Marlvern Instruments, Southborough, MA) equipped with a PP 20 parallel plate on 500  $\mu\text{m}$  of gap size. The viscosity profiles were obtained at a range of shear rates from 0.1  $\text{s}^{-1}$  to 500  $\text{s}^{-1}$  at 25  $^{\circ}\text{C}$ .

Tensile properties of the cured acrylates were estimated using a tensile tester (TT-1100, ChemInstruments, Fairfield, OH), and the acrylate film were cropped to prepare strips (1.27 cm width) as specimens for the tensile test via using a dual-blade shear cutter (JDC Precision Cutter 1000, Thwing-Albert Instrument Company, West Berlin, NJ). The specimens were applied to the two grips (one fixed and one moving parts) of the tensile tester with 5.08 cm of initial grip separation, and the grips were separated at a rate of  $2.54 \text{ cm min}^{-1}$ . Tensile strength and elongation at break were recorded as the average of the three precision values of at least five measurements. The acrylate film strip (approximately 0.15 g) was immersed in toluene (20 mL) for 10 days at room temperature to evaluated gel content of the cured acrylates (Y. Li and Sun, 2015b; Vendamme and Eevers, 2013). After the time, the sample was placed in an oven at  $130 \text{ }^{\circ}\text{C}$  for 3 hours to evaporate the solvent and then weighed. The gel content was measured to be the percentage value of dividing the weight of the sample after the immersion test by the weight before the test.

Viscoelastic properties of the cured acrylates were estimated by Dynamic mechanical analysis (DMA) acquired with TA DMA Q800 (New Castle, DE) in tension mode. Acrylate film strips (2 cm length, 1.27 cm width, and 0.13-0.14 mm thickness) were used as specimens for applying on the DMA, and the specimens were heated from  $-50 \text{ }^{\circ}\text{C}$  to  $200 \text{ }^{\circ}\text{C}$  at a rate of  $3 \text{ }^{\circ}\text{C min}^{-1}$  under a frequency of 1 Hz and a displacement amplitude of 15  $\mu\text{m}$ . Thermal stability parameters of the cured acrylates were evaluated by thermogravimetric analysis (TGA) using PerkinElmer Pyris 1 TGA (Norwalk, CT) under a nitrogen atmosphere. Approximately 10 mg of samples were tested in a heating range of  $50 \text{ }^{\circ}\text{C}$  to  $750 \text{ }^{\circ}\text{C}$  at a rate of  $20 \text{ }^{\circ}\text{C min}^{-1}$ .

## 5.4. Results and Discussion

### 5.4.1. Structure characterization of AEAU and its intermediates

The vinyl group of UA were monitored by specific peaks in the spectra of UA (Figure 5.3): the C=C stretching peak at  $1641\text{ cm}^{-1}$ , the alkene C-H stretching peak at  $3078\text{ cm}^{-1}$ , and the alkene C-H bending peak at  $908$  and  $992\text{ cm}^{-1}$ . In addition, the broad band from  $2400\text{ cm}^{-1}$  to  $3400\text{ cm}^{-1}$  and the peak at  $1706\text{ cm}^{-1}$  in UA spectra represented the O-H stretching and the C=O stretching of the carboxylic acid group of UA, respectively. After the enzymatic esterification of UA with allyl alcohol (Scheme 5.1), the O-H band disappeared in AU spectra, and the C=O stretching peak was mostly shifted from  $1706\text{ cm}^{-1}$  to  $1737\text{ cm}^{-1}$  in AU spectra. These results strongly indicated that most of carboxylic acids of UA were formed to esters groups of AU, as resulting of the esterification of UA. Furthermore, the C-C(=O)-C stretching peak of AU at  $1166\text{ cm}^{-1}$  represented the newly formed ester groups of AU.

After the epoxidation of AU, the carboxylic acid residues of UA in AU spectra (the tiny peak at  $1706\text{ cm}^{-1}$ ) clearly disappeared in EAU spectra since the purification step of EAU synthesis removed the acids. In addition, the new peak at  $835\text{ cm}^{-1}$  in EAU spectra was a result of the vibration of the new oxirane groups, and the C=C peak at  $1641\text{ cm}^{-1}$  in AU spectra was removed in EAU spectra due to the epoxidation of the double bond. In the spectra of AEAU, the peak at  $1721\text{ cm}^{-1}$  indicated the C=O stretching of the acrylic groups of AEAU, and this peak was overlapped with the C=O stretching peak at  $1737\text{ cm}^{-1}$  from the fatty acid ester groups of AEAU. The band of O-H also newly appeared around  $3300\text{ cm}^{-1}$  due to the epoxide ring-opening reaction for AEAU synthesis. The acrylation of EAU was strongly evidenced by the new peaks at  $809$ ,  $1407$ ,  $1619$ , and  $1635\text{ cm}^{-1}$  in AEAU spectra, which were attributed to the vinyl groups of the acrylate functional groups of AEAU. The peaks of the vinyl groups in AEAU spectra were mostly

reduced at the spectra of the cured AEAU due to their participations in the free-radical polymerization. AEAU, AESO, and AECO were highly cured under the UV system because all the cured acrylates showed more than 96% of gel content through the immersion test in toluene (Table 5.1).

$^1\text{H}$  NMR was used to confirm chemical structures and functionalities of AEAU and its intermediates. All peaks of protons were noted in Figure 5.4-5.7. As shown in Figure 5.4, typical fatty acid peaks appeared at 2.34 ppm (peak 1,  $\alpha$ -methylene proton) and at 11.6 ppm (not shown in Figure 5.4, carboxylic acid proton) in the UA spectra. In addition, the peaks of the terminal olefinic protons were observed at 5.8 ppm (peak 5, methine proton) and 4.91-5.0 ppm (peak 6, methylene proton) in the spectra of UA (Lluch et al., 2010). The new peak appearances at 5.91 ppm (peak 8, methine proton) and 5.21-5.33 ppm (peak 9, methylene proton) in the AU spectra (Figure 5.5) were attributed to the new C=C double bond at the ester side of AU (Lluch et al., 2010), and the peak of methylene proton (-CH<sub>2</sub>-O-) also appeared at 4.57 ppm (peak 7) in the AU spectra (Lluch et al., 2010; Luo et al., 2013), as results of the esterification of UA with allyl alcohol. In addition, the peak of the carboxylic acid proton at 11.6 ppm in the UA spectra (not shown in Figure 5.4) disappeared in the spectra of AU.

After the epoxidation of AU, the peaks of the epoxide protons appeared in a range of 2.45-3.22 ppm in the EAU spectra, as shown in Figure 5.6: the peaks at 2.46 and 2.65 ppm (peak 6, methylene protons), and at 2.9 ppm (peak 5, methine proton) representing the terminal epoxide at the aliphatic chain (Bigot et al., 2016), and the peaks at 2.74 and 2.84 ppm (peak 9, methylene protons), and at 3.2 ppm (peak 8, methine proton) representing the other epoxide at the ester side of EAU (Gadwal and Khan, 2013). Peaks 5 and 6 of the AU spectra (Figure 5.5) were clearly removed in the EAU spectra (Figure 5.6); however peaks 8 and 9 of the AU spectra reduced and

remained in the EAU spectra. Therefore, the results indicate that the C=C double bond at the ester side of AU was not completely converted to the epoxide, while the C=C double bond at aliphatic chain was mostly epoxidized. The steric hindrance of the ester group of AU might result low accessibility of m-CPBA as an oxidant toward the C=C double bond next to the ester group. Consequently, the C=C double bond residues contributed to the less epoxy functionality of EAU (1.75 epoxides per molecule, 10.94 wt% of the average epoxy content) than the theoretical value (approximately 2 epoxides per molecule). After acrylation of EAU, the corresponding peaks of epoxides (peaks 5, 6, 8, and 9 in the EAU spectra (Figure 5.6)) disappeared in AEAU spectra (Figure 5.7), and the new peaks representing three protons of the vinyl group of the acrylates were observed at 6.43, 6.15, and 5.88 ppm (peak 10 a-c) in the AEAU spectra.

The numbers of C=C double bonds in UA and AU ( $N_d$ ) and acrylate groups in AEAU ( $N_a$ ) were estimated according to Eq. (1) and (2) using the peak of  $\alpha$ -methylene proton (peak 1 in all the spectra) as internal standards (J. La Scala, 2002).

$$N_d = 0.5 \left[ \frac{A_{4.8-6.0ppm}}{A_{proton}} - 1 \right] \quad (1)$$

$$N_a = \frac{A_{5.7-6.5ppm}}{3A_{proton}} \quad (2)$$

Where  $A_{4.8-6.0ppm}$  and  $A_{5.7-6.5ppm}$  are the area of the corresponding peaks and marked in the spectra.  $A_{proton}$  is the area of the internal standard peak (peak 1) divided by the number of protons per molecule for peak 1 (i.e., 2). The numbers of the epoxides in EAU ( $N_e$ ) was determined by a titration of EAU with hydrogen bromide in acetic acid solution (ASTM D 1652-97) according to Eq. (3) (N. Kim et al., 2015).

$$N_e = (0.016 \times N \times (V - B)/W) \times \frac{MW}{16} \quad (3)$$

Where  $N$ ,  $V$ ,  $B$ ,  $W$ , and  $MW$  are normality of the titrant, amount of used titrant for sample (mL), amount of used titrant for blank (mL), mass of the sample (g), and molecular weight of EAU, respectively. From Eq. (1)-(3), the number of C=C double bonds, epoxides, and acryl groups of UA, AU, EAU, and AEAU were determined to be 0.95, 2.09, 1.75, and 1.39 per molecule, respectively, and the conversion rate of the epoxide into the acrylate was calculated to be 79.4%. The ring-opening of the epoxides of plant oils for acrylation reaction usually produces oligomers due to the reaction of the epoxide with hydroxyl groups (Y. Li and Sun, 2014; Rengasamy and Mannari, 2013). Therefore, the oligomerization during the acrylation of EAU was contributed to the low acrylate conversion rate of AEUA synthesis; however, it was greater than that of acrylation of epoxidized camelina oil (i.e., 70.2%) (Sung and Sun, Under Review); epoxidized triglycerides such as epoxidized soybean oil have multiple epoxides on one fatty acid that possibly decrease the reactivity of the epoxide in the acrylation reaction due to the steric hindrance effect (J. La Scala and Wool, 2002). Thus, we can conclude that the end-group functionalities of EAU had an advantage for obtaining better acrylate conversion due to the lack of the steric effect from the neighbor epoxides.



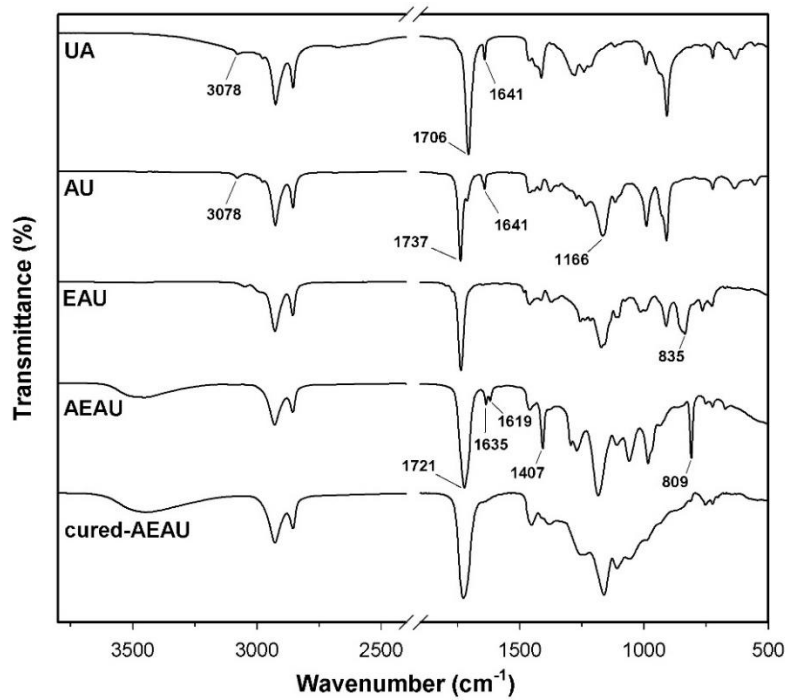


Figure 5.3: FTIR spectra of UA, AU, EAU, AEAU, and UV-cured AEAU.

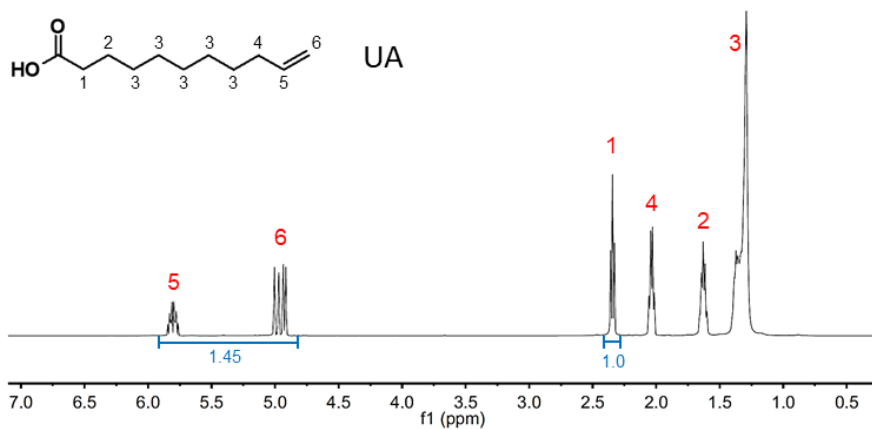
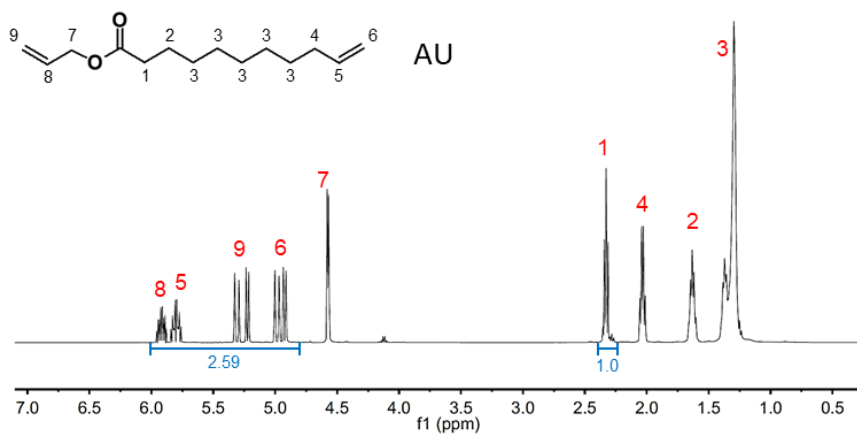
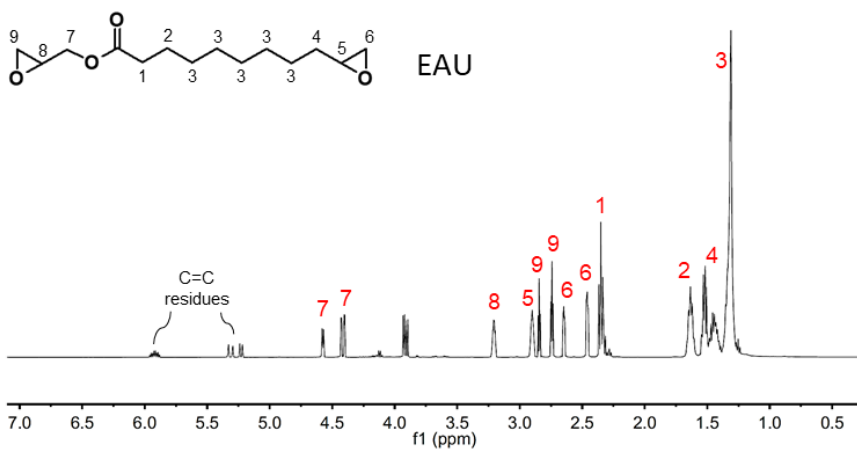


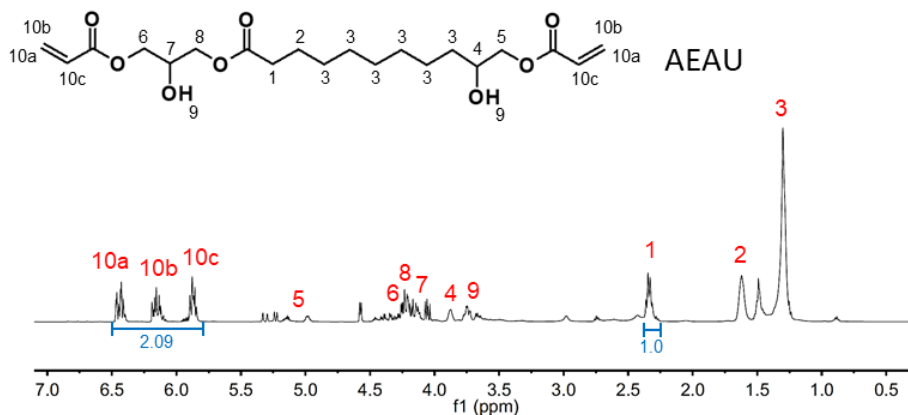
Figure 5.4: NMR spectra of UA.



**Figure 5.5: NMR spectra of AU.**



**Figure 5.6: NMR spectra of EAU.**

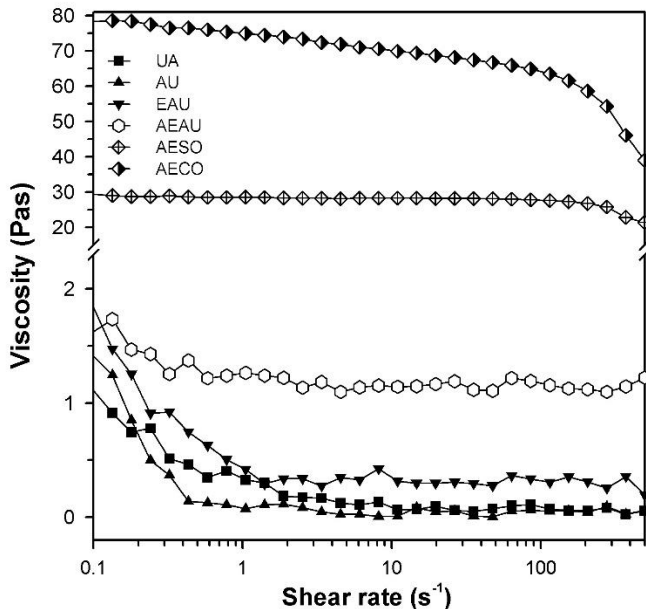


**Figure 5.7: NMR spectra of AEAU.**

#### 5.4.2. Rheological property of UA derivatives and the bio-based acrylates

Viscosities of UA, AU, EAU, and AEAU are monitored at a shear rate range of 0.1 to 500 s<sup>-1</sup> at a constant temperature (25 °C), and the rheological properties of AESO and AECO were also measured as comparison targets of AEAU (Figure 5.8). UA and all the UA derivatives showed little shear-thinning behavior at lower shear rates (approximately below 1 s<sup>-1</sup> region) and then had steady viscosities as viscosities increased. This result is because the intermolecular interaction in UA, AU, EAU, and AEAU were not high enough to exhibit shear-thinning behavior at high shear rates (Y. Li and Sun, 2015a). AU had lower polarity and weaker intermolecular forces such as hydrogen bonding than those of UA due to its ester form compared with acid groups of UA, and consequently, the viscosity of AU (0.073 Pa·s at 1 s<sup>-1</sup>) was less than that of UA (0.327 Pa·s at 1 s<sup>-1</sup>) at the low shear rates. After the epoxidation of AU, the increased viscosity was obtained for EAU (0.418 Pa·s at 1 s<sup>-1</sup>) at the experimental shear rate because of the modification of the polar epoxides. The viscosity of AEAU (1.264 Pa·s at 1 s<sup>-1</sup>) were greatly higher than that of UA derivatives since high polar hydroxyl and ester groups of AEAU resulted increments in intermolecular forces such as dipole-dipole interaction and hydrogen bonding (Y. Li and Sun,

2015a). AESO and AECO had very high viscosities at the entire shear rates and shear-thinning properties at the high shear rates due to their large number of polar groups such as hydroxyl, ester, and acrylic groups with the high molecular weights. The viscosity of AESO (28.5 Pa·s at  $1 \text{ s}^{-1}$ ) was lower than that of AECO (70.8 Pa·s at  $1 \text{ s}^{-1}$ ) because AESO contained fewer acrylic and hydroxyl groups. Similarly, the structure of AEAU contained the same polar groups as AESO and AECO had. However, compared to AESO and AECO, the viscosity of AEAU were much lower although AEAU had higher acrylate content per one fatty acid (1.75 per one fatty acid); AESO and AECO had the acrylate content of 0.8 and 1.12 per one fatty acid, respectively, which were calculated based on the acryl content per triglyceride of AESO (2.4) and AECO (3.36), respectively (Sung and Sun, Under Review). Therefore, the significantly low viscosity of AEAU was attributed to the structural advantages of AEAU, which were short and less branched shape with low molecular weight due to the less carbons of the single fatty acid chains of UA (11 carbons) with the terminal unsaturated carbons, as compared to triple fatty acids of soybean and camelina oil (mainly 18 carbons with one to three unsaturation sites such as oleic, linoleic, and linolenic acids in triglyceride form) (Scheme 5.1 and Figure 5.1).



**Figure 5.8: Viscosities of UA and its derivatives, AESO, and AECO as a function of shear rate.**

### 5.4.3. Viscoelastic properties of the UV-cured acrylates

Viscoelastic properties of the cured acrylates were estimated using DMA in tension mode, and storage modulus and  $\tan \delta$  were plotted in Figure 5.9 and 5.10, respectively. Important parameter of the analysis such as glass transition temperature ( $T_g$ ), half peak width of  $\tan \delta$  peak ( $W_{0.5}$ ), and crosslink density ( $\nu_e$ ) were summarized in Table 5.1. All the  $E'$  plots had rubbery plateau above 145 °C in Figure 5.9, and  $T_g$  of the cured acrylates were determined as the temperatures of the maximum peaks of  $\tan \delta$  plots in Figure 5.10. Estimation of  $\nu_e$  was based on rubber elasticity theory according the following Eq. (4) (Campanella et al., 2009; Khot et al., 2001; Wool and Sun, 2005):

$$\nu_e = \frac{E'}{3RT} \quad (4)$$

Where  $R$  is the gas constant,  $T$  is the absolute temperature (K), and  $E'$  is storage modulus at rubbery region (Pa) at 100 °C greater than  $T_g$ .  $\nu_e$  and  $T_g$  of the AEAU polymer were estimated to

be 56.9 °C and 6.0 kmol m<sup>-3</sup>, which were higher than those of the AESO polymer, but lower than those of the cured AECO. The highest  $\nu_e$  and  $T_g$  of the AECO polymer were expected due to the higher molecular weight and acryl functionality of AECO. Interestingly, the difference between the  $\nu_e$  of the AEAU and the AECO polymers (0.5 kmol m<sup>-3</sup>) was not remarkably large, whereas the significantly lower  $T_g$  was obtained for the AEAU polymer in comparison with the AECO polymer. This result might be due to the short fatty acid length of the AEAU backbone, which resulted the tightly crosslinked network of the polymer (J. J. La Scala et al., 2004). In the case of AESO and AECO, the higher  $\nu_e$  of the AECO polymer was undoubtedly due to the higher functionality of AECO because they were similarly composed of triglycerides as the backbone structures with different functionality.

The width of  $\tan \delta$  peak is related with homogeneity of polymeric networks; more homogeneous polymer structure shows the narrower peak of  $\tan \delta$  plot (H. Lu et al., 2001; B. S. Rao and Palanisamy, 2008), as demonstrated with the values of  $W_{0.5}$  in Table 5.1. The AEAU polymer exhibited the obviously smaller  $W_{0.5}$ , as compared to the AESO and AECO polymers, and it concluded that the polymeric structure of AEAU was mostly homogeneous among the bio-based acrylates. The higher heterogeneities of AESO and AECO polymers were mainly due to the fatty acids distributions of their triglycerides, as compared to AEAU polymer derived from UA with high purity. Besides, the homogeneity of the AEAU polymer might be attributed to the less functional groups per molecule of AEAU because more functional groups per molecule could lead relatively heterogeneous polymeric networks due to the different reactivity of the acrylic groups of multi-functional acrylates (Anseth and Bowman, 1995; Dušek and Ilavský, 1975a; Dušek and Ilavský, 1975b).

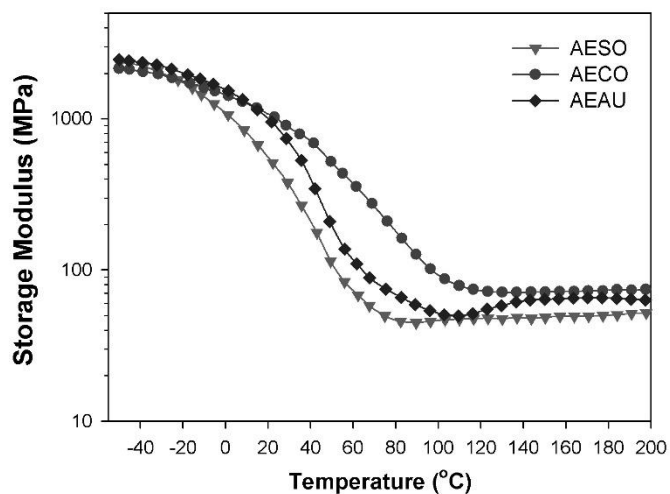


Figure 5.9: Storage modulus of the UV-cured acrylates as a function of temperature.

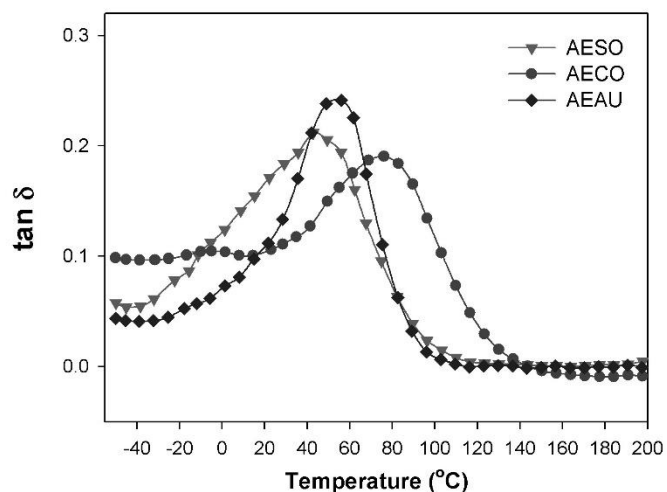


Figure 5.10:  $\tan \delta$  of the UV-cured acrylates as a function of temperature.

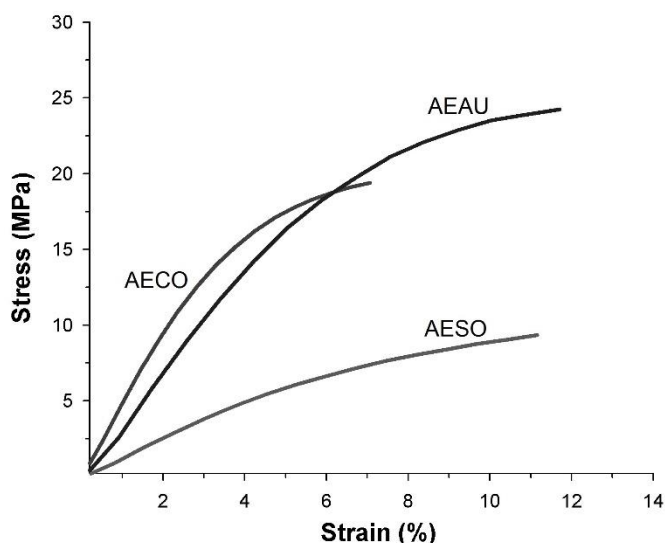
Table 5.1: Properties of the UV-cured acrylates;  $\sigma$  is tensile strength, and  $\epsilon$  is elongation at break.

Samples	$T_g$ (°C)	$v_e$ ( $\text{kmol m}^{-3}$ )	$W_{0.5}$ (°C)	$\sigma$ (MPa)	$\epsilon$ (%)	gel content (%)	$T_{d,5\%}$ (°C)	$T_{d,30\%}$ (°C)	$T_{d,max}$ (°C)	$T_s$
AEAU	56.9	6.0	45.4	$25.0 \pm 1.6$	$12.0 \pm 2.0$	96.2	340	428	478	192
AESO	46.9	4.6	78.5	$9.5 \pm 0.5$	$11.5 \pm 1.5$	96.0	313	413	428	183
AECO	75.1	6.5	94.1	$19.5 \pm 0.6$	$7.7 \pm 0.8$	96.4	345	412	431	189

#### 5.4.4. Tensile properties of the UV-cured acrylates

Figure 5.11 exhibits stress-strain curves of the UV-cured acrylates under the tensile test. Tensile strengths and elongations at break are summarized in Table 5.1. The curves show typical rigid behaviors, so the breaking strength was determined as a tensile strength. The tensile strength of the AECO polymer (19.5 MPa) were more than twice that of the AESO polymer (9.5 MPa), but the flexibility of the AECO polymer was less than 70% that of the AESO polymer, as demonstrated with the elongations at break. This result clearly indicates that the higher crosslink density lead to the improved mechanical strength as well as the brittleness (Can et al., 2006). Therefore, AECO can be an alternative to AESO for rigid thermoset applications, but the brittleness of the AECO polymer will limit its applications of flexible thermosets. Compared with the triglyceride-based acrylates, the tensile strength of the AEAU polymer (25.0 MPa) was significantly higher at maintaining the flexibility (12.0% of elongation at break). Interestingly,  $\nu_e$  of the AEAU polymer was even  $0.5 \text{ kmol m}^{-3}$  lower than that of the AECO polymer, but the tensile strength of the AEAU polymer was approximately 25% higher. This result indicates that the relatively higher functional groups based on the small size of AEAU molecule could contribute to the enhanced mechanical strength of the thermoset; the large molecular size of AESO and AECO caused relatively low functionality based on the weight of monomer although AESO and AECO had more total acryl content per molecule than that of AEAU.





**Figure 5.11: Tensile stress of the UV-cured acrylates as a function of strain.**

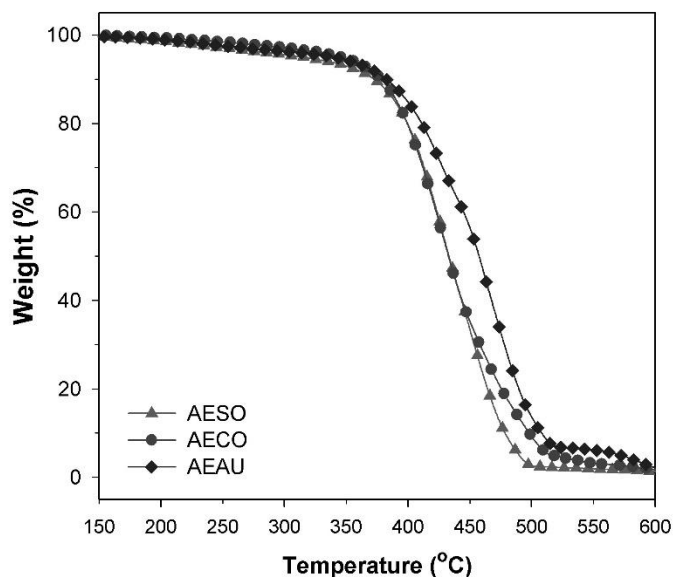
### 5.5.5. Thermal stability factors of the UV-cured acrylates

The degradation temperatures of 5% weight loss ( $T_{d,5\%}$ ) and 30% weight loss ( $T_{d,30\%}$ ) were monitored by TGA thermograms (Figure 5.12), and the temperature of maximum degradation rate ( $T_{d,max}$ ) was determined at the temperature of the maximum height of derivative weight loss curves in Figure 5.13. Using  $T_{d,5\%}$  and  $T_{d,30\%}$ , static heat-resistant index ( $T_s$ ) was calculated following Eq. (5) (Aouf et al., 2013; Lehrle and Williams, 1994):

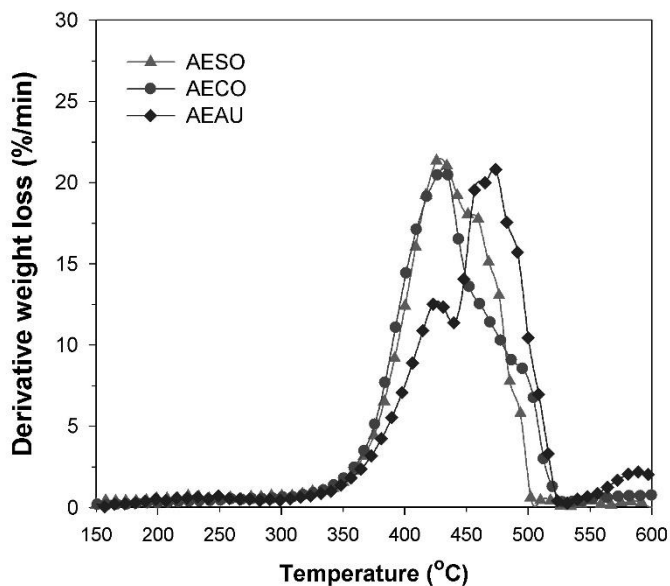
$$T_s = 0.49[T_{d,5\%} + 0.6(T_{d,30\%} - T_{d,5\%})] \quad (5)$$

All the stability factors of the cured acrylates are listed in Table 5.1. The initial degradation stage was observed at a temperature range from 200 to 330 °C for all the samples through decompositions of monomer residues in the polymers (C. Zhang et al., 2015). Major degradations of the cured acrylates were then occurred by depolymerization and formation of char in the polymer systems at a temperature range of 330 to 520 °C (K. Liu et al., 2015). The AESO polymer firstly decomposed at the major degradation range, as demonstrated with the lowest  $T_{d,5\%}$  (313 °C),

due to its low crosslink density, while the AECO and AEAU polymers showed 345 and 340 °C of  $T_{d,5\%}$ , respectively. The AEAU polymer exhibited the better thermal stability, as compared to the AESO and AECO polymers, since the highest  $T_{d,max}$  and  $T_s$  were obtained for the AEAU polymer. This result may be due to the compact chemical structure and high acryl functionality per weight of the monomer, which was previously mentioned to explain the highest tensile strength of the AEAU polymer.



**Figure 5.12: Residual weight of the UV-cured acrylates as a function of temperature.**



**Figure 5.13: Derivative weight loss of the UV-cured acrylates as a function of temperature.**

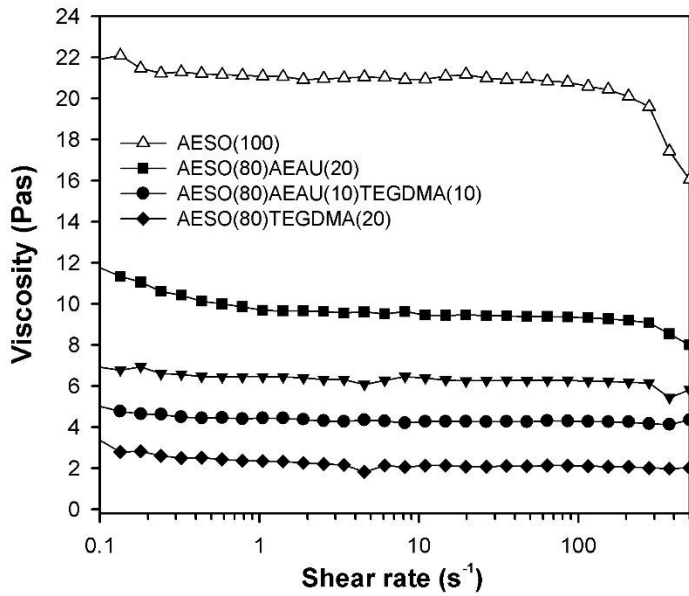
### 5.5.6. Possibility of AEAU as a reactive diluent for AESO resin

Although mechanical and thermal properties of AESO thermoset were poor, AESO is one of the commercially available bio-based acrylates due to its inexpensive and abundant raw material (J. La Scala and Wool, 2013; K. Liu et al., 2015). Therefore, AEAU was tested as a bio-based reactive diluent to enhance an easiness of processing and performance properties of the AESO resin due to its di-functionality with low viscosity and the excellent mechanical properties of the AEAU polymer. TEGDMA was also used as a petrochemical reactive diluent, which has two terminal acrylic groups (Figure 5.1), and AESO was formulated with the corresponding reactive diluents at weight ratio of 80 to 20 (Table 5.2), and the resins were cured by the same UV system with an addition of Darocur 1173 (3 wt% of total resins). Viscosities of the AESO resins with the reactive diluents are plotted as a function of shear rate in Figure 5.14, and listed in Table 5.2. The viscosity of AESO (21.1 Pa·s) was reduced by all the formulations with the reactive diluents, and the viscosity reductions were increased as TEGDMA content was increased. The least viscosity

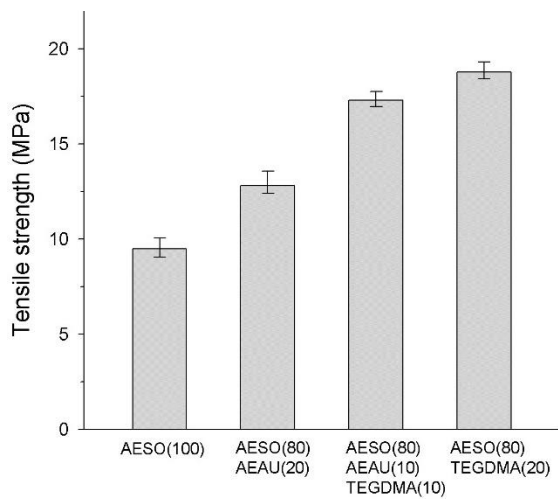
reduction was obtained for AESO(80)-AEAU(20) resin (9.7 Pa·s of viscosity) because of the longer chain of the backbone and more polar groups such as the ester group of fatty acid and hydroxyl groups of AEAU, as compared to TEGDMA. However, the bio-content of the resins were decreased as increments in TEGDMA (Table 5.2); the bio-content was determined as a term of bio-based content according to the specification from United States Department of Agriculture (USDA) as “a percent of the mass of the bio-based carbon in the total organic carbon of the product” (Dai et al., 2015; Kunioka et al., 2014). The bio-content of AESO and AEAU were determined as 100% and 85%, respectively, since acrylic acid was considered as a bioproduct derived from renewable resources (Ondrey, 2014).

As shown in  $\tan \delta$  plots (Figure 5.18), the temperature of the peak was shifted to high temperatures as the reactive diluents were added in AESO, and the AESO(80)-TEGDMA(20) polymer showed the highest temperature of the  $\tan \delta$  peak (62.8 °C), as demonstrated with  $T_g$  values in Table 5.2. The AESO(80)-AEAU(10)-TEGDMA(10) polymer exhibited significantly higher  $T_g$  (57.9 °C) than that of the AESO(100) and AESO(100)-AEAU(20) polymers (46.9 and 50.9 °C, respectively). The enhanced  $T_g$  corresponding TEGDMA additions was expected because methyl groups of methacrylic groups impeded the rotational motion of the segments in polymeric networks at the elevated temperature (Chattopadhyay et al., 2005). In addition to  $T_g$ , the polymer network of AESO was more homogeneous through the additions of the reactive diluents since all the samples including the reactive diluents had greatly narrower  $\tan \delta$  peaks than that of the neat cured AESO, as shown in  $W_{0.5}$  values in Table 5.2. AEAU and TEGDMA were not able to be crosslink agents for the AESO system because  $v_e$  of the cured AESO was decreased by the formulations with all the reactive diluents.

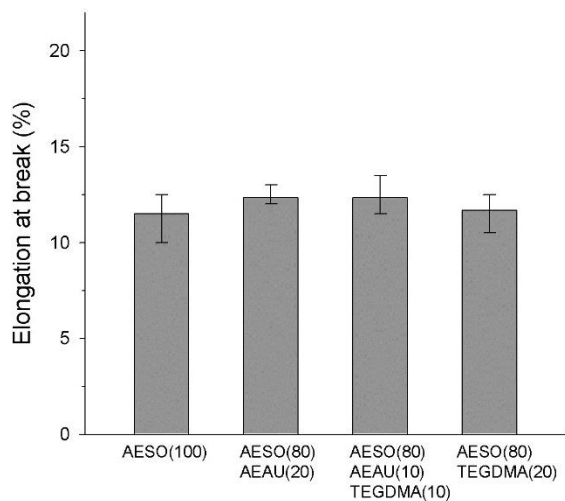
While the elongations at break of AESO and AESO with the reactive diluent polymers were not significantly different (Figure 5.16), the tensile strength of the AESO polymer (9.5 MPa) was obviously enhanced after the reactive diluents were added (Figure 5.15). The maximum tensile strength (18.8 MPa) was achieved by the addition of TEGDMA at 20% concentration (Table 5.2), and this result was corresponding to the highest storage modulus of the AESO(80)-TEGDMA(20) polymer at room temperature in Figure 5.17. Compared to the neat AESO polymer, the higher tensile strength was obtained for the AESO(80)-AEAU(20) polymer (12.8 MPa), but it was much lower than that of the AESO(80)-TEGDMA(20) polymer. Interestingly, the cured AESO including the mixed reactive diluents of AEAU and TEGDMA at 1:1 weight ratio (AESO(80)-AEAU(10)-TEGDMA(10)) showed much higher tensile strength (17.3 MPa), which was slightly below that of AESO(80)-TEGDMA(20) polymer, than that of AESO(80)-AEAU(20) polymer. Therefore, the AESO(80)-AEAU(10)-TEGDMA(10) resin was the most competitive system in this study because it achieved both high bio-content in the resin and improved performance properties of the AESO resin.



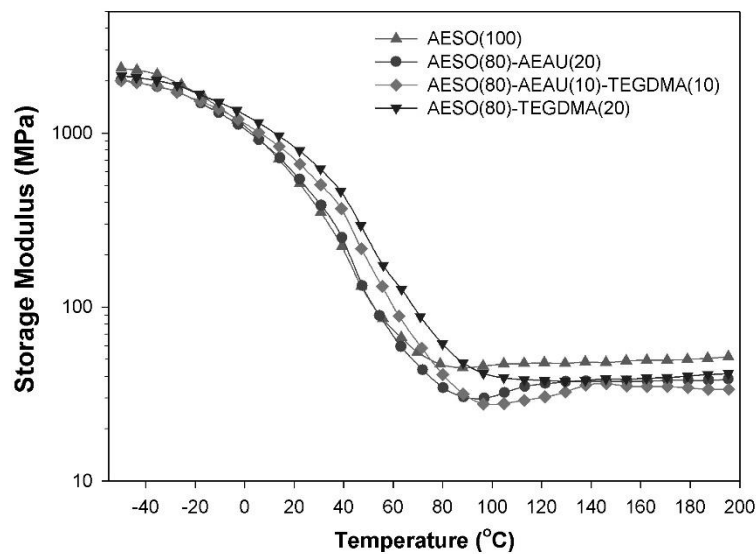
**Figure 5.14: Viscosities of the neat AESO and the AESO resins containing AEAU and/or TEGDMA as reactive diluents.**



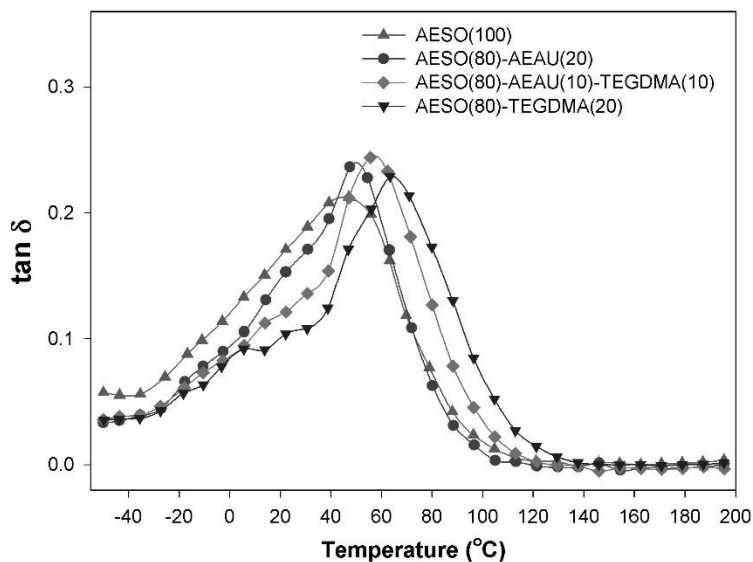
**Figure 5.15: Tensile strengths of the AESO thermosets containing AEAU and/or TEGDMA as reactive diluents.**



**Figure 5.16: Elongations at break of the AESO thermosets containing AEAU and/or TEGDMA as reactive diluents.**



**Figure 5.17: Storage modulus of the AESO thermosets containing AEAU and/or TEGDMA as reactive diluents.**



**Figure 5.18:**  $\tan \delta$  of the AESO thermosets containing AEAU and/or TEGDMA as reactive diluents.

**Table 5.2:** Bio-content and viscosity of the AESO resins formulated with AEAU and/or TEGDMA including 3 wt% of photo-initiator. Viscoelastic and tensile properties of the UV-cured resins;  $\eta$  is viscosity at shear rate of  $1 \text{ s}^{-1}$ ,  $\sigma$  is tensile strength, and  $\epsilon$  is elongation at break.

Compositions (wt%)	Bio-content (%)	$\eta$ (Pa·s)	$T_g$ (°C)	$W_{0.5}$ (°C)	$\nu_e$ ( $\text{kmol m}^{-3}$ )	$\sigma$ (MPa)	$\epsilon$ (%)
AESO(100)	97.1	21.1	46.9	78.5	4.6	$9.5 \pm 0.5$	$11.5 \pm 1.5$
AESO(80)-AEAU(20)	94.2	9.7	50.9	56.4	3.5	$12.8 \pm 0.8$	$12.3 \pm 0.7$
AESO(80)-AEAU(10)-TEGDMA(10)	85.9	4.4	57.9	55.6	3.3	$17.3 \pm 0.4$	$12.3 \pm 1.2$
AESO(80)-TEGDMA(20)	77.7	2.3	62.8	53.9	3.6	$18.8 \pm 0.5$	$11.7 \pm 1.2$

## 5.5. Conclusion

The fatty ester-based acrylate, AEAU was successfully synthesized from castor oil derivative, UA, and AEAU had extremely lower viscosity ( $1.264 \text{ Pa}\cdot\text{s}$  at  $1 \text{ s}^{-1}$ ) than that of commercial AESO ( $28.5 \text{ Pa}\cdot\text{s}$  at  $1 \text{ s}^{-1}$ ). Moreover, the AEAU thermoset showed excellent performances in all terms of strength, flexibility, glass transition temperature and crosslink density, and thermal stability, as



compared to the AESO thermoset. Even the rigid and brittle thermoset from AECO showed lower tensile strength and thermal stability factors than those of the AEAU thermoset. In addition, the AESO thermoset containing AEAU and TEGDMA equally as reactive diluents showed 1.7 times higher tensile strength (17.8 MPa) and 11 °C higher glass transition temperature (57.9 °C) maintained with the flexibility (12.3% elongation at break) and high bio-content (85.9%), as compared to the pristine AESO thermoset. These results suggested that AEAU can be a great alternative or an additive to traditional triglyceride-based acrylates such as AESO for various thermoset applications due to its low viscosity and performances of the thermoset.

## 5.6. References

- Anseth, K. S., and Bowman, C. N. (1995). Kinetic gelation predictions of species aggregation in tetrafunctional monomer polymerizations. *Journal of Polymer Science Part B: Polymer Physics*, 33: 1769-1780.
- Aouf, C., Nouailhas, H., Fache, M., Caillol, S., Boutevin, B., and Fulcrand, H. (2013). Multi-functionalization of gallic acid. synthesis of a novel bio-based epoxy resin. *European Polymer Journal*, 49: 1185-1195.
- Bigot, S., Daghbir, M., Mhanna, A., Boni, G., Pourchet, S., Lecamp, L., and Plasseraud, L. (2016). Undecylenic acid: A tunable bio-based synthon for materials applications. *European Polymer Journal*, 74: 26-37.
- Campanella, A., La Scala, J. J., and Wool, R. P. (2009). The use of acrylated fatty acid methyl esters as styrene replacements in triglyceride-based thermosetting polymers. *Polymer Engineering & Science*, 49: 2384-2392.
- Campanella, A., Scala, J. J. L., and Wool, R. (2011). Fatty acid-based comonomers as styrene replacements in soybean and castor oil-based thermosetting polymers. *Journal of Applied Polymer Science*, 119: 1000-1010.
- Can, E., Wool, R., and Küsefoğlu, S. (2006). Soybean-and castor-oil-based thermosetting polymers: Mechanical properties. *Journal of Applied Polymer Science*, 102: 1497-1504.
- Chattopadhyay, D., Panda, S. S., and Raju, K. (2005). Thermal and mechanical properties of epoxy acrylate/methacrylates UV cured coatings. *Progress in Organic Coatings*, 54: 10-19.
- Chrysanthos, M., Galy, J., and Pascault, J. (2011). Preparation and properties of bio-based epoxy networks derived from isosorbide diglycidyl ether. *Polymer*, 52: 3611-3620.
- Cousinet, S., Ghadban, A., Fleury, E., Lortie, F., Pascault, J., and Portinha, D. (2015). Toward replacement of styrene by bio-based methacrylates in unsaturated polyester resins. *European Polymer Journal*, 67: 539-550.
- Dai, J., Ma, S., Wu, Y., Han, L., Zhang, L., Zhu, J., and Liu, X. (2015). Polyesters derived from itaconic acid for the properties and bio-based content enhancement of soybean oil-based thermosets. *Green Chemistry*, 17: 2383-2392.
- Dušek, K., & Ilavský, M. (1975a). Cyclization in crosslinking polymerization. I. chain polymerization of a bis unsaturated monomer (monodisperse case). Paper presented at the *Journal of Polymer Science: Polymer Symposia*, , 53(1) 57-73.
- Dušek, K., & Ilavský, M. (1975b). Cyclization in crosslinking polymerization. II. chain polymerization of a bis unsaturated monomer (polydisperse case). Paper presented at the *Journal of Polymer Science: Polymer Symposia*, , 53(1) 75-88.
- Gadwal, I., and Khan, A. (2013). Protecting-group-free synthesis of chain-end multifunctional polymers by combining ATRP with thiol-epoxy 'click' chemistry. *Polymer Chemistry*, 4: 2440-2444.

- Khot, S. N., Lascala, J. J., Can, E., Morye, S. S., Williams, G. I., Palmese, G. R., Kusefoglou, S. H., and Wool, R. P. (2001). Development and application of triglyceride-based polymers and composites. *Journal of Applied Polymer Science*, 82: 703-723. doi:10.1002/app.1897
- Kim, N., Li, Y., and Sun, X. S. (2015). Epoxidation of camelina sativa oil and peel adhesion properties. *Industrial Crops and Products*, 64: 1-8.
- Kunioka, M., Taguchi, K., Ninomiya, F., Nakajima, M., Saito, A., and Araki, S. (2014). Biobased contents of natural rubber model compound and its separated constituents. *Polymers*, 6: 423-442.
- La Scala, J. (2002). The effects of triglyceride structure on the properties of plant oil-based polymers, PhD dissertation. University of Delaware,
- La Scala, J. J., Orlicki, J. A., Winston, C., Robinette, E. J., Sands, J. M., and Palmese, G. R. (2005). The use of bimodal blends of vinyl ester monomers to improve resin processing and toughen polymer properties. *Polymer*, 46: 2908-2921.
- La Scala, J. J., Sands, J. M., Orlicki, J. A., Robinette, E. J., and Palmese, G. R. (2004). Fatty acid-based monomers as styrene replacements for liquid molding resins. *Polymer*, 45: 7729-7737.
- La Scala, J., and Wool, R. P. (2002). The effect of fatty acid composition on the acrylation kinetics of epoxidized triacylglycerols. *Journal of the American Oil Chemists' Society*, 79: 59-63.
- La Scala, J., and Wool, R. P. (2005). Property analysis of triglyceride-based thermosets. *Polymer*, 46: 61-69.
- La Scala, J., and Wool, R. P. (2013). Fundamental thermo-mechanical property modeling of triglyceride-based thermosetting resins. *Journal of Applied Polymer Science*, 127: 1812-1826.
- Lehrle, R. S., and Williams, R. J. (1994). Thermal degradation of bacterial poly (hydroxybutyric acid): Mechanisms from the dependence of pyrolysis yields on sample thickness. *Macromolecules*, 27: 3782-3789.
- Li, C., Cai, X., Sung, J., Wang, H., Bossmann, S. H., and Susan Sun, X. (2017). Fatty acid chain combined with cycloaliphatic rings via Amberlyst-15: A promising structure for a high biocontent epoxy design. *Journal of Polymer Science Part A: Polymer Chemistry*, 55: 794-800.
- Li, C., Li, Y., Cai, X., Wang, H., Bossmann, S. H., Sung, J., and Sun, X. S. (2016). Competitive nucleophilic attack chemistry based on undecenoic acid: A new chemical route for plant-oil-based epoxies. *ACS Sustainable Chemistry & Engineering*, 4: 5718-5729.
- Li, Y., and Sun, X. S. (2014). Di-hydroxylated soybean oil polyols with varied hydroxyl values and their influence on UV-curable pressure-sensitive adhesives. *Journal of the American Oil Chemists' Society*, 91: 1425-1432.
- Li, Y., and Sun, X. S. (2015a). Camelina oil derivatives and adhesion properties. *Industrial Crops and Products*, 73: 73-80.

- Li, Y., and Sun, X. S. (2015b). Synthesis and characterization of acrylic polyols and polymers from soybean oils for pressure-sensitive adhesives. *RSC Advances*, 5: 44009-44017.
- Liu, K., Madbouly, S. A., and Kessler, M. R. (2015). Biorenewable thermosetting copolymer based on soybean oil and eugenol. *European Polymer Journal*, 69: 16-28.
- Lligadas, G., Ronda, J. C., Galià, M., and Cádiz, V. (2010). Oleic and undecylenic acids as renewable feedstocks in the synthesis of polyols and polyurethanes. *Polymers*, 2: 440-453.
- Lluch, C., Lligadas, G., Ronda, J. C., Galià, M., and Cádiz, V. (2013). Thermoplastic polyurethanes from undecylenic Acid-Based soft segments: Structural features and release properties. *Macromolecular Bioscience*, 13: 614-622.
- Lluch, C., Ronda, J. C., Galià, M., Lligadas, G., and Cádiz, V. (2010). Rapid approach to biobased telechelics through two one-pot thiol-ene click reactions. *Biomacromolecules*, 11: 1646-1653.
- Lu, H., Lovell, L. G., and Bowman, C. N. (2001). Exploiting the heterogeneity of cross-linked photopolymers to create high-T<sub>g</sub> polymers from polymerizations performed at ambient conditions. *Macromolecules*, 34: 8021-8025.
- Luo, Q., Lui, M., Xu, Y., Ionescu, M., and Petrovic, Z. S. (2013). Thermosetting allyl resins derived from soybean fatty acids. *Journal of Applied Polymer Science*, 127: 432-438.
- Ma, S., Liu, X., Fan, L., Jiang, Y., Cao, L., Tang, Z., and Zhu, J. (2014). Synthesis and properties of a Bio-Based epoxy resin with high epoxy value and low viscosity. *ChemSusChem*, 7: 555-562.
- Ondrey, G. (2014). A step closer to bio-based acrylic acid. *Chemical Engineering*, 121: 18-18.
- Pang, C., Zhang, J., Wu, G., Wang, Y., Gao, H., and Ma, J. (2014). Renewable polyesters derived from 10-undecenoic acid and vanillic acid with versatile properties. *Polymer Chemistry*, 5: 2843-2853.
- Rao, B. S., and Palanisamy, A. (2008). Synthesis, photo curing and viscoelastic properties of triacrylate compositions based on ricinoleic acid amide derived from castor oil. *Progress in Organic Coatings*, 63: 416-423. doi:10.1016/j.porgcoat.2008.07.001
- Rengasamy, S., and Mannari, V. (2013). Development of soy-based UV-curable acrylate oligomers and study of their film properties. *Progress in Organic Coatings*, 76: 78-85. doi:10.1016/j.porgcoat.2012.08.012
- Rosu, L., Cascaval, C. N., and Rosu, D. (2009). Effect of UV radiation on some polymeric networks based on vinyl ester resin and modified lignin. *Polymer Testing*, 28: 296-300.
- Sadler, J. M., Nguyen, A., Greer, S. M., Palmese, G. R., and La Scala, J. J. (2012). Synthesis and characterization of a novel bio-based reactive diluent as a styrene replacement. *Journal of Biobased Materials and Bioenergy*, 6: 86-93.
- Sharmin, E., Zafar, F., Akram, D., Alam, M., and Ahmad, S. (2015). Recent advances in vegetable oils based environment friendly coatings: A review. *Industrial Crops and Products*, 76: 215-229.
- Stanzione, J. F., Sadler, J. M., La Scala, J. J., and Wool, R. P. (2012). Lignin model compounds as Bio-Based reactive diluents for liquid molding resins. *ChemSusChem*, 5: 1291-1297.

- Sung, J., and Sun, X. S. (Under Review). Cardanol modified fatty acids from camelina oils for flexible bio-based acrylates coatings. *Progress in Organic Coatings*,
- Van der Steen, M., and Stevens, C. V. (2009). Undecylenic acid: A valuable and physiologically active renewable building block from castor oil. *ChemSusChem*, 2: 692-713.
- Vendamme, R., and Eevers, W. (2013). Sweet solution for sticky problems: Chemoreological design of self-adhesive gel materials derived from lipid biofeedstocks and adhesion tailoring via incorporation of isosorbide. *Macromolecules*, 46: 3395-3405.
- Wool, R. P., and Sun, X. S. (2005). *Bio-based polymers and composites*. Burlington: Academic Press.
- Yang, X., Li, S., Xia, J., Song, J., Huang, K., and Li, M. (2015). Renewable myrcene-based UV-curable monomer and its copolymers with acrylated epoxidized soybean oil: Design, preparation, and characterization. *BioResources*, 10: 2130-2142.
- Zhan, M., and Wool, R. P. (2010). Biobased composite resins design for electronic materials. *Journal of Applied Polymer Science*, 118: 3274-3283.
- Zhang, C., Madbouly, S. A., and Kessler, M. R. (2015). Renewable polymers prepared from vanillin and its derivatives. *Macromolecular Chemistry and Physics*, 216: 1816-1822.
- Zhang, C., Yan, M., Cochran, E. W., and Kessler, M. R. (2015). Biorenewable polymers based on acrylated epoxidized soybean oil and methacrylated vanillin. *Materials Today Communications*, 5: 18-22.

## Chapter 6 - Conclusions and future works

### 6.1. Overall conclusions

The plant oil-based acrylate, AECO, was successfully synthesized from camelina oil, followed by epoxidation of camelina oil and then acrylation of the epoxidized camelina oil, for wood coating materials. In comparison with soybean oil-based acrylate, AESO, the AECO polymer obviously had better mechanical strength, glass transition temperature, and thermal stability due to its higher acryl functionality. On the other hand, the increased acryl group content with intrinsic viscous characteristic of triglyceride structures caused too viscous feature of the AECO resin (including 3wt% of photoinitiator, 39.2 Pa·s of viscosity). Therefore, several mono- and di-functional acrylates were tested as reactive diluents (10 wt% of AECO) for viscosity reduction of the AECO resin (4.2-14.5 Pa·s). Di-functional acrylates such as EGDMA provided rigidity into the AECO polymer, but the brittle polymeric structure with the low adhesion on wood surface was also manifested in the AECO:RD copolymer. Whereas, mono-functional acrylates with small molecular weight such as MMA and HEA showed excellent viscosity reductions (4.2 Pa·s for AECO:MMA resin) and improved flexibility (8% elongation at break for AECO:HEA copolymer) maintained with mechanical strength, thermal stability and coating performances, as compared to the AECO homopolymer.

The phenolic acrylate, AECFA, was prepared from CFA, which was the new unsaturated plant oil derivative from cardanol and camelina oil containing rigid aromatic rings with flexible alkyl chains. Compared to AECO and the pristine cardanol-based acrylate, AECGE, the great flexibility (11.5% elongation at break) was achieved by the AECFA polymer. In addition, the AECFA polymer exhibited more strengthened thermoset with enhanced thermal and coating properties without losing flexibility, as compared to the AESO polymer. The results of this

research suggested that the novel plant oil-based acrylate from non-edible oils is a good alternative to the commercial AESO.

Single fatty ester-based acrylate, AEAU, was successfully synthesized from castor oil derivative through using chemical pathways such as enzymatic esterification, epoxidation, acrylation reactions. Very low viscosity was obtained for AEAU (1.264 Pa·s) while neat triglyceride-based acrylates such as AESO and AECO showed high viscosities (28.5 Pa·s and 70.8 Pa·s respectively). Compared to the commercial AESO thermoset, the AEAU thermoset showed better performances in mechanical, viscoelastic, and thermal properties. Therefore, AEAU is a promising alternative to AESO for thermoset applications due to its extremely low viscous feature with better thermoset performances. Moreover, AEAU showed a great potential to a “green” reactive diluent when it was used with petrochemical reactive diluents such as TEGDMA.

This study has finally explained that essential weakness of plant oil-based resins can be improved through chemical modifications onto the monomer backbones without using petrochemical additives such as crosslink agents, reinforcing agents, or rheology modifiers, etc. Although final resin products such as coatings, paints, and composites must contain many other ingredients to meet requirements for the end-use purpose, major polymers are undoubtedly key components of the products. Therefore, enhanced performances of the polymer itself can help to improve final resin products and reduce uses of chemical additives.

## **6.2. Future works**

This study mainly focused on using 100% bio-based raw materials with high conversion rate of chemical pathways, so future research should be considered for optimizations of the synthetic routes. For example, operation times and costs of lipase-catalyzed hydrolysis and esterification reactions for preparation AECFA and AEAU, respectively, can be reduced through optimizing

several conditions such as reaction temperature, reactants ratio, types of enzyme, agitation method, and so on. In addition, economic raw materials and other components, which have been involved in preparation of the new resins, should be found for further commercializing the resins. For example, m-CPBA, an oxygen donor in epoxidation reaction, has been used to produce EAU for AEAU synthesis due to its higher conversion rate of the reaction, as compared to using hydrogen peroxide with formic acid, which has been already used to prepare ECO and ECFA for AECO and AECFA synthesis, respectively. However, the price of m-CPBA is much higher than that of formic acid and hydrogen peroxide, and the expensive price of the material can be an obstacle to commercializing the resins. Therefore, other economic epoxidation methods should be considered to produce AEAU economically.

Only renewable resources have been considered as raw materials for synthesis the monomers in this study, and the bio-based monomers have been used as sole monomers of the target polymers. Although they showed potentials to primary acrylate monomers for coatings and thermoset applications, a combination of the bio-based acrylates with current petrochemical acrylates is still more economic and effective system for practical applications. Therefore, study of the bio-based acrylates as co-monomers will be a good step toward commercializing fully bio-based products.

Next, this study has a lack of life cycle analysis, which is an important part to evaluate how “green” the products. Thus, in addition to using renewable raw materials, other factors such as inputs in cultivation and harvesting the crop, and energy consumptions in material process, etc., should be estimated for further understand.

Finally, a task to evaluate end-use quality of the coating materials should be performed. Besides primary polymers in the resins, many other ingredients are added to typical resin products to maintain performance qualities with long lifetimes. This study paid attention to short-term



performances of the bio-based acrylic polymers. Therefore, shelf-life observations of the bio-based acrylates have to be studied, and then sub-ingredients will be added to the coating materials to preparing further bio-based coating products for end-use purposes.